

OAK RIDGE NATIONAL LABORATORY LIBRARIES



3 4456 0548436 6

8

ORNL-3488
UC-4 - Chemistry
TID-4500 (22nd ed.)



CHEMISTRY DIVISION
ANNUAL PROGRESS REPORT
FOR PERIOD ENDING JUNE 20, 1963



OAK RIDGE NATIONAL LABORATORY
CENTRAL RESEARCH LIBRARY
CIRCULATION SECTION
4500N ROOM 175

LIBRARY LOAN COPY

DO NOT TRANSFER TO ANOTHER PERSON.
if you wish someone else to see this report, send in
name with report and the library will arrange a loan.

ORNL-118 (6-97)

OAK RIDGE NATIONAL LABORATORY

operated by

UNION CARBIDE CORPORATION

for the

U.S. ATOMIC ENERGY COMMISSION

Printed in USA. Price: \$2.75 Available from the
Office of Technical Services
U. S. Department of Commerce
Washington 25, D. C.

— LEGAL NOTICE —

This report was prepared as an account of Government sponsored work. Neither the United States, nor the Commission, nor any person acting on behalf of the Commission:

- A. Makes any warranty or representation, expressed or implied, with respect to the accuracy, completeness, or usefulness of the information contained in this report, or that the use of any information, apparatus, method, or process disclosed in this report may not infringe privately owned rights; or
- B. Assumes any liabilities with respect to the use of, or for damages resulting from the use of any information, apparatus, method, or process disclosed in this report.

As used in the above, "person acting on behalf of the Commission" includes any employee or contractor of the Commission, or employee of such contractor, to the extent that such employee or contractor of the Commission, or employee of such contractor prepares, disseminates, or provides access to, any information pursuant to his employment or contract with the Commission, or his employment with such contractor.

ORNL-3488
UC-4 - Chemistry
TID-4500 (22nd ed.)

Contract No. W-7405-eng-26

CHEMISTRY DIVISION ANNUAL PROGRESS REPORT
for Period Ending June 20, 1963

E. H. Taylor, Director
M. A. Bredig, Associate Director

DATE ISSUED

OCT 8 1963

OAK RIDGE NATIONAL LABORATORY
Oak Ridge, Tennessee
operated by
UNION CARBIDE CORPORATION
for the
U. S. ATOMIC ENERGY COMMISSION

OAK RIDGE NATIONAL LABORATORY LIBRARIES



3 4456 0548436 6



Summary

1. NUCLEAR CHEMISTRY

A new nuclear isomer, Ce^{135m} , was discovered and a tentative decay scheme was suggested. A recently discovered nuclear isomer, Ba^{131m} , was produced by a new method, and earlier work on the decay properties was confirmed.

Energy spectra and angular distributions of inelastically scattered 11-Mev protons from Ni^{62} , Ni^{64} , Cu^{63} , and Cu^{65} were obtained by use of the tandem Van de Graaff. Some of the nuclear energy levels in the odd-*A* nuclides were interpreted in terms of the "excited-core" model by comparison of the relative strengths of excitation and the angular distributions with those predicted by the model.

Three neutron groups were observed in the decay of 4.1-sec N^{17} with energies in Mev (and intensities) of 0.406 ± 0.015 (45%), 1.22 ± 0.02 (45%), and 1.79 ± 0.03 (5%). The results indicate neutron emission from the 5.94-Mev ($\frac{1}{2}^-$), 5.38-Mev ($\frac{3}{2}^-$), and 4.55-Mev ($\frac{3}{2}^-$) levels of O^{17} .

The angular correlation of the 613-319-keV gamma-ray cascade in V^{51} was determined. It was fitted to the function $W(\theta) = 1 + (0.013 \pm 0.030)P_2(\cos \theta) - (0.03 \pm 0.05)P_4(\cos \theta)$.

The fractional independent fission yield of Sb^{127} was measured to be $(5.5 \pm 4.2)\%$ in the slow-neutron fission of U^{235} . This leads to a calculated value of 49.5 ± 0.2 for the most probable nuclear charge formed in fission at mass 127 and implies that there is no pronounced 50-proton shell effect on the division of nuclear charge in fission.

An upper limit of ~ 7 barns was measured for the thermal-neutron cross section of the 35-day Nb^{95} .

A determination of the half-life of Bi^{208} more precise than previously reported yielded a revised value of 3.68×10^5 yr with a standard error of 1%.

Extensive calculations of properties of cadmium, gadolinium, samarium, and boron as neutron filters were completed.

Preliminary results for the activation cross section of the 8.0-day I^{131} , $\sigma_{th} \cong 0.7$ barn and $I \cong 8$ barns, were obtained.

A redetermination of the neutron-capture cross section of Rh^{105} was undertaken because of the large degree of uncertainty involved in the earlier determination and because a source of enriched Ru^{104} was available that would permit a more accurate measurement to be made by neutron activation. Several samples of Ru^{104} were irradiated in the ORR with a cadmium-ratio technique to produce Pd^{105} and Pd^{106} through neutron capture by the Rh^{105} intermediate. From the ratio of Pd^{106} to Pd^{105} in the separated palladium fraction, measured with a two-stage mass spectrometer, a neutron cross-section value of 25,400 barns for Rh^{105} was determined. A value of 3.65 barns for the neutron cross section of Ru^{104} was indicated by the Pd^{105} and Pd^{106} yields in one irradiated sample.

2. ISOLATION AND CHEMICAL PROPERTIES OF SYNTHETIC ELEMENTS

The Raman spectra of $TcO_4^-(aq)$ and $MoO_4^{2-}(aq)$ and of crystalline $KTcO_4$, $KReO_4$, Na_2MoO_4 , Na_2WO_4 , $Na_2MoO_4 \cdot 2H_2O$, and $Na_2WO_4 \cdot 2H_2O$ were measured. Infrared spectra of $KReO_4$, $Na_2MoO_4 \cdot 2H_2O$, and $Na_2WO_4 \cdot 2H_2O$ were also observed. Examination of all the spectra led to the conclusion that the structure of the aqueous pertechnetate ion is tetrahedral.

3. CHEMICAL SEPARATION OF ISOTOPES

The kinetics of exchange and the selectivity coefficients of alkali metal ions in Dowex 50 resins of various cross-linkages were studied in ethylenediamine solutions. The selectivity coefficients are greater in ethylenediamine than in water, especially with the higher cross-linked

resins. A large variation in the diffusion rates was found for the different cations.

The lithium isotope separation factor for the system Amberlite ion exchanger IR-120-Li⁺ vs 2 N LiCl was determined to be 1.003 ± 0.001 .

Anhydrous LiSCN was prepared from LiOH·H₂O and NH₄SCN by the precipitation of LiSCN·(C₂H₅)₂O and desolvation by vacuum distillation.

Isotopic equilibrium constants were determined for the exchange of boron between BF₃(gas) and the BF₃-organic (liq) complexes of tetrahydrofuran, ethyl ether, ethyl sulfide, and nitrobenzene.

The single-stage separation factor for nitrogen between NO₃⁻ and NO₂⁻ was found to be 1.057 at 0°C and 1.055 at 10°C. The factor for the pair NO₂⁻/NO is 1.024 at 0°C. Nitrogen-15 is enriched in the first-mentioned species of each pair.

The nitrogen isotope effect in the thermal decomposition of *α,α*-azobisisobutyronitrile and benzenediazonium chloride at 40° is the same for both compounds: $k^{14}/k^{15} = 1.045$.

The isotope effect in the reduction of NO₃⁻ and NH₂OH by tin(II) is small and nearly equal in the two cases: k^{14}/k^{15} for NO₃⁻ = 1.007 ± 0.001 , and for NH₂OH = 1.004 ± 0.002 .

When Fe(II) was used in alkaline solution to reduce NO₃⁻, NO₂⁻, or NH₂OH to ammonia, an isotope effect favoring N¹⁴ was observed. For NO₃⁻, $k^{14}/k^{15} = 1.070$ at 25° and 1.058 at 110°. The effect is similar for NO₂⁻ and NH₂OH, being 1.033 at 25° and 1.028 at 110°.

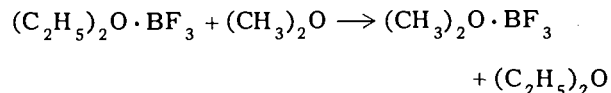
The single-stage separation factor for rubidium and cesium in the system aqueous alkali hydroxide-alkali amalgam was determined at various temperatures and concentrations. One determination was also made for each of the pairs potassium-sodium, potassium-rubidium, and potassium-cesium.

Preparation of beryllium amalgam by several electrolytic procedures was attempted without success. The heating together of beryllium and mercury to 650°C for 1 hr resulted in a solution whose beryllium content was less than 20 ppm.

Nuclear magnetic resonance chemical shifts were measured for liquid XeF₃, XeF₄, XeOF₄, and XeF₆, and ¹⁹F-¹²⁹Xe spin-spin coupling constants for XeF₄ and XeOF₄.

Kinetic data for the exchange of BF₃ between (C₂H₅)₂O·BF₃ and (CH₃)₂O·BF₃ were obtained from the ¹⁹F NMR spectra of eight mixtures of

(C₂H₅)₂O, (CH₃)₂O, and BF₃. The rate of exchange decreased as a larger portion of the ether was complexed, and the activation energies rose from 11 kcal for mixtures having >20% free ether to 16 kcal for the mixture having no free ether. Two exchange mechanisms are indicated. The equilibrium constant for the reaction



was ~ 2.5 at 26°C.

Preliminary data for five mixtures of (C₂H₅)₂O, C₆H₅OCH₃, and BF₃ indicate that this equilibrium greatly favors (C₂H₅)₂O·BF₃; the rate of exchange is about an order of magnitude slower than for the (CH₃)₂O-containing system.

Raman and infrared spectra of BF₃·diethyl ether and BF₃·tetrahydrofuran were recorded for both the B¹⁰ and B¹¹ compounds. The spectra were compared with that of BF₃·dimethyl ether and assignments made of the skeletal frequencies. The isotopic data were used to calculate theoretical equilibrium constants for isotopic exchange between the complexes and BF₃. These values were compared with experimental separation factors.

The infrared and Raman spectra of aqueous oxalate ion were investigated. The data are consistent with a staggered (*D*_{2d}) configuration for the ion rather than a planar configuration as suggested by many investigators.

The preparation at the Oak Ridge Gaseous Diffusion Plant of a series of xenon compounds presented a unique opportunity for the observation of the Raman spectra of these compounds. The Raman spectra of solid XeF₂, gaseous XeF₂, solid XeF₄, solid XeF₆, and liquid XeOF₄ were observed and assignments made of the observed bands.

The O¹⁷ enrichment facility is performing according to plan, and is now about halfway to steady-state operation. Oxygen gas or water enriched to 98% O¹⁸ or 50% O¹⁷ is expected to be available near the end of the calendar year.

4. RADIATION CHEMISTRY

Ozone yields in the radiolysis of oxygen-nitrogen solutions at 77°K were observed by alternate

gamma irradiation and absorption spectrophotometry. Earlier work was extended both to lower and intermediate oxygen concentration.

The enhancement of ozone yield, $\Delta G(O_3) = G(O_3) - \epsilon(O_2)G^o(O_3)$, is given by two equations:

$$\Delta G(O_3) = 7.69 \epsilon(N_2), \quad 0 \leq \epsilon(N_2) \leq 0.9,$$

and

$$\Delta G(O_3) = 8.05 + 1.29 \log \epsilon(O_2), \\ 0.00006 < \epsilon(O_2) < 0.1,$$

where $\epsilon(O_2)$ and $\epsilon(N_2)$ are the electron fractions of O_2 and N_2 , $G(O_3)$ the ozone yield (molecules per 100 ev), and $G^o(O_3)$ is the ozone yield (12.5 ± 0.4 molecules per 100 ev) from liquid O_2 at $77^\circ K$.

The results may be expressed as

$$\Delta G(O_3) = 7.69 \epsilon(N_2) F,$$

where F is a transfer efficiency factor, equal to unity when N_2 has, on the average, one O_2 in its shell of nearest neighbors. The value of F falls slowly with lower O_2 concentration and equals 0.5 at $[O_2] = 0.014$ mole/liter.

Charge transfer and electron capture were considered in a kinetic treatment but did not describe satisfactorily the observed enhancement.

When aqueous silver nitrate solutions were exposed to Co^{60} gamma rays, Po^{210} alpha particles, or 2537-A light, the silver ions were reduced to silver metal. Electron micrographs revealed that the metal crystal forms vary with the linear energy transfer of the incident radiations. Further modifications of the growth pattern may be effected by sweeping the solution during the irradiation with helium. Surface area measurements of the silver metal suggest that growth continues until the crystal precipitates by gravity. The radiolytically prepared metal does not have an extraordinarily high surface area.

The suppressive action of the reducible solute NO_3^- on the $G(H_2)$ was followed as a function of pH to determine the nature of the reducing species formed by the action of Co^{60} gamma rays on aqueous solutions. The postulated reducing species related as acid and conjugate base $e^-(aq) + H^+ \rightleftharpoons H$ are expected to react with NO_3^- at grossly different rates.

The suppression of the $G(H_2)$ was observed to be independent of pH, indicating that the major

reducing species was the same at pH = 1 and pH = 12.6. The $G(H_2)$ at 0 NO_3^- concentration, as determined by extrapolation of the experimental data, is about 5% greater at pH = 1 than at pH = 4.5 and 12.6. Higher $G(H_2)$ are consistent with the acid form, H atoms, having a slower reaction rate with NO_3^- than solvated electrons.

Some results from the radiolysis of dilute arsenite solutions are given. The G values for arsenate formation and hydrogen peroxide consumption in deaerated solutions are given in tabular form for neutral and 0.4 M sulfuric acid solutions. A discussion is presented of some reactions involving the hydrated electron and the hydrogen atom.

A comparison was made of the yields, and the effect of postirradiation annealing on these yields, for the decomposition of sodium chlorate by gamma rays and by alpha particles. The 100-ev yield, $G(Cl^-)$, for sodium chlorate irradiated with gamma rays at $25^\circ C$ was 1.50 ± 0.07 . Postirradiation annealing at $185^\circ C$ increased the yield to 1.92 ± 0.04 . The yield was still higher at 2.30 ± 0.04 for salt irradiated at $185^\circ C$. The yield of chloride for decomposition by alpha particles (3.3 Mev) at $25^\circ C$ was 2.12 ± 0.05 , about 40% higher than for gamma rays. Also, there was no effect of postirradiation annealing at $185^\circ C$. The results are consistent with the previous postulate that thermal effects in alpha-particle tracks are a significant factor in the radiolysis.

The radiolytic decomposition of the anhydrous alkaline earth bromates by Co^{60} gamma rays was found to increase with the atomic number of the cation from magnesium to barium. The bromate decomposition in all the salts increased less rapidly than linearly with the radiation dose up to about 4×10^{23} ev/mole. Bromine oxidation states intermediate between bromate and bromide were produced; the yield of these also was nonlinear with increasing dose. Initial radiolytic yields for bromate decomposition, $G_o(-BrO_3^-)$, were 1.75, 2.05, 2.79, and 3.02 molecules per 100 ev for $Mg(BrO_3)_2$, $Ca(BrO_3)_2$, $Sr(BrO_3)_2$, and $Ba(BrO_3)_2$, respectively. As a group the alkaline-earth bromates were more alike in their radiolytic instability than were the alkali-metal bromates reported last year.

The alpha radiolysis of a stoichiometric mixture of H_2 and O_2 admixed with CO_2 indicated: (1) CO_2 did not react chemically in this system; (2) about 60% of the energy absorbed by the CO_2 was

utilized in promoting the synthesis of water. A new kinetic expression was derived which is in good agreement with the experimental data.

Manometric and gas-chromatographic studies of the radiation-induced surface oxidation of hydrocarbons were continued and extended. Equations describing the kinetics of the postirradiation catalytic reaction were derived.

5. ORGANIC CHEMISTRY

It was found that the pinacol rearrangement of 2-*endo*-phenyl-2,3-*exo*-norbornanediol does not take place through a vinyl dehydration.

The study of small secondary isotope effects, using the differential method, was extended to several new carbonyl compounds. The primary isotope effect of C^{14} in the formation of 2,4-dinitrophenylhydrazones was found to be independent of the nature of the radical attached to the carbonyl group. A possible duality of mechanism appears to exist for the formation of hydrazones.

Irradiation of aroyl cyanides was found to produce benzils and cyanogen in two instances. Some nitriles proved to be resistant to radiation or to undergo dimerization.

Several important modifications made to the method for dry combustion of C^{14} compounds greatly increased the rate of combustion. Compounds doubly labeled with C^{14} and tritium yield carbon dioxide containing negligible tritium contamination. The effect of sample size was evaluated.

The acid-catalyzed reactions of 1,2,2-triphenylethanol and of 1,2,2-triphenylethyl acetate, labeled with deuterium and C^{14} , were studied. Isotope effects (k_H/k_D) of 2 to 2.3 during olefin formation, and of 1.1 during ester formation, were observed.

The irradiation of isophorone with ultraviolet light was found to produce several products, two of which were solid photodimers. The structures and stereochemical arrangements of the dimers were tentatively established.

The classical carbonium ion mechanism for the deamination of 1,2,2-triphenylethylamine and for the thermal decomposition of *N*-acetyl-*N*-nitroso-1,2,2-triphenylethylamine was supported by a mathematical analysis of the rate expressions for the reactions.

Pyrolysis of tributyl phosphate, dibutylphosphoric acid, monobutylphosphoric acid, barium dibutylphosphate, and barium monobutylphosphate produced mixtures of butenes. The extent of isomerization to *cis*- and *trans*-butene-2 varied with the acidity of the mixture being pyrolyzed. The composition of the butenes obtained from any of the above-mentioned starting materials differed from the thermodynamic equilibrium mixture.

The gas-chromatographic separation of a mixture of butene isomers and 1,3-butadiene was performed at 25°C using several high-boiling compounds (individually) supported on Celite. The most effective resolutions were obtained using aryl ethers modified by nitro or amine groups, aryl aldehydes and ethers, and an organic phosphorus compound. The butenes produced by pyrolysis of butyl phosphates were analyzed using a 13-ft column of *o*-nitrophenetole on Celite.

6. CHEMISTRY OF AQUEOUS SYSTEMS

The optical absorptions of hydrolyzed uranyl perchlorate solutions at 4300 Å, in conjunction with acidity measurements, were used to evaluate the formation quotients for the species $(UO_2)_2(OH)_2^{2+}$ and $(UO_2)_3(OH)_5^+$. The spectra over the wavelengths studied (3600 to 5000 Å) were shown to be consistent with the scheme postulating these as the major hydrolyzed species. From equilibrium ultracentrifugation, acidity measurements, and comparison of Raman spectra of solids and solutions, it appears that the major aggregated species formed on the addition of acid to molybdate solutions, up to $1\frac{1}{2}$ hydrogen ions per molybdate, are heptameric and octameric.

The second dissociation constant of deuterio-sulfuric acid was computed from 25 to 225°C from data on the solubility of Ag_2SO_4 in D_2SO_4 solutions. In addition, the thermodynamic constants for the reaction $DSO_4^- = D^+ + SO_4^{2-}$ are presented. A comparison with the corresponding values for the H_2SO_4 system is given.

The activity coefficient of HBr in HBr-KBr mixtures was studied to 150°C. At constant temperature and ionic strength the logarithm of the activity coefficient of HBr in the mixtures varies linearly with the molality of KBr. With the parameters describing this variation it is possible to calculate the activity coefficient of the KBr in the

mixtures. It was found that the activity coefficient of KBr varies less with changing ionic strength and temperature than does the activity coefficient of HBr in the same mixtures.

The activity coefficients of HCl and NaCl in HCl-NaCl mixtures were computed from literature data. The calculations are based on the observation that at constant ionic strength and temperature the logarithm of the activity coefficient of HCl in HCl-NaCl mixtures varies linearly with NaCl concentration.

Cryostat and cooling controls were incorporated in a redesigned spectrophotometer chamber and cell assembly. The range of automatic control of both sample and reference cells is now from at least -70 to 280°C .

The thermal stability (25 to 250°C) and absorbance in the wavelength range 0.2 to $2.0\ \mu$ of HNO_3 (0.07 to $4.0\ f$), H_2SO_4 (0.1 to $0.4\ f$), and DClO_4 (0.01 to $1.0\ f$) respectively, were investigated with the use of titanium cells with sapphire windows. Each of the acids reacts measurably with both of these materials at rates which increase with acidity and temperature. However, the acids are essentially transparent solvents for the spectrophotometry of inorganic ions up to at least 250°C in the indicated concentration and spectral ranges: HNO_3 (0 to $1.0\ f$; 0.6 to $1.2\ \mu$), H_2SO_4 (0 to $0.2\ f$; 0.25 to $1.2\ \mu$), and DClO_4 (0 to $1.0\ f$; 0.25 to $1.8\ \mu$).

A survey was completed of the cation exchange behavior of the elements in HCl and HClO_4 solutions with special emphasis on the high ionic strength range. The data are summarized as plots of $\log D_v$ vs molarity of acid in two Periodic Tables.

Another survey was completed of the cation exchange behavior of the elements in $8.5\ M\ \text{HClO}_4$ – $0.5\ M\ \text{HCl}$ – $0.1\ M\ \text{HF}$, a medium found particularly useful for major group separations. A table of distribution coefficients for this medium at 25 , 50 , and 75°C is given.

The ion exchange behavior of approximately 15 elements in citrate media has been examined in detail and techniques developed for group separations.

In continuing studies with inorganic ion exchangers and adsorbents, zirconium antimonate was found to have extremely high selectivity for strontium, rare-earth oxides were shown to have anion exchange properties, and heavy-metal sulfides were found to be remarkably fast materials for chromatographic applications.

The symmetrical quaternary ammonium halides present an opportunity for studying the effect of cation size on electrolyte behavior in aqueous solution. Osmotic and activity coefficients, measured by the gravimetric isopiestic vapor pressure technique, are reported for tetramethyl-, tetraethyl-, tetrapropyl-, and tetrabutylammonium chlorides, bromides, and iodides.

For concentrations below $1\ m$ the osmotic coefficients for the chlorides increase with the size of the cation: $\text{Bu}_4\text{N}^+ > \text{Pr}_4\text{N}^+ > \text{Et}_4\text{N}^+ > \text{Me}_4\text{N}^+$. The bromides and iodides, however, show the reverse order. At higher concentration the osmotic coefficients of the larger cation salts decrease sharply and some of these sequences are reversed.

This behavior is explained as the result of three effects: The order of the osmotic coefficients of the chlorides in dilute solution is due to the ability of large organic cations to enforce the water structure, and the more carbon atoms on an ion, the larger this effect will be. The strong ion association of the bromide and iodide salts overshadows the "structure making" ability of these cations, giving rise to the opposite order in the osmotic coefficients. At higher concentrations the tetrapropyl- and tetrabutylammonium salts form micelles, and hence a sharp lowering of the osmotic coefficients is observed.

7. ELECTROCHEMICAL KINETICS AND ITS APPLICATION TO CORROSION

Aqueous ions were found to enter into ion exchange with chromate ions bound by the film on passive iron and steel. The kinetics of the process was investigated with various systems and at temperatures from 24 to 77.5°C .

The dissolution of crystal-bar zirconium in aqueous solutions containing HF and H_2SO_4 was investigated by means of electrochemical techniques. Capacities were determined by measuring the initial slope of the voltage-time curve resulting from the application of galvanostatic pulses. Steady-state polarization curves were obtained potentiostatically whenever possible, and galvanostatic polarization curves were determined by a pulse technique. The data are explained by assuming that the dissolution reaction involves the continuous formation and dissolution

of a film on the surface of the metal. The conventional anodizing equation describes the formation of the film, and the dissolution reaction is controlled by the rate of mass transfer of undissociated HF to the surface of the film.

A comparative study of the electrochemical behavior of active iron electrodes in deoxygenated acidic sulfate and benzoate solutions was made. In sulfate solutions, the pH and potential dependencies of the iron dissolution and hydrogen evolution reactions were determined. These results served as a basis for the interpretation of the complex polarization phenomena observed in the benzoate solutions, where a potential-dependent specific adsorption of the benzoate ion is accompanied by an increase in rate of the hydrogen evolution reaction and a decrease in the rate of iron dissolution.

8. NONAQUEOUS SYSTEMS AT HIGH TEMPERATURE

The heats of fusion and the heat capacities of the solids and liquids in the vicinity of the melting points were determined for a number of rare-earth trihalides, including the trichlorides and tribromides of lanthanum, praseodymium, neodymium, and gadolinium, the triiodides of cerium and praseodymium, and the trichlorides of holmium and erbium.

In measurements of the heat content of strontium chloride from 298 to 1200°K, a second-order transition was observed near 1000°K, which is ascribed to the occurrence of disorder in either the anion or cation lattice.

Solutions of lanthanum, praseodymium, and neodymium metals in their molten tribromides were found to exhibit similar behavior to solutions in the trichlorides and triiodides, namely, gradually decreasing conductance by the metal solute, that is, increasing stability of the M^{2+} ion, in going from lanthanum to neodymium. Solutions of gadolinium, dysprosium, holmium, and erbium in their molten trichlorides behave irregularly both in regard to solubility and electrical conductance.

A maximum in conductivity near 50 mole % MX_2 dissolved in MX_3 , similar to that in the NdI_3-NdI_2 system, was found for $NdBr_3-NdBr_2$. Merely positive deviation from additivity occurs in $DyCl_3-DyCl_2$ as it does in $NdCl_3-NdCl_2$. This and the

absence of the effect in $NdCl_3-SrCl_2$ and NdI_3-SrI_2 support an earlier explanation based on electron exchange between adjacent oxidation states ($Nd^{3+}-Nd^{2+}$, $Dy^{3+}-Dy^{2+}$).

9. CHEMICAL PHYSICS

Parameters are reported for an axially symmetric spectrum in gamma-irradiated KNO_3 , and the spectrum is identified with NO_3 . This species is produced in high yield by short intense irradiations at 77°K. The spectrum disappears in about 2 hr at 77°K.

A paramagnetic species in irradiated single crystals of dimethylglyoxime was identified as a ground-state triplet. Measurements of both the allowed and the forbidden spectrum are well under way. Hyperfine structure from two equivalently or nearly equivalently coupled nitrogen atoms is present.

Parameters of a previously reported spectrum which is stable at room temperature were remeasured with increased accuracy.

Five distinct paramagnetic resonance spectra were observed in single crystals of hydrogen peroxide after photolysis with uv. Measurements were made on a species formed in high yield upon photolysis at 64°K. This species is not stable at 77°K. Of two species formed in small yield, one has an extremely large anisotropy in g and the other is clearly a triplet-state species.

A neutron-diffraction study of single crystals of XeF_2 and XeF_4 gave accurate parameters for their molecular spacings. Anisotropic thermal analysis indicated similar libratory motion of the molecular species in these molecular crystals.

The crystal and molecular structure of the important biochemical compound sucrose ($C_{12}H_{22}O_{11}$) has been determined in what appears to be the largest neutron-diffraction problem ever undertaken, with precision that compares favorably with that attainable in the best x-ray studies of complex molecules. All hydrogen atoms have been located. Distances C-C are 1.514 to 1.536 Å; C-O, 1.408 to 1.443 Å; C-H, 1.087 to 1.107 Å; O-H, 0.951 to 0.976 Å. The conformation of the furanose ring differs from that known to exist in sucrose $\cdot NaBr \cdot 2H_2O$. Hydrogen bonds (two of them intramolecular) utilize every hydroxyl group except one.

Some programs for the IBM 7090 computer have been written as needed in the structure analyses of chloral hydrate and sucrose to carry out the following calculations: averaging of intensity or F^2 data; producing data for extinction plots for detection of residual extinction errors; calculating approximate coordinates of hydrogen atoms; computing composite three-dimensional Fourier maps; preparing the type of structure-factor table often presented in crystallographic papers.

The crystalline phase reported elsewhere as a "high-density form of XeF_4 " is shown, by crystal structure analysis, to be a distinct compound with the composition $\text{XeF}_2 \cdot \text{XeF}_4$. There are no close contacts between molecules in this crystal such as to indicate molecular association; instead all intermolecular, as well as intramolecular, distances are comparable with those in crystals of the two components. Thus, it seems appropriate to describe this as a molecular addition compound.

Work on the structure of aqueous solutions, molten salts, and powders by x-ray diffraction continued. Initial attempts to describe the x-ray scattering from molten CsCl in terms of a model were made. A study of the structure of the cubic phase of CaC_2 , stable above 450°C , is nearly complete, and the results strongly favor a pyrite arrangement disordered with respect to the orientation of the C_2 anions. A study of the structure of aqueous NH_4F solutions is currently in progress.

There are four anomalies in the heat capacity data on K_2ReCl_6 . The lowest anomaly occurs at 11.9°K and is associated with an antiferromagnetic transition, whereas the anomalies at 76 , 103 , and 111°K are related to structural changes. A neutron study was made on powder and single-crystal specimens at 4.2 , 77°K , and room temperature, with a limited amount of data collected at intermediate temperatures. The space group at room temperature is $Fm\bar{3}m$, but below 76°K it is $Pn\bar{3}$ or $Pn\bar{3}m$, which requires the ReCl_6^{2-} ion to be trigonally distorted from octahedral symmetry. The room-temperature data were also interpreted in terms of a trigonal distortion but statistically disordered about the octahedral positions. Also, anomalies in the thermal expansion coefficients were observed accompanying the heat capacity anomalies in the liquid-nitrogen region.

A commercially available Polaroid film holder was extensively modified for use in x-ray and

neutron diffraction. Exposure times for routine x-ray precession alignment photographs are often as short as 1 min and seldom more than 5 min with only 10 sec development time.

An anomaly near 15°K resembling a Schottky anomaly was observed in the heat capacity of ReCl_3 . The anomaly is discussed in relation to the magnetic susceptibility. The data give $29.59 \text{ cal deg}^{-1} (\text{mole ReCl}_3)^{-1}$ for the entropy at 298.15°K .

A new detector incorporating a magnetic filter for separating atoms from molecules was added to the molecular beam apparatus.

The study of interactions between gases and surfaces was continued with an improved apparatus.

Special use was made of mass spectrometry to obtain data on ions that result as the direct consequence of nuclear decay. From these data information was obtained on (1) the angular correlation in beta decay between the β^- particle and the neutrino, (2) the extent of electron shakeoff as the result of a sudden change in nuclear charge, and (3) the nature of molecular fragmentation following nuclear decay.

10. WATER RESEARCH PROGRAM

As part of the water research program, carried out at the Oak Ridge National Laboratory under an Inter-Agency Agreement between the Department of Interior (Office of Saline Water) and the AEC, work was carried out on thermodynamic and transport properties of solutions, membranes, and ion exchangers, on electrode kinetics of porous conducting materials, and on the electrochemistry of corrosion.

As part of this work, it was shown that special glass electrodes, in conjunction with Ag/AgCl electrodes, can be used for determination of activity coefficients of salts in aqueous media and mixed water-organic solvents. Activity coefficients of HBr and KBr in their mixtures were determined; their logarithm varies linearly with composition at constant ionic strength. Activity coefficients of NaCl in HCl - NaCl mixtures were computed from literature data. The dissociation constant of DSO_4^- was evaluated and compared with that of HSO_4^- . The activity coefficients of salts, particularly NaCl , were determined in a

large number of water-organic mixtures over a broad composition range. Most of these measurements were carried out with saturated salt solutions. Some were established through distribution coefficient measurements. Ion exchange studies with conventional organic and new inorganic ion exchange materials were carried out. An excellent method of separation of calcium from magnesium, using cation exchange at high ionic strength, was developed. The adsorptive properties of a variety of sulfides were investigated. Work was initiated on hyperfiltration studies of various types of membranes; suitable equipment was assembled. A special ion exchange membrane was developed and tested; it combines good salt rejection properties with reasonable flow rates.

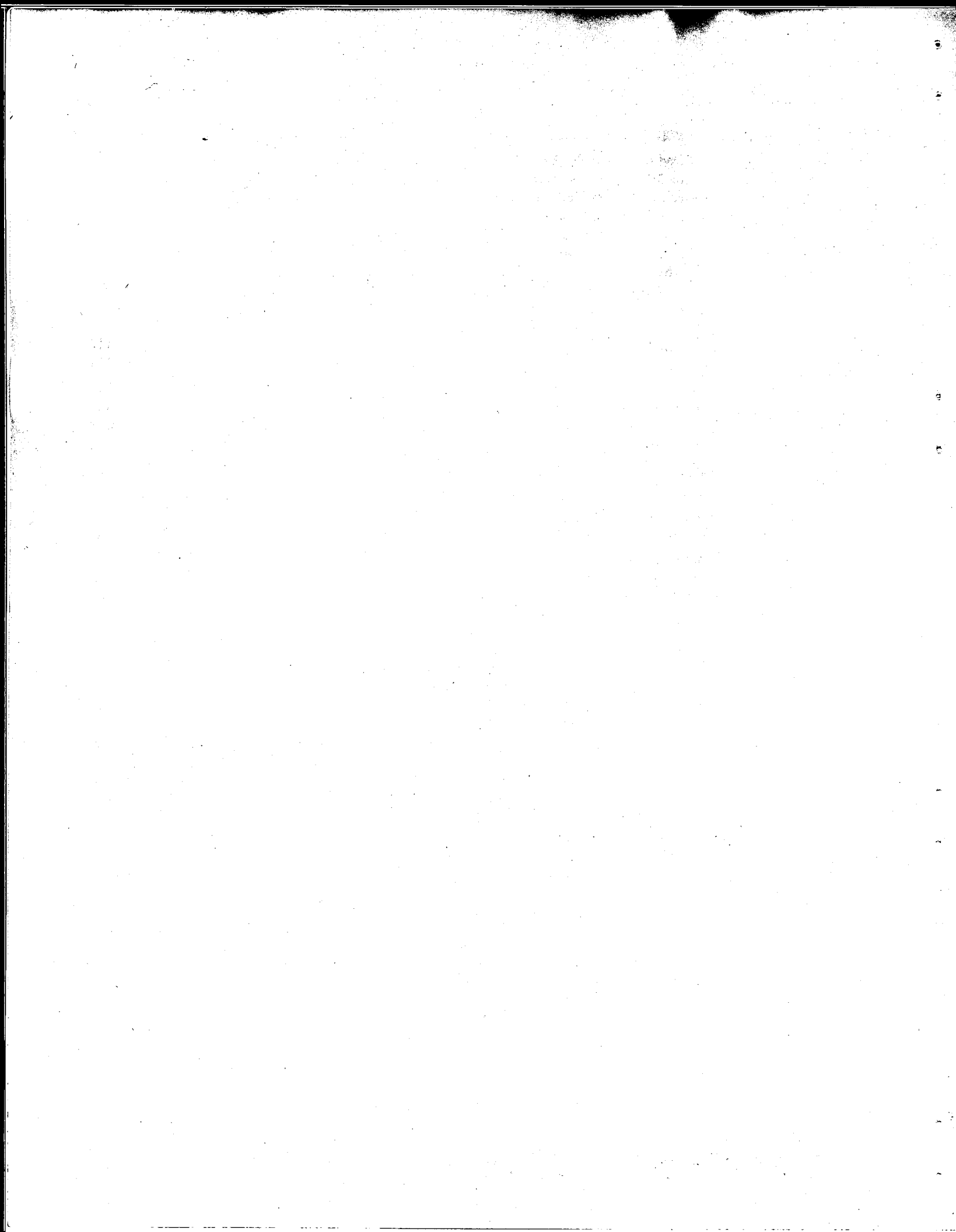
A comprehensive theory of Faradaic processes in porous conducting electrodes was developed and measurements carried out on the Fe(II)-Fe(III) system in a variety of media. The electrochemistry of corrosion of polycrystalline zone-refined iron was investigated in chloride solutions as a function of temperature, acidity, and chloride ion concentration. Corrosion was relatively insensitive to salt concentration at all temperatures and acidities studied. An electrochemical pH-stat was developed which automatically controls the acidity of unbuffered solutions in the range pH 3 to 11. This pH-stat can also be used to directly measure rates of corrosion and in some instances can be applied to evaluation of acid constants of ions.

Contents

SUMMARY	iii
1. NUCLEAR CHEMISTRY	1
Isomeric Transitions in Ce ¹³⁵ and Ba ¹³¹	1
Nuclear Energy-Level Studies Using Inelastic Proton Scattering	2
Spectroscopy of Delayed Neutrons: N ¹⁷	4
Gamma-Gamma Angular Correlation in V ⁵¹	7
Independent Fission Yield of Sb ¹²⁷	8
An Upper Limit for the Thermal Neutron Cross Section of Nb ⁹⁵	9
Half-Life of Bi ²⁰⁸	10
Effective Cutoff Energies for Cadmium, Gadolinium, Samarium, and Boron Filters	11
Thermal Neutron Cross Section and Resonance Integral of I ¹³¹	15
Neutron-Capture Cross Section of 36-hr Rh ¹⁰⁵	16
2. ISOLATION AND CHEMICAL PROPERTIES OF SYNTHETIC ELEMENTS	18
Chemistry of Technetium	18
Structure of the Aqueous Pertechnetate Ion	18
3. CHEMICAL SEPARATION OF ISOTOPES	21
Ion Exchange Studies in Nonaqueous Solvents	21
Lithium Isotope Separation Factors by Ion Exchange in Concentrated Solutions	22
Anhydrous LiSCN	22
Isotopic Chemistry of Boron	23
Nitrogen Isotopic Separation Factors Between Selected Pairs of NO ₃ ⁻ , NO ₂ ⁻ , and NO	24
Isotope Kinetic Effect in the Thermal Decomposition of Diazo Compounds	26
Isotope Effect in the Acid Reduction of Nitrate and Hydroxylamine	26
Isotope Effect in the Alkaline Reduction of Nitrate, Nitrite, and Hydroxylamine	27
Alkali Metal Separation	28
Preparation of Beryllium Amalgam	28
Fluorine-19 NMR Spectra of Xenon Fluorides	28
NMR Studies of BF ₃ Addition Compounds	29
Isotopic Mass Spectral Program	32
Raman and Infrared Spectral Studies	33
Oxygen-17 Enrichment	41
4. RADIATION CHEMISTRY	42
Radiolysis of Liquid Oxygen and Oxygen-Nitrogen at 77°K	42
Radiolytic and Photolytic Reduction of Aqueous Silver Nitrate Solutions	43
Primary Reducing Species in the Co ⁶⁰ Radiolysis of Aqueous NaNO ₃ Solutions	45
Radiolysis of Arsenite Solutions	47

Radiation Decomposition of Sodium Chlorate; Comparison of Yields and the Postirradiation Annealing Behavior for Irradiation by Gamma Rays and Alpha Particles	48
Radiolysis of Alkaline-Earth Bromates by Co^{60} Gamma Rays	48
Alpha-Particle-Induced Synthesis of Water in the Presence of CO_2	49
Radiation-Induced Surface Oxidation of Hydrocarbons	51
Postirradiation Reaction Kinetics	53
5. ORGANIC CHEMISTRY	55
Pinacol Rearrangement of 2- <i>endo</i> -Phenyl-2,3- <i>exo</i> -norbornanediol	55
Primary and Secondary Carbon-14 and Deuterium Isotope Effects	55
Coupling of Aroyl Cyanides in Photochemical Reactions	56
Method for the Rapid Combustion and Assay of C^{14} Compounds	57
Carbon-14 and Deuterium Equilibration in the 1,2,2-Triphenylethyl System	57
Photochemical Dimerization of Isophorone	59
Mechanism of the Deamination Reaction	59
Pyrolysis of Butyl Phosphate Esters and Salts	61
Separation of Butene Isomers and Butadiene by Gas-Liquid Chromatography	62
6. CHEMISTRY OF AQUEOUS SYSTEMS	65
Hydrolysis of Metal Ions	65
Second Dissociation Constant of Deuteriosulfuric Acid from 25 to 225°C	68
Activity Coefficient of HBr in HBr-KBr Mixtures	70
Activity Coefficients of Hydrochloric Acid and Sodium Chloride in Hydrochloric Acid-Sodium Chloride Mixtures	74
Inorganic and Physical Chemistry: Spectrophotometry of Solutions at High Temperatures and Pressures	78
An Improved High-Temperature Aqueous Spectrophotometric Cell Assembly	78
Spectrophotometry of Aqueous HNO_3 , H_2SO_4 , and DClO_4	78
Ion Exchange Studies	82
Ion Exchange in Concentrated HCl and HClO_4	82
Development of an Ion Exchange Separation Scheme	84
Adsorption on Inorganic Materials	84
Physical Chemistry of Ion Exchangers	88
Osmotic and Activity Coefficients of Some Quaternary Ammonium Halides in Aqueous Solution at 25°C	88
7. ELECTROCHEMICAL KINETICS AND ITS APPLICATION TO CORROSION	91
The Electrochemistry of the Dissolution of Zirconium in Aqueous Solutions of Hydrofluoric Acid	91
Ion Exchange Properties of the Passive Film on Iron and Steel	93
Electrochemical Behavior of the Active Iron Electrode	93
8. NONAQUEOUS SYSTEMS AT HIGH TEMPERATURE	96
The Electrical Conductivity of Solutions of Metals in Their Molten Halides	96
The Heats of Fusion of Some Rare-Earth-Metal Halides	99
The Heat Content and Entropy of Strontium Chloride from 298 to 1200°K	100

9. CHEMICAL PHYSICS	102
Microwave and Radio-Frequency Spectroscopy	102
Paramagnetic Resonance Study of NO_3 in Irradiated KNO_3	102
Paramagnetic Resonance Study of Irradiated Dimethylglyoxime	102
Paramagnetic Resonance Study of Photolyzed Hydrogen Peroxide	103
Neutron Diffraction Structural Chemistry	105
Neutron-Diffraction Studies of Two Xenon Fluoride Compounds, XeF_2 and XeF_4	105
Sucrose: Precise Determination of Crystal and Molecular Structure by Neutron Diffraction	108
Miscellaneous Computer Programs for Crystallography	111
Edit Program for Crystallographic Data	112
The Crystal Structure of the Molecular Addition Compound Xenon Difluoride-Xenon Tetrafluoride	112
X-Ray Diffraction Studies of Molten Salts, Powders, and Aqueous Solutions	114
Modified Polaroid Film Holder for X-Ray and Neutron Diffraction	116
Neutron Study of K_2ReCl_6 at 4.2°K, 77°K, and Room Temperature	118
Calorimetry	119
Low-Temperature Heat Capacity of Rhenium Trichloride	119
Molecular Beam Studies	121
Reactions of Alkali Metals	121
Interactions of Gases and Surfaces	121
Mass Spectrometry	122
Two-Stage Mass Spectrometer	122
Charge Spectrometry	122
10. WATER RESEARCH PROGRAM	123
Measurement of Activities of Salts by EMF Methods	123
Activity Coefficients of HBr and KBr in HBr-KBr Mixtures	124
Activity Coefficients of HCl and NaCl in HCl-NaCl Mixtures	124
Dissociation Constant of HSO_4^- and DSO_4^-	124
Solubility and Activity Coefficients of Salts in Water-Organic Mixtures	125
Ion Exchange	125
Hyperfiltration Studies of Membranes	126
Electrode Kinetics of Porous Conducting Electrodes	127
Electrochemical Studies of Corrosion of Iron	127
Development and Use of an Electrochemical pH-Stat	128
PUBLICATIONS	129
PARTICIPATION IN COLLEGE INSTRUCTION	134
PAPERS PRESENTED AT SCIENTIFIC AND TECHNICAL MEETINGS	135



1. Nuclear Chemistry

Isomeric Transitions in Ce^{135} and Ba^{131}

A. R. Brosi B. H. Ketelle

The probable existence of an unreported isomeric transition in Ce^{135} could be postulated on the basis of the energy-level systematics of nuclides with vacancies in the 82-neutron shell. A detailed study of the radiations of Ce^{135} produced by a proton bombardment of Ce^{136} gave no evidence of an isomeric state in Ce^{135} . Bombardment of Ce^{136} with epicalcium neutrons in the ORR gave high yields of interfering n, γ products. For instance, the yield of 9-hr Ce^{137} in disintegrations per min per mg of Ce^{136} at saturation was 10^4 times the yield of 55-sec Ce^{139m} in disintegrations per min per mg of Ce^{140} . In order to reduce the yield of n, γ products, bombardments were made with 14-Mev neutrons produced by a d, t reaction. Evidence for a 20-sec decay period was found which further work showed to be the Ce^{135} isomeric transition. A scintillation counter spectrum of the gamma radiation associated with the 20-sec period is shown in Fig. 1.1. The Compton distribution of the 740-kev gamma ray of 55-sec Ce^{139m} produced by an $n, 2n$ reaction on Ce^{140} in the target has not been subtracted from the curve in Fig. 1.1. In addition to x rays, gamma-ray peaks with energies of 83, 153, 213, and 296 kev are shown. Measurements at three different geometries indicate that most of the

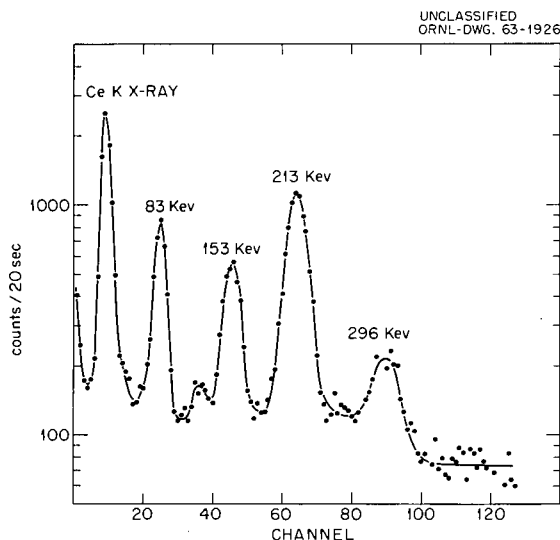


Fig. 1.1. Gamma Spectrum of 20-sec Ce^{135m} .

events in the peak at 296 kev result from coincidences. All these radiations decay with a half-life of 20 ± 1 sec.

The assignment of this decay period to Ce^{135} is supported by the fact that the 83-, 213-, and 296-kev radiations are emitted in the decay of Pr^{135} . In addition, bombardments of CeO_2 with two different enrichments of Ce^{136} resulted in yields of the 20-sec activity shown in Table 1.1. The gamma-ray disintegrations observed in the

Table 1.1. Yields of 213-kev Gamma Rays in Disintegrations per 20 sec per mg of Isotope

Sample	Yield			
	Ce^{136}	Ce^{138}	Ce^{140}	Ce^{142}
30% Ce^{136}	2440 ± 68	$104,000 \pm 2900$	1140 ± 32	$17,800 \pm 500$
8.0% Ce^{136}	2410 ± 120	$48,200 \pm 2350$	233 ± 11	2.090 ± 103

two bombardments are computed per milligram of each of the cerium isotopes present. It can be seen that the yields are consistent only with the assumption of production by a reaction of Ce^{136} . The yields observed were consistent with the cross section expected for an $n,2n$ reaction on a cerium isotope and not with the cross sections expected for n, p or n, α reactions.

The x rays emitted in the 20-sec transition were shown to be cerium x rays by measurement of the spectrum observed in a xenon-filled proportional-counter spectrometer. The x rays of elements in the rare-earth region with adjacent atomic numbers are readily resolved and identified with this spectrometer.

Since the 153-keV gamma ray is observed in the decay of the 20-sec transition and not in the decay of Pr^{135} , it may be assumed that it is emitted in the transition from the metastable level of Ce^{135} . On the basis of this assumption, a tentative decay scheme can be postulated, and conversion coefficients can be computed. These lead to the spin assignments shown in Fig. 1.2. Although further work should be done, present evidence indicates that Ce^{135m} decays by an $E3$ transition and not an $M4$ transition as in the case of Ce^{137m} and Ce^{139m} .

After the successful production of Ce^{135m} , bombardments of Ba^{130} and Ba^{132} with 14-MeV neutrons were made to produce the unknown Ba^{129} and Ba^{131} isomers. The results with Ba^{130} were not definitive, but with Ba^{132} a 14.5-min period was produced. Bombardment of $\text{Ba}(\text{NO}_3)_2$ with two different isotopic enrichments showed that yields were proportional to the amount of Ba^{132} . Xenon-filled proportional-counter-spectrometer measurements showed that the x rays were those of barium.

After these measurements were completed it was learned that 14.5-min Ba^{131m} had been made several months earlier by Tilbury and Yaffee by the reaction $\text{Cs}^{133}(p,3n)\text{Ba}^{131m}$. The work reported here corroborates their results.

Nuclear Energy-Level Studies Using Inelastic Proton Scattering

F. Perey¹ R. J. Silva
G. R. Satchler²

The energy spectra of protons inelastically scattered from targets of Ni^{62} , Ni^{64} , Cu^{63} , and Cu^{65} were obtained as a function of angle by use of an 11-MeV proton beam from the ORNL tandem Van de Graaff and surface-barrier silicon detectors. The overall resolution of the detection system, including target thickness, was about 40 keV fwhm. Typical energy spectra are shown in Fig. 1.3.

In addition to a search for previously unreported energy levels, an attempt is being made to interpret some of the energy levels of the odd- A nuclei on the basis of the "excited-core" model.³ The model predicts a multiplet for the first four excited states of Cu^{63} with spins and parities $\frac{1}{2}^-$, $\frac{3}{2}^-$, $\frac{5}{2}^-$, and $\frac{7}{2}^-$. In addition, each level should be excited with a relative intensity of $2I + 1$ and have an angular distribution similar in shape to that observed for inelastic scattering from the 2^+ level of Ni^{62} ($I = 2$). Because it has the same spin and parity as the ground state, the $\frac{3}{2}^-$ member of the multiplet would be expected to be out of the order given above (higher in energy than expected) and to be excited with less relative intensity than expected due to admixing of the two wave functions.

The experimental angular distributions obtained for the first five excited states of Cu^{63} and the 2^+ level of Ni^{62} are shown in Fig. 1.4. The angular distribution expected for an angular momentum transfer of 2 given by a distorted-wave Born calculation is also shown in Fig. 1.4. From this analysis, the 1.327- and 1.412-MeV levels of Cu^{63} have been assigned spins and parities of $\frac{7}{2}^-$ and $\frac{3}{2}^-$ respectively.⁴ A similar analysis of

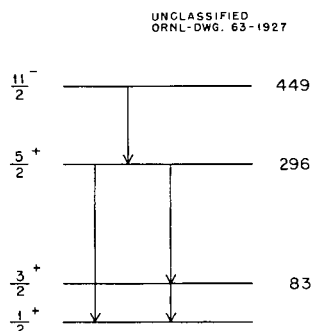


Fig. 1.2. Tentative Decay Scheme of Ce^{135m} .

¹Neutron Physics Division.

²Physics Division.

³A. DeShalit, *Phys. Rev.* **122**, 1530 (1961); A. Bronstein and A. DeShalit, *Phys. Letters* **1**, 264 (1962).

⁴F. Perey, R. J. Silva, and G. R. Satchler, *Phys. Letters* **4**, 25 (1963).

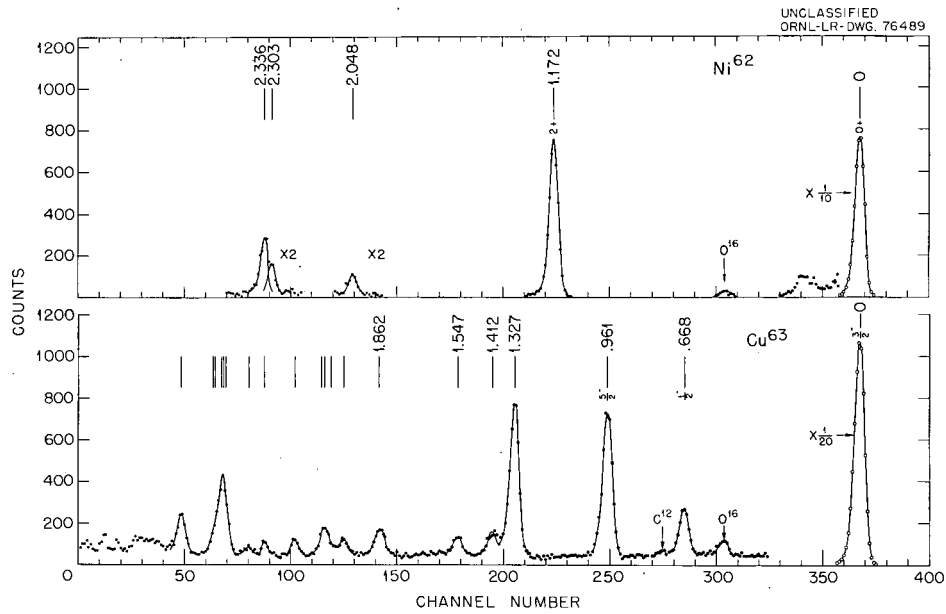


Fig. 1.3. Pulse-Height Spectra of Scattered 11-Mev Protons. The energy levels shown were taken from *Nuclear Data Sheets*.

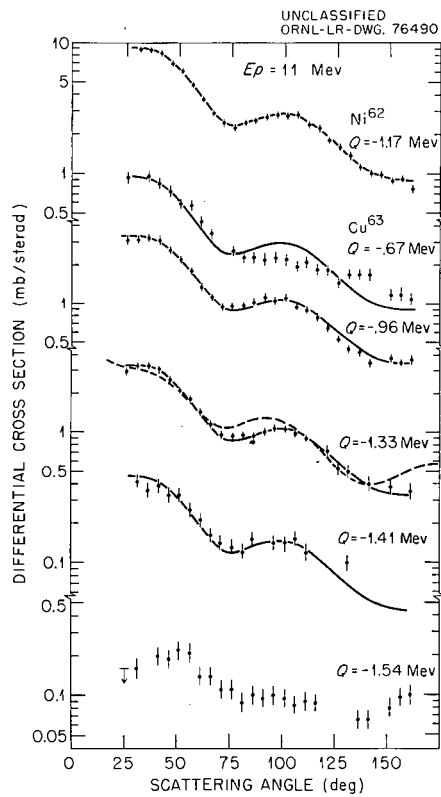


Fig. 1.4. Angular Distribution of Inelastically Scattered Protons to the First 2^+ State of Ni^{62} and the First Five Excited States in Cu^{63} . The full curves are the shape of the Ni^{62} angular distribution. The dashed curve is the result of preliminary distorted-wave Born calculation with angular momentum transfer of 2.

scattering data obtained from Ni^{64} and Cu^{65} is being carried out.

An analysis of the inelastic scattering data obtained for higher excited states of these four nuclides is in progress as well as more extensive and detailed distorted-wave Born calculations.

Spectroscopy of Delayed Neutrons: N^{175}

J. Gilat⁶ G. D. O'Kelley
E. Eichler

As part of a program to investigate the process of delayed-neutron emission, 4.1-sec N^{17} has been studied by time-of-flight and scintillation spectrometry. The term "delayed neutron" is a misnomer, because the rate-determining step in the process

is the beta transition to excited states of the daughter nucleus which lie above the neutron binding energy. These states promptly deexcite by neutron emission, since particle emission is highly favored over electromagnetic radiation. This time coincidence between the excitation of an energy level and its decay by neutron emission is the basis of our time-of-flight neutron spectrometry of N^{17} .

The experimental method is sketched in Fig. 1.5. A beta-ray event was detected in a plastic scintillator and thus announced the emission of a neutron. The neutron traversed a path of 50 or

⁵Abstract published in *Bull. Am. Phys. Soc.* 8(2), 320 (1963).

⁶Visiting scientist from the Israel Atomic Energy Commission/Laboratories, Rehovot, Israel.

UNCLASSIFIED
ORNL-DWG. 63-1929

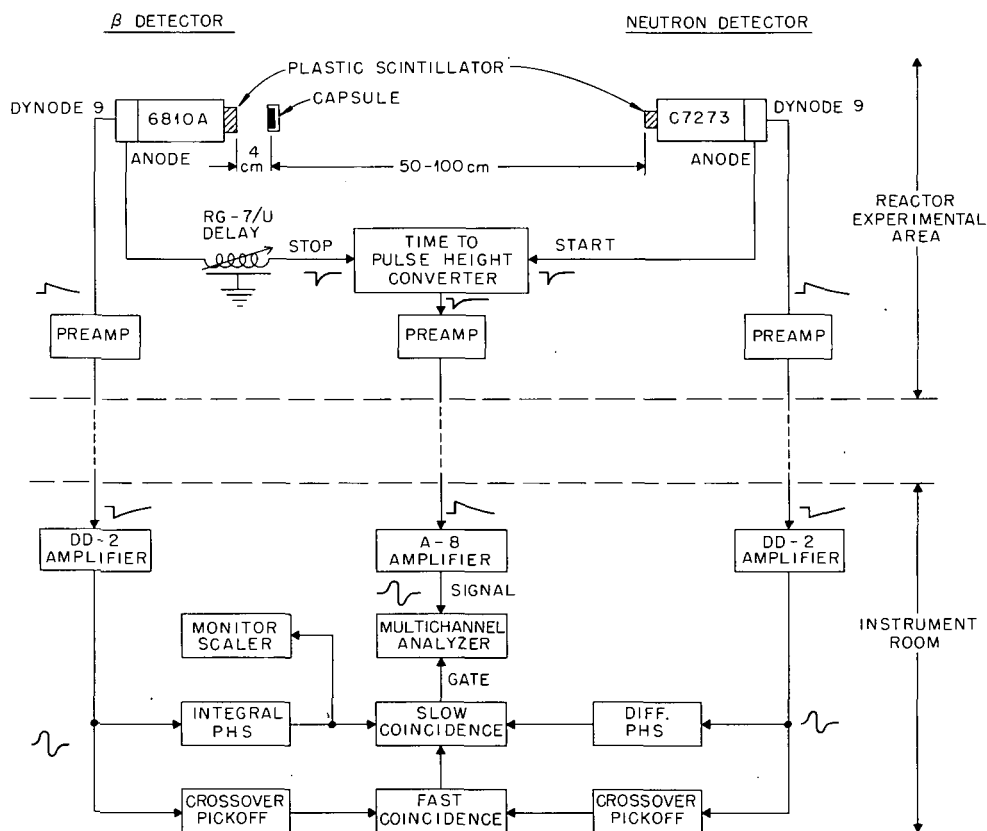


Fig. 1.5. Experimental Arrangement for Determination of Delayed-Neutron Energies by Time-of-Flight. The multichannel analyzer is gated to record only those events for which the beta detector pulses exceed the level set by the integral pulse-height selector and the neutron detector pulses fall within the upper and lower limits of the differential pulse-height selector.

100 cm and then was detected by its proton recoil in another plastic scintillator. The time interval between the beta and neutron events was converted to pulse-height information by use of a modified Neiler-type time-to-height converter.⁷ Because the method is basically a beta-neutron coincidence experiment, beta-ray spectra could be obtained in coincidence with selected neutron energy groups by a simple rearrangement of the electronic system.

Sources of 4.1-sec N^{17} were prepared in the ORNL Graphite Reactor by neutron irradiation of the chemical compound Li_3N^{15} , which served the combined functions of triton source and target. The tritons produced by the reaction $Li^6(n, \alpha)H^3$ irradiated the N^{15} nuclei, causing the reaction $N^{15}(t, p)N^{17}$ to occur. A fast pneumatic tube transported the sample into the reactor for an 8-sec irradiation, ejected the capsule, paused 5 sec, recorded an 8-sec count, and then recycled automatically. Several thousand irradiation cycles were required in a typical experiment. The 5-sec delay permitted a shorter-lived component (believed to be 0.85-sec Li^8) to decay to an acceptable level.

⁷J. H. Neiler and W. M. Good, p 509 in *Fast Neutron Physics*, ed. by J. B. Marion and J. L. Fowler, Interscience, New York, 1960.

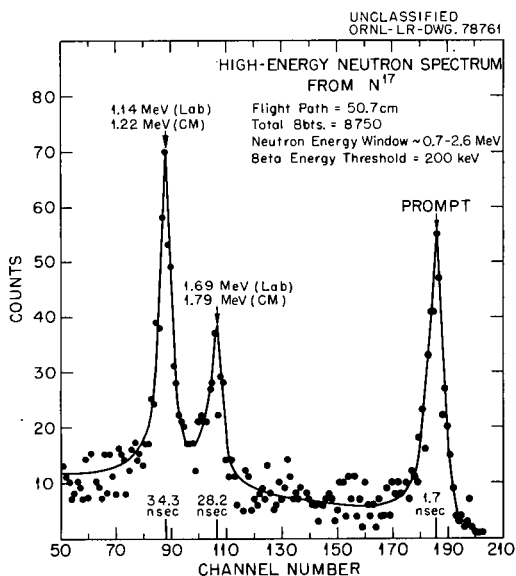


Fig. 1.6. High-Energy Portion of the Neutron Time-of-Flight Spectrum from N^{17} . Settings for the neutron and beta pulse-height selectors were chosen to favor the highest-energy neutrons.

The time-of-flight spectrum of Fig. 1.6 is typical of those obtained when the pulse-height selectors on the beta and neutron pulse amplifiers were set to emphasize the high-energy part of the neutron spectrum. In Fig. 1.7, the energy requirements favored the low-energy portion. Best values for the center-of-mass energies in Mev (and intensities) of the three neutron groups observed were 0.406 ± 0.015 (45%), 1.22 ± 0.02 (45%), and 1.79 ± 0.03 (5%). Perlow *et al.*⁸ found neutron groups at 0.426 and 1.22 Mev by use of a proportional-counter recoil spectrometer. The relative intensities of the neutron groups were corrected for the variation in neutron-detector efficiency with energy by calibrations with pulsed monoenergetic neutrons from the $H^3(p, n)He^3$ reaction on the ORNL 2.5-Mev Van de Graaff accelerator. Absolute intensities were calculated by combining the relative intensities with absolute values obtained

⁸G. J. Perlow *et al.*, *Phys. Rev.* **122**, 899 (1961).

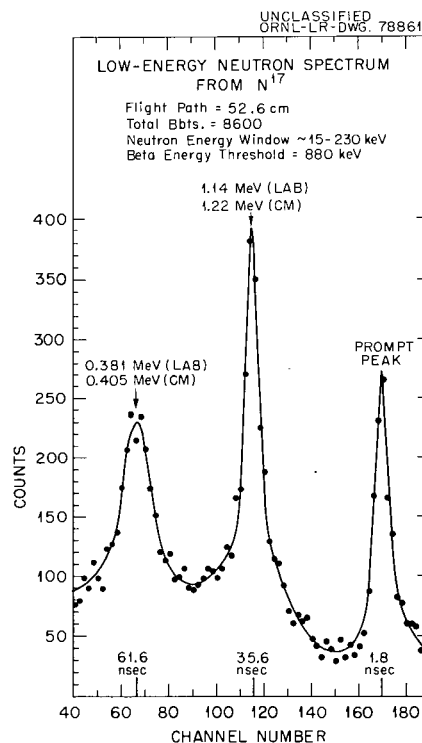


Fig. 1.7. A Neutron Spectrum of N^{17} with the Neutron and Beta Pulse-Height Selectors Adjusted for Best Sensitivity to the Low-Energy Neutron Group.

by Hopkins and Silbert⁹ for the N^{17} beta branching to the first three states in O^{17} .

The energy of the beta-ray group in coincidence with 1.22-Mev neutrons was measured as 3.23 ± 0.09 Mev, in agreement with the 3.30 Mev expected from nuclear reaction data¹⁰ (see Fig. 1.8). Although in this situation the beta energies can be computed from the known level scheme, in the case of a poorly understood scheme our method could measure the beta energies by coincidence

⁹J. C. Hopkins and M. G. Silbert, private communication; abstract submitted for presentation at the American Physical Society Meeting, Edmonton, Alberta, Aug. 28-30, 1963.

¹⁰T. Lauritsen and F. Ajzenberg-Selove (eds.), *Nuclear Data Sheets - Energy Levels of Light Nuclei*, National Academy of Sciences-National Research Council, Washington, D.C., 1962.

scintillation spectrometry and the beta-ray intensities (equal to neutron intensities) by time-of-flight.

The neutron groups which we observed can be readily fitted into the established level schemes of O^{17} and O^{16} as shown in Fig. 1.8. Perhaps the most interesting result of this work is that while the beta transitions to the neutron-emitting states at 5.94 Mev ($1/2^-$), 5.38 Mev ($3/2^-$), and 4.55 Mev ($3/2^-$) all exhibit allowed log ft values, the allowed transition to the lower state at 3.06 Mev ($1/2^-$) is found to be hindered. This situation suggests that the configurations of the ground state of N^{17} and the upper three states of O^{17} are similar, but that the configuration of the 3.06-Mev state must be different to account for the hindered transition to that state. Alternatively, chance cancellation

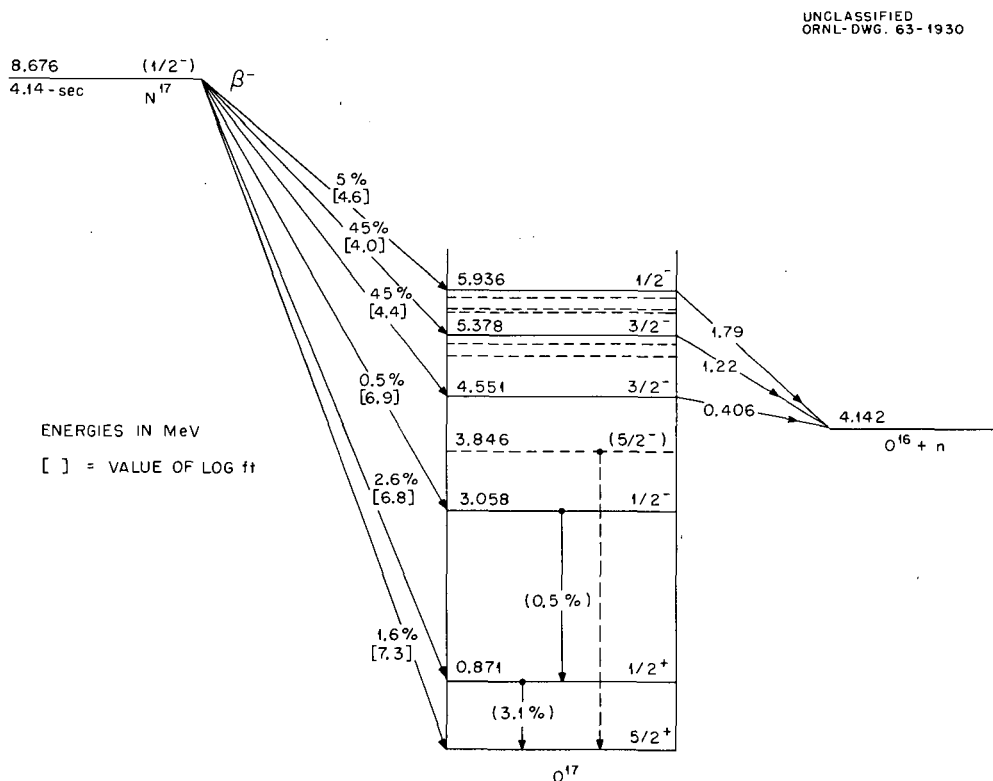


Fig. 1.8. Decay Scheme for N^{17} . Energies of levels were taken from the *Nuclear Data Sheets* (ref 10). Solid lines show levels and transitions involved in the decay of N^{17} ; dashed lines show data on additional levels as obtained from nuclear reaction work. The percent beta branching to the ground and first two excited states of O^{17} is from Hopkins and Silbert (ref 9).

of terms in the beta-decay matrix element¹¹ might give rise to the large value of $\log ft$ for the transition to the 3.06-Mev state.

Gamma-Gamma Angular Correlation in V⁵¹

R. L. Robinson¹² N. R. Johnson
G. D. O'Kelley

The nucleus V⁵¹ has the relatively simple structure of three $f_{7/2}$ particles beyond a doubly magic core configuration. According to the jj coupling shell model, the three $f_{7/2}$ particles can couple to give levels with spins of $\frac{3}{2}$, $\frac{5}{2}$, $\frac{7}{2}$, $\frac{9}{2}$, $\frac{11}{2}$, and $\frac{15}{2}$. For a nucleus like V⁵¹, which has a ground-state spin of $\frac{7}{2}$ (ref 13), this model predicts that the first and second levels will have spins of $\frac{5}{2}$ and $\frac{3}{2}$ respectively.^{14,15} Ritter *et al.*¹⁶ have verified this prediction for the spin

of the first level in V⁵¹ at 319 kev by means of Coulomb-excitation studies.

It has been suggested that the second level of the $(f_{7/2})^3$ configuration is the one observed¹⁷ at 933 kev. In an effort to ascertain the nature of this level, we investigated the angular correlation of the 613-319-kev gamma-ray cascade which deexcites it. This study was made with the 5.8-min isotope Ti⁵¹, produced by irradiation of normal titanium in the ORNL Graphite Reactor. The gamma rays were detected with two 3×3 in. NaI crystals which were each placed 10 cm from the source. One detector with its associated electronics was adjusted to accept gamma rays with energies between 300 and 340 kev. Spectra in coincidence with these gamma rays were taken at 10° intervals for angles from 90 to 180° between the two detectors. A least-squares fit of the data was made to the equation $W(\theta) = 1 + A_2 P_2(\cos \theta) + A_4 P_4(\cos \theta)$ on an IBM 7090 computer.

The experimental angular correlation coefficients which have been corrected for the finite angular resolution of the detectors are listed in Table 1.2. Those obtained with the solid and liquid sources

¹¹E. C. Halbert, private communication, May 1963.

¹²Physics Division.

¹³B. Bleaney, D. J. Ingram, and H. E. Scovil, *Proc. Phys. Soc. (London)* **64A**, 601 (1951).

¹⁴Dieter Kurath, *Phys. Rev.* **80**, 98 (1950).

¹⁵A. R. Edmonds and B. H. Flowers, *Proc. Roy. Soc. (London)* **A215**, 120 (1952).

¹⁶R. C. Ritter *et al.*, *Phys. Rev.* **128**, 2320 (1962).

¹⁷J. E. Schwäger, *Phys. Rev.* **121**, 569 (1961).

Table 1.2. Angular Correlation of the 613-319-kev Gamma-Ray Cascade
For the theoretical coefficients, δ_{319} has been taken as $+0.45 \pm 0.03$

	δ_{613}	A_2	A_4
Experimental			
Solid sources		$+0.025 \pm 0.038$	-0.05 ± 0.07
Liquid sources		$+0.002 \pm 0.038$	-0.02 ± 0.06
Average		$+0.013 \pm 0.030$	-0.03 ± 0.05
Theoretical			
Sequence			
$\frac{1}{2} (Q) \frac{5}{2} (D+Q) \frac{7}{2}$		-0.366	-0.01
$\frac{3}{2} (D+Q) \frac{5}{2} (D+Q) \frac{7}{2}$	$+0.18 \pm 0.02$	+0.013	0.00
	-9 ± 2	+0.013	+0.01
$\frac{5}{2} (D+Q) \frac{5}{2} (D+Q) \frac{7}{2}$	-0.41 ± 0.05	+0.013	0.00
	$+6.3 \pm 1.7$	+0.013	-0.01
$\frac{7}{2} (D+Q) \frac{5}{2} (D+Q) \frac{7}{2}$	-0.08 ± 0.03	+0.013	0.00
	-4.5 ± 0.8	+0.013	0.00

are in good agreement. In order to deduce information about the 613-keV transition from these coefficients, it is first necessary to know the mixing ratio of the 319-keV transition, δ_{319} , where $\delta = (E2/M1)^{1/2}$. This has been measured by Ritter *et al.*¹⁶ and by Krause.¹⁸ They reported, respectively, values of $+0.52 \pm 0.07$ and $+0.43 \pm 0.03$. For an average value of $+0.45 \pm 0.03$, a comparison has been made between the theoretical and experimental coefficients for spins of the 933-keV level which are consistent with an $E2-M1$ character for the 613-keV transition. The theoretical coefficients are included in Table 1.2. Values listed for δ_{613} give theoretical A_2 's that are identical to the measured A_2 . It can be seen that the correlation results are in agreement with a spin assignment of $3/2$, $5/2$, or $7/2$ for the 933-keV level. Spin $7/2$, however, has been ruled out by beta decay studies.^{19,20}

If the level has spin $3/2$, as expected for the second excited state of the $(f_{7/2})^3$ configuration, the correlation coefficients are compatible with a δ_{613} of $+0.18$ or -9 . For these values and a half-life for the 933-keV level of 4×10^{-12} sec, as determined from Coulomb-excitation results,²¹ the 613-keV $E2$ transition probability is, respectively, 1 and 32 times that given by the single-particle model. For these two δ_{613} 's, the $M1$ transition probability is smaller than the single-particle estimate by factors of 170 and 14,000 respectively. According to the jj coupling theory, $M1$ transitions between pure states of the $(f_{7/2})^3$ configuration are forbidden. Thus, a large retardation in the $M1$ transition rate as obtained here for either value of δ_{613} supports this type of description for the 319- and 933-keV levels. If instead the states result from the coupling of the single-particle to the first core state,²² the $M1$ transition probability should only be a factor of 2 smaller than the single-particle prediction. To obtain this estimate the gyromagnetic ratios of the collective motion and particle configuration were taken as Z/A and $+1.47$ respectively.

¹⁸I. Y. Krause, *Phys. Rev.* **129**, 1330 (1962).

¹⁹W. C. Jordan, S. B. Burson, and J. M. LeBlanc, *Phys. Rev.* **96**, 1582 (1954).

²⁰M. E. Bunker and J. W. Starnes, *Phys. Rev.* **97**, 1272 (1955).

²¹*Nuclear Data Sheets*, National Academy of Sciences-National Research Council, Washington, D.C. An average value for $B(E2)$ of $0.8 \times 10^{-50} e^2 \text{cm}^4$ was used.

²²A. DeShalit, *Phys. Rev.* **122**, 1530 (1961).

Independent Fission Yield of Sb^{127}

D. E. Troutner²³ A. C. Wahl²⁴
R. L. Ferguson

The fraction of the mass-127 fission-product chain formed directly as Sb^{127} has been measured in slow-neutron fission of U^{235} . This value of the fractional independent fission yield of Sb^{127} has been used with an empirical charge-dispersion curve²⁵ to determine the most probable nuclear charge Z_P of mass-127 fission products. Since this isobaric chain contains the "magic number" nuclide ${}_{50}\text{Sn}^{127}$, the experimental value of Z_P gives information concerning the effect of the closed 50-proton shell on the division of nuclear charge in fission.

A modification of the radiochemical procedure of Love²⁶ was used to separate antimony from its beta-decaying, fission-product precursors. The amount of Sb^{127} radioactivity separated at various times following brief thermal-neutron irradiations of U^{235} was compared with Sb^{127} radioactivity from samples in which the separation was made after complete decay of Sn^{127} . Any precursors of Sn^{127} are assumed to decay very quickly compared with the decay of Sn^{127} . Figure 1.9 summarizes

²³University of Missouri, Columbia.

²⁴Washington University, St. Louis, Mo.

²⁵A. C. Wahl *et al.*, *Phys. Rev.* **126**, 1112 (1962).

²⁶D. L. Love, quoted in W. J. Maeck, "The Radiochemistry of Antimony," *U.S. At. Energy Comm. NAS-NS-3011* (1960).

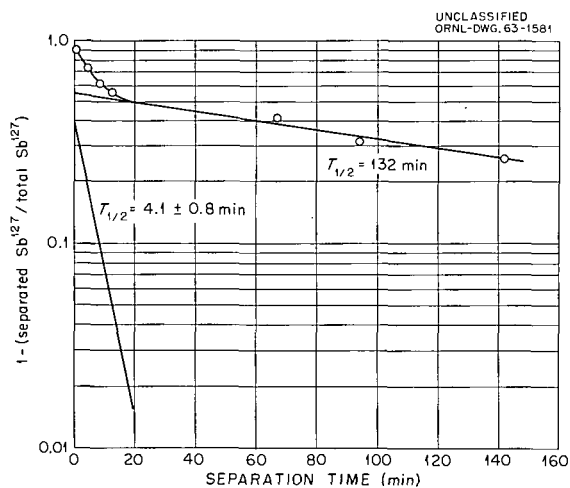


Fig. 1.9. Decay of Sb^{127} Precursors.

the results of these experiments. The ordinate is $(1 - Q)$, where Q is the ratio of the amount of Sb^{127} present at the time of separation to the amount from initially formed Sb^{127} plus complete decay of its precursors. Therefore, the quantity $(1 - Q)$ essentially represents the fraction of the chain present as Sn^{127} at a particular time after irradiation. Separation times are shown on the abscissa of the figure.

The "decay curve" of Fig. 1.9 has been resolved into two components with half-lives of 132 min and 4.1 ± 0.8 min. The 132-min value is the value reported by Hagebo, Kjelberg, and Pappas for an isomer of Sn^{127} . The 4.1-min value is a result of a least-squares analysis of our data; it is in agreement with the (4.6 ± 0.4) -min value given by Hagebo, Kjelbert, and Pappas²⁷ for another isomer of Sn^{127} and is consistent with the (2.5 ± 1) -min result of Droupesky and Orth.²⁸

The ordinate intercepts of the 4.1-min and 132-min components are 0.40 ± 0.03 and 0.55 ± 0.03 respectively. Preliminary calculations with these values give $(5.5 \pm 4.2)\%$ for the fractional independent yield of Sb^{127} and $\sim 55\%$ for the fraction of the mass-127 chain that passes through the longer-lived Sn^{127} isomer.

²⁷E. Hagebo, A. Kjelberg, and A. C. Pappas, *J. Inorg. Nucl. Chem.* **24**, 117 (1962).

²⁸B. J. Droupesky and C. J. Orth, *J. Inorg. Nucl. Chem.* **24**, 1301 (1962).

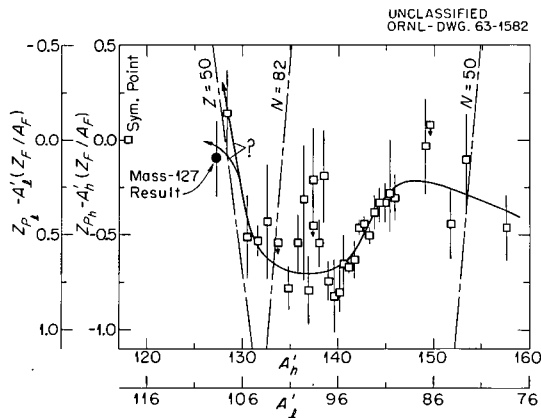


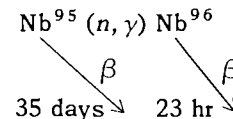
Fig. 1.10. Empirical Z_p Function [A. C. Wahl *et al.*, *Phys. Rev.* **126**, 1112 (1962)]. Scales are folded so that data for light (*l*) and heavy (*h*) fission products overlap. Primed quantities refer to fragment masses before prompt neutron emission.

If the empirical charge dispersion curve, determined by Wahl *et al.*²⁵ for several other mass chains in U^{235} slow-neutron fission, is assumed to apply to the mass-127 chain, then our result for the Sb^{127} independent yield gives a value of 49.5 ± 0.2 for the Z_p of this mass. This result, plotted in Fig. 1.10 with the empirical Z_p curve of Wahl *et al.*,²⁵ indicates that the curve should swing away from the "Z = 50" line toward the indicated symmetry point. This suggests that there is no pronounced 50-proton shell effect on the Z_p function.

An Upper Limit for the Thermal Neutron Cross Section of Nb^{95}

Joseph Halperin R. E. Druschel

The cross section of the 35-day beta-emitting Nb^{95} is of some interest since it is formed in high yield in fission. The activation cross section for this reaction



can be determined by measuring the activity of Nb^{96} formed in an irradiation of Nb^{95} .

Approximately 99% of the beta decay²⁹ of the 35-day Nb^{95} is via the 158-keV transition to the 768-keV level in Mo^{95} . This soft beta component may be absorbed almost completely by ~ 20 mg/cm² of absorber. Niobium-96 emits two beta groups (92% of 750 keV and 8% of 370 keV).²⁹ Approximately one-half of the beta particles will penetrate a 20-mg/cm² absorber in a slab geometry. Thus by counting the irradiated Nb^{95} sample with two 20-mg/cm² absorbers sandwiching the source and using a proportional gas counter in a 4π geometry configuration, an approximately fiftyfold enhancement of Nb^{96} to Nb^{95} counting efficiency could be obtained in an arrangement of high counting efficiency.

Following the irradiation the niobium was dissolved from the quartz capsule into a 9 M HCl, 5 M HF medium, and then passed through an anion exchanger to remove 24-hr W^{187} which was present.

²⁹D. Strominger, J. M. Hollander, and G. T. Seaborg, *Rev. Mod. Phys.* **30**(2), 585 (1958).

This was followed by a 0.1 M HCl, 1 M HF elution which removed 12.9-hr Cu⁶⁴, and followed by a 4 M HCl, 4 M HF elution which removed Mo⁹⁹. The niobium fraction was then eluted with 4 M HCl, 0.1 M HF. Two cycles of this purification appeared to free the sample of almost all observable radiochemical impurities.³⁰

By irradiating microcurie-size samples of Nb⁹⁵ in the hydraulic tube of the ORR at fluxes of $\sim 1.3 \times 10^{14}$ neutrons cm⁻² sec⁻¹, we were unable to see evidence for the 24-hr Nb⁹⁶. On the basis of being able to detect a 10% effect attributable to Nb⁹⁶, an upper limit for the reactor activation cross section for Nb⁹⁵ of ~ 7 barns can be reported. This cross section for Nb⁹⁵ is sufficiently low so that it could not be a significant poison in a reactor system.

Half-Life of Bi²⁰⁸

Joseph Halperin C. R. Baldock
R. E. Druschel J. H. Oliver
R. W. Stoughton

A more precise determination has been made of the half-life of Bi²⁰⁸ than has previously been reported.³¹ A revised value of 3.68×10^5 years has been measured with a standard error of 1%.

A sample of reactor-irradiated³² bismuth which had been calutron concentrated³³ was collected in four batches. The samples were carefully purified by a TTA extraction procedure to be free of lead, precipitated as the carbonate, and converted to the oxide Bi₂O₃. The spectrum was examined with a 3-in. NaI crystal-Dumont 6363 phototube assembly and multichannel analyzer. The specific activity of the 2.615-Mev full-energy peak was measured in a geometry in which the sample was 5.0 cm from the face of the crystal.

The efficiency of the counting arrangement in this geometry was calibrated using the 2.754-Mev

gamma of the 15.0-hr Na²⁴. The Na²⁴ tracer was added to quantities of normal Bi₂O₃ to simulate the Bi²⁰⁸ specific activity measurements. The absolute decay rate of the Na²⁴ sample was in turn determined by the 4 π beta-gamma coincidence method. A correction of 5.8% was applied for the difference in the full-energy-peak efficiency of the 2.754- and 2.615-Mev gamma rays.^{34,35}

The Bi²⁰⁸ content of each of the bismuth samples was determined³⁶ using a two-stage mass spectrometer.³⁷ The bismuth oxide was deposited upon a rhenium filament, and Bi⁺ metal ions were produced by a surface ionization technique; the ions were detected with a 14-stage electron multiplier tube. The data are summarized in Table 1.3.

The weights of the samples (accurate to ± 0.05 mg) are given in the second column; the specific counting rates and their associated error (both statistical counting and weighing) are shown in the third column. The measured efficiency (accurate to $\sim 1\%$) of the 2.754-Mev gamma of Na²⁴ for each sample is shown in the fourth column. The calculated efficiency for a 2.615-Mev gamma is shown in the fifth column; this was obtained by increasing the efficiency of column 4 by $(5.8 \pm 0.1)\%$. The specific activity of column 6 is obtained by dividing column 3 by column 5. The mass spectrographic ratios of Bi²⁰⁸/Bi²⁰⁹ (accurate to $\sim 1\%$) are given in the seventh column. The ratio of the specific activity to the mass ratio is given in the last column for each of the four samples. Thus the weighted mean of the ratio of the specific activity to the Bi²⁰⁸/Bi²⁰⁹ mass ratio is determined as $(1.031 \pm 0.010) \times 10^7$ dis/min per mg of Bi²⁰⁸. The corresponding half-life of Bi²⁰⁸ is therefore $3.68_3 \times 10^5$ years with a standard error of 1.0%. The internal precision of the measurement is better than 0.5%; however, the propagation of the estimated uncertainties from the various sources of error leads to the larger uncertainty of a 1.0% standard error.

³⁰The authors wish to acknowledge the help of F. Nelson of the Chemistry Division in devising the chemical separation.

³¹*Chem. Div. Ann. Progr. Rept. June 20, 1962, ORNL-3320, p 7.*

³²The authors are indebted to J. R. Huizenga of the Argonne National Laboratory for making this reactor sample available.

³³The authors are grateful to L. O. Love of ORNL and numerous associates in the calutron groups for making this separation.

³⁴M. H. Lazar, R. C. Davis, and P. R. Bell, *Nucleonics* 14(4), 52 (1956).

³⁵R. L. Heath, *Scintillation Spectrometry Gamma Ray Spectrum Catalogue*, Phillips Petroleum Co., Atomic Energy Division Report IDO-16408 (1957).

³⁶The authors wish to thank L. E. Idom for his aid in the mass measurements.

³⁷*Chem. Div. Ann. Progr. Rept. June 20, 1962, ORNL-3320, p 118.*

Table 1.3. Half-Life Determination of Bi²⁰⁸

Sample	Weight of Bi ₂ O ₃ (mg)	Specific Counting Rate (counts min ⁻¹ mg ⁻¹)	Full-Energy-Peak Efficiency		Specific Activity (dis min ⁻¹ mg ⁻¹)	Bi ²⁰⁸ / Bi ²⁰⁹ ×10 ⁻⁶	Bi ²⁰⁸ / Bi ²⁰⁹ (dis min ⁻¹ mg ⁻¹) ×10 ⁷	
			2.754 Mev (measured)	2.615 Mev (calculated)				
			×10 ⁻²	×10 ⁻²	×10 ³	×10 ⁻⁶	×10 ⁷	
1	88.3	11.99 ± 0.05	0.589 ₃	0.623 ₂	1.92 ₄	187.7	1.025	
2	14.7	7.98 ± 0.10	0.614 ₄	0.650 ₀	1.22 ₈	117.7	1.043	
3	7.4	23.85 ± 0.29	0.616 ₂	0.651 ₉	3.65 ₉	356.0	1.028	
4	5.2	22.60 ± 0.36	0.616 ₈	0.652 ₆	3.46 ₃	335.0	1.034	
Weighted Av = 1.031								

Effective Cutoff Energies for Cadmium, Gadolinium, Samarium, and Boron Filters

R. W. Stoughton Joseph Halperin

The calculations of effective neutron cutoff energies previously described³⁸ for cadmium, gadolinium, samarium, and boron filters and for spherical, cylindrical, and slab geometries have been completed. The model assumed a point 1/v detector inside the filter and a Maxwellian plus a 1/E epithermal flux, both isotropic with respect to the detector. On the assumptions made, the results for spherical geometry are the same as for a beam-flux case. The parameters varied were the Maxwellian temperature T_m (where $E_m = kT_m$), the ratio r of Maxwellian flux to 1/E flux per lethargy unit, the filter thickness l_o , and, in the case of cylindrical filters, the height/diameter ratio.

Also calculated were differential reaction rates vs energy and the fraction *FRACT* of total reactions occurring below the cutoff, both of which give a measure of the filter efficiency. The effective cutoff was defined in terms of the cutoff of a perfect filter (infinitely sharp) which gave the same reaction rate, for the filtered sample, as the filter actually used.

In the cases of cadmium and gadolinium the cross sections were set equal to Breit-Wigner

expressions for the resonances at 0.178 and 0.03 ev respectively. In the case of samarium the resonance most pertinent to its properties as a filter is that at 0.0976 ev. However, because of other relatively near higher-energy resonances, particularly that at 0.88 ev, the cross section does not continue to decrease as $E^{-5/2}$ above 0.0976 ev, and the 0.88-ev resonance causes a perturbation on the filter properties. The cross section of samarium for most calculations was set equal to a single Breit-Wigner expression (one level: $E_r = 0.0976$ ev) plus a 1/v term; the results of such calculations are indicated in the figures by samarium (1 level). For comparative purposes some calculations were conducted in which the cross section was set equal to the sum of two Breit-Wigner expressions (two levels: $E_r = 0.0976$ and 0.88 ev) plus a 1/v term. The boron cross section was set equal to a 1/v term normalized to 755 barns at 0.0253 ev.

In all the results presented below the lower limit of the 1/E flux was taken as $5E_m$.

Cutoffs and Filter Efficiencies. — The effective cutoff E_c and *FRACT* are shown in Figs. 1.11 and 1.12 for the various filter materials for spherical geometry (beam-flux case) as a function of thickness l_o , thermal to 1/E flux ratio r , and characteristic Maxwellian energy E_m (equal to kT_m). From the results of the differential rate calculations and the values of *FRACT* in Fig. 1.12 it appears that filter thicknesses of at least 25 mils of cadmium, 100 mg/cm² of gadolinium, 500 mg/cm² of samarium, or 300 mg/cm² of boron are required to make

³⁸Chem. Div. Ann. Progr. Rept. June 20, 1962, ORNL-3320, p 3; also see ORNL TM-236 and Nucl. Sci. Eng. 15, 314 (1963) for more details and numerical results.

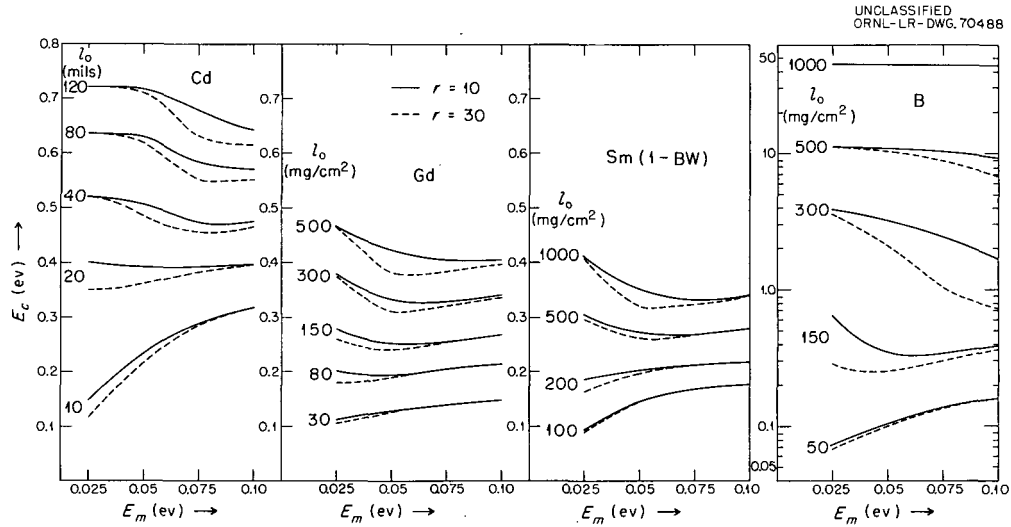


Fig. 1.11. Effective Cutoff for Spherical Filters (Beam-Flux Case).

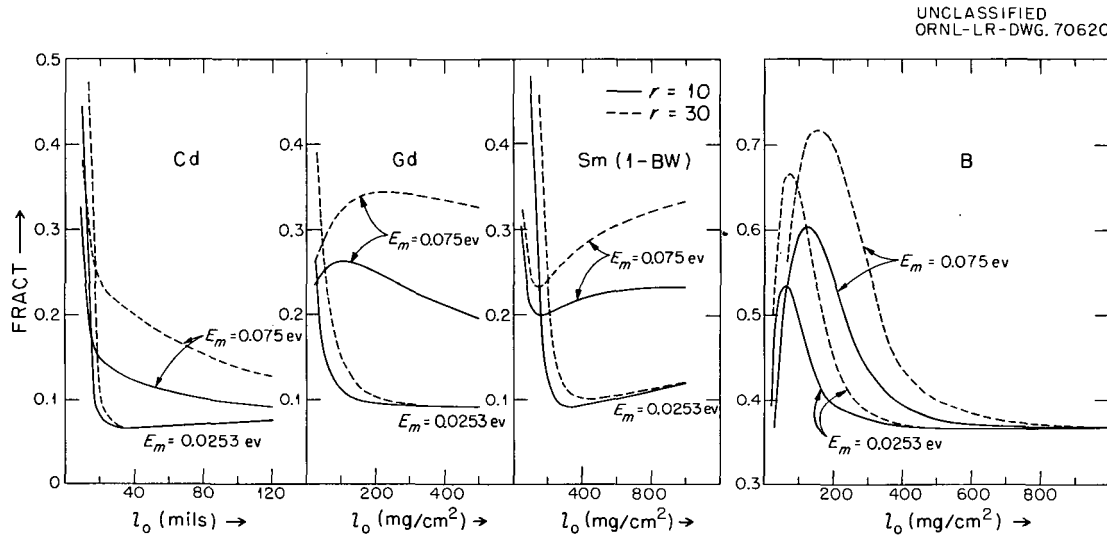


Fig. 1.12. Fractions of Reactions Below Cutoff for Spherical Filters (Beam-Flux Case).

the contribution of Maxwellian neutrons to the filtered reaction rate relatively unimportant.

According to Fig. 1.11, as expected from the higher-energy resonance in the case of cadmium (0.178 vs 0.03 and 0.0976 ev for gadolinium and samarium), the cutoffs are also higher for reasonable thicknesses. It is somewhat surprising that gadolinium and samarium do not show a greater difference in this regard.

In the case of cadmium, for thin filters the transmission of Maxwellian neutrons at relatively low energies causes the value of the cutoff E_c to depend rather strongly on r at low values of E_m . At 10 mils of cadmium and at the higher E_m 's the transmission of Maxwellian neutrons is so high that these neutrons alone tend to determine E_c , and hence the latter becomes insensitive to r . At higher thicknesses (40 mils and above) and at

low E_m values, relatively few Maxwellian neutrons are transmitted so that E_c is insensitive to r . However, as E_m rises the fraction of Maxwellian neutrons existing and being transmitted in the cutoff region and above also rises and again E_c becomes a more sensitive function of r .

The curves for gadolinium and samarium are generally similar to those for cadmium, except that with the greater thicknesses there is less tendency for the E_c values to become independent of r at $E_m = 0.0253$ ev. This situation undoubtedly results from the fact that the resonances of gadolinium (0.03 ev) and samarium (0.0896 ev) are closer to 0.0253 ev than is that of cadmium (0.178 ev). If the cadmium curves at about 0.04 ev and above are compared with the other two at 0.025 ev and above, a greater similarity is seen. Since boron, which obeys the $1/v$ law, does not show any tendency toward a "sharp" cutoff, the E_c values were plotted on a log scale.

Effect of Filter Geometry. — Effective cutoffs for the various filter materials for spherical (beam-flux case), cylindrical [height (H)/diameter (D) = 2], and slab geometries at a flux ratio r of 20 are shown in Fig. 1.13. As can be seen the effect of geometry is large, with the E_c values for spheres being not greatly different from those for cylinders ($H/D = 2$) but with the slabs ($\cos \theta$ law) showing much higher values. In fact the slab values are so much larger than those for the spheres that unless widely different values of thickness are used, the slab values for a given actual thickness would be higher than those of the thicker spheres (and cylinders).

Figure 1.14 shows the effect of height/diameter for cylindrical cadmium filters at $E_m = 0.0253$ ev and $r = 20$. The cutoffs are at a minimum for $H/D = 1$ and show relatively little change with increasing H/D , especially above about 3. With decreasing H/D , however, there is a rapid rise below

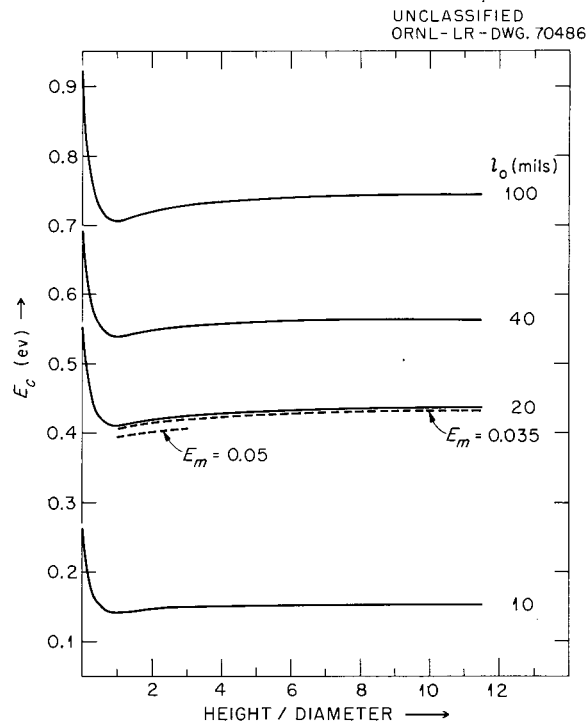


Fig. 1.14. Variation of Effective Cutoff with Height/Diameter for Cylindrical Cadmium Filters ($E_m = 0.0253$ ev, $r = 20$).

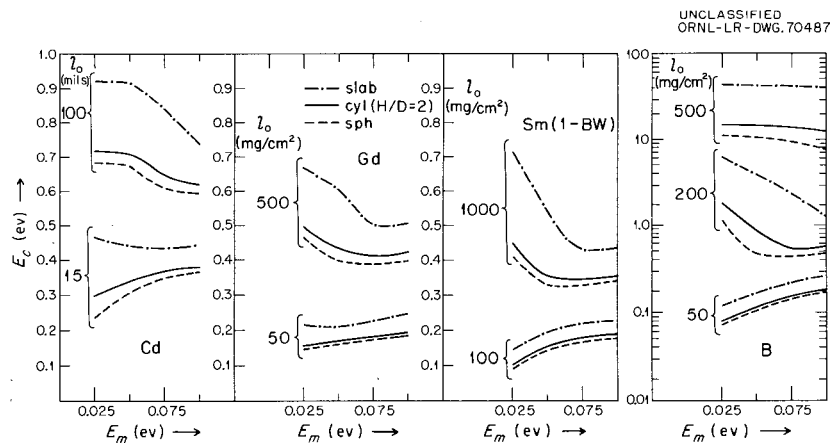


Fig. 1.13. Effect of Geometry of Filter on Cutoff (for $r = 20$).

about 0.5 and the limiting values at $H/D = 0$ (the slab values) are shown by breaks on the ordinate axis.

The effects of varying H/D in the cases of the other filter materials may be expected to be similar to those of cadmium.

Cutoffs for Very Thick Cadmium Filters. — In a long irradiation (large flux time) appreciable

amounts of Cd^{113} in a cadmium filter may be destroyed by neutron capture. For example, in a thermal flux of 10^{14} neutrons $\text{cm}^{-2} \text{sec}^{-1}$ about 0.6 mil of cadmium is destroyed per day. Thus, in a few weeks the effective filter thickness may be reduced substantially. In order to have a useful filter throughout such an irradiation it would be necessary to start with a thickness such that

Table 1.4. Effective Cutoffs for Cadmium Filters

Mils of Cadmium	E_m (ev)							
	0.0253		0.050		0.075		0.100	
	E_c	FRACT	E_c	FRACT	E_c	FRACT	E_c	FRACT
Spherical Geometry (Beam-Flux Case), $r = 10$								
100	0.681	0.074	0.677	0.075	0.632	0.095	0.607	0.146
150	0.773	0.076	0.771	0.077	0.636	0.088	0.688	0.128
200	0.848	0.077	0.847	0.078	0.821	0.084	0.761	0.115
250	0.912	0.078	0.911	0.079	0.892	0.083	0.830	0.107
Spherical Geometry (Beam-Flux Case), $r = 30$								
100	0.681	0.074	0.668	0.078	0.591	0.137	0.584	0.243
150	0.773	0.076	0.767	0.078	0.688	0.112	0.654	0.210
200	0.848	0.077	0.844	0.078	0.777	0.099	0.714	0.182
250	0.912	0.078	0.910	0.079	0.856	0.093	0.770	0.160
Cylindrical Geometry ($H/D = 2$), $r = 10$								
100	0.719	0.076	0.715	0.077	0.673	0.093	0.637	0.141
150	0.817	0.078	0.816	0.078	0.785	0.087	0.728	0.123
200	0.897	0.079	0.897	0.080	0.875	0.085	0.811	0.111
250	0.966	0.080	0.966	0.080	0.950	0.084	0.887	0.103
Cylindrical Geometry ($H/D = 2$), $r = 30$								
100	0.719	0.076	0.708	0.079	0.626	0.129	0.610	0.235
150	0.817	0.078	0.812	0.079	0.736	0.106	0.686	0.198
200	0.897	0.079	0.895	0.080	0.835	0.096	0.753	0.170
250	0.966	0.080	0.965	0.081	0.919	0.091	0.817	0.149
Slab Geometry, $r = 10$								
100	0.921	0.099	0.919	0.100	0.880	0.108	0.792	0.143
150	1.054	0.101	1.052	0.102	1.030	0.106	0.942	0.127
200	1.161	0.103	1.160	0.103	1.146	0.105	1.072	0.120
250	1.253	0.104	1.253	0.104	1.243	0.105	1.184	0.115
Slab Geometry, $r = 30$								
100	0.921	0.099	0.915	0.100	0.813	0.127	0.718	0.223
150	1.054	0.101	1.051	0.102	0.985	0.115	0.834	0.180
200	1.161	0.103	1.160	0.103	1.116	0.110	0.952	0.155
250	1.253	0.104	1.253	0.104	1.223	0.108	1.072	0.140

the effective filter thickness at the end of the irradiation has not been reduced to below the equivalent of about 25 mils of unirradiated cadmium. Hence the actual cadmium thickness might need to be appreciably higher depending upon the flux and length of irradiation. The previous calculations for cadmium spheres (beam-flux case), cylinders ($H/D = 2$), and slabs have therefore been extended to include 250-mil thickness, and the results are given in Table 1.4 as a function of thickness, $E_m (= kT_m)$, and $r = \phi_{th}/\phi_r$.

Conclusions. — Cadmium — with a thickness of 30 or preferably 40 mils — is perhaps the most useful all-around filter, with gadolinium as a second choice. In the case of samarium a correction may have to be made for the second higher resonance above thermal energies (i.e., that at 0.88 ev) and possibly for others.

For low values of the Maxwellian temperature ($E_m = 0.0253$ to about 0.05 ev) and thicknesses of 30 mils or higher, the effective cadmium cutoff is insensitive to the Maxwellian to $1/E$ flux ratio, as very few Maxwellian neutrons are transmitted; for thinner filters or higher Maxwellian temperatures the flux ratio is more important. For gadolinium and samarium the sensitivity to transmission of Maxwellian neutrons at low values of E_m is enhanced due to the lower energy of their resonances and their consequent lower cutoffs. On the other hand, the lower resonance of gadolinium (0.03 ev) allows a cutoff closer to the lower limit of the $1/E$ flux (some $5E_m$).

It is not necessary to know (accurately) the resonance-flux lower limit in order to calculate effective cutoffs. The variations in the cutoffs for filters of practical thicknesses appear to be less than about 3% at worst (and more typically 1%) due to variations of the resonance-flux lower limit over a range as wide as ordinarily encountered in well-thermalized reactors, that is, a lower limit of (5 ± 2) times E_m .

In all cases the cutoffs for cylinders were between those of spheres and slabs. This is to be expected since the effective thicknesses (at a given actual thickness) for these geometries are in that order. The variation of cutoff with ratio of height to diameter for cylinders is relatively minor and (as expected) is more noticeable at the lower values.

By the use of gadolinium and cadmium (and perhaps samarium, too) and by comparisons of

monitors of known cross section it should be possible to detect resonances in the thermal to cut-off regions in an unknown sample.

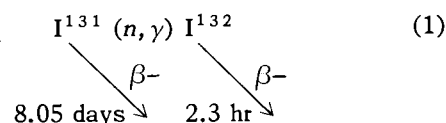
Thermal Neutron Cross Section and Resonance Integral of I^{131}

Joseph Halperin

R. E. Druschel

The cross section of I^{131} had been reported in the early literature as 600 ± 300 barns³⁹ and more recently by Kennett and Thode⁴⁰ as 50 ± 40 barns. The latter workers separated the xenon daughters from an irradiated sample of I^{131} and mass spectrographically determined the Xe^{132}/Xe^{131} ratio. They recognized the complicating aspect of the high cross section in Xe^{131} , which gave rise to most of the large uncertainty in their experiment (i.e., the contribution to the Xe^{132} due to neutron capture in Xe^{131} exceeded that due to capture in I^{131}).

The direct measurement [see Eq. (1)] of the I^{131} activation cross section is made difficult by the necessity of determining the content of the 2.3-hr I^{132} in the presence of the relatively large amount of 8.0-day I^{131} ;



Irradiating samples of I^{131} to saturation at fluxes of $\sim 10^{14}$ neutrons $\text{cm}^{-2} \text{sec}^{-1}$, yields I^{132} with decay rates of $\sim 10^{-4}$ that of the I^{131} . However since I^{131} emits gamma rays with a maximum energy of only 722 kev and I^{132} emits several gamma rays at higher energy although in low yield,⁴¹ it would appear possible to detect I^{132} by NaI gamma-ray spectroscopy techniques. A further complication is due to the presence of the 12.5-hr I^{130} which is formed because of the presence of I^{129} in the I^{131} tracer (since they are both produced with comparable yields in fission). The relatively high cross section of I^{129} accentuates the interference of I^{130} , which emits gamma rays at 1150 kev.

³⁹D. J. Hughes and J. A. Harvey, *Neutron Cross Sections*, BNL-325 (July 1, 1955).

⁴⁰T. J. Kennett and K. G. Thode, *J. Inorg. Nucl. Chem.* 5, 253 (1958).

⁴¹D. Strominger, J. M. Hollander, and G. T. Seaborg, *Rev. Mod. Phys.* 30(2), 585 (1958).

By irradiating millicurie quantities of "fresh" I^{131} (so as to minimize the I^{129} content – yet old enough for the 21-hr I^{133} with its gamma interference to have died out) in a high-flux position in the ORR, rapidly retrieving and purifying the irradiated sample, and analyzing the gamma-ray spectrum through ~ 60 g/cm² of lead, we find that we can measure and follow the decay of the 1.40-Mev gamma ray in I^{132} . This gamma ray has an intensity of approximately 10% in I^{132} decay.

The samples are irradiated in sealed quartz ampuls. The radioiodine is dissolved, isotopically equilibrated, and purified using an oxidation-reduction procedure followed by a CCl_4 extraction.⁴²

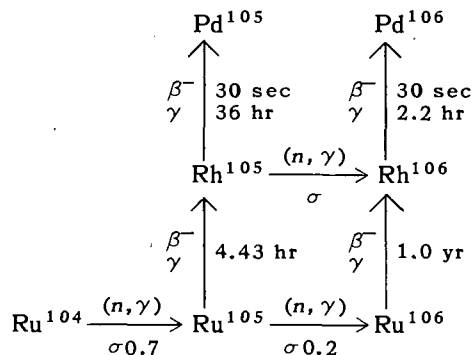
Preliminary results have been obtained with both bare and cadmium-filtered irradiations. On this basis, using cobalt monitors, a thermal cross section, $\sigma_{th} \cong 0.7$ barn, and a resonance integral, $I \cong 8$ barns, have been measured. These cross sections are substantially below the previous estimates and imply a negligible neutron loss to I^{131} in a reactor system.

Neutron-Capture Cross Section of 36-hr Rh^{105}

P. M. Lantz C. R. Baldock
L. E. Idom

The neutron-capture cross section of Rh^{105} has been found by Cuninghame *et al.*⁴³ to be $\cong 1.8 \times 10^4$ barns based on a flux calculated by three different methods. They observed that the yields of Pd^{105} and Pd^{106} relative to those of Pd^{107} , Pd^{108} , and Pd^{110} were considerably altered from what was expected when they measured mass spectrometrically the thermal fission yields of Pu^{239} . In view of the significance of so large a cross section in reactor technology, it was suggested by L. E. Glendenin that a more accurate measurement could be made by neutron activation of Ru^{104} and mass spectrometric measurement of the Pd^{105}/Pd^{106} separated from the Ru^{104} . The reaction below indicates how this

determination can be performed;



Approximately 56 mg of enriched Ru^{104} (98.2%) metal was irradiated to 5.0×10^{20} nvt in the ORR by use of a cadmium-ratio technique.⁴⁴ The "stringer" irradiation tube contained a sample in a cadmium can in the middle and an unfiltered sample at each end, so three samples were irradiated simultaneously. A cobalt monitor in the form of a cobalt-aluminum alloy (0.15% cobalt) was placed on two sides of each Ru^{104} sample. Following the irradiation the samples were subjected to extensive chemical processing.

After several weeks cooling time to permit Ru^{105} to decay to stable Pd^{105} , the ruthenium metal was dissolved in a sodium hydroxide–sodium hypochlorite solution. The ruthenium tetroxide was distilled from an $HClO_4$ solution in a quartz still and trapped in SO_2 -saturated 6 M HCl. The residue containing the palladium was reduced by evaporation to a nearly dry salt mass to remove the excess $HClO_4$. The residue was transferred in 2 M HCl to a conditioned Dowex-2 (ref 45) resin column to adsorb the chloride complex ion, $PdCl_4^{2-}$, and to remove NaCl and the trace of silver that was present in the unirradiated Ru^{104} metal. After washing the excess acid from the resin column, the palladium was stripped with 0.25 M NH_4OH as the $Pd(NH_3)_4^{2+}$ ion. The palladium solution was reduced to dryness and heated to drive off the NH_4Cl . The residue was dissolved in weak HNO_3 for examination with a two-stage 12-in. mass spectrometer with a thermal ionization source and electron-multiplier detectors. Ratios of Pd^{106}/Pd^{105} relative to Pd^{108} , which

⁴²J. Kleinberg and G. A. Cowan, "The Radiochemistry of Fluorine, Chlorine, Bromine, and Iodine," U.S. At. Energy Comm. NAS-NS-3005 (1960).

⁴³J. G. Cuninghame, L. E. Glendenin, and A. L. Harkness, Neutron Capture Cross-Section of 36 hr Rh^{105} , TID-11967 (November 1960).

⁴⁴R. W. Stoughton and Joseph Halperin, *Nucl. Sci. Eng.* 6, 100 (1959).

⁴⁵H. G. Hicks *et al.*, *The Qualitative Anionic Behavior of a Number of Metals with an Ion Exchange Resin, "Dowex 2,"* LRL-65 (December 1953).

was present in micro amounts due to the presence of natural palladium, were determined.

Enriched Pd¹⁰² (50.9%) was added to a sample of the Ru¹⁰⁴ starting material, and the material was subjected to the same chemical treatment employed with the irradiated sample. This permitted a determination, by the isotope-dilution technique, of the natural palladium content of the starting material plus any introduced by the reagents. The values obtained by mass spectrometric analysis were 8.14×10^{-6} g of mass 106 and 6.76×10^{-6} g of mass 105 per gram of Ru¹⁰⁴.

In order to measure the amount of Pd¹⁰⁵ and Pd¹⁰⁶ produced in the irradiation, enriched Pd¹⁰² was introduced into one of the bare-irradiation Ru¹⁰⁴ samples before processing. After making a correction for the chemical yield (82%), it was found that the sample contained 6.39×10^{-4} g of mass 106 and 12.02×10^{-4} g of mass 105 per gram of Ru¹⁰⁴.

Based on an approximate flux ratio $\Phi_{th}/\Phi_r = 15.4$ observed in the ORR and the yield of Pd¹⁰⁵ and Pd¹⁰⁶, the effective cross section of Ru¹⁰⁴ was found to be ~ 3.65 barns. This value is approximately five times that observed by Seren *et al.*⁴⁶ by thermal neutron activation of natural ruthenium. The effective cross section of 36-hr Rh¹⁰⁵ was observed as $25,400 \pm 2,500$ barns,⁴⁷ under the conditions previously stated and with no consider-

ation given to the loss of product due to neutron capture by Ru¹⁰⁵, Pd¹⁰⁵, Rh¹⁰⁶, and Pd¹⁰⁶.

During the course of this investigation it was found that the recovery of trace amounts of palladium from the Dowex-2 resin column was adversely affected by small amounts of HClO₄ present in the column feed solution, and by permitting the palladium to remain on the resin several hours before stripping. It was further observed that very small amounts of salt remaining in the palladium solution caused ionization instability during examination in the mass spectrometer. This, however, was not critical when the total palladium in the source material was increased by the addition of the enriched isotope.

It was found that these difficulties can be avoided by precipitating the trace palladium as the sulfide with copper as a carrier, dissolving the Cu-Pd sulfide in H₂O₂-HCl solution, and adsorbing the palladium on an anion resin column. The palladium is stripped with a 0.25 M NH₄OH solution, evaporated, and then dissolved in a weak HNO₃-H₂SO₄ solution for electroplating on a 1/4-in. section of 6-mil rhenium wire. Eighty percent recovery of $\leq 1 \times 10^{-7}$ g of palladium from the chemical processing has been demonstrated.

The improved techniques developed during the course of the preliminary experiments reported here will be applied to refine the cross-section values obtained. Another sample of Ru¹⁰⁴ has been prepared and is currently in the ORR for two reactor cycles. This Ru¹⁰⁴ metal was purified by ruthenium tetroxide distillation to remove the natural palladium, silver, and other impurities. The Ru¹⁰⁴ was then electroplated from a weak H₂SO₄ solution on a thin copper foil, which was dissolved from the ruthenium metal with NHO₃.

⁴⁶Leo Seren, H. N. Friedlander, and S. H. Turkel, *Phys. Rev.* **72**, 888 (1947).

⁴⁷The authors gratefully acknowledge the assistance of R. W. Stoughton and Joseph Halperin in making these measurements.

2. Isolation and Chemical Properties of Synthetic Elements

CHEMISTRY OF TECHNETIUM

Structure of the Aqueous Pertechnetate Ion

R. H. Busey O. L. Keller, Jr.

The structures of $\text{ReO}_4^-(aq)$ and $\text{WO}_4^{2-}(aq)$ have been shown to be tetrahedral by Raman and infrared spectroscopy by comparison with the known tetrahedral $\text{OsO}_4(l)$.¹ Three Raman lines were observed for all three molecules, whereas four are expected for T_d symmetry. The absence of the fourth line, $\nu_2(E)$, was explained¹ by showing (force field calculation) that it could lie close to $\nu_4(F_2)$ and thus be unresolved. It was considered of interest to determine if the Raman spectrum of $\text{TcO}_4^-(aq)$, which is presumably tetrahedral, would exhibit four lines since the mass ratio, Tc/O, is considerably different from that of the other molecules.

The Raman spectrum of $\text{TcO}_4^-(aq)$ (Fig. 2.1) was observed to have only two lines, whereas the spectrum of the isoelectronic $\text{MoO}_4^{2-}(aq)$ was observed to have three lines similar in shape and relative intensities to those of $\text{WO}_4^{2-}(aq)$, $\text{ReO}_4^-(aq)$, and OsO_4 . In order to interpret the Raman spectrum of the $\text{TcO}_4^-(aq)$, an extensive investigation of the Raman and infrared spectra of crystals of several salts of all the above ions was undertaken.

$\text{Na}_2\text{MoO}_4(\text{cryst})$ and $\text{Na}_2\text{WO}_4(\text{cryst})$ are isostructural and have a spinel structure with space group $Fd\bar{3}m$, $Z = 8$ (ref 2). The MoO_4^{2-} and WO_4^{2-} are in site symmetry³ T_d . The Raman spectrum of $\text{Na}_2\text{WO}_4(\text{cryst})$ is very similar to

that of $\text{Na}_2\text{MoO}_4(\text{cryst})$ (Fig. 2.1) with the exception that the symmetrical stretch vibration, $\nu_1(A_1)$, is located at 928 cm^{-1} instead of 892 cm^{-1} . The tetrahedral (T_d) assignment of the lines is (reading left to right) $\nu_1(A_1)$, $\nu_3(F_2)$, $\nu_2(E)$, and $\nu_4(F_2)$. The 116-cm^{-1} line is a lattice vibration. The very weak line at 835 cm^{-1} arises from excitation of ν_1 by the weak 4347.50-\AA line present in the mercury exciting source (4358.35 \AA) not removed by the filter solution. The low intensity of $\nu_2(E)$ explains its absence in the aqueous solution spectra, and the previous explanation¹ is invalid. The $\nu_1(A_1)$ lines in the spectra of $\text{MoO}_4^{2-}(aq)$ and $\text{WO}_4^{2-}(aq)$ are coincident with $\nu_1(A_1)$ of the crystal spectra. The corresponding $\nu_4(F_2)$ and $\nu_3(F_2)$ lines in the spectra of $\text{MoO}_4^{2-}(aq)$ and $\text{WO}_4^{2-}(aq)$ lie a number of cm^{-1} above the corresponding lines in the crystal spectra.

To investigate the difference between the $\nu_3(F_2)$ in the solution and in the crystal spectra, the Raman spectra of $\text{Na}_2\text{MoO}_4 \cdot 2\text{H}_2\text{O}(\text{cryst})$ and $\text{Na}_2\text{WO}_4 \cdot 2\text{H}_2\text{O}(\text{cryst})$ were measured. These salts are isostructural with space group $Pbca$, $Z = 8$ (refs 4, 5). The MoO_4^{2-} and WO_4^{2-} are in site symmetry C_1 . Thus the degeneracy of doubly and triply degenerate vibrations in T_d symmetry, $\nu_2(E)$, $\nu_3(F_2)$, and $\nu_4(F_2)$, are completely removed, and all nine fundamentals become Raman and infrared active. The spectrum of $\text{Na}_2\text{WO}_4 \cdot 2\text{H}_2\text{O}(\text{cryst})$ is similar to that of $\text{Na}_2\text{MoO}_4 \cdot 2\text{H}_2\text{O}(\text{cryst})$ (Fig. 2.1) except that the resolved lines at 844 and 837 cm^{-1} and the almost resolved line centered at 330 cm^{-1} are not resolved in the tungstate spectrum. Infrared spectra observed on Nujol mulls of the salts from 650 to 4000 cm^{-1}

¹L. A. Woodward and H. L. Roberts, *Trans. Faraday Soc.* 52, 615 (1956).

²L. N. Becka and R. J. Poljak, *Anales Asoc. Quim. Arg.* 46, 204 (1958).

³R. S. Halford, *J. Chem. Phys.* 14, 8 (1946).

⁴R. J. Poljak and L. N. Becka, *Anales Asoc. Quim. Arg.* 46, 199 (1958).

⁵C. W. F. T. Pistorious and W. E. Sharp, *Acta Cryst.* 14, 316 (1961).

showed bands essentially coincident with the Raman lines consistent with the C_1 symmetry.

The $\nu_3(F_2)$ Raman lines at 843 and 833 cm^{-1} in the respective $\text{MoO}_4^{2-}(\text{aq})$ and $\text{WO}_4^{2-}(\text{aq})$ spectra are coincident with strong Raman lines of the solid dihydrates. Thus it appears that the $\nu_3(F_2)$ vibration is more subject to a shift

in frequency in changing the environment of the ion than $\nu_1(A_1)$ and $\nu_4(F_2)$. It is an interesting empirical observation that the increase in frequency (wave number) of $\nu_3(F_2)$ in going from the anhydrous salts (T_d symmetry) to the aqueous solutions is approximately inversely proportional to the mass of the central metal atom.

The space group of isostructural $\text{KTcO}_4(\text{cryst})$ and $\text{KReO}_4(\text{cryst})$ is $I4_1/a$, $Z = 4$ (ref 6) (CaWO_4 type). The TcO_4^- and ReO_4^- are in site symmetry S_4 . The correlation table for the species of the two point groups is⁷

T_d	S_4
A_1	A
E	$A + B$
F_2	$B + E$

All species in S_4 are Raman active (seven lines), and B and E are infrared active (five bands). The Raman spectra of both crystals are given in Fig. 2.1. The infrared spectrum of a Nujol mull of $\text{KReO}_4(\text{cryst})$ was observed to have a group of four bands centered around 913 cm^{-1} , where for S_4 symmetry two fundamentals should be observed. In the overtone-combination region 1750 to 1950 cm^{-1} , a group of five bands appeared which are readily interpreted as an overtone (or combination) and the overtone in combination with each of four lattice vibrations. The fourth lattice vibration at 40 cm^{-1} was unobservable in the Raman spectrum. Combination bands between fundamentals and lattice vibrations cause the complexity centered at 913 cm^{-1} .

Again the $\nu_1(A_1)$ (971 cm^{-1}) and $\nu_4(F_2)$ (332 cm^{-1}) of $\text{ReO}_4^-(\text{aq})$ ¹ are nearly coincident with strong Raman lines of $\text{KReO}_4(\text{cryst})$, whereas $\nu_3(F_2)$ (916 cm^{-1}) lies at a higher wave number than the strong Raman line at 897 cm^{-1} for the crystal.

The Raman spectra of both crystals are consistent with the tetrahedral ion being in site symmetry S_4 . The point of interest in the $\text{KTcO}_4(\text{cryst})$ spectrum is the relatively narrow separation of the two most intense lines, 887 and 913 cm^{-1} , the latter line undoubtedly arising

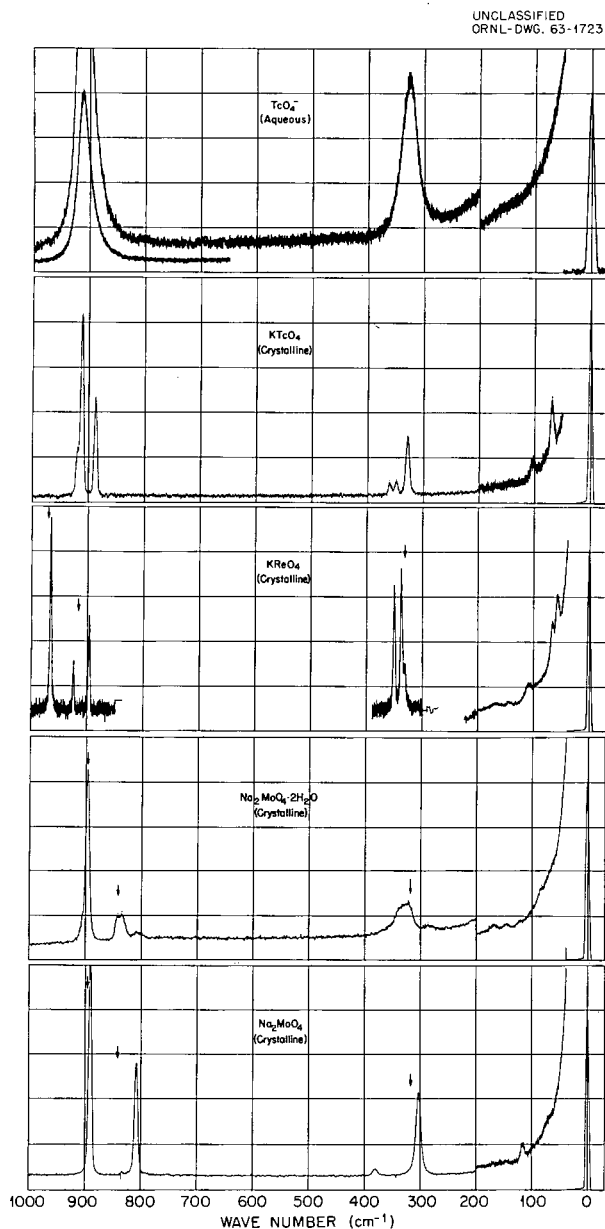


Fig. 2.1. Raman Spectra of $\text{TcO}_4^-(\text{aq})$, $\text{KTcO}_4(\text{cryst})$, and Related Crystals. Arrows indicate location of the Raman lines of the corresponding aqueous ion.

⁶B. J. McDonald and G. J. Tyson, *Acta Cryst.* 15, 87 (1962).

⁷E. B. Wilson, Jr., J. C. Decius, and P. C. Cross, *Molecular Vibrations*, McGraw-Hill, New York, 1955.

from the symmetrical stretch vibration. The separation of these two lines is expected to be reduced in going from the crystal to the aqueous solution, similar to that observed in the tungstate and molybdate spectra. This appears to be the case as one line at 912 cm^{-1} is observed in the $\text{TcO}_4^-(\text{aq})$ spectrum, indicating the separation is sufficiently reduced to where the two lines are not resolved. Consistent with this is the

observation that the 912-cm^{-1} line is only partially polarized instead of completely polarized or unpolarized. Thus the TcO_4^- is tetrahedral in aqueous solution in spite of the observed Raman spectrum exhibiting only two of the four lines expected. The 912-cm^{-1} line represents $\nu_1(A_1)$ and $\nu_3(F_2)$ unresolved, the 326-cm^{-1} line is $\nu_4(F_2)$, and $\nu_2(E)$ is unobserved because of its very weak intensity.

3. Chemical Separation of Isotopes

Ion Exchange Studies in Nonaqueous Solvents

D. A. Lee

The study of ion exchange phenomena in nonaqueous systems was continued: selectivity and diffusion coefficients were determined for alkali metal ions in Dowex 50 and ethylenediamine. Alkali metal thiocyanates were used as solutes because of their high solubility in ethylenediamine. The results of these studies are summarized in Table 3.1.

The larger cations, Cs^+ and K^+ , exchange at a slow rate, while Na^+ and Li^+ exchange rapidly, that is, approximately at the same rate as in aqueous solutions. The great difference between the exchange rates may be due to the relative solvating power of the alkali metal ions with ethylenediamine. The selectivities increase as

the resin cross-linkage increases, but this effect is much more pronounced for lithium and sodium than for potassium.

The effect of salt concentration on the diffusion and selectivity coefficients was determined for the system NaSCN-EDA vs the Na^+ form of Dowex 50-X8 with Cs^{134} tracer. The results are given in Table 3.2. The most rapid diffusion rate was associated with the dilute electrolyte solutions, in which film diffusion was presumably the limiting consideration. As the concentration of the electrolyte was increased to the range in which particle diffusion may be limiting, the diffusion rate decreased. Since other factors may contribute importantly to the diffusion rate at such concentrations, these data do not necessarily reflect pure particle diffusion coefficients; however, they

Table 3.1. Ion Exchange Diffusion and Selectivity Coefficients in Ethylenediamine

System	D_i (cm^2/sec)	K_M^{Cs}
Dowex 50-X1- Li^+ - Cs^* vs 0.1 N LiSCN-EDA	1.2×10^{-7}	16.1
Dowex 50-X8- Li^+ - Cs^* vs 0.1 N LiSCN-EDA	2.6×10^{-7}	58.5
Dowex 50-X16- Li^+ - Cs^* vs 0.1 N LiSCN-EDA	1.9×10^{-7}	400
Dowex 50-X1- Na^+ - Cs^* vs 0.1 N NaSCN-EDA	1.4×10^{-7}	11.0
Dowex 50-X8- Na^+ - Cs^* vs 0.1 N NaSCN-EDA	1.1×10^{-7}	27.9
Dowex 50-X16- Na^+ - Cs^* vs 0.1 N NaSCN-EDA	8.1×10^{-8}	~200
Dowex 50-X1- K^+ - Cs^* vs 0.1 N KSCN-EDA	1.1×10^{-9}	1.4
Dowex 50-X8- K^+ - Cs^* vs 0.1 N KSCN-EDA	4.7×10^{-10}	2.5
Dowex 50-X16- K^+ - Cs^* vs 0.1 N KSCN-EDA	1.4×10^{-10}	3.5
Dowex 50-X1- Cs^+ - Cs^* vs 0.1 N CsSCN-EDA	2.5×10^{-9}	
Dowex 50-X8- Cs^+ - Cs^* vs 0.1 N CsSCN-EDA	1.2×10^{-9}	
Dowex 50-X16- Cs^+ - Cs^* vs 0.1 N CsSCN-EDA	4.0×10^{-10}	

Table 3.2. The Effect of Solute Concentration on Diffusion and Selectivity Coefficients in Ethylenediamine

System	D_1 (cm^2/sec)	$K_{\text{Na}}^{\text{Cs}}$
Dowex 50-X8- Na^+ -Cs* vs 0.01 N NaSCN-EDA	3.6×10^{-7}	29
Dowex 50-X8- Na^+ -Cs* vs 0.05 N NaSCN-EDA	3.3×10^{-7}	27
Dowex 50-X8- Na^+ -Cs* vs 0.15 N NaSCN-EDA	1.3×10^{-7}	25
Dowex 50-X8- Na^+ -Cs* vs 0.29 N NaSCN-EDA	9.5×10^{-8}	26

are useful for comparison. The selectivity coefficients were not affected by concentration differences. It was observed that the selectivity coefficients varied from one batch of resin to another of the same labeled composition.

Lithium Isotope Separation Factors by Ion Exchange in Concentrated Solutions

D. A. Lee

The fractionation of lithium isotopes by means of ion exchange reactions has been studied extensively. For reasons of experimental convenience, essentially all of these studies have been performed with aqueous electrolyte concentrations of 0.25 N or less, there being no theoretical grounds for supposing any appreciable concentration dependence of the fractionation factor at higher electrolyte concentrations. Recently, however, Ciric and Pupezin reported¹ abnormally large lithium isotopic fractionation factors for systems employing the cation exchanger Amberlite IR-120 and 2 N solutions of LiCl. These results, if confirmed, would have important theoretical and practical consequences for the separation of lithium isotopes. Therefore an attempt was made to substantiate these findings. Amberlite IR-120 (lithium form) was equilibrated with an aqueous solution of 2 N LiCl. Thirty-six individual samples of each phase were carefully analyzed with a 6-in.-radius 60°-sector dual-collector mass spectrometer equipped for integrated measurements of m/e positions 6 and 7. The conditions and results of this experiment as well as those of Ciric and

Pupezin are given in Table 3.3. It may be seen that the results of Ciric and Pupezin were not substantiated. It seems likely that their abnormally large factors arose because of undetected isotopic fractionation of their samples in the mass spectrometer.

Anhydrous LiSCN

D. A. Lee

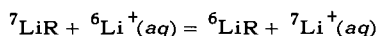
In the course of the study of nonaqueous ion exchange, a need arose for anhydrous LiSCN. No satisfactory method for the preparation of this salt could be found in the literature.² The following is a useful procedure which was developed for the preparation of this salt. Granular NH_4SCN and $\text{LiOH} \cdot \text{H}_2\text{O}$ were stirred together and gently warmed. Water and NH_3 were removed by vacuum distillation at low temperature ($\sim 60^\circ\text{C}$) until the solution recrystallized. Sufficient $(\text{C}_2\text{H}_5)_2\text{O}$ was then added to dissolve these crystals. The $\text{LiSCN} \cdot (\text{C}_2\text{H}_5)_2\text{O}$ was precipitated by the addition of petroleum ether to the ether solution. Some $(\text{C}_2\text{H}_5)_2\text{O}$ and traces of H_2O were removed from the $\text{LiSCN}(\text{C}_2\text{H}_5)_2\text{O}$ crystals by vacuum distillation with a slow increase in temperature ($\sim 25\text{--}110^\circ\text{C}$). The product contained 0.09% H_2O by Karl Fischer determination.

The melting point of LiSCN was determined from a heating curve to be 281°C . The heat of fusion was measured by the method of mixtures to be 5.0 ± 1.0 kcal (95% confidence interval). The

¹M. M. Ciric and J. D. Pupezin, *Bull. Inst. Nucl. Sci. "Boris Kidrich"* (Belgrade) 13(2), 29-45 (1962).

²D. W. Plester, S. E. Rogers, and A. R. Ubbelohde, *Proc. Roy. Soc. (London)* A235, 469 (1956); F. A. Schimmel, *J. Chem. Eng. Data* 5, 519 (1960); J. T. Shuttle, "The Alkali Metals," p 64 in *Comprehensive Inorganic Chemistry* (ed. by M. C. Sneed and R. C. Brasted), vol 6, Van Nostrand, Princeton, N.J., 1957.

Table 3.3. Single-Stage Batch Equilibration



	This Work	Ciric and Pupezin
Resin	Amberlite IR-120	Amberlite IR-120
Resin capacity, meq/ml wet resin	1.9	1.9
Resin size, mesh	20-50	50-100
Resin porosity	Medium	
Resin form	Li ⁺	Li ⁺
Volume wet resin, ml	28	1
Volume aqueous phase, ml	100	100
Concentration of LiCl in aqueous phase, <i>N</i>	2.0	2.0
Temperature, °C	24	
Equilibration time, min	30	5
Number of individual samples taken from each phase	36	
Mean ⁶ Li/ ⁷ Li, resin phase	12.594 ± 0.003	11.032 ± 0.004
Mean ⁶ Li/ ⁷ Li, liquid phase	12.626 ± 0.013	11.228 ± 0.005
Mean separation factor	1.003 ± 0.001	1.018 ± 0.001

entropy of fusion was 9.0 cal deg⁻¹ mole⁻¹. The change of volume on melting was determined by using a dilatometer. The molar volume change at 281°C was 2.58 ml. A thermogravimetric analysis of LiSCN showed that at 100°C there was a 1% increase in weight. However, this increase was lost at 150°C. From 150 to 400°C the weight did not change; above 400°C extensive weight loss occurred.

The solubility of LiSCN in about 40 organic solvents was determined. Generally, LiSCN was very soluble in amines, amides, ethers, alcohols, aldehydes, and esters, but insoluble in aliphatic and aromatic hydrocarbons.

Isotopic Chemistry of Boron

A. A. Palko

The exchange of boron between BF₃(gas) and the BF₃ complexes of nitrobenzene, ethyl ether, tetrahydrofuran, and ethyl sulfide was studied at several temperatures. The experimental techniques

were similar to those previously reported.³ Isotopic equilibrium constants, determined from these studies, are shown in Table 3.4. These data were corrected for solubility of BF₃ in the 1:1 liquid complex, assuming that the isotopic equilibrium constant for the reaction BF₃(gas) ⇌ BF₃(soln) is small compared to the data reported. The solubility of BF₃ in nitrobenzene and tetrahydrofuran is shown in Table 3.5. Corresponding data for ethyl ether were reported earlier.⁴

The solubility of BF₃ in nitrobenzene was considerably smaller than in the other solvents studied. However, at 7°C the isotopic equilibrium constant for this system was 1.032, a value very nearly equal to that observed in the ethyl ether-BF₃ system.

Isotopic equilibrium constants for the ethyl sulfide-BF₃ system are somewhat larger than those of other systems; nevertheless, for purposes

³A. A. Palko, *Chem. Div. Ann. Progr. Rept. June 20, 1961*, ORNL-3176, p 18.

⁴A. A. Palko, *Chem. Div. Ann. Progr. Rept. June 20, 1961*, ORNL-3176, p 19.

Table 3.4. Isotopic Equilibrium Constants for Several BF_3 Exchange Systems

$\text{Et}_2\text{O}\text{-BF}_3$		$\text{Et}_2\text{S}\text{-BF}_3$		Tetrahydrofuran- BF_3	
Temperature ($^{\circ}\text{C}$)	α	Temperature ($^{\circ}\text{C}$)	α	Temperature ($^{\circ}\text{C}$)	α
-32	1.052	-34	1.054	7	1.030
-22	1.040	-20	1.056	14	1.028
-10	1.037	-10	1.052	19	1.025
-3	1.039	0	1.045	29	1.023
22	1.032	8	1.046		
		10	1.047		
		20	1.038		
			1.037		
		28	1.033		

Table 3.5. Solubility of BF_3 in Tetrahydrofuran and Nitrobenzene

Temperature ($^{\circ}\text{C}$)	Moles of BF_3 per Mole of Organic			
	Nitrobenzene		Tetrahydrofuran	
	400 mm Hg	760 mm Hg	400 mm Hg	760 mm Hg
25	0.0255	0.050		
22	0.030	0.057	1.0050	1.0316
14	0.046	0.083	1.0111	1.0476
8	0.063	0.110	1.0206	1.0622
5	0.074	0.126		

of isotope separation, the anisole- BF_3 system possesses greater stability and general attractiveness.

Nitrogen Isotopic Separation Factors Between Selected Pairs of NO_3^- , NO_2^- , and NO

L. L. Brown

The isotopic separation factor for the exchange of nitrogen between NO_3^- and NO_2^- is of considerable theoretical interest because of its contribution to the overall isotopic fractionation achievable in the popular Nitrox system for enriching N^{15} . It has not been previously observed

in the laboratory because of the practical difficulties involved in separating the ionic species. These difficulties have now been overcome; the separation factors were measured in the following manner. Solutions 1 *M* in NaNO_2 and 1.5 *M* in HNO_3 were cooled to either 0° or 10°C long enough to reach isotopic equilibrium and then quenched with sodium hydroxide. The nitrogen species were chemically separated, by a variation of the Varner method,⁵ and individually converted to N_2 for isotopic assay. The observed separation

⁵J. E. Varner *et al.*, *Anal. Chem.* **25**, 1528 (1953).

factors (α) expressed in the form

$$\alpha = \frac{(N^{15}/N^{14})NO_3^-}{(N^{15}/N^{14})NO_2^-}$$

are shown in Table 3.6. The experimentally observed factors are lower than those calculated from spectroscopic data.⁶ This same situation exists for the NO_3^-/NO system measured earlier.^{7,8} The differences are probably due to the combination of experimental effects and spectroscopic uncertainties of the nitrogen species actually present in solution.

The only isotope data on the pair NO_2^-/NO are those of Nankane.⁹ His data show the dependence of the exchange rate on the acidity of the reaction media. Basic solutions of NO_2^- will not exchange with NO ; at the other extreme, highly acid solutions destroy the HNO_2 . New data show

that enriched NO will exchange with 1 M $NaNO_2$ (normal) in 0.027 M H_2SO_4 with moderate speed:

Time (hr)	NO Enrichment (% N^{15})
0	96.5
4.5	42.0
12.5	36.3
25	36.3
48	36.3
Equilibrium	36.6 (calc)

The single-stage separation factor was determined at 0° on the type of solution described above, using normal NO . From a series of four equilibrations and eight isotopic analyses, a value of 1.024 ± 0.002 (95% confidence interval) was obtained. Nitrogen-15 enriches in the NO_2^- .

Another estimate of the NO_2^-/NO factor may be had from the ratios of the NO_3^-/NO and NO_3^-/NO_2^- experimental separation factors. The quotient of these two factors eliminates the common NO_3^- term, and yields 1.029 for the NO_2^-/NO ratio. This value agrees well with the direct observation, but neither of them substantiates the value calculated from spectroscopic data.

⁶G. M. Begun and W. H. Fletcher, *J. Chem. Phys.* **33**, 1083 (1960).

⁷L. L. Brown and G. M. Begun, *J. Chem. Phys.* **30**, 1206 (1959).

⁸L. N. Kauder, T. I. Taylor, and W. Spindel, *J. Chem. Phys.* **31**, 232 (1959).

⁹R. Nankane, S. Isomaura, and O. Kurchara, *Kagaku Kenkyusho Hokoku* **33**, 335 (1957).

Table 3.6. Summary of Observed and Calculated Separation Factors of Some Nitrogen Exchange Systems

System	Temperature (°C)	Separation Factor ^a (α)		Reference
		Calculated	Observed	
$N^{15}O + N^{14}O_3^-$	0	1.092	1.088 ^b	c
	25	1.080	1.073	d
			1.065	e
$N^{15}O_2^- + N^{14}O_3^-$	0	1.074	1.057	c, this work
	10	1.071	1.055	
$N^{15}O + N^{14}O_2^-$	0	1.016	1.024	c, this work
			1.029	Line 1/line 4

$$^a \alpha = [(N^{15}/N^{14})NO_3^-] / [(N^{15}/N^{14})\text{Other}] \text{ or } [(N^{15}/N^{14})NO_2^-] / [(N^{15}/N^{14})NO].$$

^bExtrapolated as $\alpha = A/T + B/T^2$ from Stern, *J. Chem. Phys.* **34**, 333 (1961).

^cG. M. Begun and W. H. Fletcher, *J. Chem. Phys.* **33**, 1083 (1960).

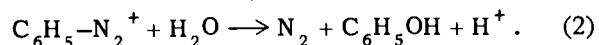
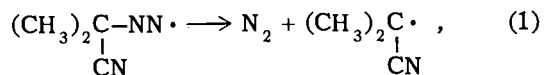
^dL. N. Kauder, T. I. Taylor, and W. Spindel, *J. Chem. Phys.* **31**, 232 (1959).

^eL. L. Brown and G. M. Begun, *J. Chem. Phys.* **30**, 1206 (1959).

Isotope Kinetic Effect in the Thermal Decomposition of Diazo Compounds

L. L. Brown

Nitrogen isotope effects in the thermal decomposition of two diazo compounds were measured at 40 and 60°C. The compounds were α, α' -azobisisobutyronitrile and benzenediazonium chloride, which decompose by first-order reactions to give nitrogen:



The rate constants for both reactions are well established in the literature, and are included in Table 3.7 for reference.

The isotope effect was determined by fractionally decomposing some of the material and comparing the isotope ratio of the product nitrogen with nitrogen from a 100% decomposed sample.

If one ascribes all of the kinetic effect to the nitrogen bonded to carbon, then an adjustment must be made in the observed isotope ratios because of an "inert" nitrogen atom in the sample. The kinetic effect equation has the form:

$$\frac{k^{14}}{k^{15}} = \frac{\log(1-f)}{\log(1-r_c f)}$$

where

f = fraction decomposed,

$$r_c = 2r_{ms} - 1,$$

$r_{ms} = (29/28)_{\text{sample}} / (29/29)_{\text{substrate}}$ which is obtained directly from isotope ratio mass spectrometer,

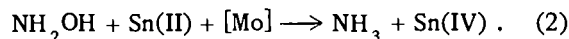
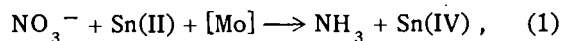
k^{14}/k^{15} = ratio of rate constants for the decomposition of pure N^{14} and N^{15} compounds.

The observed kinetic effects are collected in Table 3.7. Nitrogen-14 reacts more rapidly than N^{15} . Each value of k^{14}/k^{15} is the average of three or four individual determinations.

Isotope Effect in the Acid Reduction of Nitrate and Hydroxylamine

L. L. Brown

The reduction of nitrate to ammonia by Sn(II) in HCl solution first produces hydroxylamine as an intermediate. A subsequent reaction, the reduction of hydroxylamine to ammonia, is the rate-determining step.¹⁰ For this reason, any nitrogen isotope effect should be the same for the two single reactions:



¹⁰G. P. Haight, Jr., et al., *Acta Chem. Scand.* 15, 2026 (1961); 16, 221, 659 (1962).

Table 3.7. Rate Constants and Isotope Effects for Thermal Decomposition of Two Diazo Compounds

Compound	Temperature (°C)	k	Reference	k^{14}/k^{15} (±95% confidence interval)
Azobisisobutyronitrile	40	0.00405 hr ⁻¹	a	1.045 ± 0.001
	60	0.01196		1.046 ± 0.001
Benzenediazonium chloride	40	0.0246 min ⁻¹	b	1.044 ± 0.001

^aC. F. H. Bawn and S. F. Mellish, *Trans. Faraday Soc.* 47, 1216 (1951).

^bH. A. H. Pray, *J. Phys. Chem.* 30, 1417-77 (1926).

To confirm this observation experimentally, samples of NaNO_3 and NH_2OH were partially reduced at 25° and isotopic analyses were obtained from the product ammonia. The isotope ratios $\text{N}^{15}/\text{N}^{14}$ obtained in every run were quite precise and the isotope effects were small. Within experimental limits, the isotope effects are equal and support the mechanism of Haight. The observations of this work are summarized in Table 3.8.

Table 3.8. Isotope Effect in Reduction of NO_3^- and NH_2OH to NH_3 in HCl Solution

Reaction	$(k^{14}/k^{15})^a$	Number of Samples
$\text{NO}_3^- + \text{Sn(II)}$	1.007 ± 0.001^b	8
$\text{NH}_2\text{OH} + \text{Sn(II)}$	1.004 ± 0.002	13

^aSee following section for calculation of k^{14}/k^{15} .

^b95% confidence interval on average value of k^{14}/k^{15} .

Isotope Effect in the Alkaline Reduction of Nitrate, Nitrite, and Hydroxylamine

L. L. Brown

Ferrous ion was used to reduce NaNO_3 , NaNO_2 , and NH_2OH to ammonia in 5 M NaOH. In order to reduce nitrate, a catalyst such as silver sulfate is necessary. The other two reductions proceed without catalysis.

Various fractions of the nitrogen components were reduced by adding a controlled deficiency of ferrous sulfate solution. The product ammonia was distilled into standard HCl for quantitative analysis, and then converted to N_2 for isotopic analysis. Experiments were performed at 25 and 110°C . Isotopic analyses were obtained as the ratio of $\text{N}^{15}/\text{N}^{14}$ in the product NH_3 to that of the nitrogen in the original compound.

The isotope effect between N^{14} and N^{15} was calculated from the equation

$$\frac{k^{14}}{k^{15}} = \log(1-f)/\log(1-rf),$$

where

k^{14}/k^{15} = the ratio of the rate constants for reduction of the pure N^{14} and N^{15} species,

f = the fraction of material reduced,

$r = (\text{N}^{15}/\text{N}^{14})_{\text{product}}/(\text{N}^{15}/\text{N}^{14})_{\text{original}}$.

This equation is based on a first-order reaction of nitrogen and is plausible but not yet established. The values of k^{14}/k^{15} obtained are shown in Table 3.9. Since mechanisms have not yet been determined for these reactions, the significance of the isotope effects is not clear. Evidently, the rate-determining step for the reduction of NO_2^- is similar to that for NH_2OH and quite different from that for NO_3^- . As expected, N^{14} is reduced more rapidly than N^{15} for all three compounds.

Table 3.9. Nitrogen Isotope Effect in the Reduction of Certain Nitrogen Compounds

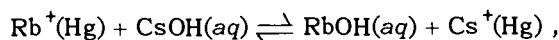
Reaction	25°		110°	
	k^{14}/k^{15}^a	Number of Samples	k^{14}/k^{15}^a	Number of Samples
$\text{NO}_3^- \rightarrow \text{NH}_3$	1.070 ± 0.007	5	1.058 ± 0.007	4
$\text{NO}_2^- \rightarrow \text{NH}_3$	1.033 ± 0.001	3	1.028 ± 0.003	12
$\text{NH}_2\text{OH} \rightarrow \text{NH}_3$	1.032 ± 0.003	3	1.029 ± 0.002	6

^a95% confidence interval on average value of k^{14}/k^{15} .

Alkali Metal Separation

Donald Zucker

The single-stage separation factor, α , for rubidium and cesium in the system



$$\alpha = \frac{(\text{Cs}^+/\text{Rb}^+)(\text{Hg})}{(\text{CsOH}/\text{RbOH})(\text{aq})},$$

was measured at temperatures from 0 to 70°C and at total concentrations (i.e., rubidium plus cesium) of 0.02, 0.2, and 1.0 *M*. In each equilibration the total alkali metal concentration in moles per liter was the same in aqueous and amalgam phases, and the total moles of rubidium in the entire system the same as the total moles cesium. Amalgams were prepared electrolytically, with a very small holding current being applied to maintain the proper concentration during equilibration. Assay was by flame analysis.

Separation was greater at lower temperatures and at lower concentrations, with cesium concentrating in the amalgam phase in all cases. The least-squares plots of $\log_{10} \alpha$ vs $1/T$ fit the experimental data quite well. Values taken from the least-squares equations are given in Table 3.10.

In order to predict the effects of alkali metal impurities on the assay of potassium isotopes separated by an amalgam process, separation factors for low concentrations of sodium, rubidium, and cesium were measured with respect to potassium in an aqueous hydroxide and amalgam system, both phases being about 0.22 *M* in potassium. The sodium, rubidium, and cesium, each present initially to about 1% of the total alkali content, all concentrated in the amalgam phase. The temperature was $25 \pm 0.5^\circ\text{C}$. Results for the

single-stage separation factors,

$$\alpha = \frac{(\text{M}^+/\text{K}^+)_{\text{Hg}}}{(\text{M}^+/\text{K}^+)_{\text{aq}}},$$

were: sodium, 1.9; rubidium, 1.19; cesium, 3.0.

Preparation of Beryllium Amalgam

Donald Zucker

Liquid amalgams are interesting and useful vehicles for the study of chemical exchange reactions. For this reason, attempts were made to prepare an amalgam of beryllium. In initial experiments, attempts were made to electrolyze beryllium into mercury from aqueous solutions of $\text{Be}(\text{OH})_2$ and BeSO_4 or BeCl_2 .

Subsequently these efforts were repeated, using, instead of the aqueous solutions, organic solutions of beryllium acetylacetonate dissolved in 2-aminoethanol, 1,2-diaminopropane, 1,2-diaminoethane, or a mixture of *N*-methylacetamide and ethanol. Dimethylberyllium dissolved in ethyl ether was also tried. Finally, powdered beryllium metal was heated with mercury in a sealed quartz tube at 650°C for 1 hr. None of these attempts produced solutions containing as much as 20 ppm of beryllium at room temperature. Thus, it appears that this figure represents an upper limit of the solubility of beryllium in mercury.

Fluorine-19 NMR Spectra of Xenon Fluorides

A. C. Rutenberg

The ^{19}F magnetic resonance spectra of XeF_2 , XeF_4 , XeOF_4 , and XeF_6 were obtained using a

Table 3.10. Rubidium-Cesium Separation Factor, α

Concentration Rubidium + Cesium (moles/liter)	Temperature ($^\circ\text{C}$)								95% Confidence Limit
	0	10	20	30	40	50	60	70	
0.02	3.34	3.01	2.73	2.49	2.29	2.11	1.96	1.80	0.18
0.2	3.11	2.78	2.52	2.29	2.09	1.92	1.77	1.65	0.09
1.0	2.65	2.43	2.23	2.06	1.92	1.79	1.68	1.58	0.09

Varian high-resolution spectrometer operating at a fixed frequency of 56.4 Mc. The samples were in quartz capillaries, each containing about 10 mg of a xenon compound.

No signals were obtained with solid XeF_2 or XeF_4 . A single broad peak was observed for both solid and molten XeF_6 . Molten XeF_2 gave a broad peak barely visible above the background noise. Liquid XeF_4 and XeOF_4 both gave spectra consisting of two lines symmetrically distributed about a stronger center line. The center line results from fluorine atoms bonded to the zero-spin isotopes of xenon. The two outside lines result from the spin coupling of ^{19}F with ^{129}Xe (spin $\frac{1}{2}$). The ^{19}F spin coupling with ^{131}Xe was not observed, presumably due to quadrupole relaxation. The experimental data obtained in this study are presented in Table 3.11.

The spectra of XeF_4 and XeOF_4 both indicate the magnetic equivalence of the four fluorine atoms in each of the compounds. This is in agreement with the square planar structure reported¹¹ for XeF_4 and the fourfold symmetry axis shown¹² by the Raman and infrared spectra of XeOF_4 .

The chemical shifts for the four compounds are in a logical order; the higher numbers indicate a greater degree of shielding of the ^{19}F nuclei.

¹¹J. H. Burns, P. A. Agron, and H. A. Levy, *Science* **139**, 1208 (1963).

¹²D. F. Smith, *Science* **140**, 899 (1963).

Table 3.11. Chemical Shifts and Spin Coupling Constants for Xenon Fluorides

Compound	Temperature (°C)	Chemical Shift ^a (ppm)	J (cps) ^b
XeF_2 (liquid)	132	~600 ^c	
XeF_4 (liquid)	114	445	3836
XeOF_4 (liquid)	26	329	1127
XeF_6 (solid)	26	330	
XeF_6 (liquid)	56	340	

^aFrom $\text{F}_2 \equiv 0$.

^b ^{19}F - ^{129}Xe spin-spin coupling constant.

^cEstimate from scope trace.

The δ values seem to bear closest resemblance to the iodine fluorides.¹³

Table 3.12 shows a comparison of spin-spin coupling constants for fluorides of xenon, antimony, and tellurium. The J values have been adjusted (J^*) to compensate for the difference in magnetogyric ratios of the nuclei involved. It is reasonable to expect XeF_4 to have a larger J value than XeF_6 , as is true of other series of fluoride compounds.¹⁴ Assuming a J^* value for XeF_6 comparable to FeF_6 , the J^* value for XeF_4 does not seem out of line. Data for compounds analogous to XeOF_4 are not available.

The NMR spectra to date fail to reveal any major difference between the xenon compounds and compounds of their analogous neighbors in the periodic table. The compounds used in this investigation were prepared by D. F. Smith, Technical Division, Oak Ridge Gaseous Diffusion Plant, Oak Ridge, Tennessee.

Table 3.12. Spin-Spin Coupling Constants for Fluorides of Xenon, Antimony, and Tellurium

Compound	J (cps)	J^* (cps)	Reference
$^{129}\text{XeF}_4$	3836	13,040	This work
$^{129}\text{XeOF}_4$	1127	3,830	This work
$^{121}\text{SbF}_6^-$	1937	7,610	b
$^{125}\text{TeF}_6$	3688	10,980	c

$${}^a J^* = \frac{J_{\text{MF}}}{\gamma_{\text{M}}/\gamma_{\text{F}}}$$

^bW. G. Proctor and F. C. Yu, *Phys. Rev.* **81**, 20 (1951).

^cE. L. Muetterties and W. D. Phillips, *J. Am. Chem. Soc.* **81**, 1084 (1959).

NMR Studies of BF_3 Addition Compounds

A. C. Rutenberg A. A. Palko

Boron trifluoride forms stable 1:1 molecular addition compounds with methyl and ethyl ethers. In systems containing BF_3 and mixtures of these

¹³H. S. Gutowsky and C. J. Hoffman, *J. Chem. Phys.* **19**, 1259 (1951).

¹⁴E. L. Muetterties and W. D. Phillips, *J. Am. Chem. Soc.* **81**, 1084 (1959).

ethers, exchange of BF_3 occurs between the ether species. Although this exchange is too rapid to be observed by conventional techniques, it may be measured conveniently with a nuclear magnetic resonance spectrometer. The ^{19}F resonance for BF_3 addition compounds offers the combination of a strong signal, which is fairly narrow in the absence of chemical exchange, plus large chemical shifts between different BF_3 addition compounds. It is, therefore, suitable for quantitative kinetic studies. The spectra for two ether· BF_3 complexes are very simple, consisting at low temperature of a pair of peaks which, as the temperature is raised, broaden, merge, and fuse to a single peak. The mean lifetimes (τ) of the BF_3 complexes were calculated from line-width and peak-separation data obtained by use of audio sideband techniques. A discussion of time-dependent factors influencing signal shape and method of calculating τ are described by Pople, Schneider, and Bernstein.¹⁵

¹⁵J. A. Pople, W. G. Schneider, and H. J. Bernstein, *High-Resolution Nuclear Magnetic Resonance*, chap. 10, McGraw-Hill, New York, 1959.

A study of the exchange of BF_3 between $(\text{CH}_3)_2\text{O}\cdot\text{BF}_3$ and $(\text{C}_2\text{H}_5)_2\text{O}\cdot\text{BF}_3$ has been completed. The ^{19}F resonance for BF_3 complexed with $(\text{CH}_3)_2\text{O}$ appears at a field strength 5.3 ppm above the corresponding $(\text{C}_2\text{H}_5)_2\text{O}\cdot\text{BF}_3$ complex. This large chemical shift permits very rapid exchanges to be observed, and mean lifetimes (τ) as short as 1.5×10^{-5} sec were measured for this system.

The initial and equilibrium compositions of the eight mixtures studied are presented in Table 3.13.

For mixtures A through F, the quantities of the four species at equilibrium were calculated from the known amounts of the three components used to prepare the mixture, and the measured location of the single peak at 26°. The equilibrium constants indicate a preference of the BF_3 for $(\text{CH}_3)_2\text{O}$. Values of these constants in the temperature range -40 to -60°C based on peak-area measurements differed only slightly from the 26°C results.

The mean lifetimes of the BF_3 addition compounds are shown in Table 3.13. The τ values

Table 3.13. Characteristics of the $(\text{CH}_3)_2\text{O}\text{-}(\text{C}_2\text{H}_5)_2\text{O}\text{-BF}_3$ Systems

	A	B	C	D	E	F	G	H
Initial composition								
$(\text{C}_2\text{H}_5)_2\text{O}$ (moles)	1.00	1.00	1.00	1.00	1.00	1.00	1.00	1.00
$(\text{CH}_3)_2\text{O}$ (moles)	0.30	0.34	0.51	0.69	0.34	1.01	1.00	1.00
BF_3 (moles)	0.41	0.67	0.78	1.06	0.89	1.61	1.91	2.00
Equilibrium composition at 26°C								
$(\text{C}_2\text{H}_5)_2\text{O}\cdot\text{BF}_3$ (moles/liter)	1.78	3.17	2.79	3.56	4.17	3.52	4.46	4.59
$(\text{CH}_3)_2\text{O}\cdot\text{BF}_3$ (moles/liter)	1.28	1.56	2.18	2.56	1.92	4.15	4.55	4.59
$(\text{C}_2\text{H}_5)_2\text{O}$ (moles/liter)	5.73	3.87	3.63	2.21	2.63	1.27	0.13	0.00
$(\text{CH}_3)_2\text{O}$ (moles/liter)	0.99	0.86	1.09	1.42	0.42	0.67	0.06	0.00
K_{eq} (exp) ^a	4.2	2.2	2.6	1.1	2.9	2.2	2.2 ^b	
$\tau \times 10^5$ at 0°C (sec)	3.1	3.6	6.7	10	17	28	260	670
95% confidence limits on τ	0.4	0.8	0.3	1	2	1	10	64
ΔE (kcal/mole)	11.1	11.1	11.4	11.7	11.0	10.1	14.0	16.1
95% confidence limits on ΔE	0.8	0.7	0.7	0.5	0.8	0.2	0.3	0.7
Peak coalescing temperature (°C)	-37.6	-34.5	-28.0	-23.0	-20.5	-14.5	+13.8	+22.0

$${}^a K_{\text{eq}} = \frac{[(\text{CH}_3)_2\text{O}\cdot\text{BF}_3][(\text{C}_2\text{H}_5)_2\text{O}]}{[(\text{C}_2\text{H}_5)_2\text{O}\cdot\text{BF}_3][(\text{CH}_3)_2\text{O}]}$$

^b Assumed and used to compute composition.

at 0°C for the various mixtures were obtained from the least-squares line. At a τ of 7.6×10^{-4} sec, the NMR peaks for the two addition compounds merge to give a single peak.

Figure 3.1 shows the experimentally determined τ values plotted as a function of reciprocal temperature. The lines shown are the least-squares straight lines.

In the temperature range of this study, the rate of exchange decreased as a larger portion of the ethers was complexed. The 0°C τ value increased 215-fold on going from 31 to 100% complexed ether.

An activation energy of about 11 kcal was measured for the exchange of BF_3 between $(\text{C}_2\text{H}_5)_2\text{O} \cdot \text{BF}_3$ and $(\text{CH}_3)_2\text{O} \cdot \text{BF}_3$ for those mixtures which had a significant excess of the uncomplexed ether. There was a sharp increase in ΔE when most of the ether had been complexed, rising to 16.1 kcal for the completely complexed mixture. Mixture F, which exhibited a slightly lower ΔE , was overheated during a malfunction of the equipment and, as a result, contained several percent of the mixed ether $\text{C}_2\text{H}_5\text{OCH}_3$.

The data indicate the existence of two modes of exchange. The prevailing mechanism when little free ether is present is associated with a higher activation energy and a much slower rate of exchange (large τ) than is the process which predominates when an appreciable quantity of free ether is present. In the presence of uncomplexed

ether, the exchange mechanism undoubtedly involves the transfer of a BF_3 molecule from the complex to the free ether. This exchange appears to proceed by way of a displacement rather than by a dissociation mechanism since the activation energy for the exchange is somewhat less than the heat of formation of the BF_3 -ether complexes.^{16,17} An exchange reaction proceeding by a BF_3 transfer to an uncomplexed ether should require less rearrangement of the solution, and, hence, be characterized by a smaller activation energy than the exchange of BF_3 between $(\text{CH}_3)_2\text{O} \cdot \text{BF}_3$ and $(\text{C}_2\text{H}_5)_2\text{O} \cdot \text{BF}_3$. Accordingly, the completely complexed mixture displays a slower rate of exchange and a higher activation energy than the other mixtures.

A study of the system $\text{C}_6\text{H}_5\text{OCH}_3 - (\text{C}_2\text{H}_5)_2\text{O} \cdot \text{BF}_3$ is in progress. This system differs from the previous one in several respects. The equilibrium constant greatly favors the $(\text{C}_2\text{H}_5)_2\text{O} \cdot \text{BF}_3$ complex; therefore, the mixture contains almost no free $(\text{C}_2\text{H}_5)_2\text{O}$ and the composition does not change with temperature. The chemical shift between $\text{C}_6\text{H}_5\text{OCH}_3 \cdot \text{BF}_3$ and $(\text{C}_2\text{H}_5)_2\text{O} \cdot \text{BF}_3$ is smaller than the $(\text{C}_2\text{H}_5)_2\text{O} \cdot \text{BF}_3 - (\text{CH}_3)_2\text{O} \cdot \text{BF}_3$

¹⁶D. E. McLaughlin and M. Tamres, *J. Am. Chem. Soc.* **82**, 5618 (1960).

¹⁷P. Diehl, *Helv. Phys. Acta* **31**, 685 (1958).

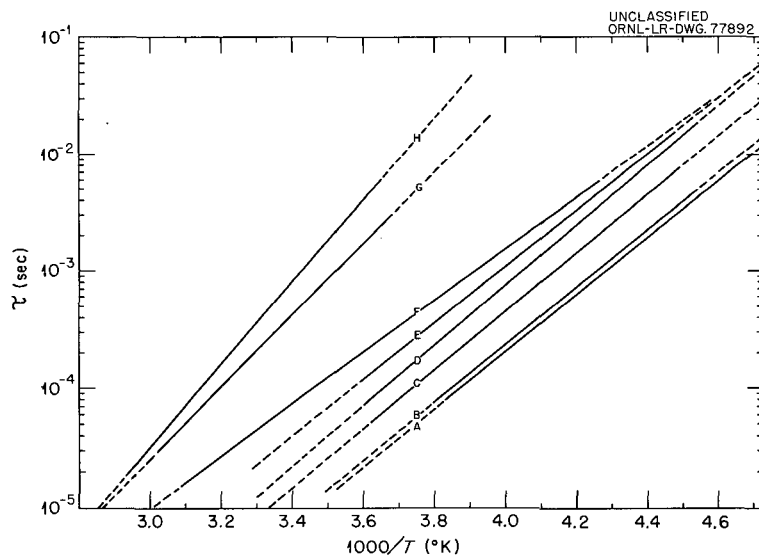


Fig. 3.1. Temperature Dependence of τ for Various Mixtures of BF_3 , $(\text{CH}_3)_2\text{O}$, and $(\text{C}_2\text{H}_5)_2\text{O}$. Solid portion of lines indicates range over which data were taken. Compositions of mixtures are listed in Table 3.13.

shift and is temperature and composition dependent. A mixture containing a significant excess of anisole at -25°C would display an anisole $\cdot\text{BF}_3$ peak 1.5 ppm below $(\text{C}_2\text{H}_5)_2\text{O} \cdot \text{BF}_3$.

Some preliminary data for five mixtures studied to date are presented in Table 3.14. The mean lifetimes are about an order of magnitude longer than in the corresponding $(\text{CH}_3)_2\text{O}$ system.

It is of interest to compare the results of the $\text{BF}_3\text{-(CH}_3)_2\text{O-(C}_2\text{H}_5)_2\text{O}$ study with the ^{19}F data of Diehl¹⁷ for the system $\text{BF}_3\text{-CH}_3\text{OH-C}_2\text{H}_5\text{OH}$. His values of $\tau \times 10^5$ at 0° , estimated from a graph in his paper, were 87 at $\text{BF}_3/\Sigma \text{ alcohol} = 0.8$ and 1000 at $\text{BF}_3/\Sigma \text{ alcohol} = 0.4$. The activation energies for the corresponding systems were reported, respectively, as 7.3 ± 1 kcal, and "about the same within greater limits of error." The rate of exchange in the alcohol system increased rapidly with BF_3 content for mixtures of $\text{BF}_3/\text{alcohol} > 0.5$. The effect of changing the BF_3 content, thus, was opposite in direction to that observed in the present study.

This divergent behavior of the alcohol systems appears to result from a hydrogen bonding effect which has no counterpart in the ether system. For $\text{BF}_3/\text{alcohol}$ ratios less than 0.5, dialcohol complexes of BF_3 are formed in which two alcohol molecules are associated through hydrogen bonding. With increasing $\text{BF}_3/\text{alcohol}$ ratios, progressively smaller mole fractions of the more stable BF_3 -dicomplex are to be found in the system, qualitatively accounting for the increase in exchange rate.

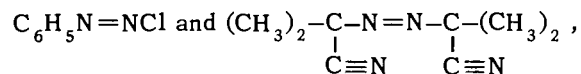
Isotopic Mass Spectral Program

L. Landau

The $\text{B}^{10}/\text{B}^{11}$ ratios were determined from BF_3 samples by measuring the mass spectral peak heights at mass positions 10 and 11 and also at 48 and 49. The BF_3 samples were obtained from $(\text{C}_2\text{H}_5)_2\text{O} \cdot \text{BF}_3$, $(\text{C}_2\text{H}_5)_2\text{S} \cdot \text{BF}_3$, $\text{C}_6\text{H}_5\text{NO}_2 \cdot \text{BF}_3$, and tetrahydrofuran $\cdot \text{BF}_3$, each equilibrated with BF_3 at several temperatures, and each was compared with the $\text{B}^{10}/\text{B}^{11}$ ratios in tank BF_3 . There were some discrepancies between separation factors measured at 10 and 11 compared with those measured at 48 and 49, but the combined data yielded separation factors reliable to ± 0.002 at the 95% confidence level.

The percent of O^{17} and O^{18} in water from the "O¹⁷ Pilot Plant" was determined routinely by equilibrating the water with a small quantity of CO_2 , of known $\text{C}^{13}/\text{C}^{12}$ ratio, for 30 min in a shaker. The CO_2 was then assayed by measuring the heights of the mass peaks at 44, 45, 46, 47, 48, and 49.

From experiments concerned with the isotope kinetic effects during the thermal decomposition of



and the chemical reduction of NH_2OH , NO_2^- , and NO_3^- , nitrogen samples were prepared and compared with reference nitrogen samples. The NO_2^- and NO_3^- were equilibrated at several temperatures, and each phase separately converted to

Table 3.14. Characteristics of the $\text{C}_6\text{H}_5\text{OCH}_3\text{-(C}_2\text{H}_5)_2\text{O-BF}_3$ System

$\text{BF}_3/\Sigma \text{ ether}$ (mole ratio)	0.13	0.30	0.50	0.73	0.885
Equilibrium concentration (moles/liter)					
$(\text{C}_2\text{H}_5)_2\text{O} \cdot \text{BF}_3$	0.59	1.29	2.04	2.71	3.76
$\text{C}_6\text{H}_5\text{OCH}_3 \cdot \text{BF}_3$	0.57	1.28	2.04	2.95	2.93
$\text{C}_6\text{H}_5\text{OCH}_3$	7.80	6.00	4.09	2.09	0.86
$\tau \times 10^5$ at 0°C (sec)	39	60	92	155	280
ΔE (kcal/mole)	10.6	12.5	12.0	13.1	14.4
95% confidence limits on ΔE	0.5	0.5	0.6	0.4	0.5

nitrogen; NO and NO₂⁻ were also equilibrated and each phase converted to nitrogen. The nitrogen samples from the separate phases were compared at mass positions 29 and 28 by dual collection to give a value for the instantaneous 29/28 ratio in one sample and then the 29/28 ratio in the other. This comparison was made between five and ten times for each pair of samples to obtain separation factors, or relative rates of decomposition of the N¹⁴ and N¹⁵ species. Separation factors, when comparable, agreed approximately to ±0.0015 at the 95% confidence level. These deviations were largely due to experimental difficulties of sample preparation; the internal consistency for any one pair of samples was about ±0.0003.

Two sets of CO₂ samples were prepared by L. L. Brown in 1958, one set having a higher C¹³/C¹² ratio than normal. Since that time pairs of these samples have been compared for their 45/44 (set 1)/45/44 (set 2) ratio. The average of 13 such determinations was 1.03032 ± 0.00009 at the 95% confidence level. Each determination represents approximately ten comparisons of 45/44 in set 1 to 45/44 in set 2. These data are shown in Table 3.15.

Table 3.15. Precision of CO₂ Analyses

Run No.	45/44 Set 1	Δ	Δ ²
	45/44 Set 2		
		× 10 ⁻⁵	× 10 ⁻¹⁰
1	1.03020	12	144
2	1.03025	7	49
3	1.03030	2	4
4	1.03038	6	36
5	1.03058	26	676
6	1.03060	28	784
7	1.03025	7	49
8	1.03033	1	1
9	1.03020	12	144
10	1.03045	13	169
11	1.03017	15	225
12	1.03013	19	361
13	1.03028	4	16

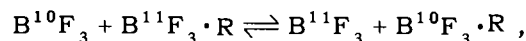
$$S = \frac{\sum \Delta^2}{n - 1} = 14.9 \times 10^{-5}$$

$t(0.05, 12) = 2.179$
 Average = 1.03032 ± 0.00009 (95% confidence limit)

Raman and Infrared Spectral Studies

G. M. Begun¹⁸

Infrared and Raman spectral studies of isotopic molecules provide fundamental information from which isotopic exchange equilibrium constants can be calculated. For a number of years a program of studying the spectra of addition complexes of BF₃ substituted with B¹⁰ and B¹¹ isotopes has been under way. The studies of the BF₃·dimethyl ether complex were previously published.¹⁹ The isotopic exchange equilibrium constant calculations and measurements for the system BF₃·BF₃·(CH₃)₂O described in last year's report²⁰ were completed and published.²¹ Infrared and Raman spectral studies of the boron isotopic species of BF₃·diethyl ether and BF₃·tetrahydrofuran were completed and published. Representative spectra can be found in this publication.²² The results were compared with those obtained for the BF₃·dimethyl ether complex, and assignments of the skeletal vibrations were made. These assignments are summarized in Table 3.16. Isotopic equilibrium constants were calculated for the reaction



where R is diethyl ether or tetrahydrofuran. These are shown in Table 3.17 along with previous results for the BF₃·dimethyl ether complex. The calculated equilibrium constants are compared with experimental values in Table 3.18. The agreement between the calculated and observed equilibrium constants is quite good.

The vibrational spectrum of aqueous oxalate ion has been studied by a number of investigators, and the frequency assignments and structure have been discussed several times. In several cases it was assumed that the oxalate ion had planar (*D*_{2h}) symmetry and assignments were made by analogy

¹⁸W. H. Fletcher of the University of Tennessee Chemistry Department consulted on much of this work.

¹⁹G. M. Begun, W. H. Fletcher, and A. A. Palko, *Spectrochim. Acta* **18**, 655-65 (1962).

²⁰G. M. Begun and W. H. Fletcher, *Chem. Div. Ann. Progr. Rept. June 20, 1962*, ORNL-3320, p 26.

²¹A. A. Palko, G. M. Begun, and L. Landau, *J. Chem. Phys.* **37**, 552-55 (1962).

²²G. M. Begun and A. A. Palko, *J. Chem. Phys.* **38**, 2112 (1963).

Table 3.16. Assignment of Skeletal Frequencies for $\text{BF}_3 \cdot \text{Dimethyl Ether}$,
 $\text{BF}_3 \cdot \text{Diethyl Ether}$, and $\text{BF}_3 \cdot \text{Tetrahydrofuran}$

$\text{BF}_3 \cdot \text{Dimethyl Ether}$		$\text{BF}_3 \cdot \text{Diethyl Ether}$		$\text{BF}_3 \cdot \text{Tetrahydrofuran}$		Assignment
B^{10}	B^{11}	B^{10}	B^{11}	B^{10}	B^{11}	
322	322	306	306	299	299	O (R) ₂ wag
344	344	333	333	337	337	O (R) ₂ rock
499	499	425	425	374	374	C—O—C deformation
506	506	504	502	505	503	BF_3 deformation
672	661	678	664	637	626	B—O stretch
810	805	758	756	729	727	B—F stretch (sym)
		833	831	871	871	C—C stretch
925	918	887	879	814	806	C—O stretch
		904	904			CH_3 rock
				924	922	C—C stretch (sym)
1020	1020	1005	1005	1007	1007	C—O stretch
		1097	1097	1049	1049	C—C stretch
1225	1177	1210	1163	1192	1156	BF_3 stretch (antisym)
1259	1216	1252	1210	1258	1206	BF_3 stretch (antisym)

with N_2O_4 . The bond joining the two carbon atoms in the oxalate ion is essentially a single bond, and there seems to be no reason to expect the ion to assume a planar configuration in solution. Further study of the oxalate ion was undertaken when our work showed that several bands of N_2O_4 ,²³ on which oxalate assignments had been based by analogy, were erroneously assigned. A special effort was made to observe as many Raman and infrared lines as possible in concentrated aqueous oxalate solutions.

Representative Raman spectra of oxalate solutions in H_2O and D_2O are shown in Fig. 3.2. The Raman line at $\sim 1650 \text{ cm}^{-1}$, which has been used in previous assignments, is seen to shift to 1220 cm^{-1} when D_2O is substituted for H_2O . This clearly demonstrates that this band is due to the bending vibration of water. The medium-strength line at 1579 cm^{-1} was not reported by previous workers although it has been seen in the infrared.

The infrared spectra of aqueous oxalate solutions were also studied using both H_2O and D_2O as solvent. It was found necessary to study the spectra of KBr disks and mineral oil mulls of sodium and potassium oxalates in order to observe the low vibrational frequencies. Table 3.19 lists the fundamental vibrational frequencies selected from the data and our assignments of the vibrations. The existence of three coincidences between the infrared and Raman spectra indicates that the free ion cannot have D_{2h} (planar) symmetry. The small number of Raman lines points to D_{2d} symmetry, and our assignment of the fundamental vibrational frequencies has been made on this basis.

The synthesis of the xenon fluorides at Argonne National Laboratory²⁴ has opened the door to a whole series of new compounds. A number of these compounds were prepared at the Oak Ridge Gaseous Diffusion Plant by D. F. Smith, and we

²³G. M. Begun and W. H. Fletcher, *J. Mol. Spectry.* 4, 388 (1960).

²⁴H. H. Claassen, H. Selig, and J. G. Malm, *J. Am. Chem. Soc.* 84, 3593 (1962).

Table 3.17. Calculated Equilibrium Constants for Boron Isotope Exchange

T (°K)	$\frac{Q(\text{B}^{11}\text{F}_3)}{Q(\text{B}^{10}\text{F}_3)}$	$\frac{Q[\text{B}^{11}\text{F}_3 \cdot \text{O}(\text{CH}_3)_2]}{Q[\text{B}^{10}\text{F}_3 \cdot \text{O}(\text{CH}_3)_2]}$	$\frac{Q[\text{B}^{11}\text{F}_3 \cdot \text{O}(\text{C}_2\text{H}_5)_2]}{Q[\text{B}^{10}\text{F}_3 \cdot \text{O}(\text{C}_2\text{H}_5)_2]}$	$\frac{Q[\text{B}^{11}\text{F}_3 \cdot \text{OC}_4\text{H}_8]}{Q[\text{B}^{10}\text{F}_3 \cdot \text{OC}_4\text{H}_8]}$	α^a		
					$\text{BF}_3 \cdot \text{O}(\text{CH}_3)_2$	$\text{BF}_3 \cdot \text{O}(\text{C}_2\text{H}_5)_2$	$\text{BF}_3 \cdot \text{OC}_4\text{H}_8$
250	1.310	1.256	1.258	1.243	1.043	1.041	1.053
273.16	1.270	1.222	1.224	1.211	1.039	1.038	1.048
298.16	1.235	1.193	1.194	1.183	1.035	1.034	1.044
325	1.205	1.167	1.168	1.159	1.032	1.031	1.040
350	1.182	1.148	1.148	1.126	1.030	1.029	1.036
400	1.146	1.118	1.118	1.112	1.025	1.025	1.031

$$^a\alpha = \frac{[\text{B}^{10}\text{F}_3 \cdot \text{R}](\text{liq})/[\text{B}^{11}\text{F}_3 \cdot \text{R}](\text{liq})}{[\text{B}^{10}\text{F}_3](\text{g})/[\text{B}^{11}\text{F}_3](\text{g})}, \text{ where R} = (\text{CH}_3)_2\text{O}, (\text{C}_2\text{H}_5)_2, \text{ or tetrahydrofuran.}$$

Table 3.18. Equilibrium Constants for Boron Isotope Exchange Between BF_3 and BF_3 Ether Complexes

T ($^{\circ}\text{K}$)	Equilibrium Constant (α) ^a								
	$\text{BF}_3 \cdot \text{O}(\text{CH}_3)_2$			$\text{BF}_3 \cdot \text{O}(\text{C}_2\text{H}_5)_2$			$\text{BF}_3 \cdot \text{O}(\text{C}_4\text{H}_{10})$		
	Calculated	Observed	Ref	Calculated	Observed	Ref	Calculated	Observed	Ref
250	1.043	1.041	<i>b</i>	1.041			1.053		
273	1.039	1.034	<i>b</i>	1.038			1.048		
293	1.035	1.029	<i>b</i>	1.035	1.034	<i>c</i>	1.044	1.036	<i>f</i>
					1.031	<i>d</i>		(298 $^{\circ}\text{K}$)	
343	1.030			1.029	1.028	<i>e</i>	1.037		
					1.026	<i>c</i>			
					(348 $^{\circ}\text{K}$)				

$${}^a\alpha = \frac{[\text{B}^{10}\text{F}_3 \cdot \text{ether}](\text{liq})/[\text{B}^{11}\text{F}_3 \cdot \text{ether}](\text{liq})}{[\text{B}^{10}\text{F}_3](\text{g})/[\text{B}^{11}\text{F}_3](\text{g})}$$

^bG. M. Begun and W. H. Fletcher, *Chem. Div. Ann. Progr. Rept. June 20, 1962*, ORNL-3320, p 26.

^cR. W. McIlroy and F. C. W. Pummery, p 180 in *Proceedings of the International Symposium on Isotope Separation*, North Holland Publishing Co., Amsterdam, 1958.

^dS. V. Ribnikar, *ibid.*, p 204.

^eK. E. Holmberg, *ibid.*, p 201.

^fS. V. Ribnikar and G. A. Bootsma, *Bull. Inst. Nucl. Sci. "Boris Kidrich" (Belgrade)* 1, 91 (1959).

were afforded the opportunity of observing the Raman spectra of solid and gaseous XeF_2 , solid XeF_4 , solid XeF_6 , and liquid XeOF_4 . The techniques used were by no means routine, and special cells were developed in most cases. Conical glass cells were used for the solid XeF_2 and XeF_4 . For gaseous XeF_2 a quartz cell wrapped with heating wire was used in order to obtain sufficient vapor pressure in the gas phase. Liquid XeOF_4 was found to attack glass rapidly, and a sealed quartz liquid cell was developed in which to observe its spectrum. This cell is shown in Fig. 3.3 filled with liquid XeOF_4 . Since XeF_6 attacks quartz, a conical fluorothene cell was developed to hold the solid XeF_6 . This cell failed shortly after the spectral observations and subsequently exploded while immersed in potassium hydroxide solution for disposal of the sample.

Representative Raman spectra of solid XeF_2 , solid XeF_4 , solid XeF_6 , and liquid XeOF_4 are shown in Figs. 3.4–3.7 respectively. The Raman spectrum of XeF_2 shows two strong lines at 108

Table 3.19. Fundamental Vibrational Frequencies of Aqueous Oxalate Ion

Species	Frequency	Activity	Mode of Motion
$A_1 \nu_1$	1486	R, polarized	C–O stretch
ν_2	900	R, polarized	C–C stretch
ν_3	449	R, polarized	CO_2 deformation
$B_1 \nu_4$		R, depolarized	Torsion
$B_2 \nu_5$	$\sim 1519^a$	IR, R, depolarized	C–O stretch
ν_6	$\sim 524^b$	IR, R, depolarized	CO_2 deformation
$E \nu_7$	1310	IR, R, depolarized	C–O stretch
ν_8	761	IR, R, depolarized	CO_2 rock
ν_9	301	IR, R, depolarized	CO_2 wag

^aCorrected for Fermi resonance.

^bObserved only in the crystal.

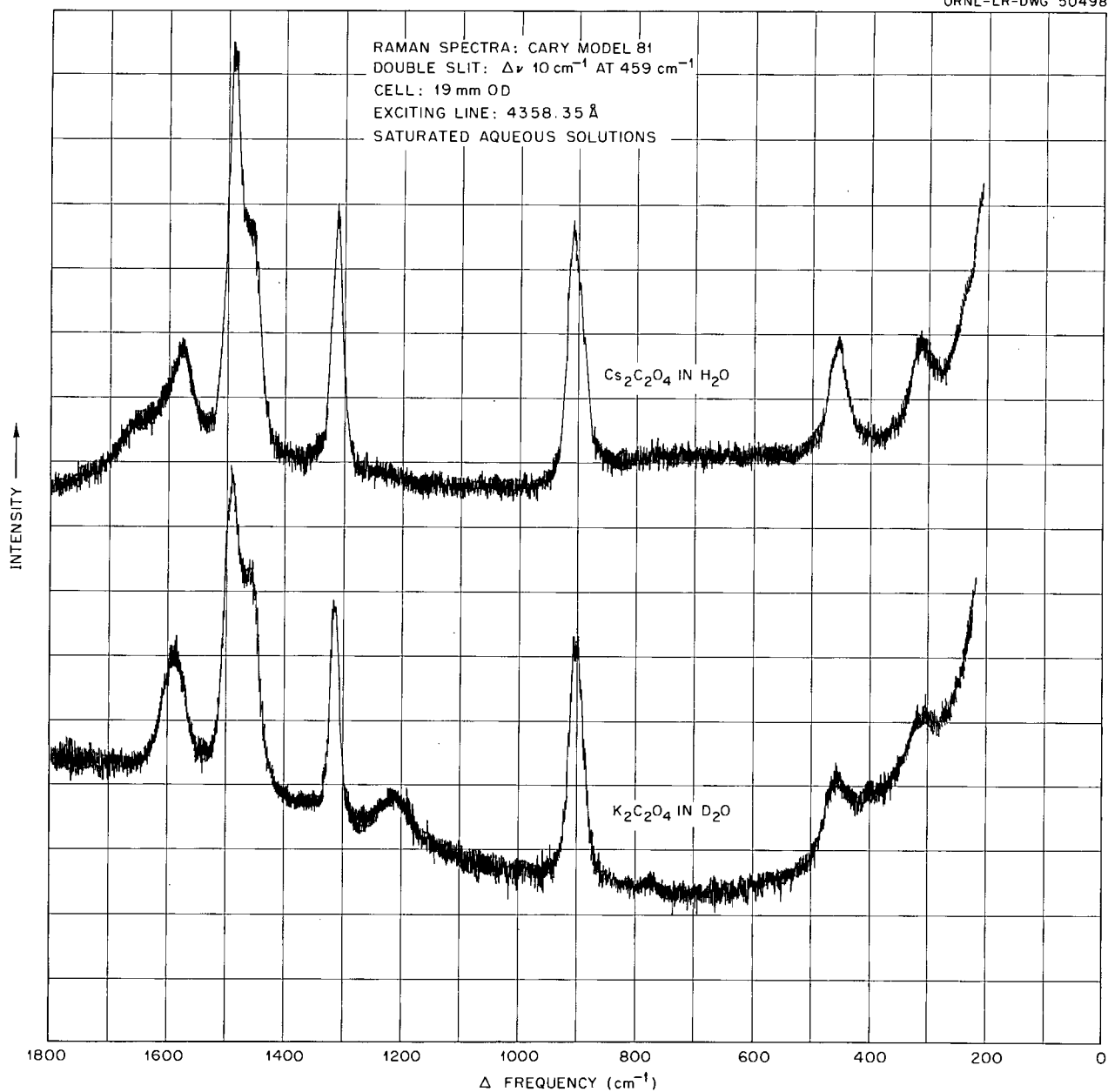


Fig. 3.2. Raman Spectra of Aqueous Oxalate Solutions.

and 496 cm^{-1} respectively. The two other Raman bands, shown at 508 and 547 cm^{-1} in Fig. 3.4, are due to XeF_4 impurity in the sample. The infrared spectrum²⁵ of the vapor shows fundamental bands at 213.2 and 555 cm^{-1} and a weak over-

tone band at 1070 cm^{-1} . These data establish the structure of XeF_2 as linear F-Xe-F , and the observed frequencies were assigned as shown in Table 3.20. It is interesting to note the shift of the ν_1 frequency from 514 cm^{-1} in the vapor to 496 cm^{-1} in the solid, indicating considerable interaction between the molecules in the solid state.

²⁵D. F. Smith, Oak Ridge Gaseous Diffusion Plant.

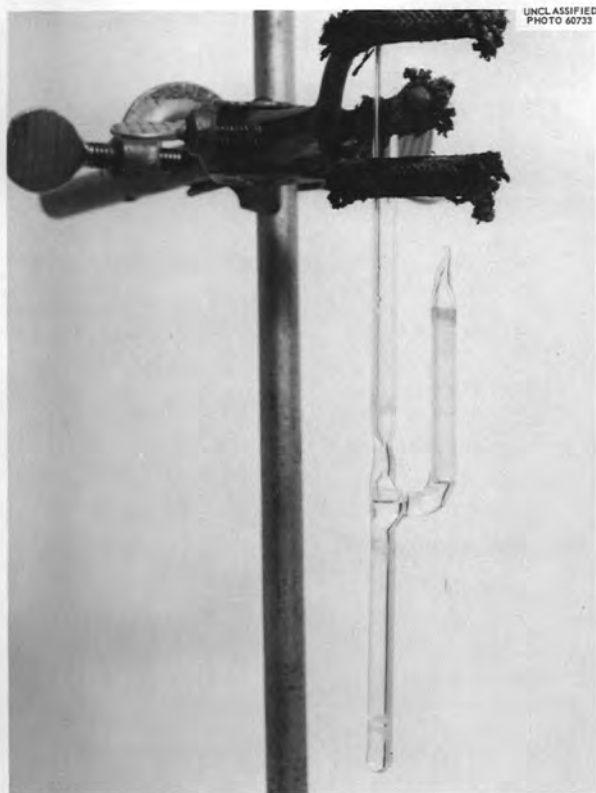


Fig. 3.3. Quartz Raman Cell Containing Liquid XeOF_4 .

The XeF_4 Raman spectrum is similar to that obtained at Argonne National Laboratory²⁶ with the addition of the 215 cm^{-1} band, the unresolved band at 552 cm^{-1} , and the lattice frequencies at 74 and 99 cm^{-1} . These data, along with the infrared data, show XeF_4 to be planar (as concluded by the Argonne workers). Our assignments of the Raman bands are listed in Table 3.21.

The Raman spectrum of solid XeF_6 is shown in Fig. 3.6. The twin peaks at 504 and 544 cm^{-1} are almost certainly due to XeF_4 impurity. A weak lattice vibration observed at 75 cm^{-1} may be

²⁶C. L. Chernick *et al.*, *Science* 138, 136 (1962).

Table 3.20. Raman and Infrared Frequencies of XeF_2

Frequency (cm^{-1})	Assignment
108	Lattice vibration (libration)
213.2	ν_2 - bending vibration
514	ν_1 - symmetric stretch
555	ν_3 - antisymmetric stretch
1070	$\nu_1 + \nu_3$ - combination band

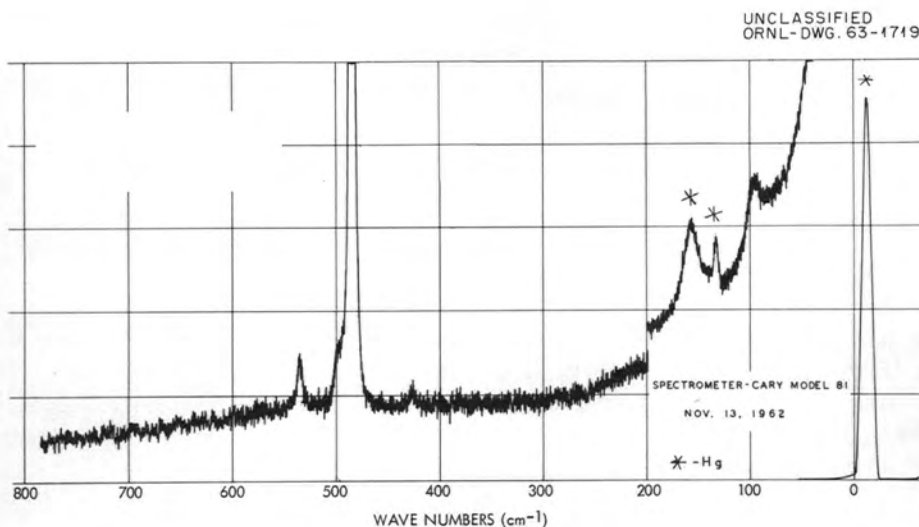


Fig. 3.4. Raman Spectrum of XeF_2 Solid.

either XeF_6 or XeF_4 impurity. The remaining bands and their relative intensities are 582 cm^{-1} [4], 636 cm^{-1} [8], and 655 cm^{-1} [10]. Two infrared bands have been observed by D. F. Smith at the Oak Ridge Gaseous Diffusion Plant. These are at 520 and 611 cm^{-1} . These spectra, showing no coincidences between the infrared and Raman spectra, indicate a considerable degree of symmetry in the XeF_6 molecule. The spectra to date are most compatible with a D_{4h} structure but do not rule out the O_h (octahedral) structure.

After being sealed in a quartz cell, XeOF_4 , a clear water-white liquid at room temperature, gave a very good Raman spectrum. The Raman and infrared spectra of the compound are in accord

Table 3.21. Raman Frequencies of XeF_4

Frequency (cm^{-1})	Assignment
74	Lattice vibration (libration)
99	Lattice vibration (libration)
215	$\nu_3 (B_{1g})$ - in plane scissor-type bend
237	$2\nu_7$ - overtone band
504	$\nu_5 (B_{2g})$ - Xe-F antisymmetric stretch
543	$\nu_1 (A_{1g})$ - Xe-F symmetric stretch
552	$2\nu_2$ - overtone band

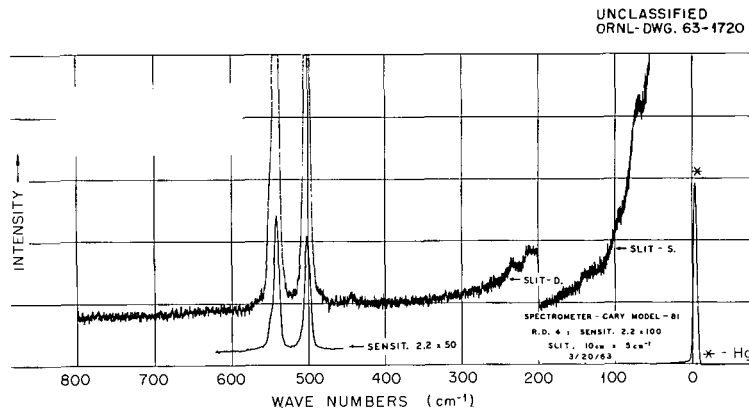


Fig. 3.5. Raman Spectrum of XeF_4 Solid.

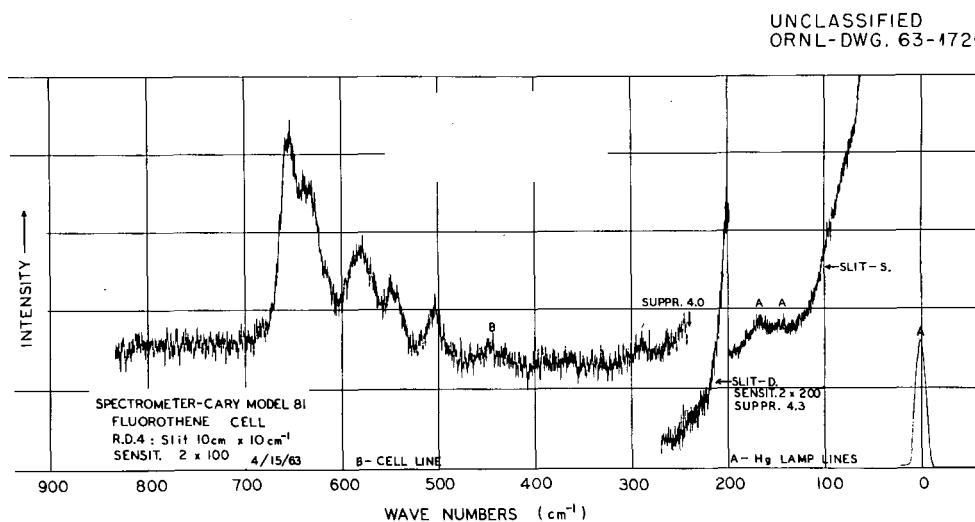
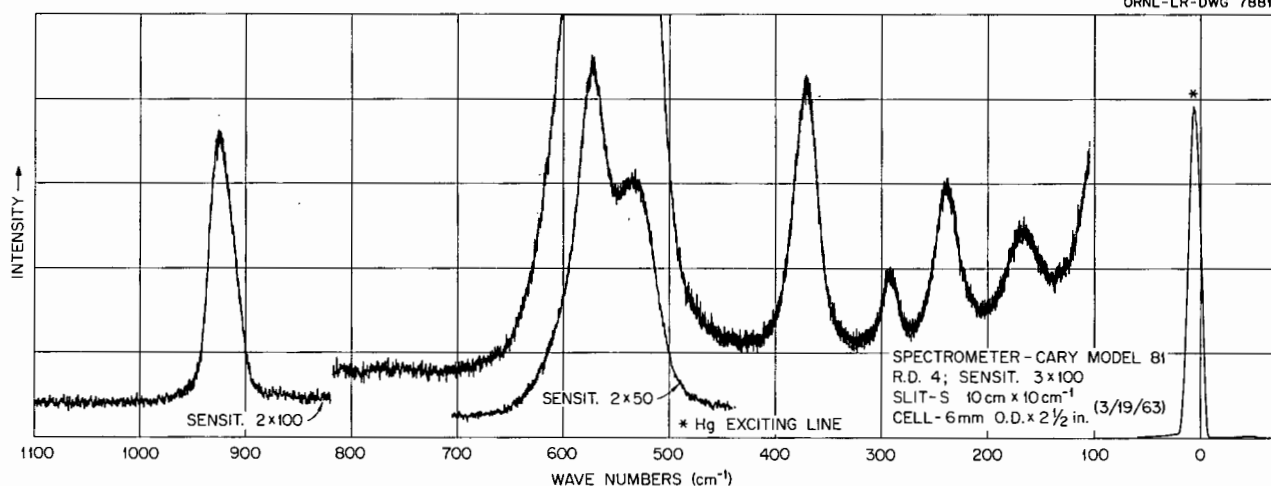


Fig. 3.6. Raman Spectrum of XeF_6 Solid.

Fig. 3.7. Raman Spectrum of XeOF_4 Liquid.Table 3.22. Spectral Data for Liquid XeOF_4

Assignment	Raman Frequency (I)			Infrared Frequency (g) ^b		Description ^c
	cm^{-1}	Intensity	Polarization ^a	cm^{-1}	Intensity	
$\nu_1 (A_1)$	920	20	P	926	s^d	$\nu (\text{Xe}-\text{O})$
$\nu_2 (A_1)$	567	100	P	576	s	$\nu (\text{Xe}-\text{F})$ sym
$\nu_3 (A_1)$	285	2	P	294	s	$\delta (\text{F}-\text{Xe}-\text{F})$ sym, out of plane
$\nu_4 (B_1)$	527	40	D			$\nu (\text{Xe}-\text{F})$ antisym
$\nu_5 (B_1)$						$\delta (\text{F}-\text{Xe}-\text{F})$ antisym, out of plane
$\nu_6 (B_2)$	233	6	D			$\delta (\text{F}-\text{Xe}-\text{F})$ antisym, in plane
$\nu_7 (Eu)$				608	vs	$\nu (\text{Xe}-\text{F})$ antisym
$\nu_8 (Eu)$	365	15	D	361	s	$\delta (\text{F}-\text{Xe}-\text{O})$
$\nu_9 (Eu)$	161	3	D			$\delta (\text{F}-\text{Xe}-\text{F})$ antisym, in plane

^aP, polarized; D, largely depolarized.^bObserved by D. F. Smith, ORGDP.^c ν , stretching vibration; δ , bending vibration.^ds, strong; vs, very strong.

with a molecular structure having C_{4v} symmetry and closely resemble the spectra of IF_5 and BrF_5 . A square pyramid structure is indicated for XeOF_4 with the xenon atom close to the plane of the four fluorine atoms and the oxygen atom at the apex

of the pyramid. The spectral data are presented in Table 3.22 along with our assignment of the frequencies. There is one missing frequency, and it is possible that the value of 233 cm^{-1} belongs to ν_5 rather than ν_6 . The assignment to ν_6 has

been made by analogy with XeF_4 , which has frequencies very similar to XeOF_4 .

Oxygen-17 Enrichment

A. H. Narten

An isotope separation facility capable of producing research quantities of high-purity O^{17} and O^{18} has been constructed at ORNL. At midyear the water distillation cascade had been in continuous operation for 48 weeks and was performing

satisfactorily. The maximum concentrations of O^{17} and O^{18} attained at this time were 1.1 and 61.4% respectively. Projections, based upon the present performance of the cascade, indicate that steady-state operation will be achieved near the end of this calendar year. At that time the peak concentrations of O^{17} and O^{18} are expected to be about 3 and 98% respectively.

The hot-wire thermal diffusion cascade, which will be used to upgrade the O^{17} product from the water distillation cascade, is now operational. It has been designed to yield 50 mg per day of 50%-pure O^{17} gas.

4. Radiation Chemistry

Radiolysis of Liquid Oxygen and Oxygen-Nitrogen at 77°K

J. F. Riley

By means of alternate gamma irradiation and absorption spectrophotometry, the formation of ozone may be observed in oxygen-nitrogen solutions at 77°K. The work previously reported^{1,2} has been extended both to lower and intermediate oxygen concentrations. Figure 4.1 shows how the ozone yield, $G(O_3)$, varies with the electron fraction of oxygen, $\epsilon(O_2)$. The simple assumption of an ozone yield proportional to the electron fraction of oxygen is indicated by the dotted line. Any difference between the experimental yields and the simply assumed linearity of yield is loosely termed "energy transfer."

Extensive "energy transfer" or enhanced ozone yields were observed. The enhancement may be expressed as

$$\Delta G(O_3) = G(O_3)_{\text{exptl}} - \epsilon(O_2)G^0(O_3), \quad (1)$$

where $\Delta G(O_3)$ is the ozone-yield enhancement, $G(O_3)_{\text{exptl}}$ is the observed ozone yield, $\epsilon(O_2)$ is the electron fraction of oxygen, and $G^0(O_3)$ is the ozone yield (12.5 ± 0.4 molecules per 100 ev) from pure oxygen at 77°K.

Figure 4.2 shows how the ozone enhancement $\Delta G(O_3)$ varies with the electron fraction of oxygen. The enhancement increases as $\epsilon(O_2)$ decreases, passes through a maximum, and then falls off rapidly with decreasing oxygen concentration. Over the region from $\epsilon(O_2) = 1$ to $\epsilon(O_2) = 0.1$, $\Delta G(O_3)$ may be approximated by a linear function

¹Chem. Div. Ann. Progr. Rept. June 20, 1961, ORNL-3176, pp 33-34.

²Chem. Div. Ann. Progr. Rept. June 29, 1962, ORNL-3320, pp 43-44.

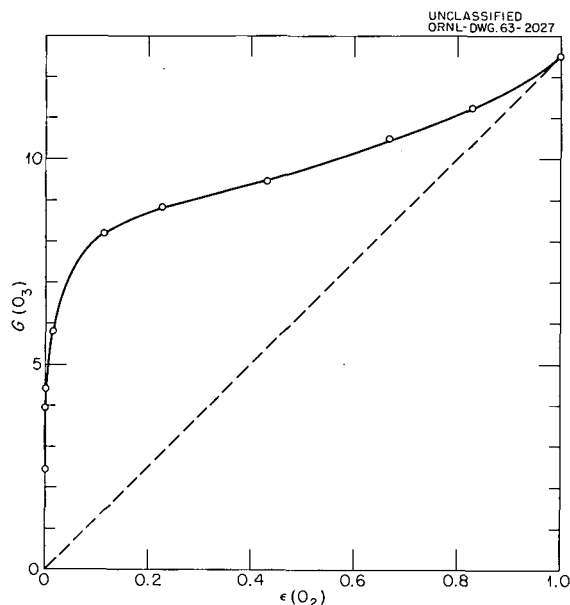


Fig. 4.1. Ozone Yield $G(O_3)$ from the Radiolysis of Oxygen-Nitrogen at 77°K vs Electron Fraction of Oxygen $\epsilon(O_2)$.

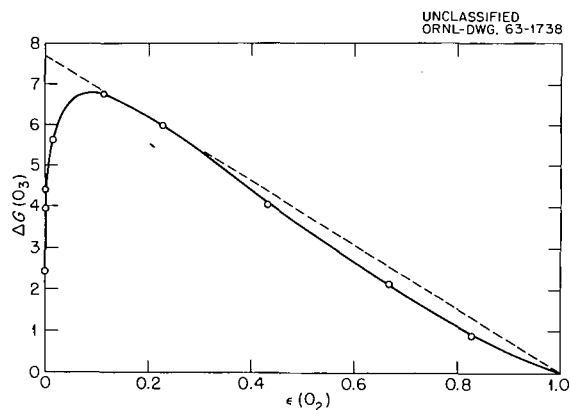


Fig. 4.2. Enhancement of Ozone Yield $\Delta G(O_3)$ from the Radiolysis of Oxygen-Nitrogen at 77°K vs Electron Fraction of Oxygen $\epsilon(O_2)$.

of the electron fraction of nitrogen, $\epsilon(N_2)$. The dotted line of Fig. 4.2 represents the linear function

$$\Delta G(O_3) = 7.69\epsilon(N_2), \quad 0 \leq \epsilon(N_2) \leq 0.9. \quad (2)$$

Figure 4.3 allows us to examine the enhancement at very low oxygen concentrations. Over a considerable range, $\Delta G(O_3)$ is approximately a logarithmic function of $\epsilon(O_2)$;

$$\Delta G(O_3) = 8.05 + 1.29 \log_{10} \epsilon(O_2), \quad 0.00006 < \epsilon(O_2) < 0.1. \quad (3)$$

One treatment of these results suggests that they may be expressed as

$$\Delta G(O_3) = 7.69\epsilon(N_2)F, \quad (4)$$

where F is an efficiency factor for energy transfer between nitrogen and oxygen. The efficiency factor F reaches the value of unity as each N_2 has one O_2 in its shell of nearest neighbors. If in Fig. 4.2, $\Delta G(O_3)$ were given exactly by Eq. (2) over its specified range, then the efficiency factor F would equal unity as long as each N_2 had, on the average, at least one O_2 in its shell of nearest neighbors. The value of F falls slowly

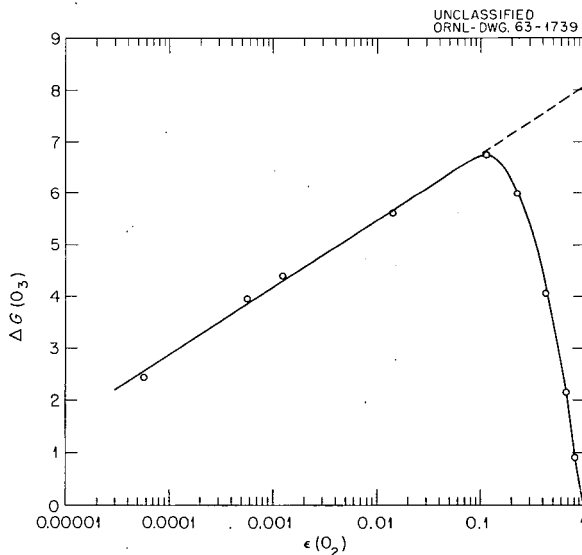


Fig. 4.3. Enhancement of Ozone Yield $\Delta G(O_3)$ vs Log Electron Fraction of Oxygen $\log \epsilon(O_2)$.

with further decrease in oxygen concentration, as shown in Fig. 4.4. The transfer efficiency factor F has the value 0.5 when the concentration of oxygen is 0.014 mole/liter [$\epsilon(O_2) = 0.0006$].

A second treatment is to consider particular reaction steps and the competition between degradation and transfer of energy from nitrogen to oxygen; in this way, the ratio of rate constants for the competing reactions might be evaluated. Of special interest are the reactions of charge transfer, $N_2^+ + O_2 \rightarrow O_2^+ + N_2$, and electron capture, $O_2 + e \rightarrow O_2^-$. To date, no kinetic scheme or combination of reactions has been found to describe satisfactorily the observed enhancement.

Alternatively, the entire assumption of energy deposition or localization proportional to electron fraction may require replacement by a detailed description of the deposition.

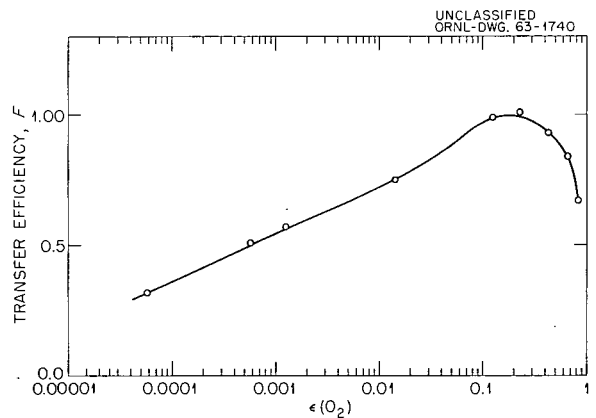


Fig. 4.4. Transfer Efficiency F vs Log Electron Fraction of Oxygen $\log \epsilon(O_2)$.

Radiolytic and Photolytic Reduction of Aqueous Silver Nitrate Solutions

H. A. Mahlman

The reduction of solid silver salts to silver metal by light or ionizing radiations is well known. A similar result has been observed for aqueous silver nitrate solutions. Of particular interest is the characteristic growth pattern of the metal particles.

Aqueous silver nitrate solutions were prepared from reagent grade $AgNO_3$ and triple-distilled

water. These solutions were deaerated and exposed to Co^{60} gamma rays, Po^{210} alpha particles, or 2537-A light. The silver metal formed was separated from the solution by centrifugation, washed with water, and examined with an electron microscope. Representative electron micrographs, which illustrate the characteristic features of the silver particles formed by each type of incident radiation, are presented as Figs. 4.5-4.7.

Figure 4.5 is an electron micrograph of the silver particles prepared by Co^{60} gamma irradiations and illustrates two general forms, spheres and flat crystals. The finely divided background metal particles are small spheres about 70 Å in diameter. The crystals appeared in the electron micrographs to be flat and diamond shaped. The two acute angles were 60° , while the two obtuse angles were 120° . Some of the crystals possessed a projection or tail. If the sample was swept with helium during gamma irradiation, the tail length was increased from several hundred angstroms to an unmeasurable length due to the physical contortions of its growth as shown by the electron micrograph in Fig. 4.8.

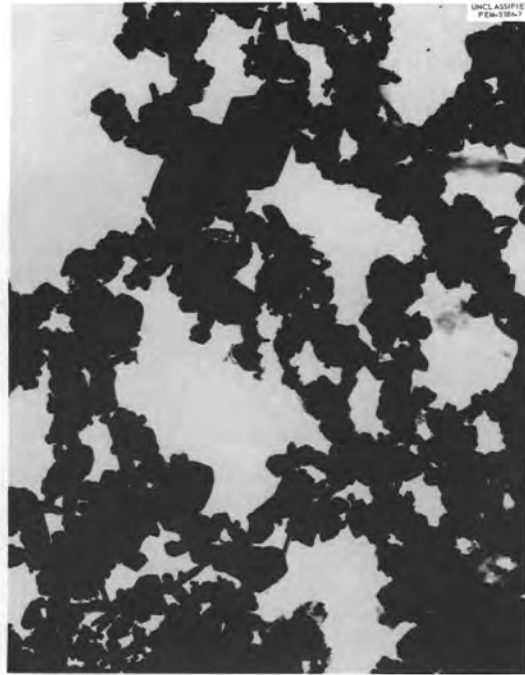


Fig. 4.6. Silver Metal Formed by Po^{210} Alpha-Particle Irradiation. 18,000X. Reduced 61%.



Fig. 4.5. Silver Metal Formed by Co^{60} Gamma-Ray Irradiation. 18,000X. Reduced 61%.



Fig. 4.7. Silver Metal Formed by 2537-A Light from a Mercury Vapor Lamp. 18,000X. Reduced 61%.



Fig. 4.8. Silver Metal Tail Growth when Solution Is Swept with Helium During Co^{60} Gamma-Ray Irradiation. 18,500X. Reduced 61%.

The metallic silver formed by polonium alpha-particle irradiation is in the form of large flat crystals interconnected by irregular bridges, as illustrated by Fig. 4.6. The crystal angles are predominantly 60° and 120° . The bridges vary both in width and length and show no preferred oriented growth. In regions where extensive bridging has occurred the electron micrographs show essentially solid irregular metal masses. The well-defined tail formation present in the gamma radiolysis is absent.

The photolytic reduction of aqueous silver nitrate gives particles that are essentially spherical (see Fig. 4.7). Some of the particles have minor irregularities that make them appear as gears. For short exposures (20 hr) the spheres had a maximum diameter of about 87,500 Å, and there is some evidence of agglomeration of the particles. For longer exposures (70 hr) the maximum diameter of the spheres was about 137,000 Å. The electron micrographs show more extensive agglomeration for the 70-hr exposure than was observed for the shorter exposure. One interesting feature of these photolytic experiments is that the volumes of the spheres are directly proportional to the exposure time.

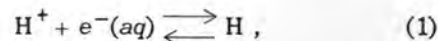
The use of radiolytically prepared silver metal as a catalyst has been considered. For Co^{60} -gamma-ray-prepared silver metal the surface area of the particles was found to be $0.44 \text{ m}^2/\text{g}$ as measured by nitrogen absorption. This would indicate that about 0.05% of the silver atoms are surface atoms. If surface area is the criterion for catalysis, this material would not be particularly outstanding.

A second sample of silver was prepared by subjecting an aqueous silver nitrate solution to successive gamma-ray doses. The metal formed was separated from the solution after the completion of each irradiation. The surface area of this metal was $1.23 \text{ m}^2/\text{g}$, where about 0.4% of the silver atoms are on the surface. The increased surface area indicates that the metal suspended in the solution continues to grow until it precipitates. Thus one would expect the surface area of the silver metal to be higher for smaller doses and repeated separation of the metal from the solution.

Primary Reducing Species in the Co^{60} Radiolysis of Aqueous NaNO_3 Solutions

H. A. Mahlman

Until recently the radiation chemistry of water has been explained by the assumed decomposition of water molecules into H atoms and OH radicals. These primary products reacted with each other, as they diffused from the point of origin, to form water and the detected molecular products H_2 and H_2O_2 . Contrary to this simple concept, current experimental evidence indicates that the reducing entity may be partially or totally solvated electrons.³ Recognition of two types of hydrogen atoms related as acid and conjugate base, according to Eq. (1),

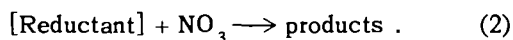


depends upon the H atom or solvated electron either reacting with the same reagent to give different products or at grossly different rates.

At $\text{pH} = 1$ the acid form, H atoms, should predominate, whereas at $\text{pH} = 12.6$ the basic form should predominate. The suppressive action of

³Any current review of radiation chemistry.

the reducible solute NO_3^- on the $G(\text{H}_2)$ should serve as an excellent monitor for the investigation since the suppression of H_2 is indicative of the reaction rate



Thus, the purpose of this research was to measure the $G(\text{H}_2)$ as a function of NO_3^- concentration, calculate the reaction rate constant of the reducing species with NO_3^- , and identify the reducing species.

Aqueous NaNO_3 solutions were prepared from recrystallized reagent grade NaNO_3 and triple-distilled water. They also contained $10^{-3} M$ halide ion to protect the molecular hydrogen formed from OH radical attack. One series of NaNO_3 solutions was prepared to about $\text{pH} = 13$ (measured $\text{pH} = 12.6$), while the pH of another series was adjusted with reagent grade H_2SO_4 to be 1.0. These solutions were individually deaerated, irradiated with Co^{60} gamma rays at a dose rate of $1.8 \times 10^{21} \text{ ev liter}^{-1} \text{ min}^{-1}$, and analyzed for the amount of molecular hydrogen formed by vapor fractometry. The $G(\text{H}_2)$, defined as the number of hydrogen molecules formed for each 100 ev of energy absorbed by the sample, are tabulated in Table 4.1 as well as the $G(\text{H}_2)$ previously obtained at $\text{pH} = 4.5$.⁴

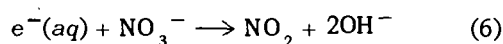
From least-squares analyses of the $G(\text{H}_2)$ as a function of the cube root of the nitrate ion concentration in the concentration range 0.001 to 0.3 M , the following equations were obtained with standard errors of 0.018 on the intercept and 0.015 on the slope:

$$\text{pH} = 1, \quad G(\text{H}_2) = 0.479 - 0.405[\text{NO}_3^-]^{1/3}; \quad (3)$$

$$\text{pH} = 4.5, \quad G(\text{H}_2) = 0.456 - 0.403[\text{NO}_3^-]^{1/3}; \quad (4)$$

$$\text{pH} = 12.6, \quad G(\text{H}_2) = 0.455 - 0.405[\text{NO}_3^-]^{1/3}. \quad (5)$$

Since the slopes of these equations are essentially equal, it is concluded that the reducing entity reacting with NO_3^- in this concentration range is the same at all pH 's. The reactions under consideration are



⁴H. A. Mahlman and J. W. Boyle, *J. Chem. Phys.* 27, 1434 (1957).

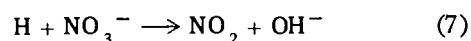
Table 4.1. Hydrogen Yields from Co^{60} Gamma-Ray-Irradiated Aqueous NaNO_3 Solutions at Various pH 's

NaNO_3 Molarity	$G(\text{H}_2)$		
	$\text{pH} = 1.0$	$\text{pH} = 4.5$	$\text{pH} = 12.6$
0.001	0.444 ^a	0.416	0.430 ^a
0.010	0.378 ^a	0.370 ^b	0.358 ^a
0.040	0.359 ^a	0.315 ^b	0.302 ^a
0.100	0.278 ^a	0.263	0.269 ^a
0.300	0.212 ^a	0.193	0.187 ^a

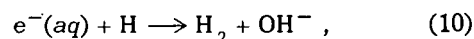
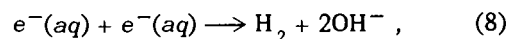
^aAverage of two to four individual determinations at each sodium nitrate concentration.

^bCalculated value from Eq. (4).

and



in competition with



where the reaction rate constants have been reported as $k_6 = 1 \times 10^{10} \text{ liters mole}^{-1} \text{ sec}^{-1}$ (ref 5), $k_7 = 1 \times 10^7 \text{ liters mole}^{-1} \text{ sec}^{-1}$ (ref 6), $k_8 = 1 \times 10^{10} \text{ liters mole}^{-1} \text{ sec}^{-1}$ (ref 5), $k_9 = 1.3 \times 10^{10} \text{ liters mole}^{-1} \text{ sec}^{-1}$ (ref 5), and $k_{10} = 3 \times 10^{10} \text{ liters mole}^{-1} \text{ sec}^{-1}$ (ref 5). The absolute rate constant for the reaction of NO_3^- and the reducing species that normally produces molecular hydrogen was calculated from the diffusion kinetic calculations of Flanders and Fricke⁷ and found to be $1.3 \times 10^{10} \text{ liters mole}^{-1}$

⁵H. A. Schwarz, *Special Effects*, paper presented at the Conference on Basic Mechanisms in the Radiation Chemistry of Aqueous Media, Gatlinburg, Tennessee, May 8-10, 1963.

⁶Calculated from data by A. O. Allen, *Radiation Yields and Reactions in Dilute Solutions*, paper presented at the Conference on Basic Mechanisms in the Radiation Chemistry of Aqueous Media, Gatlinburg, Tennessee, May 8-10, 1963.

⁷D. A. Flanders and H. Fricke, *J. Chem. Phys.* 28, 1126 (1958).

sec⁻¹. This is in good agreement with the rate constant $k_6 = 1 \times 10^{10}$ liters mole⁻¹ sec⁻¹ for the reaction of the solvated electron with nitrate ion.

It is noted that all $G(H_2)$ measured at pH = 1 are larger than the $G(H_2)$ at pH = 4.5 and 12.6 as given in Table 4.1 or by the calculated intercepts of Eqs. (3-5). If significance is attached to this small increase, it can be interpreted as indicative of the conversion of some solvated electrons to H atoms by hydronium ions. The lower rate constant for k_7 would favor the formation of some additional H_2 by Eqs. (9) and (10) and thus a somewhat larger $G(H_2)$. This interpretation must be considered initially as competitive reactions between Eqs. (1) and (6).

Radiolysis of Arsenite Solutions

J. W. Boyle

Peroxymonosulfuric acid (Caro's acid) is formed by radiolysis in concentrated sulfuric acid solutions. In order to learn more about the formation of this acid and the radical precursors associated with its formation, a study has been started using arsenite ion as a radical and Caro's acid scavenger. However, before irradiating concentrated acid solutions, a thorough understanding of the radiation chemistry of arsenite ion in dilute acid is needed, and the work so far has been directed toward this latter goal.

The results in these relatively dilute acid solutions have been obtained from two systems - aerated arsenite solutions and deaerated arsenite solutions which contain hydrogen peroxide. Yields (number of molecules changed per 100 ev of absorbed gamma-ray energy) of the products in these two systems are given in Table 4.2 for 0.4 M H_2SO_4 and neutral solutions. For simplicity, arsenite and arsenate are listed as As(III) and As(V). Yields at intermediate acidities gave intermediate values.

These results are explained on the basis of the following intermediates produced by the radiolysis of water; $H_2O \rightsquigarrow e^-(aq)$ (or H), OH, H_2O_2 , H_2 . The reducing radical produced in the radiolysis of aqueous solutions is now considered to be present in two forms - mainly hydrated electrons [$e^-(aq)$] in neutral solutions and mostly hydrogen atoms (H) in acid solutions. The results

in Table 4.2 can be qualitatively explained by the $e^-(aq)$ and H reactions. The OH radical oxidizes arsenite in all solutions. The pertinent reactions are listed in Table 4.3 with their respective absolute reaction rate constants.

In air-saturated neutral solutions the hydrogen peroxide yield is lowered and the arsenate yield raised upon addition of hydrogen peroxide prior to irradiation. The explanation is that in the absence of hydrogen peroxide essentially all the hydrated electrons react according to reaction 2; whereas in the presence of hydrogen peroxide some hydrated electrons react with hydrogen peroxide (reaction 3), the hydrogen peroxide yield is lowered, and the arsenate yield raised. In acid solutions the hydrated electrons that are converted

Table 4.2. Product Yields from Co⁶⁰ Gamma Radiolysis of 10⁻³ M Arsenite Solutions

G	Aerated As(III)		Deaerated As(III)-H ₂ O ₂	
	0.4 M H ₂ SO ₄	Neutral	0.4 M H ₂ SO ₄	Neutral
H ₂	0.4	0.4	0.4	0.4
O ₂	-3.2	-2.9		
As(V)	2.9	2.9	0.4	4.4
H ₂ O ₂	3.9	3.2	~0	-4.0

Table 4.3. Some Important Radical Reactions in Aqueous Solutions and Their Absolute Reaction Rate Constants^a

Reaction	Reaction Rate Constant, k (liters mole ⁻¹ sec ⁻¹)
(1) $e^-(aq) + H_3O^+ \rightarrow H + H_2O$	2.3×10^{10}
(2) $e^-(aq) + O_2 \rightarrow O_2^-$	2.1×10^{10}
(3) $e^-(aq) + H_2O_2 \rightarrow OH + OH^-$	1.2×10^{10}
(4) $H + O_2 \rightarrow HO_2$	2×10^{10}
(5) $H + H_2O_2 \rightarrow OH + H_2O$	4×10^7

^aThese rate constants were reported by H. A. Schwartz, M. S. Matheson, and A. O. Allen at the Conference on Basic Mechanisms in the Radiation Chemistry of Aqueous Media, Gatlinburg, Tenn., May 8-10, 1963.

to hydrogen atoms by reaction 1 react according to reaction 4, which is equivalent to reaction 2. The relatively slow reaction 5 does not compete effectively, and the addition of hydrogen peroxide prior to irradiation has no effect on subsequent hydrogen peroxide and arsenate yields.

In deaerated solutions reactions 2 and 4 are absent. The difference between neutral and acid solutions is due primarily to reaction 1. In a neutral solution that contains hydrogen peroxide the hydrated electrons are converted to OH radicals which in turn oxidize arsenite. Therefore, high yields of hydrogen peroxide consumption and arsenate production result. The yields are higher than expected, however. In acid solution the hydrated electrons are converted to hydrogen atoms by reaction 1. These hydrogen atoms then apparently react much more rapidly with As(III) [or As(V)] than with hydrogen peroxide. The reaction rate constant of the hydrogen atom with the arsenic species can then be bracketed between 4×10^7 and 1.2×10^{10} liters mole⁻¹ sec⁻¹. The rate constant is possibly about half-way between the above limits.

An as yet unexplained observation is that, in strong acid in the absence of oxygen, hydrogen peroxide is neither formed nor consumed. This seems to be true, independent of the amount of hydrogen peroxide present. This suggests that something in these arsenite solutions reacts with the precursors of the molecular hydrogen peroxide, thus preventing any molecular hydrogen peroxide from being formed.

A continuation of this study is expected to give an evaluation of reaction rate constants for some reactions with hydrated electrons and hydrogen atoms. It is hoped also to obtain quantitative yields of the hydrated electron and hydrogen atom as a function of pH.

**Radiation Decomposition of Sodium Chlorate;
Comparison of Yields and the Postirradiation
Annealing Behavior for Irradiation by
Gamma Rays and Alpha Particles⁸**

C. J. Hochanadel

Patrick and McCallum⁹ found that the yield of chloride in the gamma-ray decomposition of sodium chlorate was about doubled by postirradiation annealing for several hours at 185 to 210°C. On

the basis of a comparison of nitrate yields in the radiolysis of several alkali nitrates by gamma rays and alpha particles, the author¹⁰ had suggested that thermal effects in alpha-particle tracks may be a significant factor in the radiolysis. If this is true, then it was thought that the chloride yield in the radiolysis of sodium chlorate should be larger for alpha-particle decompositions than for gamma-ray decomposition and that the effect of postirradiation annealing should be less.

The 100-ev yield, $G(\text{Cl}^-)$, for samples irradiated with gamma rays at 25°C was 1.50 ± 0.07 . The yield was increased to 1.92 ± 0.04 by postirradiation annealing at 185°C. The yield was still higher at 2.30 ± 0.04 for samples irradiated at 185°C.

The yield of chloride for decomposition by alpha particles (3.3 Mev) at 25°C was 2.12 ± 0.05 , about 40% higher than for gamma rays. Also, there was no effect of postirradiation annealing at 185°C.

The results are consistent with the previous postulate that thermal effects in alpha-particle tracks are a significant factor in the radiolysis.

**Radiolysis of Alkaline-Earth Bromates
by Co⁶⁰ Gamma Rays**

J. W. Chase G. E. Boyd

A study of the radiolysis of the molecular bromate ion by Co⁶⁰ gamma rays¹¹ has been extended to include the anhydrous crystalline alkaline-earth bromates to further elucidate the role of crystal "free space" in determining the susceptibility of this ion to radiolytic decomposition.

The irradiations were conducted in the 10.5 × 10.5 × 12 in. cavity of the ORNL Cobalt Storage Facility, where dose rates of 8.0 to 8.7×10^{17} ev g⁻¹ min⁻¹ in water were observed. The temperature in the chamber was uniform and varied

⁸Paper submitted for publication in the *Journal of Physical Chemistry*.

⁹P. F. Patrick and K. J. McCallum, *Nature* 194, 776-77 (1962).

¹⁰C. J. Hochanadel, *Radiation Res.* 16, 286-302 (1962).

¹¹G. E. Boyd, E. W. Graham, and Q. V. Larson, *J. Phys. Chem.* 66, 300 (1962).

only from 35 to 40°. The pure, anhydrous alkaline-earth bromates were rotated during the irradiation to ensure a uniform dose in the samples. Gamma-ray dose rate measurements were made with approximately 0.032 M ceric sulfate solutions 0.4 M in H₂SO₄. Initial 100-ev radiolytic yields or "G₀" values for bromate decomposition were estimated to be 1.49, 1.75, 2.05, 2.79, and 3.02 for KBrO₃, Mg(BrO₃)₂, Ca(BrO₃)₂, Sr(BrO₃)₂, and Ba(BrO₃)₂ respectively. The radiation stability of BrO₃⁻ ion was found to decrease progressively from Mg(BrO₃)₂ to Ba(BrO₃)₂ for the alkaline earths. The radiolytic decomposition in the crystalline bromates produced by the gamma rays in this source increased nonlinearly with the radiation dose. The yield of bromine oxidation states intermediate between bromate and bromide (oxidizing fragments) also was found to increase nonlinearly with dose.

Potassium and barium bromate samples were also irradiated at a fixed geometry in the ORNL Radiation Chemistry Group's 2900-curie Co⁶⁰ source.^{12,13} The dose rate determined with the Fricke dosimeter was 1.82 × 10¹⁸ ev g⁻¹ min⁻¹. The radiolytic decomposition in these samples produced by the gamma rays of this source was found to be considerably lower than that produced by gamma rays of the Cobalt Storage Facility. However, a nonlinear increase in decomposition with radiation dose as well as in the formation of oxidizing fragments with dose was observed. Work is continuing in this area.

Alpha-Particle-Induced Synthesis of Water in the Presence of CO₂

P. S. Rudolph S. C. Lind

The alpha radiolysis of H₂ and O₂, in varying proportions, has been studied extensively by Lind.¹⁴ He concluded that the energy absorbed by either H₂ or O₂ was equally effective in the synthesis of H₂O. Lind and Bardwell¹⁵ subsequently investigated the sensitizing effect of

several chemically inert gases on this reaction. In the cases studied, the sensitizing gas, which had the highest ionization potential (IP) in the mixture, accelerated the reaction rate in proportion to its partial pressure. This was explained on the basis of charge transfer from the additive gas ion to the reactants. Rosenblum¹⁶ studied the water synthesis from a stoichiometric mixture of H₂ and O₂ with CO₂ as an additive gas. The IP of CO₂ is intermediate to those of H₂ and O₂. Thus, in this mixture the CO₂⁺ can transfer charge only to O₂. Using the rate equation of Lind¹⁴ and neglecting the energy absorbed by the CO₂ (see footnote b, Table 4.4, where *i* is

¹⁶Charles Rosenblum, *J. Phys. Chem.* 37, 53 (1933).

Table 4.4. Experimental Data and Reaction Rates Calculated on the Basis of Lind's Equations for the 2H₂ + O₂ + xCO₂ System

Volume of sphere, 7.55 cm³; initial Rn (E₀) = 0.1417 curie; diameter of sphere, 2.43 cm;
P_{CO₂} = 291 mm

$e^{-\lambda t}$	P_{H_2}	P_{O_2}	$\left(\frac{k\mu}{\lambda}\right)^a$	$\left(\frac{k\mu}{\lambda}\right)''^b$
1.000	395	197		
0.920	310	155	18.4	21.3
0.866	266	133	16.7	20.0
0.768	200	100	16.4	20.3
0.701	163	81.5	16.7	21.9
0.641	134	67.0	16.6	22.9
0.488	80.4	40.2	15.4	23.6
0.407	61.3	30.6	13.2	23.7
0.340	48.7	24.4	11.9	23.9
0.115	23.1	11.5	8.9	23.4
0.002	15.5	7.8		
				Av 22.3

$$^a \left(\frac{k\mu}{\lambda}\right)' = \frac{2.30}{E_0} \left\{ \frac{\Delta \log \left[P_{H_2} + P_{O_2} + \frac{i_{CO_2}}{i_{(H_2+O_2)}} P_{CO_2} \right]}{\Delta e^{-\lambda t}} \right\}$$

$$^b \left(\frac{k\mu}{\lambda}\right)'' = \frac{2.30}{E_0} \left[\frac{\Delta \log (P_{H_2} + P_{O_2})}{\Delta e^{-\lambda t}} \right]$$

¹²J. A. Ghormley and C. J. Hochanadel, *Rev. Sci. Instr.* 22, 473 (1951).

¹³J. F. Riley and C. J. Hochanadel, *Chem. Div. Ann. Progr. Rept.* June 20, 1962, ORNL-3320, p 44.

¹⁴S. C. Lind, *J. Am. Chem. Soc.* 41, 531 (1919).

¹⁵S. C. Lind and D. C. Bardwell, *J. Am. Chem. Soc.* 48, 1575 (1926).

the specific ionization of the gas and $e^{-\lambda t}$ is the fraction of radon remaining), Rosenblum calculated a reaction rate which appeared to be constant. This value, however, was higher than the value for $2\text{H}_2 + 1\text{O}_2$ without a sensitizing gas. This indicated that CO_2 did contribute energetically to the reaction. He then attempted to correct for the effect of the CO_2 by use of Lind and Bardwell's equation¹⁵ for sensitizing gases (see footnote a, Table 4.4). He assumed that the CO_2 was 14.5% efficient in transferring energy to the reactants. Although the equation used is an equation for a straight line, his "corrected" reaction rate showed a definite trend, decreasing by a factor of over 2 from initial to final readings.

In view of the above discrepancies the $\text{H}_2\text{-O}_2$ reaction in the presence of CO_2 under radon alpha irradiation was reinvestigated. A stock mixture of electrolytic proportions of H_2 and O_2 plus CO_2 was prepared. An aliquot of this stock mixture was introduced into a small sphere that contained radon, and the pressure was recorded periodically as previously described.¹⁷ Pertinent data are given in Table 4.4.

Rosenblum,¹⁶ on the basis of cryogenic separations in situ, concluded there was "no appreciable loss of CO_2 until the greater part of the reactants had been used up." We found, using standard analytical techniques on a replicate sample of the stock mixture and on the final gas mixture after decay of the radon, that within experimental error, no CO_2 was consumed. The initial and final values for CO_2 were 2.65 and 2.60 cm^3 , STP, respectively.

Table 4.4 shows that $(k\mu/\lambda)'$ is not constant, indicating that CO_2 is not 100% efficient in promoting reaction by energy transfer. Neglecting the energy absorbed by the CO_2 gives $(k\mu/\lambda)''$ an apparent constancy with a mean value of 22.3. This is in excellent agreement with Rosenblum's¹⁶ value (when corrected for differences in diameter of the spheres) of 21.3, especially when one considers that the $P_{\text{CO}_2}/(P_{\text{H}_2} + P_{\text{O}_2})$ in the two respective studies were 0.49 and 0.47. However, the reaction rate for $2\text{H}_2 + 1\text{O}_2$ in a 2.43-cm sphere should be 15.4 if the CO_2 made no contribution to the reaction.

¹⁷P. S. Rudolph and S. C. Lind, *J. Chem. Phys.* 33, 705 (1960).

A plot, Fig. 4.9, of the data from Table 4.4 shows that the "apparent" constancy is not real. The data give two straight lines with a definite break at 245 mm of $\text{H}_2 + \text{O}_2$. The same observation is evident in Rosenblum's data,¹⁶ although undetected by him.

A kinetic expression which fits the experimental data has been derived on the basis of the known and energetically possible reactions listed below. These reactions produce reactive species, which subsequently react with H_2 or O_2 and ultimately produce water, although this is not indicated in the reactions shown below:

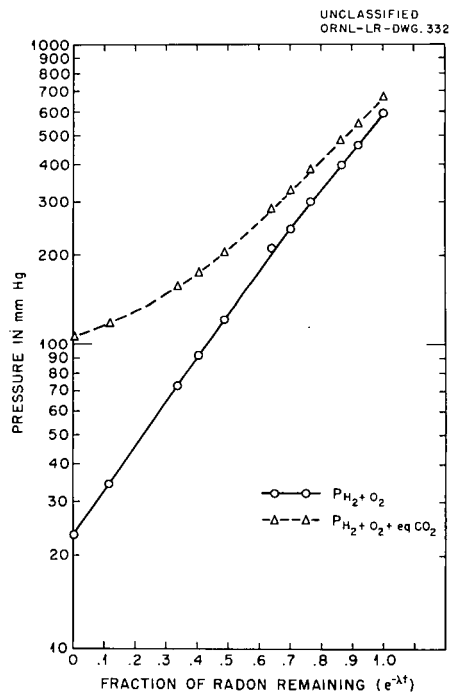
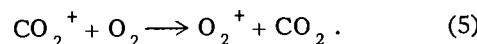
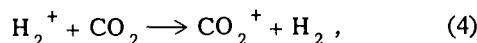
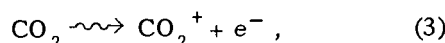
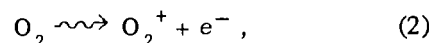
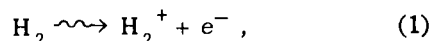


Fig. 4.9. Plot of Pressure vs $e^{-\lambda t}$ (Fraction of Radon Remaining) for the $2\text{H}_2 + \text{O}_2 + x\text{CO}_2$ System. Solid line neglects P_{CO_2} . Broken line includes equivalent pressure of CO_2 , that is, $[i_{\text{CO}_2}/i_{(2\text{H}_2+\text{O}_2)}]P_{\text{CO}_2}$, where i is the specific ionization.

In addition to the above reactions the following assumptions were made in deriving the kinetic expression.

1. Since all the alpha particles lose most of their energy in the wall and since P_{CO_2} is constant, the energy absorbed by the CO_2 is constant.

2. Since the ratio H_2/O_2 remains constant, these two gases can be treated as a single gas and the energy absorbed by them is a function of their total pressure.

3. The energy absorbed by either H_2 or O_2 is equally effective in the formation of H_2O .¹⁴

4. Carbon dioxide is chemically inert but energetically active; it transfers energy to O_2 .

5. A certain fraction (Φ) of the total possible ion-molecule collisions that can give rise to energy transfer do so.

6. The value of Φ for the reaction $\text{H}_2^+ + \text{CO}_2 \rightarrow \text{CO}_2^+ + \text{H}_2$ is taken as unity.

7. The number of ions produced by alpha particles in a gas is proportional to the energy absorbed by that gas.

The processes leading to a decrease in the pressure of H_2 are reactions (1) + (2) + (5)₃ + (5)₄ - (4), where the subscripts refer to the reaction that produces the reactant CO_2^+ ion, or

$$\begin{aligned} \frac{-dP_{\text{H}_2}}{dt} = E_0 DK e^{-\lambda t} & \left(i_{\text{H}_2} P_{\text{H}_2} + i_{\text{O}_2} P_{\text{O}_2} \right. \\ & + \Phi i_{\text{CO}_2} P_{\text{CO}_2} \frac{P_{\text{O}_2}}{P_T} + \Phi i_{\text{H}_2} P_{\text{H}_2} \frac{P_{\text{CO}_2} P_{\text{O}_2}}{P_T^2} \\ & \left. - i_{\text{H}_2} P_{\text{H}_2} \frac{P_{\text{CO}_2}}{P_T} \right), \quad (6) \end{aligned}$$

where

$$D = 2.43 \text{ cm,}$$

$$P_{\text{O}_2} = 0.5 P_{\text{H}_2},$$

$$P_{\text{CO}_2} = 291 \text{ mm,}$$

$$P_T = 1.5 P_{\text{H}_2} + 291,$$

$$E_0 = 0.1417 \text{ curie,}$$

$$i_{\text{H}_2} = 0.21,$$

$$i_{\text{O}_2} = 1.16,$$

$$i_{\text{CO}_2} = 1.53,$$

$$\Phi = 0.6.$$

Equation (6) simplifies to

$$\begin{aligned} \frac{-dP_{\text{H}_2}}{dt} = K' e^{-\lambda t} & \left(0.79 P_{\text{H}_2} \right. \\ & \left. + 72.2 \frac{P_{\text{H}_2}}{P_T} + 18.3 \frac{P_{\text{H}_2}^2}{P_T^2} \right). \quad (7) \end{aligned}$$

Integrating (7) between limits gives

$$\frac{K'}{\lambda} = \frac{2.3 [f(P_{\text{H}_2})_1 - f(P_{\text{H}_2})_2]}{e^{-\lambda t_1} - e^{-\lambda t_2}}, \quad (8)$$

where

$$\begin{aligned} f(P_{\text{H}_2}) = 0.968 \log P_{\text{H}_2} + 0.151 \log (8.77 \times 10^4 \\ + 814 P_{\text{H}_2} + 1.78 P_{\text{H}_2}^2) \\ - 0.193 \log \frac{3.56 P_{\text{H}_2} + 617}{3.56 P_{\text{H}_2} + 1011}. \quad (9) \end{aligned}$$

A plot of $f(P_{\text{H}_2})$ vs $1 - e^{-\lambda t}$ (the fraction of radon decayed) is shown in Fig. 4.10. The points are the experimental values and the line is the least-squares line. Values of $\Phi > 0.6$ give curves with decreasing slopes, whereas values of $\Phi < 0.6$ give curves with increasing slopes.

The excellent linearity supports the postulated mechanisms and assumptions on which the kinetic expression [Eq. (7)] is based.

Radiation-Induced Surface Oxidation of Hydrocarbons

H. W. Kohn

Work begun last year on the reactions of adsorbed hydrocarbons during and after Co^{60} gamma irradiations has been extended. The oxidation of 17 hydrocarbons on three adsorbents (silica, alumina, and silica-alumina) has been studied.

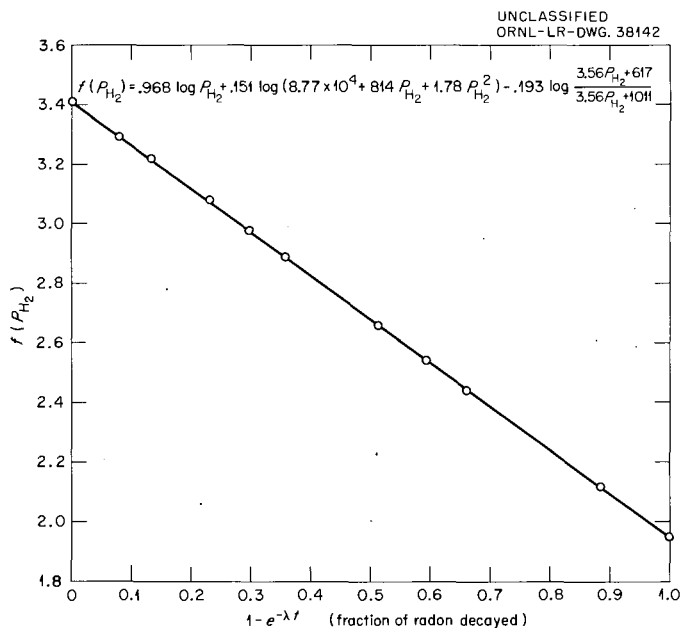


Fig. 4.10. Plot of Function of P_{H_2} vs $1 - e^{-\lambda t}$ (Fraction of Radon Decayed) for the $2H_2 + O_2 + xCO_2$ System. The function of P_{H_2} is based on a newly derived equation that assumes that CO_2 is 60% efficient in transferring energy to promote reaction.

Only two of the 51 cases have failed to show appreciable oxidation; in four other cases, oxidation begins as soon as the reagents are added, that is, radiation is not required for oxidation.

Yields. - Radiation yields, $G(-O_2)$, are calculated on the basis of molecules of oxygen which disappear per 100 ev of energy absorbed by the adsorbent. These values are summarized in Table 4.5.

The initial pressure of oxygen varied for different experiments because of the vapor pressure differences between the different organic compounds over the adsorbent. Detailed examination of the toluene/oxygen/alumina system showed, moreover, that there was a linear dependence of the initial $G(-O_2)$ on the pressure of O_2 and on the extent of surface coverage. One would expect similar dependence with other compounds and adsorbents. Therefore the yields cited in Table 4.5 should be granted only a qualitative significance. Even so, several trends are apparent. Unsaturated compounds are generally easier to oxidize than saturates. Silica is generally the least efficient radiation energy transfer medium;

alumina seems generally to be better than silica-alumina. Oxidation on silica gives tarry-looking residues. This darkening is less noticeable on silica-alumina and is nearly absent on alumina.

The reaction induced during irradiation is remarkably insensitive to temperature. Samples irradiated at $-196^\circ C$ and subsequently warmed to $25^\circ C$ (so that the pressure could be read) showed, within experimental error, no difference in $G(-O_2)$ from those irradiated at $25^\circ C$. The postirradiation catalytic reaction, however, could be completely suppressed by cooling to $-78^\circ C$.

Separation and Identification of Products. - Toluene oxidation produces benzyl alcohol, benzaldehyde, phenol, and cresols. Xylene oxidation gives rise to similar species. These products are tightly bound to the adsorbent and cannot be removed by extraction with, for example, dry ether. The adsorbent will even remove milligram amounts of product from dry ether solution. Therefore, the recovery and identification of products was carried out by refluxing the adsorbent first with ammonia and then with HCl and extracting. The solutions (acidified when

Table 4.5. Radiation Oxidation of Adsorbed Hydrocarbons

Initial $G(-O_2)$ based on energy dissipated in 10 g of adsorbent. Adsorbent degassed $>400^\circ\text{C}$

Adsorbate	Silica Ge1	Silica-Alumina	Alumina
Methane ^a	1.4	2.9	~2
Ethane ^a	2.6	3.0	4.8
Ethylene ^a	5.9	8.4	3.1
<i>n</i> -Propane ^a	0.8	8.1	3.7
Naphthalene ^b	3.3	<1	7.0
Anthracene ^b	28.4	^c	^c
Phenanthrene ^b	1.8	^c	^d
Biphenyl ^b	1.5	<1	^d
<i>n</i> -Hexane ^e	6.5	14.7	2.3
Hexene-1 ^e	13	110 ^f	28 ^f
Cyclohexane ^e	2.9	30.5	30.4
Cyclohexene ^e	14	78 ^f	54 ^f
Toluene ^e	3.6	11.5	18.1
<i>o</i> -Xylene ^e	<1	12.5	40.2
<i>m</i> -Xylene ^e	<1	19.1	29.5
<i>p</i> -Xylene ^e	<1	10.5	36.7
Mesitylene ^e	4.0	17.1	29.0

^aTotal adsorbate equals 50 micromoles.

^bTotal adsorbate equals 1 millimole.

^cConsiderable reaction occurs also in the absence of radiation.

^dLess than background [$G(-O_2) \approx 2$ to 4] for the radiation reaction of oxygen and alumina with no added adsorbent.

^eTotal adsorbate equals 7.2–10 millimoles (1 ml).

^fReaction occurs also in the absence of radiation.

necessary) were extracted with several small portions of ether. The ether extract was reduced in volume to 50 μl by passing a stream of N_2 through it and was then analyzed gas chromatographically with a column of tricresyl phosphate–phosphoric acid on glass beads.¹⁸

The product distributions are shown in Table 4.6. Different conditions for toluene oxidation give nearly the same product distribution. The most marked variations are the absence of benzyl alcohol when silica-alumina is the adsorbent, and the absence of phenol when silica is the adsorbent, or when oxygen is not present (with

¹⁸This analysis was perfected by A. D. Horton of the Analytical Chemistry Division.

alumina). Benzaldehyde can usually be detected (but not measured accurately). The total amount of products recovered, however, accounts for less than 10% of the oxygen consumed. Recovery and analysis experiments on standards are not quantitative either. Therefore, these products may be only surface intermediates in the oxidation process.

Postirradiation Reaction Kinetics

H. W. Kohn M. H. Lietzke

Following irradiation there is a slow but extended decrease of oxygen pressure. Examples of this postirradiation catalytic reaction for two different systems are shown in Fig. 4.11. The rate data for seven postirradiation oxidations were fitted to the Elovich equation¹⁹ and to a new equation, derived below. In five of the seven cases, the data fitted both equations excellently. However, if the (alumina) catalyst is first irradiated, and the toluene and oxygen are then added, the data can be fitted only by the new equation. Other potentially suitable expressions have been derived and are presently under investigation.

¹⁹S. Yu. Elovich and G. M. Zhabrova, *Zh. Fiz. Khim.* 13, 1761 (1939).

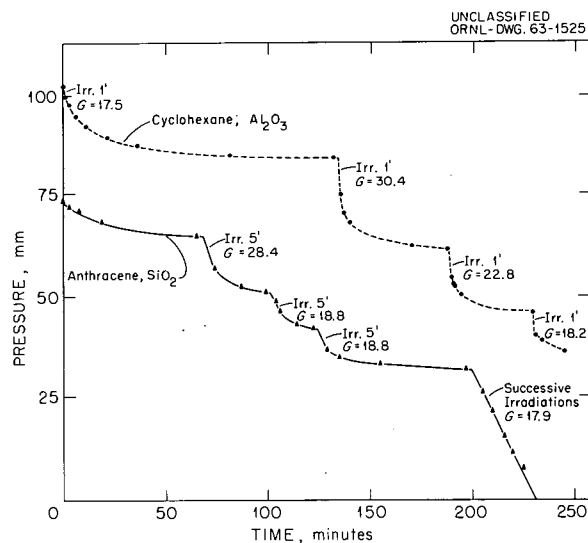


Fig. 4.11. Radiation-Induced Consumption of Oxygen by Two Hydrocarbon-Adsorbent Systems.

If one assumes a first-order rate law, then

$$-dx/dt = Kx, \quad (1)$$

where the rate constant K is proportional to the number of sites N . Hence,

$$K = K_1 N. \quad (2)$$

The sites themselves are disappearing with rate constant K_2 , and according to a second-order law

$$-dN/dt = K_2 N^2. \quad (3)$$

Upon integration of Eq. (3),

$$1/N = K_2 t + c_1. \quad (4)$$

Substitution of Eq. (4) into Eq. (1) gives

$$dx/x = K_1/K_2 \frac{dt}{(t + c_1/K_2)}. \quad (5)$$

Integration of Eq. (5) leads to

$$\ln x = a \ln(t + b) + c, \quad (6)$$

where $a = K_1/K_2$, $b = c_1/K_2$, and c is a constant of integration.

Table 4.6. Product Distributions for Hydrocarbon/Adsorbent/Oxygen Systems

Preparative Conditions	Relative Concentration of Products (<i>o</i> -Cresol Equals 1)			
	Benzyl Alcohol	<i>p</i> -Cresol	<i>m</i> -Cresol	Phenol
Toluene, irradiated 20 to 30 min with ϕCH_3 , O_2 , and Al_2O_3 present	1.7–1.8	1.2–1.5	~0.5	1.5–2.0
Silica-alumina adsorbent	Very small	1.5–2.0	~0.3–0.4	2.0–3.3
Silica adsorbent ^a	~2.4	~1.0	~1.1	~0.3
Irradiated Al_2O_3 <i>in vacuo</i> , add $\phi\text{CH}_3 + \text{O}_2$	0.75–1.0	0.5–0.9	~0.5	Trace to 0.5
Irradiated $\text{Al}_2\text{O}_3 + \phi\text{CH}_3$ <i>in vacuo</i> , dissolve and extract immediately	~2–4	1.2–2.0	Trace to 0.7	1.3–2.4
Al_2O_3 , ϕCH_3 , and O_2 , no irradiation (5 days auto-oxidation)	2.6	1.0	0.5	1.3
Irradiated <i>o</i> -xylene-oxygen-alumina		<i>(o</i> -methylbenzyl alcohol)/ <i>o</i> -cresol = 4.1		
Irradiated <i>p</i> -xylene-oxygen-alumina		<i>(p</i> -methylbenzyl alcohol)/ <i>p</i> -cresol = 6.5		
Irradiated <i>m</i> -xylene-oxygen-alumina		<i>(m</i> -methylbenzyl alcohol)/ <i>m</i> -cresol = 12		

^aToluene oxidation on silica gives dark-orange oxidation products and very little (i.e., a few micrograms) of the materials shown in the table.

5. Organic Chemistry

Pinacol Rearrangement of 2-endo-Phenyl-2,3-exo-norbornanediol

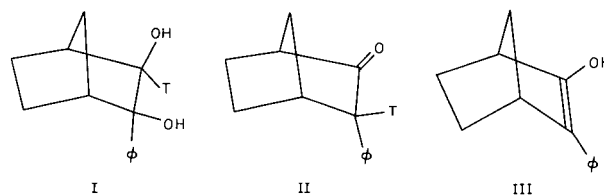
B. M. Benjamin R. G. Werth
Z. K. Cheema C. J. Collins

It has been shown that the pinacol rearrangement with strong acids of deuterated 1,2-diols¹ takes place without loss of deuterium. This indicates that the reaction occurs through carbonium ion intermediates followed by migration of hydrogen or some other group to produce product, rather than taking place through vinyl dehydration,^{2,3} which would result in loss of deuterium. Recently it was reported⁴ that 2-endo-phenyl-2,3-exo-norbornanediol (I), when treated with sulfuric acid, was converted to 2-endo-phenylnorbornanone (II) through a mechanism that involved a vinyl-like intermediate.

We synthesized I labeled at the 3-endo-hydrogen position with tritium in tracer amounts. The compound was treated with cold concentrated sulfuric acid, and the resultant ketone II was isolated and purified by quickly washing its ether solution with dilute sodium bicarbonate and then distilling it. The starting glycol had a molar radioactivity of 0.4901 mc/mole, and the ketone product had 0.4148 mc/mole, which is 85.2% of the starting radioactivity. The bicarbonate wash solution contained some tritium activity. In another run the ketone product was washed for a longer time with bicarbonate, after which it contained only 48.8% of the starting radioactivity. Therefore, during pinacol rearrangement of I the radioactivity is

retained. Some tritium is lost after formation and during subsequent workup by exchange of the acidic hydrogen at position 3. That all the tritium was in position 3 of ketone II was shown by treating an ether solution of a sample of it with dilute sodium hydroxide. The reisolated ketone had essentially no radioactivity. Tritium in any other position is not removed under these conditions.

These results show that vinyl dehydration that involves intermediates such as III does not occur. Since tritium remains in this molecule during the reaction it must migrate from position 2 to the carbon atom which bears the phenyl substituent. We are now attempting to determine the course of this rearrangement.



Primary and Secondary Carbon-14 and Deuterium Isotope Effects

V. F. Raaen R. G. Werth⁵
C. J. Collins

The differential method has been used in the continuation of the study of small isotope effects.⁶ The investigation has been extended to several

¹C. J. Collins *et al.*, *J. Am. Chem. Soc.* **81**, 460 (1959).

²E. S. Gould, *Mechanism and Structure in Organic Chemistry*, p 602, Henry Holt, New York, 1959.

³R. C. Fuson, *Reactions of Organic Compounds*, p 183, Wiley, New York, 1962.

⁴D. C. Kleinfelter and P. von R. Schleyer, *J. Am. Chem. Soc.* **83**, 2329 (1961).

⁵Research participant from Concordia College, Moorhead, Minn.

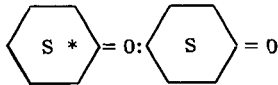
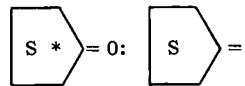
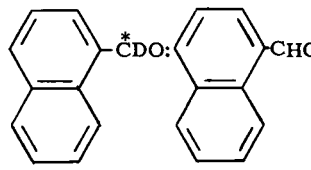
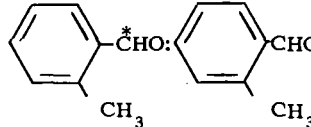
⁶*Chem. Div. Ann. Progr. Rept. June 20, 1960*, ORNL-2983, p 36; *June 20, 1961*, ORNL-3176, p 41; *June 20, 1962*, ORNL-3320, p 47; and V. F. Raaen, A. K. Tsiomis, and C. J. Collins, *J. Am. Chem. Soc.* **82**, 5502 (1960).

new ketones and aldehydes. These are listed in Table 5.1. Again, the reaction studied was the formation, at 0°, of 2,4-dinitrophenylhydrazones. In all reactions with deuterated compounds, C¹⁴ has been used to trace deuterium. Carbon-14 contributions to the isotope effects in these reactions have been evaluated separately.

The average of primary isotope effects of C¹⁴ in the reaction that forms 2,4-dinitrophenylhydrazones is $k^*/k = 0.950 \pm 0.004$. The effect is the same, within experimental error, for aldehydes and ketones. It is also unchanged by extreme steric effects.

The absence of a secondary deuterium isotope effect in the reaction of 1-naphthaldehyde-*d* (run 7, Table 5.1) is in contrast to the large isotope

Table 5.1. Experimentally Determined Values of the Isotope Effect in Conversion of Aldehydes and Ketones to Their 2,4-Dinitrophenylhydrazones

Run No.	Competing Species	k^*/k (ref a)
1	$\text{Ph}\overset{*}{\text{C}}\text{OCH}(\text{CH}_3)_2 : \text{PhCOCH}(\text{CH}_3)_2$	0.95222 ± 0.0022
2	$\text{Ph}\overset{*}{\text{C}}\text{HO} : \text{PhCDO}$	1.0031 ± 0.0015
3	$\text{Ph}\overset{*}{\text{C}}\text{DO} : \text{PhCDO}$	0.9542 ± 0.0007
4	$\text{Ph}\overset{*}{\text{C}}\text{DO} : \text{PhCHO}$	0.8999 ± 0.0026
5	 $\text{C}_6\text{H}_{10}\text{O}^* : \text{C}_6\text{H}_{10}\text{O}$	0.95960 ± 0.0032
6	 $\text{C}_5\text{H}_8\text{O}^* : \text{C}_5\text{H}_8\text{O}$	0.95658 ± 0.0024
7	 $\text{C}_{10}\text{H}_7\text{CHO}^* : \text{C}_{10}\text{H}_7\text{CHO}$	0.95076 ± 0.0067
8	 $\text{C}_{10}\text{H}_6\text{CH}_2\text{CHO}^* : \text{C}_{10}\text{H}_6\text{CH}_2\text{CHO}$	0.94879 ± 0.0009

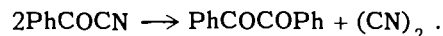
^aRatio of specific rate constants for C¹⁴-labeled (k^*) and unlabeled (k) species.

effect observed when the corresponding tritium-labeled 2-naphthaldehyde reacts with 4-nitrophenylhydrazine. The two reactions must, therefore, involve mechanisms whose rate-determining steps are very different. Study of this reaction will continue.

Coupling of Aroyl Cyanides in Photochemical Reactions

V. F. Raaen

In many reactions, cyanogen behaves chemically as if it were a halide. Similarly, benzoyl cyanide reacts in much the same way as does benzoyl chloride. There are exceptions to this pseudo-halide behavior. In one instance,⁷ cyanogen was found to give *o*-substitution in reactions with benzyl-type Grignard reagents. Aroyl nitriles exposed to unfiltered ultraviolet radiation couple to produce benzil;



In the present study, aroyl cyanides (in ether solution) are irradiated 6 hr by means of a 400-w immersion-type Hanovia lamp. Benzophenone is used as the energy-transfer agent. Benzoyl cyanide and *p*-toluyl cyanides are found to give benzil and *p*-tolil in 65 and 55% yields respectively. Other aroyl cyanides to be investigated are the *p*-nitrobenzoyl cyanide, phthaloyl cyanide, and furoyl cyanide. In a preliminary experiment, irradiation of *p*-nitrobenzoyl cyanide in an ether-tetrahydrofuran solution that contained benzophenone did not yield 4,4'-dinitrobenzil.

Irradiation of benzoyl chloride under conditions similar to those used for the aroyl cyanides yielded unchanged benzoyl chloride. Irradiation of benzoyl bromide produced four different unidentified and unstable products but no benzil. Irradiation of equimolar amounts of benzoyl cyanide and benzoyl chloride (in ether solution that contained benzophenone) yielded a solid product that, on the basis of solubility and C¹⁴ data, is believed to be a dimer or trimer of benzoyl cyanide. No benzil is produced in this reaction. It

⁷V. F. Raaen and J. F. Eastham, *J. Am. Chem. Soc.* 82, 1349 (1960).

has been observed⁸ that benzoyl cyanide adds to the C=N bond of imines and of Schiff bases. Possibly similar addition to the C≡N bond can occur in this case.

Method for the Rapid Combustion and Assay of C¹⁴ Compounds

V. F. Raaen

Pregl micro combustion methods and ionization chamber measurements provide the most accurate and generally applicable means for determining C¹⁴. Several important modifications to the apparatus described by Tolbert⁹ have been made without loss of its salient feature, that is, the use of an oxygen-carbon dioxide mixture that contains 5 to 7% carbon dioxide. The chief alterations are the provision for automatic oxygen cutoff when the ionization chamber is full and the use of cobaltcobaltic oxide (Co₃O₄) instead of quartz as the combustion-tube filling. The new filling makes it possible to burn organic samples at lower temperatures and at flow rates as high as 50 ml/min. In addition to the above changes, the pressure-relief bubbler and rotameter flowmeter were eliminated to advantage. The fritted-disk pressure regulator and lead dioxide trap, used with the Van Slyke-Folch procedure, are retained. The modifications described permit the accurate determination of C¹⁴ in a 2- to 30-mg sample in 20 min. The time required for all weighing operations and calculations is included in the 20-min period.

Compounds with an angular methyl group,¹⁰ for example, steroids and other oxidation-resistant compounds, tend to give methane on combustion. When tritium is present, cross contamination can become serious if the oxidation is incomplete. Use of the efficient cobaltcobaltic oxide catalyst reduces cross contamination from tritium to 0.2% or less at sweep rates that permit total absorption of water.

⁸A. Dornow and S. Lüpfer, *Chem. Ber.* **89**, 2718 (1956).

⁹B. M. Tolbert, *Ionization Chamber Assay of Radioactive Gases*, UCRL-3499 (August 1956).

¹⁰J. Horacek, J. Koerbl, and V. Pechanec, *Mikrochim. Acta* **1960**, 294 (1960).

The significance of sample weight on the observed molar radioactivity has usually been ignored, it being assumed that the filling gas would have a swamping effect. It has been found in this investigation that for a constant C¹⁴ content a sixfold increase in sample size causes an apparent increase in molar radioactivity of 1.0 to 1.8%. This increase in ion-pair yield with increase in carbon dioxide content seems to contradict published observations¹¹ that ion-pair yields are as much as 6% greater in oxygen than they are in carbon dioxide. Further experiments are in progress to resolve this point.

Carbon-14 and Deuterium Equilibration in the 1,2,2-Triphenylethyl System

B. M. Benjamin C. J. Collins

In previous publications¹²⁻¹⁴ accounts were given of the results of studies of the carbonium ion intermediates produced in the deamination reaction of 1,2,2-triphenylethylamine and also¹⁵⁻¹⁸ of the solvolysis reaction of 1,2,2-triphenylethyl tosylate.

In order to obtain a better understanding of the mechanisms involved in these reactions above, we have now studied similar elimination and substitution reactions of 1,2,2-triphenylethanol and its acetoxyl derivative labeled with both C¹⁴ and deuterium. The redistribution of deuterium and its effect upon the equilibration of C¹⁴ in the reaction products was determined.

1,2,2-Triphenylethanol-1-C¹⁴-1-d (I) was prepared by the reduction with lithium aluminum

¹¹W. P. Jesse and J. Sadaukis, *Phys. Rev.* **107**, 766 (1957); K. E. Wilzbach, A. R. Van Dyken, and L. Kaplan, *Anal. Chem.* **26**, 881 (1954).

¹²W. A. Bonner and C. J. Collins, *J. Am. Chem. Soc.* **78**, 5587 (1956).

¹³C. J. Collins, W. A. Bonner, and C. T. Lester, *J. Am. Chem. Soc.* **81**, 466 (1959).

¹⁴C. J. Collins, Joan B. Christie, and V. F. Raaen, *J. Am. Chem. Soc.* **83**, 4267 (1961).

¹⁵W. A. Bonner and C. J. Collins, *J. Am. Chem. Soc.* **75**, 5372 (1953).

¹⁶C. J. Collins and W. A. Bonner, *J. Am. Chem. Soc.* **75**, 5379 (1953).

¹⁷C. J. Collins and W. A. Bonner, *J. Am. Chem. Soc.* **77**, 92 (1955).

¹⁸W. A. Bonner and C. J. Collins, *J. Am. Chem. Soc.* **77**, 99 (1955).

deuteride of phenyl benzhydryl ketone-C¹⁴. The acetoxy derivative (III) was obtained by treating a pyridine solution of I with acetic anhydride.

Phenyl benzhydryl ketone labeled with C¹⁴ in the position *a* to the carbonyl group was repeatedly treated with small portions of deuterium oxide (with potassium carbonate as catalyst) until 97 to 98% of the α protons were replaced by exchange with deuterium.¹⁹ The resulting deuterated ketone was reduced with lithium aluminum hydride to give 1,2,2-triphenylethanol-2-C¹⁴-2-*d* (II).

In a typical formolysis experiment, 1.16 g of carbinol II was added to 25 ml of warm formic acid, and the solution was heated for 1 hr on the steam bath. Products were separated by crystallization and chromatography on alumina. The following quantities were obtained: 0.2284 g of 1,1,2-triphenylethylene (IV), 1.008 g of 1,2,2-triphenylethyl formate (V), and a trace of the

corresponding carbinol (VI). The olefin was analyzed for proton content by nuclear magnetic resonance (NMR); 33% of the molecules were found to contain olefinic protons, whereas the remaining 67% contained deuterium in that position. The C¹⁴ distribution was determined by standard degradation and counting procedures.¹⁴ Thirty-three percent of the C¹⁴ was found in position 2, and 67% in position 1. Deuterium distribution in the formate V was determined by first deformylizing it with lithium aluminum hydride to give the corresponding carbinol. The carbinol was then analyzed using the NMR spectrometer. The hydrogen and deuterium were found to be distributed approximately equally between positions 1 and 2 (see Table 5.2). No deuterium was lost by exchange with solvent, and therefore each molecule of the carbinol contained a deuterium atom in one position and a hydrogen atom in the other position as shown by the absence of doublets ($J = 8.1$ cps) in the NMR spectrum at $\delta \sim 4.1$ ppm and 5.1 ppm. Carbon-14 also was found to be equally distributed between the two chain positions. The carbinol I and its acetate III were submitted to the same

¹⁹As determined by the nuclear magnetic resonance (NMR) spectrum. We are indebted to the Department of Chemistry of the University of Tennessee for the use of their A-60 nuclear magnetic resonance spectrometer.

Table 5.2. Isotope Distribution in Products of the Reaction of Labeled 1,2,2-Triphenylethyl Derivatives with Acids

	Starting Compound				
	I	II	III	III	II
Reagent	98% formic acid	98% formic acid	98% formic acid + <i>p</i> -toluenesul- fonic acid	Acetic acid + <i>p</i> -tol- uenesulfonic acid	Concd H ₂ SO ₄
Olefinic product	IVa + IVb (31% yield)	IVa + IVb (19.9% yield)	IVa + IVb (31% yield)	Trace	IVa + IVb (63.7% yield)
C ¹⁴ (position 1)	70.6%	67.8%	71.9%		66.5%
C ¹⁴ (position 2)	29.4%	32.2%	28.1%		33.5%
Deuterium content	30%	33%	30.3%		47%
Formate product		Va + Vb + Vc + Vd (78.7% yield)	Vabcd (43% yield)	Va + Vb + Vc + Vd (as acetate)	
C ¹⁴ (position 1)		48.8%		49.2%	
C ¹⁴ (position 2)		51.2%		50.8%	
Deuterium (position 1)		52.2%		52.8%	
Deuterium (position 2)		47.8%		47.2%	

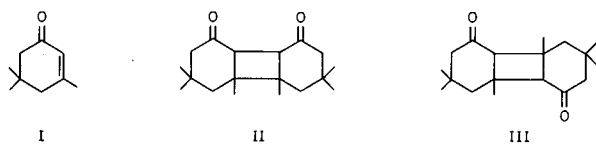
reaction conditions, and the products were analyzed for deuterium and C¹⁴ distribution.

The treatment of acetate III with acetic acid that contained *p*-toluenesulfonic acid resulted in almost quantitative yield of the ester, which had undergone complete equilibration of deuterium and C¹⁴. Only a trace of olefin was isolated. When carbinol II was treated with cold concentrated sulfuric acid, 63.7% of 1,1,2-triphenylethylene was isolated along with some unidentified tar and solid sulfonated material. The olefin had a C¹⁴ distribution of 33.5% in position 2 and 66.5% in position 1. However, it contained only 50% of the original deuterium. Further treatment of the olefin with sulfuric acid resulted in loss of more deuterium. Thus exchange of hydrogen for deuterium takes place in the presence of the strong acid, and the hydrogen exchange process is more rapid than the C¹⁴ scrambling. All data are recorded in Table 5.2.

Photochemical Dimerization of Isophorone

V. F. Raaen B. M. Benjamin
C. J. Collins

Isophorone (I), when irradiated with unfiltered ultraviolet light for 40 to 50 hr, yields a number of condensation products. All of them are viscous oils with the exception of two crystalline solids which were isolated in about 10% total yield. The solid obtained in highest yield had a melting point of 215°; the melting point of the other was 185°. On the basis of the molecular weights and of the proton counts obtained by integration of the nuclear magnetic resonance (NMR) spectra of these compounds, it was shown that both are dimeric with the starting isophorone (I) but contain no olefinic proton. From this information as well as from the carbon-hydrogen analyses and other chemical properties, these two compounds are believed to have the structures II and III, either



of which could conceivably exist in four stereoisomeric forms. The data presently available do

not permit assignment of the complete stereochemistry of the dimers. Features of the NMR spectra are ambiguous but suggest that similar molecules with fewer groups will serve as models for obtaining useful information.

The dimer of higher melting point is resistant to reduction and does not react with phenylmagnesium bromide, in contrast to the dimer of lower melting point. Isomers resulting from *trans* fusion across the double bond can be ruled out as reasonable structures for these compounds because upon being treated with strong base they do not undergo the expected isomerization which would result in a *cis* fused-ring system. Structures II and III are believed, therefore, to have been formed with *trans* position of the two six-membered rings. Further work will be required to establish which of the structures should be assigned to the material of higher melting point.

Mechanism of the Deamination Reaction

C. J. Collins B. M. Benjamin

The highly stereospecific nature of certain open carbonium ions produced during deamination reactions has been reported several times.^{20,21} An excellent example of stereospecific nonbridged intermediates can be found in the deamination of (+)-1,2,2-triphenylethyl-1-C¹⁴-amine. The data were explained by the mechanism shown in Fig. 5.1. In order to put the mechanism on a quantitative basis, rate expressions were set up for the formation and disappearance of all intermediate ions of Fig. 5.1, as well as for disappearance of reactant and appearance of products. The expressions were integrated between the limits $t = 0$ and $t = \infty$, and by use of the Heaton area theorem,²² the following four equations were derived:

$$(m_d - m_b) = \frac{k_2}{k_\phi} (m_b - 1) + \frac{k_r}{k_\phi} (m_b - m_c), \quad (1)$$

²⁰C. J. Collins, W. A. Bonner, and C. T. Lester, *J. Am. Chem. Soc.* 81, 466 (1959).

²¹C. J. Collins, J. B. Christie, and V. F. Raaen, *J. Am. Chem. Soc.* 83, 4267 (1961).

²²B. M. Benjamin and C. J. Collins, *J. Am. Chem. Soc.* 78, 4329 (1956).

$$(m_e - m_c) = \frac{k_2}{k_\phi} (m_c) + \frac{k_r}{k_\phi} (m_c - m_b), \quad (2)$$

$$(m_b - m_d) = \frac{k_2}{k_\phi} (m_d) + \frac{k_r}{k_\phi} (m_d - m_e), \quad (3)$$

$$(m_c - m_e) = \frac{k_2}{k_\phi} (m_e) + \frac{k_r}{k_\phi} (m_e - m_d), \quad (4)$$

where m_b , m_c , m_d , and m_e designate the mole fractions of product obtained through pathways B, C, D, and E respectively. Employing these equations, data from three deaminations were used to calculate²³ the best values for k_2/k_ϕ and

²³This was done using a linear least-squares program written for the IBM 7090 computer by M. H. Lietzke.

k_r/k_ϕ . The extent of error in calculating these values was obtained by using them to recalculate m_b , m_c , m_d , and m_e from Eqs. (1-4). The observed and calculated mole fractions are in good agreement and are listed in Table 5.3 (runs 1-3).

The same calculations were applied to the data obtained for the thermal decomposition of *N*-acetyl-*N*-nitroso-1,2,2-triphenylethylamine, which has been postulated to go through the same intermediates.²¹ The results are given in Table 5.3 (run 4).

These results demonstrate the compatibility of the classical carbonium ion mechanism of Fig. 5.1 with the data both for the deamination reactions^{20,21} and for the thermal decomposition²¹ of *N*-acetyl-*N*-nitroso-1,2,2-triphenylethylamine.

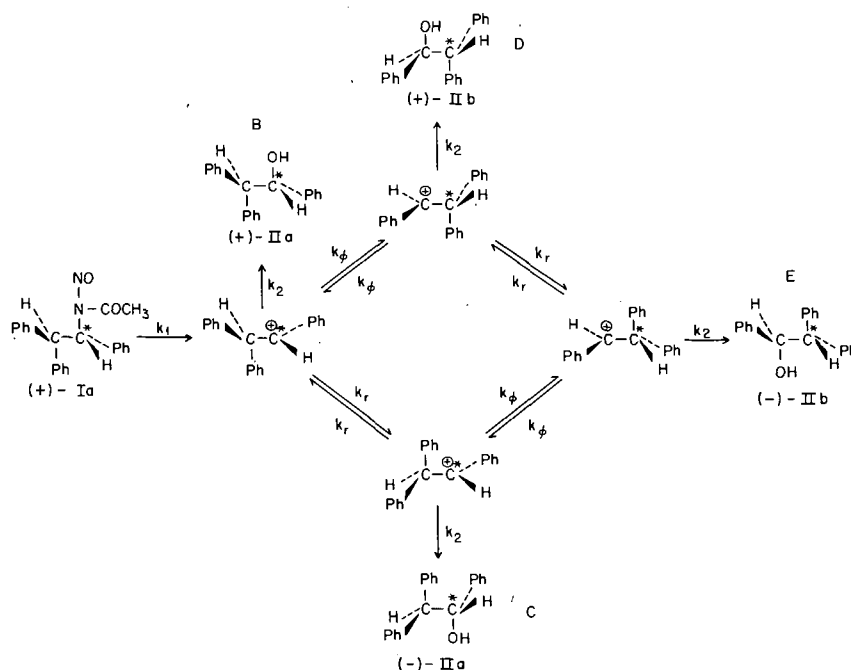


Fig. 5.1. Deamination of 1,2,2-Triphenylethylamine.

Table 5.3. Comparison of Experimental and Calculated Values of m_b , m_c , m_d , and m_e Using Eqs. (1-4) and the Data of Refs 20 and 21

Run No.		Contribution of Path				k_r/k_ϕ	k_2/k_ϕ
		B	C	D	E		
1	Observed	0.556	0.215	0.144	0.085	1.76 ± 0.15^a	2.26 ± 0.15
	Calculated	0.5530	0.2124	0.1424	0.092		
2	Observed	0.526	0.212	0.174	0.088	1.28 ± 0.3	1.55 ± 0.2
	Calculated	0.5172	0.2015	0.1714	0.1100		
3	Observed	0.470	0.253	0.170	0.110	1.89 ± 0.5	1.31 ± 0.3
	Calculated	0.4713	0.2384	0.1693	0.1266		
4 ^b	Observed	0.496	0.185	0.199	0.120	0.8875 ± 0.008	1.14 ± 0.006
	Calculated	0.4964	0.1850	0.1991	0.1195		

^aStandard error.

^bThese data are the averages of several runs for the thermal decomposition of *N*-acetyl-*N*-nitroso-1,2,2-triphenyl-ethyl-C¹⁴-amine.

Pyrolysis of Butyl Phosphate Esters and Salts

C. E. Higgins W. H. Baldwin

Extensive isomerization of the olefins formed by the pyrolysis of trialkyl phosphates was observed qualitatively by Baumgarten and Setterquist.²⁴ In determining the rate constants for the partial pyrolysis of tributyl phosphate (TBP) to form dibutylphosphoric acid (HDBP) and butene-1, we reported²⁵ that traces of the *cis-trans* isomers of butene-2 were detected after only a few percent of the TBP had been converted to HDBP. The composition of the gases evolved from the complete pyrolysis of TBP, HDPB, H₂MBP, Ba(DBP)₂, and BaMBP have now been determined.

At least four of every five butyl groups in TBP, HDBP, or H₂MBP were obtained as butene isomers by pyrolysis at 244°C (see Table 5.4). The remaining butyl groups were obtained predominantly as *n*-butyl alcohol and less as di-*n*-butyl ether.

The progressive increase of acid concentration during the pyrolysis of TBP was accompanied by an increase in the amount of isomerization. At

the beginning the gas formed was 100% butene-1, but at the end the composition was essentially that obtained from H₂MBP and showed the most extensive isomerization. The isomeric distributions for composite gas samples from each phosphate ester are listed in Table 5.4.

The barium salts of HDBP and H₂MBP were subjected to pyrolysis to test the extent to which acid catalysis is participating in isomerization. The gases from Ba(DBP)₂ contained 60% butene-1, 18% *trans*-butene-2, and 22% *cis*-butene-2, while from BaMBP only a 40% yield of butyl groups was obtained as 98% butene-1 at 300°C and 96% butene-1 at 400 to 500°C.

The ratios of the butenes produced by pyrolysis have been compared in Table 5.5 with the calculated equilibrium ratios.²⁶ While the composition of the gases from the pyrolysis of H₂MBP approaches the equilibrium composition, the agreement is not good. The probability then favors a kinetically controlled reaction over thermodynamic control. The constancy of the *cis/trans* ratio regardless of the acid concentration, the same as found even in the early stages of TBP decomposition, would appear to eliminate acid-catalyzed isomerization after rupture of the C—O bond.

²⁴H. E. Baumgarten and R. A. Setterquist, *J. Am. Chem. Soc.* **79**, 2605 (1957).

²⁵C. E. Higgins and W. H. Baldwin, *J. Org. Chem.* **26**, 846 (1961).

²⁶J. E. Kilpatrick et al., *J. Res. Natl. Bur. Std.* **36**, 559 (1946).

Table 5.4. Butene Production from the Pyrolysis of Butyl Phosphate Esters and Salts

	Heating Time (hr)	Temperature (°C)	Yield (%)	Composition (%)		
				Butene-1	<i>trans</i> -Butene-2	<i>cis</i> -Butene-2
TBP	2.5	244	80	55	26	19
HDBP	0.25	244	79	37	37	26
H ₂ MBP	0.10	244	85	19	47	34
Ba(DBP) ₂	1.5	300-470	67	60	18	22
BaMBP	2.5	300	8	98	1	1

Table 5.5. Ratio of Butene Isomers

	Temp (°C)	Ratio		
		<i>cis/trans</i>	<i>cis/1</i>	<i>trans/1</i>
TBP (composite)	244	0.73	0.35	0.47
HDBP	244	0.70	0.70	1.0
H ₂ MBP	244	0.72	1.8	2.5
Ba(DBP) ₂	300-470	1.2	0.37	0.3
BaMBP	300	1.0	0.01	0.01
	400-500	0.9	0.02	0.02
Equilibrium ^a	244	0.54	1.93	3.6
	300	0.57	1.67	2.94
	400	0.64	1.16	1.81
	500	0.65	0.86	1.31

^aJ. E. Kilpatrick et al., *J. Res. Natl. Bur. Std.* **36**, 559 (1946).

Separation of Butene Isomers and Butadiene by Gas-Liquid Chromatography

C. E. Higgins W. H. Baldwin

Gas-liquid chromatography (GLC) is the simplest and most useful method for the analysis of gaseous mixtures. In earlier work on the pyrolysis of tributyl phosphate and related compounds,²⁷ the

²⁷C. E. Higgins and W. H. Baldwin, *J. Org. Chem.* **26**, 846 (1961).

butene isomers formed were separated by GLC at 0°C with dimethyl formamide supported on Celite.²⁸ This highly efficient liquid must be used at low temperatures because of its relatively high volatility at room temperature. The comparison of the substances listed in Table 5.6 was made to see if a high-boiling compound could be found to give a comparable separation at room temperature. Although butene-1, *trans*-butene-2, and *cis*-butene-2 were the only four-carbon gaseous products formed from the pyrolysis of the butyl phosphates, 1,3-butadiene was also included to test the separation of a diolefin from olefins of the same chain length.

The relative retention ratios, related to butene-1 as standard, are listed in Table 5.6 for 27 different liquids supported on Celite in the weight ratio of 8 to 20 (liquid to support). All but dimethyl formamide were tested at 25°C. Most of the substances listed either successfully resolved the butene mixture or would do so with a longer column than the 6.75-ft test column, but many could not separate the 1,3-butadiene from the butenes.

The best overall resolution was found using aryl ethers modified with a nitro or amine group (*o*-nitrophenetole, *o*-nitroanisole, and *o*-phenetidine), aryl aldehydes and ethers (cinnamaldehyde, anisaldehyde, veratrole, and *m*-dimethoxybenzene), and an organic phosphorus compound (triethyl phosphate). Cinnamaldehyde separated *trans*-butene-2

²⁸G. W. Taylor and A. S. Dunlop, pp 73-85 in *Gas Chromatography*, ed. by V. J. Coates, H. J. Noebels, and I. S. Fagerson, Academic Press, New York, 1958.

Table 5.6. Retention Data at 25°C for Butene Isomers and 1,3-Butadiene

Liquid	Boiling Point (°C)	t_{R1} ^a Butene-1 (min)	Relative Retention Ratio ^b		
			<i>trans</i> -Butene-2	<i>cis</i> -Butene-2	1,3-Butadiene
Triethanolamine	277-79 (150 mm)	0.24	1.38	1.67	2.29
1-Naphthonitrile	299	1.83	1.41	1.60	1.73
<i>o</i> -Nitroanisole	277	2.04	1.35	1.56	2.10
Phenyl ether	259	2.05	1.30	1.54	
(TBP) ₂ ·UO ₂ (NO ₃) ₂		2.12	1.25	1.48	1.62
Anisaldehyde	247	2.16	1.38	1.59	2.01
<i>o</i> -Nitrophenetole	275	2.20	1.35	1.57	1.98
1-Bromonaphthalene	281	2.26	1.36	1.57	1.41
<i>o</i> -Phenetidine	228	2.28	1.27	1.54	1.85
<i>p</i> -Aminodiethylaniline	261	2.40	1.28	1.54	1.70
Cinnamaldehyde	252	2.42	1.41	1.63	1.94
<i>o</i> -Nitrotoluene	222	2.90	1.37	1.55	1.73
Veratrole	206	2.92	1.28	1.49	2.00
Dibenzylamine	300	2.99	1.29	1.58	1.55
Triethyl phosphate	216	3.03	1.24	1.47	2.07
12 ft dimethyl formamide, 0°C	152-54	3.62	1.38	1.68	
α -Methylnaphthalene	293	3.98	1.33	1.54	1.41
<i>m</i> -Dimethoxybenzene	216-18	4.23	1.29	1.48	1.74
Hallcomid M-18 OL	196-211 (3 mm)	4.55	1.29	1.48	1.39
Butyl dibutylphosphinate	125-26 (1 mm)	4.76	1.26	1.46	1.57
Hallcomid M-6	83-89 (3 mm)	4.83	1.28	1.47	1.76
Hallcomid M-12	147-63 (3 mm)	4.90	1.30	1.48	1.47
Tributyl phosphate	180 (20 mm)	5.19	1.27	1.46	1.63
Caprylic acid	238	5.38	1.31	1.48	
Dicyclohexylamine	256	5.88	1.27	1.50	1.13
Dibutyl dimethylphosphoramidate	85-86 (0.5 mm)	5.90	1.25	1.45	1.67
9 ft diethylacetamide	185	5.92	1.27	1.48	
9 ft diethylacetamide, 0°C		8.72	1.31	1.59	

^a t_{R1} = retention time from air peak.

^bButene-1 = 1.00.

from butene-1 better at 25°C than dimethyl formamide did at 0°C, though it did not resolve the *cis-trans* pair as well. The *cis-trans* resolution equivalent to that obtained using dimethyl formamide occurred with *o*-phenetidine or dibenzylamine. Increasing the chain length of the amide resulted in less effective separation. Resolution was still obtained employing dimethyl caproamide (Hallcomid M-6), but better resolution was found with *o*-nitrophenetole in half the retention time.

In Fig. 5.2, the separation of the butenes and 1,3-butadiene at 25°C is shown using a 13-ft column of *o*-nitrophenetole (29 wt %) on Celite 545. The relative retention ratios for this separation were 1.00, 1.35, 1.56, and 1.96 for butene-1, *trans*-butene-2, *cis*-butene-2, and 1,3-butadiene, respectively, where butene-1 emerged 4.63 min after the air peak. Fitting the column with a condenser and cooling with tap water to 16°C further improved the separation. The relative retention ratios were increased to 1.36, 1.59, and 2.01, where butene-1 (1.00) was retained 5.80 min after air.

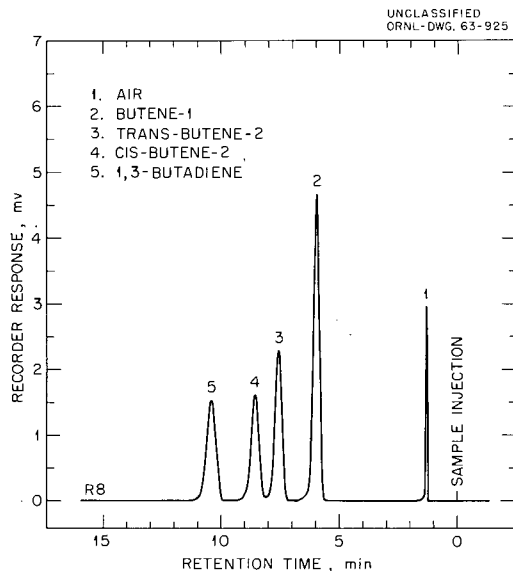


Fig. 5.2. The Separation of Butenes and 1,3-Butadiene at 25°C; Column, 13 ft by 0.25-in.-OD Coiled Copper Tubing Containing *o*-Nitrophenetole on Celite (Loading Ratio 2 to 5 by Weight); Carrier Gas, Helium; Flow Rate, 50 ml/min.

6. Chemistry of Aqueous Systems

Hydrolysis of Metal Ions

J. Aveston¹ J. S. Johnson
R. M. Rush

In previous annual reports, development of equilibrium ultracentrifugation methods for determination of activity coefficients of three-component solutions² and for estimation of formation constants for hydrolytic polymerization reactions³ was reported; refinements of these techniques have been made during the past year. Here we shall outline further work on the hydrolysis of U(VI) and results obtained in a renewed investigation⁴ of Mo(VI) hydrolysis.

Optical Absorption of Hydrolyzed Uranyl Perchlorate Solutions. — Last year a correlation of optical absorption spectra of hydrolyzed uranyl chloride solutions with a hydrolysis scheme based on ultracentrifugation and acidity measurements was reported; this scheme involved the species, written without possible complexed chloride ions, $(\text{UO}_2)_2(\text{OH})_2^{2+}$, $(\text{UO}_2)_3(\text{OH})_4^{2+}$, and $(\text{UO}_2)_3(\text{OH})_5^+$. The optical absorption curves were resolved into absorptivities for these individual species. In addition, analysis of literature acidity measurements had indicated, though not conclusively, that the same species, except for $(\text{UO}_2)_3(\text{OH})_4^{2+}$, were prominent in perchlorate media.

If it is assumed that only the species UO_2^{2+} , $(\text{UO}_2)_2(\text{OH})_2^{2+}$, and $(\text{UO}_2)_3(\text{OH})_5^+$ are present in appreciable amounts in perchlorate solutions and that the species absorptivities of the hydrolyzed species determined from analysis of spectra in

chloride media are the same in perchlorate, the fractions of the various species in a solution of given total U(VI) concentration and degree of hydrolysis can be determined from the optical absorbance. (The species absorptivity of the unhydrolyzed uranyl is obtained directly from spectrophotometric measurements of a solution sufficiently acidic to repress hydrolysis.) If the acidity of the solution is also measured, the fractions allow evaluation from measurements on a single solution of the formation quotients of the dimer, $k_{2,2}$, and the trimer, $k_{3,5}$; all species, of course, must be present in appreciable amounts.

Such a procedure was followed for eight solutions, from 0.001 to 0.1 M U(VI) and average degrees of hydrolysis between 0.4 and 1.0 hydroxyl bound per uranium, with use of the absorbances at 4300 Å. Average values of $k_{2,2} = 1.15 \times 10^{-6}$ and of $k_{3,5} = 3.9 \times 10^{-17}$ were obtained; the maximum variation of an individual solution from these numbers was 16%. A least-squares analysis of the acidity measurements alone gave 1.22×10^{-6} and 3.69×10^{-17} respectively.

With the constants obtained at 4300 Å, optical absorption curves obtained in perchlorate media were resolved by least-squares analysis into the absorptivities of the individual species over the wavelengths of the study. In Fig. 6.1, these are compared with values reported last year for chloride media. The agreement supports the assumptions made in this treatment.

Polymolybdates. — Most, though not all, who have worked in the field agree that polymeric aggregates are formed on the addition of acid to simple molybdate solutions, but there are wide differences in the species postulated. Schemes that involve one or more of almost all possibilities from dimeric to octameric, and even higher, units have been proposed at one time or another. Those which have been more frequently mentioned, or supported by more convincing evidence, are

¹Visiting scientist from the National Chemical Laboratory, Teddington, England.

²R. M. Rush *et al.*, *Chem. Div. Ann. Progr. Rept. June 20, 1961*, ORNL-3176, pp 45-47.

³R. M. Rush *et al.*, *Chem. Div. Ann. Progr. Rept. June 20, 1962*, ORNL-3320, pp 66-68.

⁴*Chem. Div. Ann. Progr. Rept. June 20, 1958*, ORNL-2584.

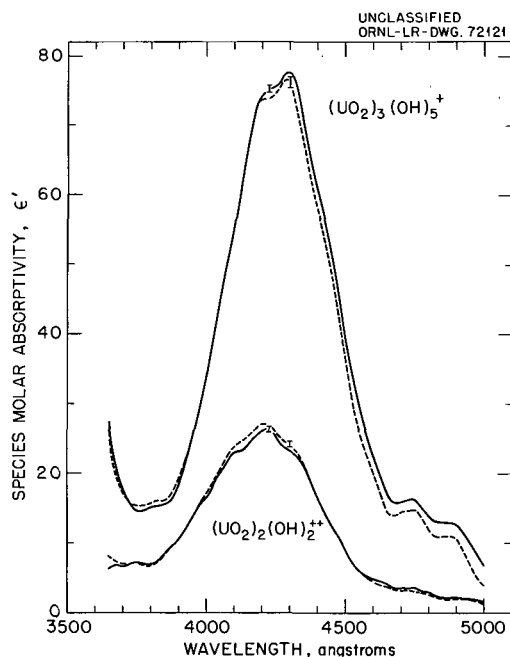


Fig. 6.1. Comparison of Species Molar Absorptivities for U(VI) in 1 M Total Chloride (—) and 1 M Total Perchlorate (---). Equilibrium quotients used: $k_{2,2} = 6.7 \times 10^{-7}$, $k_{3,4} = 4.7 \times 10^{-13}$, and $k_{3,5} = 1.0 \times 10^{-17}$ for chloride; $k_{2,2} = 1.15 \times 10^{-6}$ and $k_{3,5} = 3.9 \times 10^{-17}$ for perchlorate. Vertical lines on the curves indicate one standard error on each side of the value.

tetramers, heptamers, and octamers (though some of the evidence for tetramers could just as plausibly be explained by octamers of the same degree of neutralization). On the basis of structural studies, Lindqvist⁵ proposed that heptameric units of molybdate occur in solid ammonium paramolybdate, $(\text{NH}_4)_6\text{Mo}_7\text{O}_{24} \cdot 4\text{H}_2\text{O}$, and octameric units in tetramolybdate, $(\text{NH}_4)_2\text{Mo}_4\text{O}_{13} \cdot 2\text{H}_2\text{O}$ (or multiple); analytical ratios of ammonium to molybdenum in the solids are consistent. Sasaki, Sillén, and Lindqvist⁶ carried out titrations of Na_2MoO_4 in 3 M sodium perchlorate. They interpreted their curves up to p ca. 1.5 (p is the average number of hydrogen ions bound per molybdate) with an $\text{MoO}_4^{2-} - \text{Mo}_7\text{O}_{24}^{6-}$ equilibrium, with additional species differing from these only in that more hydrogen ions were bound.

⁵I. Lindqvist, *Arkiv Kemi* 2, 325 (1950); *Acta Cryst.* 3, 159 (1950).

⁶Y. Sasaki, L. G. Sillén, and I. Lindqvist, *J. Inorg. & Nucl. Chem.* 9, 93 (1959).

Equilibrium ultracentrifugations of acidified Mo(VI) in NaCl and NaClO_4 solutions, reported by us earlier⁴ and supplemented recently, indicate that the average degree of polymerization, N , rises rapidly from unity at p equals 0 to 1.2 and levels off in the range N equals 7 to 9 from p equals 1.2 to 1.5. The uncertainty in N stems principally from uncertainty in the charge of the species, that is, the extent of sodium complexing, and there is a slight possibility that the correct value lies outside these limits. Above $p = 1.5$, species of higher molecular weights are formed. Centrifugations with LiCl as supporting electrolyte indicate that the situation is similar in this medium, although there is some indication of higher charges on the species.

Titration of MoO_4^{2-} in 1 M total sodium (chloride) in the concentration range of 0.001 to 0.1 M Mo(VI) have been carried out; the curves are similar in shape to those in 3 M NaClO_4 (ref 6), even though they are shifted approximately half a pH unit in the acidic direction. Least-squares analysis of the results (Fig. 6.2, middle deviation plot) indicates that they are represented satisfactorily by a monomer-heptamer scheme similar to that of Sasaki, Sillén, and Lindqvist;⁶ the quotients for which values are listed in the figure are defined by the equation

$$k_{i,j} = \frac{[\text{H}_j(\text{MoO}_4)_i^{(2i-j)-}]}{(\text{H}^+)^j (\text{MoO}_4^{2-})^i}$$

The pH shifts of these curves from those in 3 M Na^+ are reflected in a shift of about 4.9 log units in the value of $k_{7,8}$; quotients for the successive binding of further protons are not greatly different from the values given⁶ for the other medium.

In order to test how firm a conclusion can be drawn from such evidence, similar schemes that involve a monomer-octamer (bottom, Fig. 6.2) and a monomer-heptamer-octamer scheme were tried. Agreement with experiment was for practical purposes as satisfactory as with the monomer-heptamer equilibrium. It appears that when a large fraction of total solute is found in species of such high aggregation, it is difficult to draw definitive conclusions from acidity data alone.

In an attempt to arrive at a more definite resolution, Raman spectra of the solids purported to be heptameric and octameric were compared with the spectra of concentrated solutions having

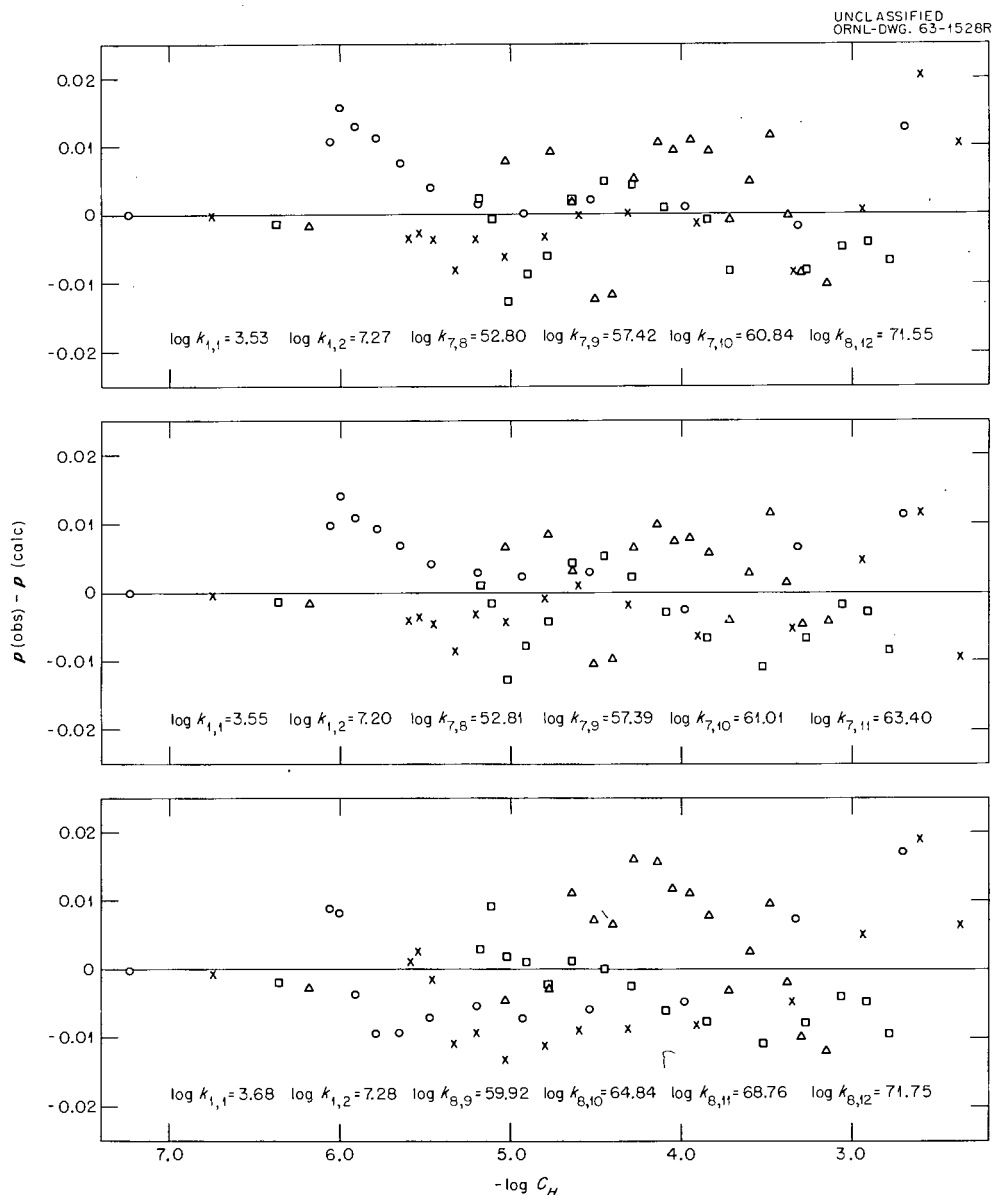


Fig. 6.2. Tests of Various Hydrolysis Schemes for Mo(VI) in NaCl. Deviation of observed proton number, $p(\text{obs})$, from values computed with constants obtained from least-squares fit, $p(\text{calc})$, of all points below $p = 1.5$. Symbols represent total molarity of Mo(VI) as: O, 0.08; x, 0.02; \square , 0.005; \triangle , 0.00125. All solutions in 1 M total sodium.

the same p as the solids. For reasons of solubility and availability of suitable crystals, it was necessary to compare the ammonium form of the solids with lithium molybdate solutions.

The comparison (Fig. 6.3) shows that the two solids have quite distinct patterns. The spectrum

of the solution with $p = 1.14$ is very similar to the corresponding paramolybdate, $(\text{NH}_4)_6\text{Mo}_7\text{O}_{24}$. The solution with $p = 1.5$ seems definitely more similar to the octamolybdate salt than to the paramolybdate. It thus appears that both the heptamer and the octamer are found in molybdate solutions below $p = 1.5$.

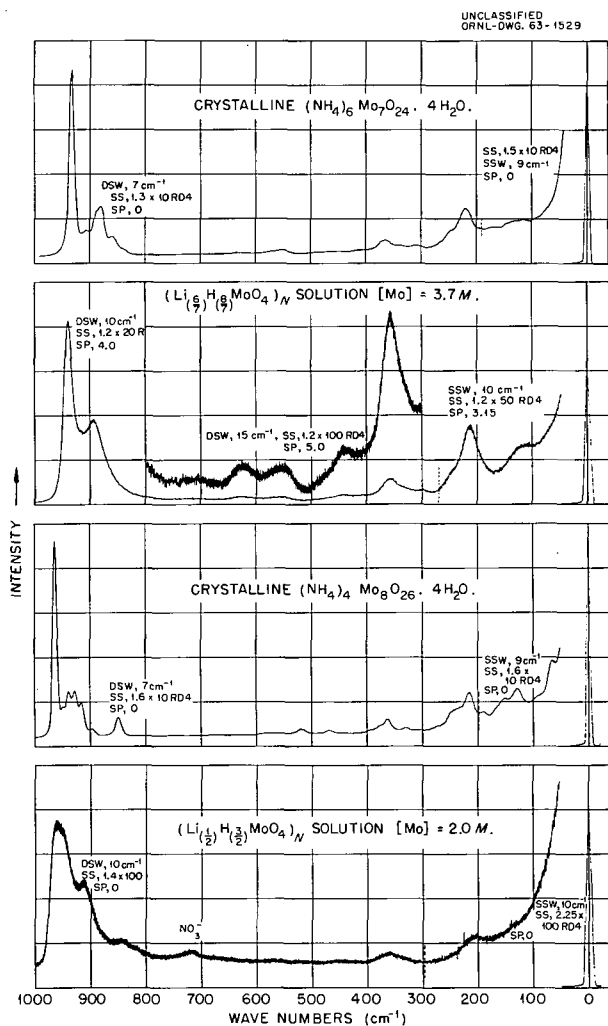


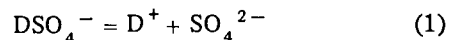
Fig. 6.3. Comparison of Raman Spectra of Solid Polymolybdates with Solutions. Cary model 81, lamp current 13.5 amp, chart speed $0.25 \text{ cm}^{-1} \text{ sec}^{-1}$, period control setting 0.5, slit length 10 cm. SS, sensitivity setting; SP, suppression setting; SSW, single slit width; DSW, double slit width.

Second Dissociation Constant of Deuteriosulfuric Acid from 25 to 225°C

M. H. Lietzke R. W. Stoughton

The second dissociation constant of deuteriosulfuric acid from 25 to 225°C has been computed

from data on the solubility of Ag_2SO_4 in D_2SO_4 solutions. In addition, the thermodynamic constants ΔF° , ΔH° , and ΔS° for the reaction



have been calculated. In carrying out the determinations the solubility of Ag_2SO_4 was measured in D_2O and in 0.1, 0.25, 0.5, 0.75, and 1.0 m D_2SO_4 from 25°C to at least 225°C. All solubility measurements were made using the synthetic method described previously.⁷

The D_2SO_4 solutions were prepared by diluting a 1 m stock solution of D_2SO_4 with D_2O . The D_2SO_4 stock solution was prepared according to the method given by Shudde⁸ which consists essentially of bubbling SO_3 vapor through D_2O . The SO_3 vapor [obtained by heating Sulfan B ($\gamma\text{-SO}_3$) from the Allied Chemical Co.] was conveyed with a stream of dry helium through the all-glass system. The D_2O was prepared by twice distilling 99.7% D_2O under an atmosphere of nitrogen that had been dried over $\text{Mg}(\text{ClO}_4)_2$; the first distillation was made from a 1 m D_2SO_4 and 0.5 m $\text{K}_2\text{Cr}_2\text{O}_7$ solution and the second from 2% KMnO_4 and 0.04 m NaOD . Extreme precautions were taken at all times to exclude any contamination by H_2O .

The experimental solubility values in each solution were fitted by the method of least squares to a cubic equation in the temperature: $s = a_0 + a_1 t + a_2 t^2 + a_3 t^3$. The coefficients of these equations are given in Table 6.1. At any temperature the solubility of Ag_2SO_4 is lower in D_2O than in H_2O (0.019 m in D_2O at 25°C compared to 0.027 m in H_2O). In 0.1 m D_2SO_4 the solubility of Ag_2SO_4 is lower than in H_2SO_4 ; in 0.25 and 0.5 m D_2SO_4 the solubility is about the same as in H_2SO_4 ; while in 0.75 and 1.0 m D_2SO_4 the solubility is higher than in the corresponding protonated systems. Thus the ionic strength effect is greater in the deuterated media.

Method of Calculation. — In carrying out the calculations it was assumed that only the species Ag^+ , D^+ , SO_4^{2-} , and DSO_4^- existed in a solution of Ag_2SO_4 dissolved in D_2SO_4 . As in previous

⁷M. H. Lietzke and R. W. Stoughton, *J. Am. Chem. Soc.* **78**, 3023 (1956).

⁸R. H. Shudde, North American Aviation Document NAA-SR-2158.

Table 6.1. Coefficients^a of Cubic Equation Describing the Molal Solubility of Ag₂SO₄ in D₂O and in D₂SO₄ Solutions

	a_0	a_1	a_2	a_3	σ_{fit}^b
		$\times 10^{-4}$	$\times 10^{-6}$	$\times 10^{-10}$	$\times 10^{-3}$
D ₂ O	0.0125795	3.04525	-1.27999	-7.74237	0.614
0.1 m D ₂ SO ₄	0.0109412	5.36589	0.687999	-59.2311	1.62
0.25 m D ₂ SO ₄	0.0138302	3.98960	6.31358	-177.706	1.89
0.5 m D ₂ SO ₄	0.0305152	-4.06263	16.4867	-350.694	2.77
0.75 m D ₂ SO ₄	0.0140920	3.17410	11.9268	-154.042	2.50
1.0 m D ₂ SO ₄	0.0325238	-6.26753	21.0097	-276.151	4.12

$$a_s = a_0 + a_1 t + a_2 t^2 + a_3 t^3.$$

^bStandard error of fit.

work⁹ it was also assumed that

$$\ln Q_2 = \ln K_2 + 4 \delta_T \left(\frac{\sqrt{I}}{1 + A\sqrt{I}} \right) \quad (2)$$

and

$$\ln S = \ln 4s_0^3 + 6 \delta_T \left(\frac{\sqrt{I}}{1 + P\sqrt{I}} - \frac{\sqrt{3s_0}}{1 + P\sqrt{3s_0}} \right), \quad (3)$$

where K_2 is the DSO₄⁻ acid constant; δ_T is the Debye-Hückel limiting slope at temperature T for a singly charged ion; S is the stoichiometric solubility product of Ag₂SO₄; s_0 is the solubility of Ag₂SO₄ in D₂O at temperature T ; P and A are adjustable parameters; and I is the ionic strength of the solution, given by

$$I = m + s + 2[\text{SO}_4^{2-}], \quad (4)$$

where s is the molal solubility of Ag₂SO₄ in D₂SO₄ of molality m and the brackets indicate molality.

Hence the overall problem involves the evaluation of $\ln K_2$, A , and P by a nonlinear least-squares procedure subject to the restrictions represented by the equation for conservation of total sulfate and those expressing the (molality)

solubility product of Ag₂SO₄ and the acid dissociation quotient in terms of the concentrations of the ionic species. Details of the calculation are very similar to those in the bisulfate acid constant calculation previously reported.¹⁰ One difference, however, should be emphasized: measurement of Ag₂SO₄ in five different concentrations of D₂SO₄ permitted the direct evaluation of all three parameters. It was not necessary, as in the HSO₄⁻ calculation (where the solubility of Ag₂SO₄ was studied in only three different concentrations of H₂SO₄), to permute over a range of set values of one of the parameters. Also, the least-squares matrix ($X^T X$) was inverted permitting a calculation of the standard error in $\ln K_2$ at each temperature.

In order to compute the value of δ_T , the Debye-Hückel limiting slope at temperature T , it is necessary to know the density and dielectric constant of D₂O as a function of temperature. Values of the density of D₂O from 30 to 250°C are given by Heiks *et al.*,¹¹ while the dielectric constant from 4 to 100°C has been measured by Malmberg.¹² Above 100°C the dielectric constant of H₂O was used in preference to extrapolating the D₂O values, since

¹⁰M. H. Lietzke and R. W. Stoughton, *J. Phys. Chem.* **65**, 2247 (1961).

¹¹J. R. Heiks *et al.*, *J. Phys. Chem.* **58**, 488 (1954).

¹²C. G. Malmberg, *J. Res. Natl. Bur. Std.* **60**, 609 (1958).

⁹M. H. Lietzke and R. W. Stoughton, *J. Phys. Chem.* **63**, 1183, 1186, 1188, 1190, 1984 (1959); **64**, 816 (1960).

Table 6.2. Values of $\log K_2$ for D_2SO_4 as a Function of Temperature

Temperature, t (°C)	P	A	$-\log K_2^a$ (DSO_4^-)	$\sigma_{\log K_2}^b$	$-\log K_2^c$ (DSO_4^-)	$-\log K_2^d$ (HSO_4^-)
25	0.635	0.234	2.326	0.043	2.342	1.987
50	0.576	0.216	2.668	0.13	2.656	2.301
75	0.461	0.210	2.976	0.13	2.969	2.636
100	0.400	0.224	3.287	0.095	3.281	2.987
125	0.417	0.307	3.591	0.061	3.593	3.352
150	0.451	0.391	3.906	0.034	3.904	3.728
175	0.481	0.456	4.208	0.024	4.215	4.113
200	0.504	0.505	4.524	0.036	4.526	4.506
225	0.515	0.539	4.842	0.042	4.836	4.905

^aEquations (2) and (3).

^bStandard error in $\log K_2$.

^cEquation (5).

^dM. H. Lietzke and R. W. Stoughton, *J. Phys. Chem.* **65**, 2247 (1961).

the experimental values for the two solvents tended to merge at 100°C and since different expressions for D_2O gave widely different values on extrapolating to higher temperatures (some higher and some lower than the H_2O values). The H_2O values used were computed at each temperature using the equation given by Åkerlöf and Oshry.¹³

The values of $\log K_2$ obtained as a function of temperature are fitted by the method of least squares;

$$\log K_2 = \frac{22.86565}{T} + 1.253986 - 0.01231753T, \quad (5)$$

where T is the absolute temperature.

In Table 6.2 are summarized the values of P , A , and $\log K_2$ computed at each 25°C interval from 25 to 225°C along with the standard error in $\log K_2$; in the last column are shown the values of $\log K_2$ for H_2SO_4 (ref 10) for comparison. It can be seen that the value of K_2 for D_2SO_4 is a factor of about 2.3 lower than the corresponding value for H_2SO_4

at 25°C, while the values are about equal at 200°C. Above 200°C the value of K_2 for D_2SO_4 is larger than the value for H_2SO_4 . At 225°C the ratio $K_{HSO_4^-} / K_{DSO_4^-}$ is about 0.87.

Activity Coefficient of HBr in HBr-KBr Mixtures

M. H. Lietzke R. W. Stoughton

Previous EMF studies have involved the determination of the standard potential of the Ag, AgCl electrode¹⁴ to 275°C, the thermodynamic properties of hydrochloric acid solutions¹⁵ to 275°C, and the determination of the standard potential of the Ag, AgBr electrode and the mean ionic activity coefficient of HBr (ref 16) to 200°C. In the present work EMF measurements have been made in HBr-KBr mixtures to 150°C so that the activity coefficient of HBr in these mixtures could be

¹⁴R. S. Greeley *et al.*, *J. Phys. Chem.* **64**, 652 (1960).

¹⁵R. S. Greeley *et al.*, *J. Phys. Chem.* **64**, 1445 (1960).

¹⁶M. B. Towns, R. S. Greeley, and M. H. Lietzke, *J. Phys. Chem.* **64**, 1861 (1960).

¹³G. C. Åkerlöf and H. J. Oshry, *J. Am. Chem. Soc.* **72**, 2844 (1950).

calculated. The cell used may be represented as



Experimental. – The experimental apparatus and the preparation of electrodes and solutions were the same as described previously.^{14,16}

Results and Discussion. – EMF measurements were made on HBr-KBr solutions of total ionic strength approximately 0.01, 0.02, 0.034, 0.05, 0.067, 1.0, 1.8, and 3.8. In all these cases the ionic strength fraction of HBr in the mixtures was 0.5. In addition measurements were made in solutions of total ionic strength approximately 0.4 and 1.0 in which the ionic strength fraction of HBr was either 0.25 or 0.75. The EMF values taken at the same temperature were reproducible to about ± 1.0 mv. In general they were more reproducible in the solutions that contained a higher fraction of HBr. No drift of EMF with time was observed.

In the calculations the solubility of AgBr was neglected, and the ionic strength was taken to be equal to the sum of the HBr and the KBr molalities. No correction was made for the loss of water or of HBr to the vapor space since these corrections had previously been shown to be unnecessary.¹⁶ The hydrogen pressure was calculated by subtracting the vapor pressure of the solution from the observed total pressure, while the vapor pressure of the solution was obtained by taking the vapor pressure of pure water at the temperature of measurement from the steam tables¹⁷ and correcting for the presence of KBr and HBr in solution by Raoult's law. Each EMF value was corrected to 1.00 atm hydrogen pressure by subtracting $(RT/2\mathfrak{J}) \ln f_{\text{H}_2}$, where the fugacity f_{H_2} of the hydrogen was taken equal to the hydrogen pressure. The corrected EMF values E at each ionic strength were plotted as a function of temperature, and the values at 25, 60, 90, 125, and 150°C were read from the curves. All further computations were done at these five temperatures.

The experimental EMF values were measured at temperatures within one degree of these round temperatures. In all cases the experimental EMF values were within 1 mv of the smooth curves and in most cases they were much closer.

¹⁷E. Schmitt (ed.), *VDI-Wasserdampftafeln*, 4th ed., Springer-Verlag, Berlin, 1956.

Since the measurements on the series of solutions in which the HBr contributed 50% to the ionic strength had been extended to low concentrations, they could be used not only to permit the computation of activity coefficients but also to provide a check on the E^0 values of the Ag, AgBr electrode which had been previously reported.¹⁶ Accordingly, values of $E^{0''}$ were computed for each ionic strength at the five temperatures mentioned above:

$$E^{0''} = E + \frac{RT}{\mathfrak{J}} \ln [m_2(m_2 + m_3)] - \frac{2RT}{\mathfrak{J}} \frac{\delta_T \sqrt{I}}{1 + A\sqrt{I}}, \quad (2)$$

where E represents the EMF of cell (1) at 1 atm hydrogen pressure and at absolute temperature T , δ_T is the Debye-Hückel limiting slope, A was taken as 1.5 at all temperatures, m_2 is the molality of the HBr in the HBr-KBr mixture, while m_3 is the corresponding molality of KBr, I is the total ionic strength of the solution ($m_2 + m_3$), and R and \mathfrak{J} have their usual meanings. The limiting slope for a univalent ion δ_T was corrected for temperature changes as in previous work;¹⁴ the correction included terms for change in dielectric constant and density of the solvent. Values of δ_T used in Eq. (2) are shown in Table 6.3.

The values of $E^{0''}$ so calculated were fitted at each temperature by the method of least squares to

$$E^{0''} = E^0 - \frac{2RT}{\mathfrak{J}} BI - \frac{2RT}{\mathfrak{J}} CI^2, \quad (3)$$

where B and C are adjustable parameters and E^0 is the standard potential of the Ag, AgBr electrode. A comparison of the values of E^0 so calculated and the values previously reported is shown in Table 6.3.

The agreement between the E^0 values for the Ag, AgBr electrode obtained in the two studies is within experimental error. It is interesting to note that the values obtained in the HBr solutions¹⁶ were derived by extrapolating EMF data taken in the range 0.005 to 0.1 m , while the values reported in the present study were derived by extrapolating EMF data measured in the total ionic strength range 0.01 to 3.9. In the former case, only a linear term was used in the extrapolation, while in the latter case both a linear and a quadratic term were used.

Table 6.3. Comparison of the Values of E^0 for the Ag, AgBr Electrode

Temperature, t (°C)	ϕ_T	E^0 mixture data (v)	E^0 previously reported ^a (v)	ΔE^0 (mv)
25	1.1697	+0.0714	+0.0712	0.2
60	1.2558	0.0507	0.0499	0.8
90	1.3483	0.0276	0.0269	0.7
125	1.4787	-0.0056	-0.0054	-0.2
150	1.5886	-0.0336	-0.0320	-1.6

^aM. B. Towns, R. S. Greeley, and M. H. Lietzke, *J. Phys. Chem.* 64, 1861 (1960).

The activity coefficients of HBr in the solutions that contain 0.5 ionic strength fraction HBr were calculated using Eq. (4) and the values of B and C obtained in the least-squares fit of Eq. (3);

$$\ln \gamma_{\text{HBr}} = \frac{-\phi_T \sqrt{I}}{1 + A \sqrt{I}} + BI + CI^2. \quad (4)$$

As indicated above, a value of 1.5 was used for A at all temperatures. The values of the parameters in Eq. (4) are given in Table 6.4.

Since the measurements on the series of solutions where the ionic strength fraction of HBr was not 0.5 had not been made at enough different total ionic strength values to permit a least-squares fitting of $E^{0''}$ values vs ionic strength, the activity coefficients were computed using the following equation:

$$\ln \gamma_{\text{HBr}} = \frac{1}{2} \frac{\int}{RT} (E^0 - E) - \frac{1}{2} \ln m_2(m_2 + m_3). \quad (5)$$

However, the EMF values in these solutions were subjected to a similar smoothing by calculating $E^{0''}$ values at each of the two ionic strengths (0.4 and 1.0) and plotting these values along with the corresponding E^0 values for pure HBr (ref 16). Then a consistent set of EMF values was calculated corresponding to the smoothed $E^{0''}$ values. The values of the mean ionic activity coefficients of HBr as a function of ionic strength fraction of HBr at total ionic strengths of 0.41 and 1.0 are

Table 6.4. Parameters of Eq. (4) for the Pure Components HBr and KBr and for HBr-KBr Mixture Where $m_2 = m_3$

t (°C)	A	B	C	D^a
			$\times 10^{-2}$	$\times 10^{-4}$
HBr^b				
25	1.500	0.3716	-3.695	
60	1.500	0.5320	-18.716	
90	1.500	0.4355	-15.433	
HBr in HBr-KBr ($m_2 = m_3$)^c				
25	1.500	0.2437	0.4805	
60	1.500	0.2425	0.1418	
90	1.500	0.2287	0.1051	
125	1.500	0.1766	0.9402	
150	1.500	-0.2500	11.304	
KBr^d				
25	1.292	0.01989	0.6511	-4.677
60	1.252	0.08151	-0.4270	3.837
90	1.368	0.07621	-0.2216	1.841

^a D is the coefficient of a cubic term in I used in the case of KBr.

^bHBr parameters for 0 to 1 m .

^cMixture parameters for I from 0 to 3.9 m .

^dKBr parameters for 0 to 4 m .

shown in Table 6.5. The values in the column labeled ionic strength fraction 0.0 were taken from Harned and Hamer¹⁸ and actually represent values at an HBr concentration of 0.01 *m* at the total ionic strength indicated.

When the values of $\ln \gamma_{\text{HBr}}$ in the mixtures (Table 6.5) are plotted against the molality of KBr (m_3) in the mixture at constant total ionic strengths of 0.41 and 1.0 the plots are linear within experimental error. At ionic strength of 1.0, the $\ln \gamma_{\text{HBr}}$ values in the pure acid solutions were not used at temperatures above 60°C, since these were appreciably lower than the linear extrapolations of the values at lower acid fractions and since there is reason to suspect that the EMF of the cell (at higher temperatures and acid concentrations) cannot be readily interpreted in terms of the activity coefficient of HBr.¹⁹ These values

¹⁸H. S. Harned and W. J. Hamer, *J. Am. Chem. Soc.* **55**, 4496 (1933).

¹⁹We wish to thank B. B. Owen (private communication, April 1963) for bringing this matter to our attention. We also would like to point out that the activity coefficients in ref 16 may be in error at 1 *m* above 60°C and at 0.5 *m* above about 125°C.

are enclosed in brackets in Table 6.5. Hence it was assumed that the activity coefficients of HBr in the mixtures could be represented at each temperature and constant total ionic strength by equations of the form

$$\ln \gamma_{\text{HBr}} = \ln \gamma_{\text{HBr}}^{\circ} - \alpha m_3. \quad (6)$$

In Eq. (6), γ_{HBr} is the activity coefficient of HBr in the mixture, while $\gamma_{\text{HBr}}^{\circ}$ is the activity coefficient of HBr in an HBr solution of the same ionic strength. In order that all the data at the five different temperatures and at each ionic strength could be used simultaneously in determining the values of α , the latter was assumed to be linear in I , t , and the product of I and t . The parameters obtained by the method of least squares are given in the following equation:

$$\alpha = 0.24847 + 0.0009330(t - 25) - 0.06058I - 0.0004683I(t - 25). \quad (7)$$

This equation may be used in Eq. (6) to calculate the values of γ_{HBr} in an HBr-KBr mixture between 25 and 150°C. It may also be used in calculating

Table 6.5. Mean Ionic Activity Coefficients of HBr in HBr and in HBr-KBr Mixtures

<i>t</i> (°C)	Ionic Strength Fraction of HBr in the Mixture				
	1.0	0.754	0.5	0.272	0.0
<i>I</i> = 0.41					
25	0.795	0.778	0.752	0.736	0.723
60	0.759	0.751	0.738	0.707	0.697
90	0.748	0.721	0.711	0.685	
125	0.713	0.679	0.667	0.645	
150	0.673	0.649	0.630	0.619	
	1.0	0.745	0.5	0.254	0.0
<i>I</i> = 1.0					
25	0.873	0.843	0.798	0.755	0.728
60	0.852	0.812	0.784	0.717	0.690
90	(0.773)	0.770	0.742	0.684	
125	(0.717)	0.711	0.672	0.634	
150	(0.653)	0.660	0.613	0.585	

the activity coefficient of KBr in the HBr-KBr mixtures. Since²⁰

$$\left(\frac{\partial \ln a_3}{\partial m_2}\right)_{m_3} = \left(\frac{\partial \ln a_2}{\partial m_3}\right)_{m_2}, \quad (8)$$

it follows that

$$\begin{aligned} \left(\frac{\partial \ln \gamma_3}{\partial m_2}\right)_{m_3} &= \left(\frac{\partial \ln \gamma_3}{\partial I}\right)_{m_3} \\ &= \left(\frac{\partial \ln \gamma_2}{\partial m_3}\right)_{m_2} = \left(\frac{\partial \ln \gamma_2}{\partial I}\right)_{m_2}. \end{aligned} \quad (9)$$

Upon differentiating²¹ Eq. (6) with respect to the total ionic strength I at constant m_2 ,

$$\left(\frac{\partial \ln \gamma_2}{\partial I}\right)_{m_2} = \frac{d \ln \gamma_2^\circ}{dI} - \alpha - m_3 \frac{d\alpha}{dI}. \quad (10)$$

Equation (10) may be inserted into (9) and the latter integrated with respect to I between the limits m_3 and $m_2 + m_3$; whence

$$\begin{aligned} \ln \gamma_3(m_2 + m_3) - \ln \gamma_3^\circ(m_3) &= \ln \gamma_2^\circ(m_2 + m_3) \\ &- \ln \gamma_2^\circ(m_3) - \int_{I=m_3}^{I=m_2+m_3} \alpha dI \\ &- \int_{I=m_3}^{I=m_2+m_3} m_3 \frac{d\alpha}{dI} dI. \end{aligned} \quad (11)$$

The second term on the left and first two terms on the right of Eq. (11) may be evaluated²² by the use of analytical expressions of the type shown in Eq. (4) for the pure components HBr and KBr from literature data^{9,23} at 25, 60, and 90°C. The parameters in Eq. (4) for the pure components and for a 50-50 mole % mixture are shown in Table 6.4. The substitution of Eq. (7), which gives the ionic strength and temperature dependence of α , into Eq. (11) permits the evaluation of the remaining integrals and hence the calculation of the activity

coefficient of KBr in the HBr-KBr mixtures. The values obtained are shown in Table 6.6.

As can be seen the activity coefficient of KBr in the mixtures is both less temperature and less ionic strength dependent than is the activity coefficient of HBr in the same mixtures.

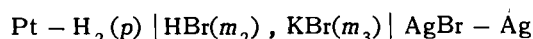
Table 6.6. Mean Ionic Activity Coefficient of KBr in HBr-KBr Mixtures

t (°C)	Ionic Strength Fraction of KBr in the Mixture			
	1.0	0.728	0.5	0.246
$I = 0.41$				
25	0.670	0.681	0.691	0.703
60	0.661	0.672	0.683	0.698
90	0.651	0.653	0.656	0.660
$I = 1.0$				
25	0.616	0.639	0.660	0.679
60	0.619	0.618	0.625	0.641
90	0.609	0.601	0.595	0.593

Activity Coefficients of Hydrochloric Acid and Sodium Chloride in Hydrochloric Acid-Sodium Chloride Mixtures

M. H. Lietzke R. W. Stoughton

In a recent study²⁴ of the cell



it was shown that at constant temperature and ionic strength the logarithm of the activity coefficient of HBr in HBr-KBr mixtures varies linearly with the molality of KBr. It was also shown that with the parameters describing this variation it is possible to calculate the activity coefficient of the KBr in the mixtures. It seems not unreasonable to assume that the thermodynamic behavior

²⁰N. Bjerrum, *Z. Physik. Chem. (Leipzig)* **104**, 406 (1923).

²¹H. A. C. McKay, *Trans. Faraday Soc.* **51**, 903 (1955).

²²M. H. Lietzke and R. W. Stoughton, *J. Phys. Chem.* **66**, 508 (1962).

²³G. C. Johnson and R. P. Smith, *J. Am. Chem. Soc.* **63**, 1351 (1941).

²⁴M. H. Lietzke and R. W. Stoughton, to be published in the *Journal of Physical Chemistry*.

observed in the HBr-KBr system would also be exhibited by the HCl-NaCl system. In fact it has already been shown²⁵ that at constant ionic strength and temperature the logarithm of the activity coefficient of HCl in HCl-NaCl mixtures varies linearly with NaCl concentration. Hence data on the activity coefficient of HCl in pure solutions²⁶ and in NaCl solutions²⁷ and of NaCl^{25,28} in pure solutions have been used to calculate the parameters describing the activity coefficients of both HCl and NaCl in HCl-NaCl mixtures. For these calculations the values of the activity coefficient of HCl ($m = 0.01$) in NaCl solutions²⁷ for 0 to 50°C were extrapolated to 60°C.

In carrying out the computation it was assumed that the ionic strength dependence of the logarithms of the activity coefficients of HCl, of NaCl, and of HCl ($m = 0.01$) in NaCl solutions could be described at each temperature by Eq. (1):

$$\ln \gamma_{\pm} = \frac{-\phi\sqrt{I}}{1 + 1.5\sqrt{I}} + BI + CI^2 + DI^3. \quad (1)$$

In this equation ϕ is the appropriate Debye-Hückel limiting slope which contains as a factor the square root of the density of water; I is the ionic strength (on a molality basis); and B , C , and D are adjustable parameters. The values of the parameters were determined in each instance by the method of least squares and are given in Table 6.7. For convenience, the value of the parameter in the denominator of the Debye-Hückel expression was taken in all cases to be 1.5.

At constant ionic strength and temperature it may be assumed that

$$\ln \gamma_{\text{HCl}} = \ln \gamma_{\text{HCl}}^{\circ} - \alpha m_{\text{NaCl}}, \quad (2)$$

where α is a function only of total ionic strength and temperature. In Eq. (2), γ_{HCl} is the activity coefficient of HCl in the HCl-NaCl mixture, and $\gamma_{\text{HCl}}^{\circ}$ is the activity coefficient of HCl in an HCl

solution of the same ionic strength. The parameters in Table 6.7 which give the ionic strength dependence of the logarithm of the activity coefficients of HCl and HCl ($m = 0.01$) in NaCl were used to calculate values of the parameter α in Eq. (2).

In order that the values of α could be used to compute the activity coefficient of NaCl in the HCl-NaCl mixtures, they were fitted by the method of least squares for ionic strength values above 0.11:

$$\alpha = a_0 + a_1 I + a_2 I^2 + a_3 t + a_4 It. \quad (3)$$

Because the activity-coefficient values appeared to be more precise at 25°C and below, two separate fits of the α values were made (1) using the α values from 0 to 25°C and (2) using the α values from 25 to 60°C. The parameters of Eq. (3) for the two fits are given in Table 6.8.

Equation (3) may be used in Eq. (2) to calculate the values of γ_{HCl} in HCl-NaCl mixtures between 0 and 60°C for a total ionic strength as low as 0.11. It may also be used in calculating the activity coefficient of NaCl in the HCl-NaCl mixtures, since according to the rules of partial differentiation it follows from the equation for the total free energy of the system in terms of the partial molal quantities that²⁹

$$\left(\frac{\partial \ln a_3}{\partial m_2} \right)_{m_3} = \left(\frac{\partial \ln a_2}{\partial m_3} \right)_{m_2}. \quad (4)$$

This equation may be expressed in terms of the variable I :

$$\begin{aligned} \left(\frac{\partial \ln \gamma_3}{\partial m_2} \right)_{m_3} &= \left(\frac{\partial \ln \gamma_3}{\partial I} \right)_{m_3} \\ &= \left(\frac{\partial \ln \gamma_2}{\partial m_3} \right)_{m_2} = \left(\frac{\partial \ln \gamma_2}{\partial I} \right)_{m_2}. \end{aligned} \quad (5)$$

Upon differentiating³⁰ Eq. (2) with respect to the total ionic strength I at constant m_2 ,

$$\left(\frac{\partial \ln \gamma_2}{\partial I} \right)_{m_2} = \frac{d \ln \gamma_2^{\circ}}{dI} - \alpha - m_3 \frac{d\alpha}{dI}. \quad (6)$$

²⁵H. S. Harned and B. B. Owen, *The Physical Chemistry of Electrolytic Solutions*, 3d ed., chap. 14 and Appendix A, Reinhold, New York, 1958.

²⁶R. S. Greeley et al., *J. Phys. Chem.* **64**, 1445 (1960); H. S. Harned and R. W. Ehlers, *J. Am. Chem. Soc.* **55**, 2179 (1933).

²⁷H. S. Harned and G. E. Mannweiler, *J. Am. Chem. Soc.* **57**, 1873 (1935).

²⁸R. A. Robinson, *Trans. Faraday Soc.* **35**, 1222 (1939).

²⁹N. Bjerrum, *Z. Physik. Chem. (Leipzig)* **104**, 406 (1923).

³⁰H. A. C. McKay, *Trans. Faraday Soc.* **51**, 903 (1955).

Table 6.7. Values of the Parameters of Eq. (1) Giving the Ionic Strength Dependence of the Activity Coefficients of HCl and NaCl

Temperature	<i>B</i>	<i>C</i>	<i>D</i>	σ_{fit}^2 ^a
		$\times 10^{-2}$	$\times 10^{-3}$	$\times 10^{-6}$
		NaCl ^b		
0	-0.0373852	3.56644	-3.03349	15
10	-0.00701016	2.95583	-2.43814	8.9
20	0.0102915	2.81899	-2.50491	7.2
25	0.0241390	2.29369	-1.96781	1.7
30	0.0265655	2.56721	-2.45514	8.1
40	0.0417905	2.11154	-1.97467	9.1
50	0.0553079	1.68468	-1.53191	8.5
60	0.0628909	1.95709	-2.28398	5.3
		HCl ^c		
0	0.253049	2.33598	-2.02789	17
10	0.247702	2.13754	-1.83070	6.2
20	0.241086	1.92351	-1.56655	2.9
25	0.237579	1.82248	-1.45024	2.8
30	0.222354	3.38269	-6.73504	2.2
40	0.218233	2.50886	-4.14886	3.2
50	0.214575	1.82417	-1.81932	1.7
60	0.213183	0.589944	2.96181	2.1
		HCl (<i>m</i> = 0.01) in NaCl ^d		
0	0.139450	4.28343	-6.23885	19
10	0.148713	3.59159	-4.98155	8.5
20	0.150904	3.33731	-4.62235	7.0
25	0.156031	2.91288	-3.89802	4.4
30	0.154654	2.95854	-4.11460	6.5
40	0.157406	2.57192	-3.64777	5.7
50	0.160227	2.07142	-2.89576	11
60	0.163973	1.61486	-2.50417	17

^aVariance of fit.

^bThe equations hold to 4 *m*.

^cAt 25°C and below, the equations hold to 4 *m*, above 25°C to 2 *m*.

^dThe equations hold to 3 *m*.

Table 6.8. Parameters of Eq. (3)^a

Temperature Range (°C)	a_0	a_1	a_2	a_3	a_4
		$\times 10^{-2}$	$\times 10^{-3}$	$\times 10^{-3}$	$\times 10^{-4}$
0-25	0.120661	-2.53234	5.32570	-1.22881	1.40681
30-60	0.108192	-2.11277	4.45109	-0.962928	1.88598

^aEquation holds over the ionic strength range 0.11 to 3.01 *m* at 0 to 25°C and 0.11 *m* to 2.01 above 25°C.

Table 6.9. Activity Coefficients of HCl and NaCl in Pure Solution and in a 50-50 Mole % Mixture

<i>I</i>	γ_{HCl} in Pure HCl	50-50 Mole % Mixture		γ_{NaCl} in Pure NaCl
		γ_{HCl}	γ_{NaCl}	
$t = 0^\circ\text{C}$				
0.2	0.780	0.771	0.749	0.736
0.5	0.777	0.756	0.704	0.674
1.0	0.840	0.799	0.694	0.636
1.5	0.943	0.878	0.714	0.625
2.0	1.078	0.984	0.748	0.628
2.5	1.247	1.114	0.793	0.642
3.0	1.455	1.266	0.843	0.662
$t = 25^\circ\text{C}$				
0.2	0.768	0.762	0.746	0.736
0.5	0.758	0.743	0.705	0.682
1.0	0.809	0.780	0.703	0.656
1.5	0.895	0.850	0.728	0.656
2.0	1.008	0.942	0.767	0.668
2.5	1.148	1.054	0.815	0.688
3.0	1.318	1.182	0.866	0.715
$t = 60^\circ\text{C}$				
0.2	0.745	0.741	0.730	0.723
0.5	0.723	0.715	0.689	0.673
1.0	0.754	0.737	0.686	0.654
1.5	0.818	0.790	0.710	0.661
2.0	0.907	0.864	0.749	0.680

Equation (6) may be inserted into Eq. (5) and the latter integrated with respect to l between the limits m_3 and $m_2 + m_3$; whence

$$\ln \gamma_3(m_2 + m_3) - \ln \gamma_3^\circ(m_3) = \ln \gamma_2^\circ(m_2 + m_3) - \ln \gamma_2^\circ(m_3) - \int_{I=m_3}^{I=m_2+m_3} \alpha dl - \int_{I=m_3}^{I=m_2+m_3} m_3 \frac{d\alpha}{dl} dl. \quad (7)$$

The second term on the left and the first two terms on the right of Eq. (7) may be evaluated by the use of Eq. (1) and the parameters given in Table 6.7 for the pure components HCl and NaCl. The substitution of Eq. (3), which gives the ionic strength and temperature dependence of α , into Eq. (7) permits the evaluation of the remaining integrals and hence the calculation of the activity coefficient of NaCl in HCl-NaCl mixtures. Values of the activity coefficients of HCl and NaCl in pure solution and in a 50-50 mole % mixture at 0, 25, and 60°C are given in Table 6.9.

As expected, at any temperature and ionic strength the activity coefficients are in the order (greatest to least) $\gamma_{\text{HCl}}^\circ$, $\gamma_{\text{HCl}}(m_2 = m_3)$, $\gamma_{\text{NaCl}}(m_2 = m_3)$, $\gamma_{\text{NaCl}}^\circ$; and at any temperature the changes of activity coefficients with ionic strength are in the same order.

INORGANIC AND PHYSICAL CHEMISTRY: SPECTROPHOTOMETRY OF SOLUTIONS AT HIGH TEMPERATURES AND PRESSURES

An Improved High-Temperature Aqueous Spectrophotometric Cell Assembly

W. C. Waggener A. J. Weinberger
R. W. Stoughton

Cryostat and cooling controls have been incorporated in the redesigned spectrophotometer chamber and cell assembly previously described³¹ permitting simultaneous and automatic control of both sample and reference cells in the range 25°C to at least -70°C.

Spectrophotometry of Aqueous HNO₃, H₂SO₄, and DClO₄

W. C. Waggener A. J. Weinberger
R. W. Stoughton

The study of the DClO₄-D₂O-H₂O system reported last year³¹ has been continued and expanded to include exploratory runs with HNO₃ and H₂SO₄ solutions. All experiments have been conducted with a second prototype high-temperature

³¹W. C. Waggener, A. J. Weinberger, and R. W. Stoughton, *Chem. Div. Ann. Progr. Rept.*, June 20, 1962, ORNL-3320, pp 73-74.

Table 6.10. High-Temperature-Pressure Spectrophotometric Cell Corrosion Data

Cell length, 3.81 cm; sample volume at 25°C, 4.4 ml

Material of Construction	Area in Contact with Sample	
	cm ²	% Crevice
Titanium (body)	25.6	30
Sapphire (windows)	9.87	80
Teflon (seals)	<0.02	100

Temperature (°C)	Acid	Concentration Range (f)	Sample Pickup [micromoles ml ⁻¹ hr ⁻¹ (unit formality) ⁻¹]	
			Titanium	Aluminum
250	HNO ₃	0-1.0	0.020	0.75
250	DClO ₄	0-1.0	0.015	0.70
250	H ₂ SO ₄	0-0.2	0.011	3.8
250	H ₂ SO ₄	0.2-0.4	2.20	3.8
25	DClO ₄	0.1-1.0	<9 × 10 ⁻⁴	<3 × 10 ⁻⁴

spectrophotometric cell designed to allow gas-liquid equilibration.³²

After the initial experiments with DClO_4 (ref 32) the severely pitted windows of the sample cell were replaced with windows cut so as to expose the $(10\bar{1}1)$ planes (60° orientation) instead of the (0001) planes (0° orientation) of sapphire to the solutions. The new windows have been exposed successively to HNO_3 , H_2SO_4 , and DClO_4 solutions in a series of experiments involving 31 temperature cycles above 100°C , 600 hr above 25°C , and 200 hr above 245°C . The change in crystal orientation had no discernible effect on the corrosion rates for the three acids, and DClO_4 also was found to be an etchant for the $(10\bar{1}1)$ faces of sapphire.

The amount of titanium and aluminum appearing in cell samples (determined by spectrographic analysis) increased with the time and temperature of exposure and, except for H_2SO_4 , was roughly proportional to the acid concentration. A summary of corrosion rates expressed in terms of micromoles $\text{ml}^{-1} \text{hr}^{-1}$ (unit formality)⁻¹ is given in Table 6.10.

HNO_3 . — Figures 6.4 and 6.5 represent exploratory experiments with dilute HNO_3 , using a titanium cell which had been pretreated by numerous earlier experiments with HNO_3 and DClO_4 solutions. All runs were made with H_2O in the reference cell at 25°C . The curves are direct overlays from chart data and are illustrative of the spectrophotometry of the system.

Curve (2) of Fig. 6.4 shows the characteristic profile of the lowest-energy electronic band ($\epsilon_{0.3\mu}^{\text{max}} \sim 7$) of the nitrate ion and the optical cutoff by the next higher-energy band ($\epsilon_{0.2\mu}^{\text{max}} \sim 1.5 \times 10^4$). Solutions of HNO_3 tend to absorb in the 0.35 to 0.8μ region because of the presence of molecular HNO_2 ($\epsilon_{0.37\mu}^{\text{max}} \sim 50$) and NO_2 ($\epsilon_{0.4-0.5\mu}^{\text{max}} \sim 200$). The characteristic vibrationally perturbed electronic band of HNO_2 can be used for its estimation at 25°C . Estimation of NO_2 is less straightforward because of the diffuseness of its spectrum and because the amount of NO_2 appears significant only above 200°C and for $\text{HNO}_3 > 0.1 f$.

The effects of $[\text{H}^+]$, $[\text{NO}_3^-]$, $[\text{O}_2]$, and temperature upon the amount of HNO_2 and NO_2 present are correlated approximately by the following

reactions:

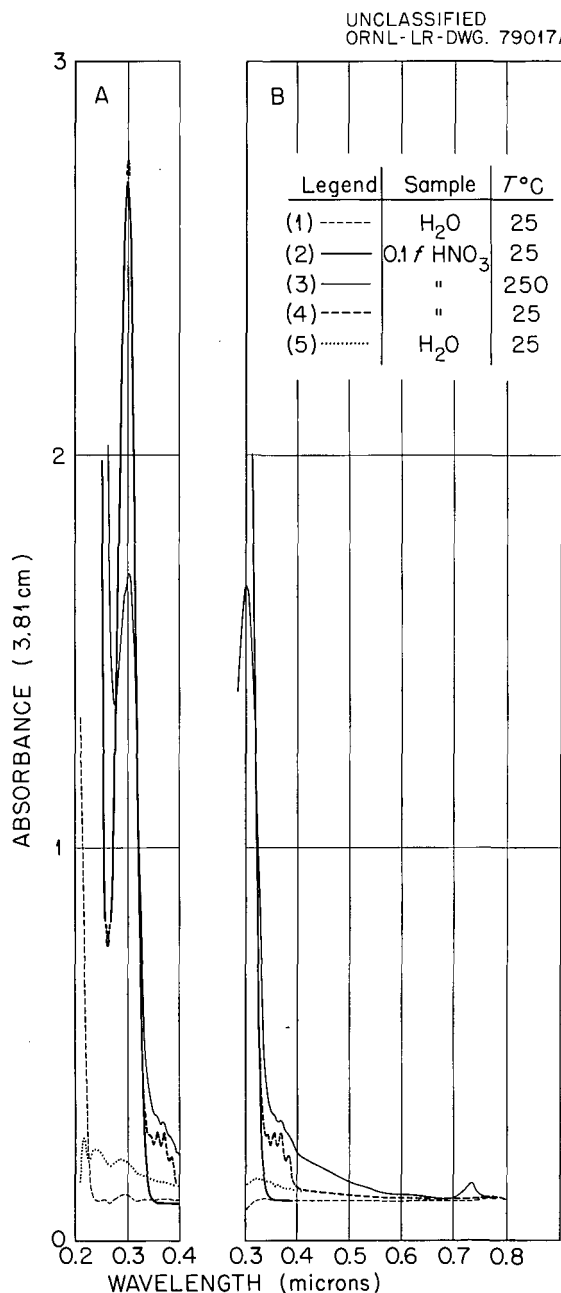
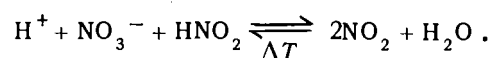
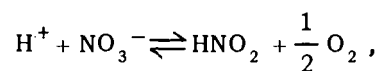
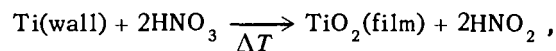


Fig. 6.4. Spectra of $0.1 f \text{HNO}_3$ Under Argon as a Function of Temperature vs H_2O at 25°C . Source used: Graph A, hydrogen arc; Graph B, tungsten-filament lamp.

³²W. C. Waggener, A. J. Weinberger, and R. W. Stoughton, *Chem. Div. Ann. Progr. Rept.* June 20, 1961, ORNL-3176, pp 58-59.

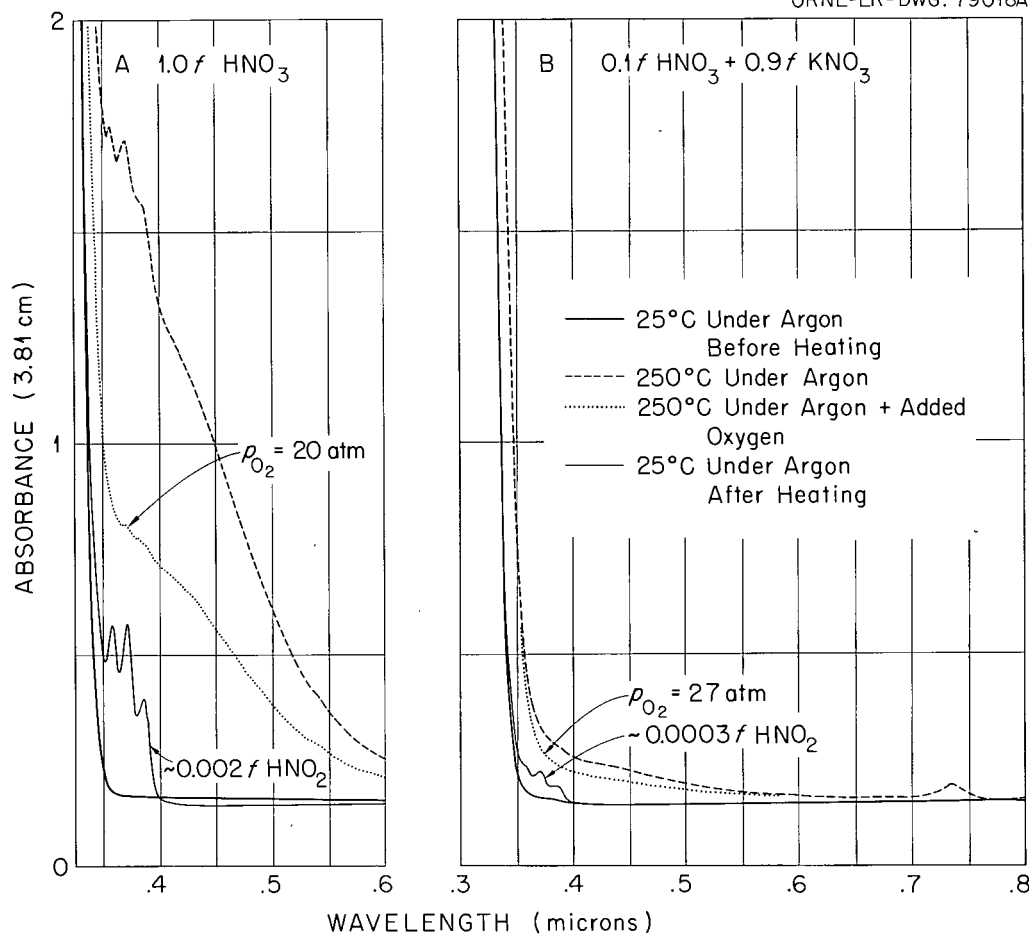


Fig. 6.5. Effect of Acidity on the Thermal Stability of 1 f Aqueous Nitrate Solutions. Source used: tungsten-filament lamp. Graph A, 1.0 f HNO₃; Graph B, 0.1 f HNO₃ + 0.9 f KNO₃.

The titanium cell became relatively unreactive to solutions of HNO₃ of lower concentration and at temperatures below that employed for passivation. Solutions 0.1 to 1.0 f in HNO₃, following runs at 250°C for several days in the absence of an overpressure of O₂, showed 0.01 to 0.5% HNO₂ after cooling to 25°C.

For HNO₃ solutions at 250°C the passivity of titanium breaks down completely in the concentration range between 1 and 4 f.

H₂SO₄. — Figures 6.6–6.8 represent exploratory experiments with dilute H₂SO₄. These spectra were measured vs H₂O at 25°C and were corrected for background absorbance. Figure 6.6 shows the absorbance of 0.1 f H₂SO₄ under an inert atmosphere as a function of time and temperature. The

absorption band at 0.3 μ which appeared after filling at 25°C presumably is due to hydrolytic titanium species, which either absorb strongly (estimated $\epsilon_{0.3 \mu}^{\max} \sim 2 \times 10^4$) or exhibit non-Rayleigh light scattering. When the solution was heated this band disappeared between 40 and 70°C. At 250°C a new absorption band centered at 0.275 μ was discernible after 10 to 12 hr. Figure 6.7 shows the effect of an O₂ overpressure on 0.1 f H₂SO₄; the absorbance cutoff at 0.25 μ was sharpened and there was no evidence of the 0.275-μ band after more than 15 hr at 250°C. The spectra of 0.2 f H₂SO₄ (not shown) were qualitatively similar to those of 0.1 f acid. However, the absorbance of the 0.3-μ band (25°C) was one-half, and the 0.275-μ band (250°C) was twice that observed for the more dilute acid.

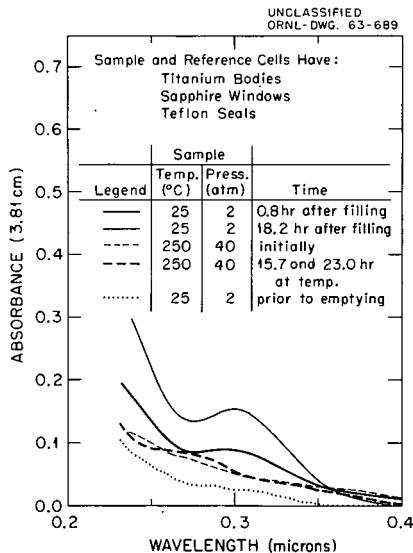


Fig. 6.6. Spectra of 0.1 f H_2SO_4 Under Argon as a Function of Time and Temperature vs H_2O at $25^\circ C$.

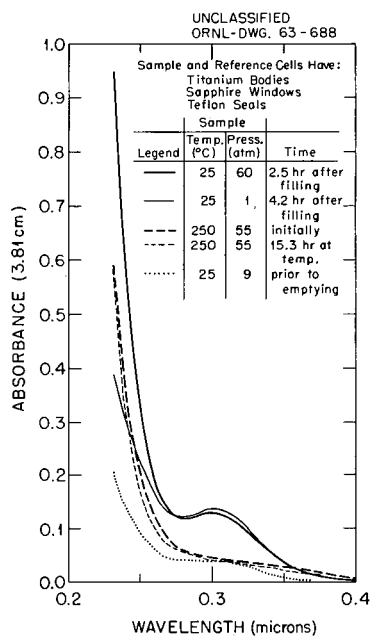


Fig. 6.7. Spectra of 0.1 f H_2SO_4 Under O_2 as a Function of Time and Temperature vs H_2O at $25^\circ C$.

Solutions 0.4 f in H_2SO_4 under argon remained transparent in the wavelength range above 0.25μ and the temperature range from 25 to $200^\circ C$ as shown in Fig. 6.8. Above $200^\circ C$ the $0.275\text{-}\mu$

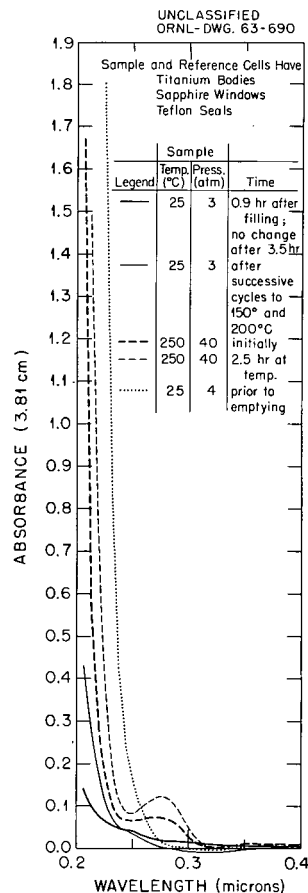


Fig. 6.8. Spectra of 0.4 f H_2SO_4 Under Argon as a Function of Time and Temperature vs H_2O at $25^\circ C$.

absorption band developed rapidly. This band possibly is due to a titanium complex associated with decomposition of H_2SO_4 , which is known to have occurred since H_2S was detected in the sample at the end of the run.

Higher concentrations than 0.4 f H_2SO_4 caused gross attack of the titanium even at temperatures under $100^\circ C$.

DCIO₄. — Figures 6.9 and 6.10 give an idea of the absorbance of 0.1 and 0.5 f $DCIO_4$ solutions, respectively, as a function of time and temperature. The sapphire windows were etched progressively during 57.5 hr at $250^\circ C$, and the observed increase in absorbance shown in Fig. 6.10, particularly in the base line, is attributed to increased light scattering at the window surfaces and in the solution. It is noteworthy that reduction products (*viz.*, Cl_2 , $HOCl$, $HClO_2$, and $HClO_3$) which absorb

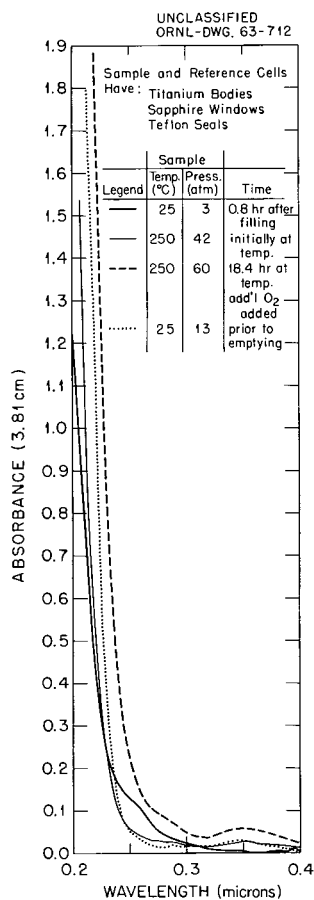


Fig. 6.9. Spectra of 0.1 f DClO_4 Under O_2 as a Function of Time and Temperature vs H_2O at 25°C .

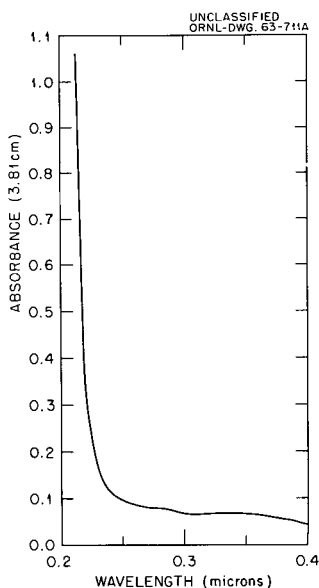


Fig. 6.10. Absorbance Increase in 0.5 f DClO_4 During 57.5 hr at 250°C and 49 atm Total Pressure.

in the visible and ultraviolet regions were below the limit of spectral detection.

Perchloric acid above 1 f as yet has not been studied at 250°C , and it is not known at what concentration titanium ceases to be passive for this system.

ION EXCHANGE STUDIES

Ion Exchange in Concentrated HCl and HClO_4

F. Nelson T. Murase³³
K. A. Kraus

A systematic study of the cation exchange behavior of most elements was carried out in HCl and HClO_4 solutions over a wide range of acid concentrations. Principal emphasis was placed on the more concentrated solutions. The results are summarized in the form of two "periodic tables" in Figs. 6.11 and 6.12. The adsorption functions are given as plots of $\log D_v$ (amount per liter of bed/amount per liter of solution) vs molarity of acid. The data refer to measurements at 25°C with a 4% cross-linked Dowex 50. Loading of the resin was usually less than 1% of capacity.

From an examination of Figs. 6.11 and 6.12, the following generalizations can be made:

1. A surprisingly large number of elements show moderate or even excellent adsorbability in concentrated HCl or HClO_4 solutions. Further, there are striking differences between these two media.

2. Adsorbability from concentrated HClO_4 is generally substantially larger than from concentrated HCl . The principal exceptions, Fe(III) , Ga(III) , and presumably also Au(III) , form ions of the type MCl_4^- , whose special adsorption characteristics on cation exchangers were described earlier.³⁴

3. In concentrated HCl , only Sc(III) , Fe(III) , Ga(III) , Au(III) , Tl(III) , Th(IV) , and Sb(V) have D_v values larger than 10.

4. The elements which in 9 M HClO_4 have $D_v > 10$ include the rare earths, Sc(III) , Y(III) , and, interestingly, all the actinides. This group also includes the two alkaline earth elements Ca(II) and Sr(II) , a number of other divalent ions [Mn(II) , Cd(II) , and Pb(II)], trivalent ions [Fe(III) , Ga(III) , and Bi(III)], tetravalent ions [Ti(IV) , Zr(IV) ,

³³ Guest scientist from Atomic Fuel Corporation, Tokyo, Japan.

³⁴ K. A. Kraus, D. C. Michelson, and F. Nelson, *J. Am. Chem. Soc.* **81**, 3204 (1959).

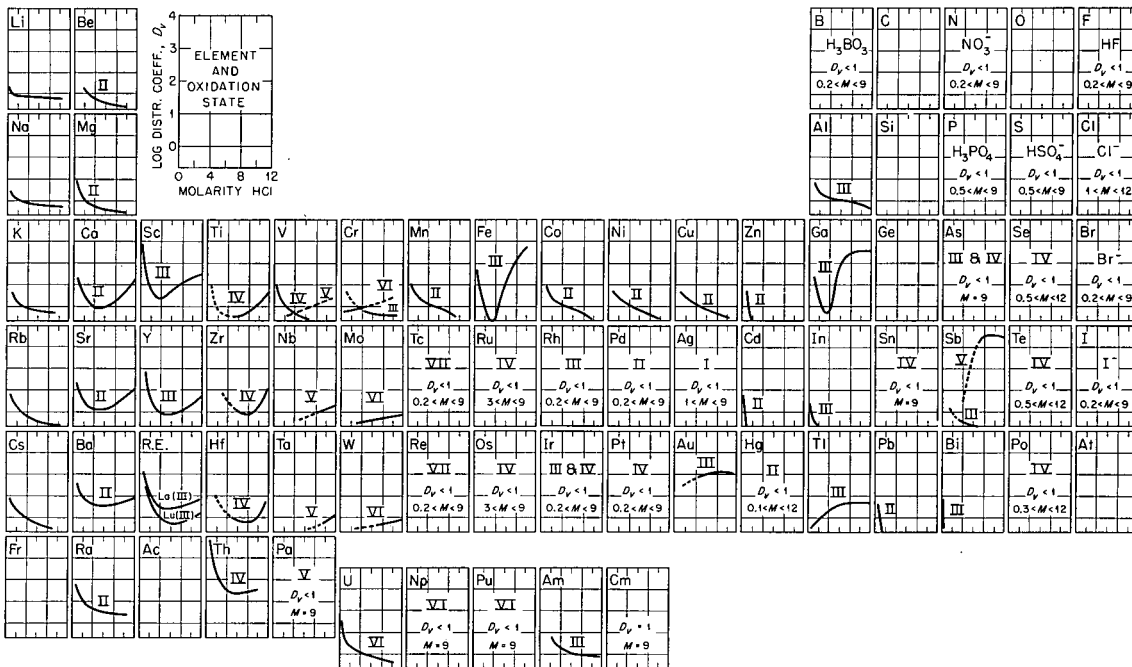


Fig. 6.11. Adsorption of the Elements from HCl Solutions by a Cation Exchange Resin.

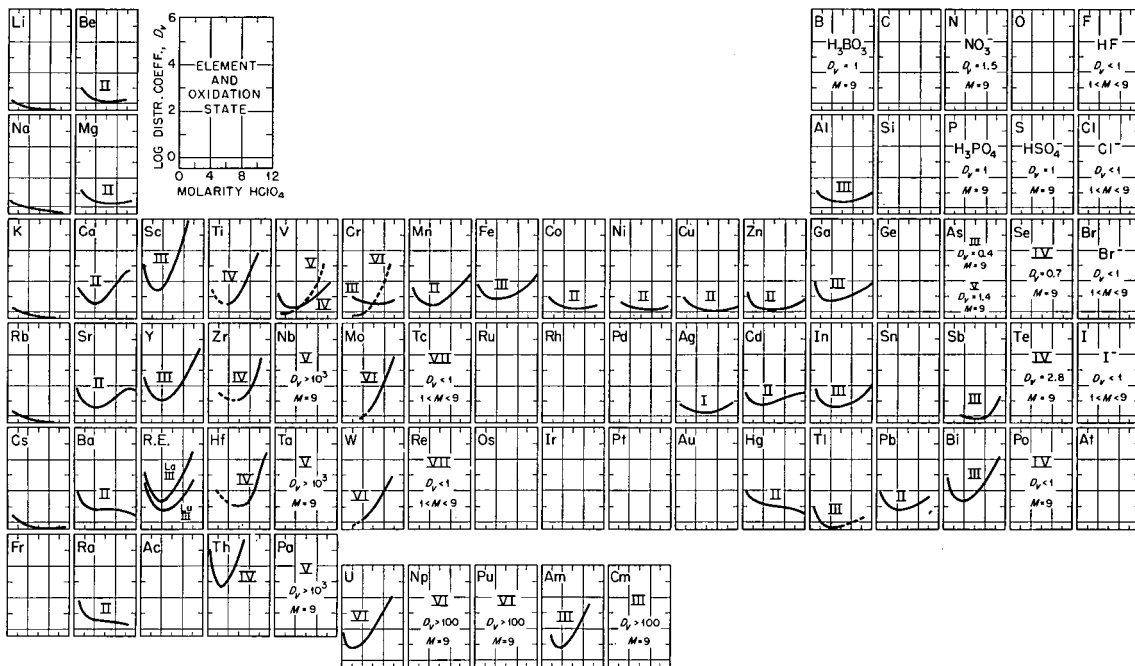


Fig. 6.12. Adsorption of the Elements from HClO₄ Solutions by a Cation Exchange Resin.

Hf(IV), and V(IV)], and ions of oxidation number 5 [V(V), Nb(V), Ta(V), and Pa(V)] and 6 [Cr(VI), Mo(VI), W(VI), and U(VI)]. For most of these elements D_v is larger than 100.

On the basis of the information summarized in Figs. 6.11 and 6.12, a large number of separations may be devised and many have been tested, particularly with the concentrated acids. These high-ionic-strength separations are of very wide applicability. However, for efficient use of these media it is desirable to compensate for the relatively slow equilibration rates by operating with very-fine-mesh resins, at moderately slow flow rates, and at elevated temperatures.

Development of an Ion Exchange Separation Scheme

F. Nelson E. L. Lind³⁵
K. A. Kraus

Work on the development of an ion exchange separation scheme to cover essentially all the elements continued. Methods for separating elements into major groups³⁶ were tested further, and progress was made on the breakdown into smaller subgroups and individual components.

A scheme was developed for the resolution of approximately 15 elements which are not adsorbed by the proposed anion and cation exchange techniques in concentrated mineral acids. Resolution of these elements into three subgroups was achieved with an anion exchange column in the citrate form. Adsorption is carried out from ammonium citrate solution; the alkali metals, Ba(II), and Ra(II) are not adsorbed. The column is then treated with 0.5 M citric acid; Be(II), Mg(II), Cu(II), Mn(II), and Ni(II) are eluted. The third subgroup is then removed with 4 M HNO₃; it includes Al(III), V(IV), and Cr(III).

In continuation of a survey of the cation exchange behavior of essentially all the elements in concentrated electrolyte solutions, the studies on the system 8.5 M HClO₄-0.5 M HCl-0.1 M HF were substantially completed. This medium was originally chosen because it combined the high selectivity of high-ionic-strength cation exchange

with the complexing properties of Cl⁻ and F⁻, which are needed to keep many elements in solution. This medium, further, seems to be of near-optimum composition for a major division of the elements into groups with little overlap between them.

A summary of our measurements of the distribution coefficients (D_v) is given in Table 6.11. Most of the measurements were carried out either at 25 or 50°C; a few measurements were carried out at 75°C. Whenever possible, on the basis of previous information and measurements of temperature coefficients, estimates of distribution coefficients are given. For comparison, Table 6.11 also includes values of the distribution coefficients D_v at 25°C for 9 M HCl and 9 M HClO₄ solutions.

Inspection of Table 6.11 shows that in 8.5 M HClO₄-0.5 M HCl-0.1 M HF at 50°C there are no elements with D_v between 4.5 and 9. Thus a natural "gap" exists for the separation of an adsorbable from a nonadsorbable group.

Adsorption on Inorganic Materials

H. O. Phillips R. R. Brown³⁷
K. A. Kraus

The adsorption and ion exchange behavior of a variety of inorganic materials was studied. While a considerable number of new materials were prepared and evaluated with respect to rates of adsorption or exchange, selectivity, uptake of ions, and stability in acids and bases, this report will deal only with zirconium antimonate, rare-earth oxides, and various sulfides since these received special emphasis during the year.

We have earlier reported³⁸ that the zirconium antimonate shows unusual selectivity when compared with similar acid salts such as zirconium phosphate, tungstate, or molybdate. Particularly striking is its selectivity for sodium (in acid solutions), which is very much higher than for the other alkali metals. It now appears that this material also seems to have a unique selectivity for strontium. Capacity of the exchanger is at least 0.8 mole of Sr²⁺ per liter of bed.

³⁵ORINS Research Participant, Central Washington State College, Wash.

³⁶F. Nelson et al., *Chem. Div. Ann. Progr. Rept.* June 20, 1962, ORNL-3320, pp 79-80.

³⁷ORINS research participant, summer 1962. Allen University, Columbia, S. C.

³⁸H. O. Phillips and K. A. Kraus, *J. Am. Chem. Soc.* **84**, 2267 (1962).

Table 6.11. Distribution Coefficients of Elements in 9 M HCl, HClO₄, and HCl-HClO₄-HF Mixtures (Dowex 50-X4)

Element	Distribution Coefficient, D_v				
	9 M HCl, 25°C	9 M HClO ₄ , 25°C	8.5 M HClO ₄ -0.5 M HCl-0.1 M HF		
			25°C	50°C	75°C
Ac(III)	~10.0 ^a	(>100) ^b	(>100)	(>100)	(>100)
Ag(I)	<1.0	2.4	<1	<0.5	(<1)
Al(III)	0.6	3.8	<1	(<1)	(<1)
Am(III)	1.2	2000	1500	(1000)	(600)
As(V)	<1.0	1.4	1	(1)	(1)
Au(III)	120		10	4.4	2.0
B (H ₃ BO ₃)	<1	1	(<1)	(<1)	(<1)
Ba(II)	4.5	4.9	5	4.0	2.8
Be(II)	0.3	1.3	1	0.8	(<1)
Bi(III)	<1	860	<1	(<1)	(<1)
Br (Br ⁻)	<1	<1	(<1)	(<1)	(<1)
Ca(II)	3.2	140	160	64	30
Cd(II)	<1	17	0.8	<0.5	(<1)
Cl (Cl ⁻)	<1	<1	<1	<1	<1
Cm(III)	1	(>1000)	(>100)	(>100)	(>100)
Co(II)	0.3	1.5	<1	0.5	(<1)
Cr(III)	<1	2.0	1.5	(<2)	(<2)
Cs(I)	<1	0.6	<1	<0.5	<1
Cu(II)	0.4	1.2	<1	<0.5	<1
F (HF)	<1	<1	<1	<1	<1
Fe(III)	300	18	120	37	15
Fr(I)	(<1)	(<1)	(<1)	(<1)	(<1)
Ga(III)	330	13	47	21	11
Hf(IV)	<1	96	<1	<1	(1.5)
Hg(II)	<1	7	<1	<0.5	(<1)
I (I ⁻)	<1	<1	(<1)	<1	(<1)
In(III)	<1	9.5	<1	<0.5	(<1)
Ir(IV)	<1		<1	<0.5	(<1)
K(I)	<1	0.3	<1	<1	<1
Li(I)	<1	0.5	<1	<1	<1
Mg(II)	0.3	1.9	1	(1)	(1)
Mn(II)	0.4	19	2.0	2.8	3.8
Mo(VI)	<1	870	4.6	2.9	2.0
N (NO ₃ ⁻)	<1	1.5	(<2)	(<2)	(<2)

Table 6.11 (continued)

Element	Distribution Coefficient, D_v				
	9 M HCl, 25°C	9 M HClO ₄ , 25°C	8.5 M HClO ₄ -0.5 M HCl-0.1 M HF		
			25°C	50°C	75°C
Na(I)	<1	0.5	<1	<0.5	(<1)
Nb(V)	1.6	>1000	0.4	<1	1.6
Ni(II)	<1	1.0	<1	<1	(<1)
Np(VI)	<1	>100	(>10)	>10	(>10)
P (H ₃ PO ₄)	<1	1	(1)	(1)	(1)
Pa(V)	<1	>1000	1.5	1.9	2.4
Pb(II)	<0.5	19	<1	<1	(<1)
Pd(IV)	<1		<1	<0.5	(<1)
Po(IV)	<1	1	<1	<0.5	(<1)
Pt(IV)	<1		<1	(<1)	(<1)
Pu(VI)	<1	>100	(>10)	>10	(>10)
Rare Earths					
La(III)	4.5	3300	(>2000)	(>1000)	(>500)
Ce(III)			1800	940	520
Eu(III)		2000	710	460	3200
Yb(III)	1.0	130	(>50)	(>50)	(>50)
Lu(III)	0.8	87	52	54	50
Ra(II)	2.5	2.0	(2)	2	(<2)
Rb(I)	<1	<0.5	<1	<0.5	(<1)
Re(VII)	<0.8	<1	<1	(<1)	(<1)
Rh(III)	<1		0.6	<0.5	(<1)
S (HSO ₄ ⁻)	<1	1	(1)	(1)	(1)
Sb(V)	2000		>100	>10	(>10)
Sc(III)	17	7.2×10^5	970	1300	1600
Se(IV)	<1	0.7	1	(1)	(1)
Sn(IV)	<1		<1	0.5	(<1)
Sr(II)	3.5	29	25	13	7.7
Ta(V)	1	>1000	(1)	0.4	<1
Tc(VII)	<0.5	<1	(1.5)	1	0.8
Te(IV)	<1	2.8	1	1.0	(1)
Th(IV)	28	$>1 \times 10^7$	820	1000	1200
Ti(IV)	1	1900	(1)	(1)	1.0
Tl(III)	5.3	1	20	10	5.1

Table 6.11 (continued)

Element	Distribution Coefficient, D_v				
	9 M HCl, 25°C	9 M HClO ₄ , 25°C	8.5 M HClO ₄ -0.5 M HCl-0.1 M HF		
			25°C	50°C	75°C
U(VI)	0.5	3800	51	39	33
V(IV)	<1	21	3.2	4.1	5.3
W(VI)	<1	>500	1.4	1.3	1.1
Y(III)	1.6	580	180	150	110
Zn(II)	<1	1.8	0.6	<0.5	(<1)
Zr(IV)	1.0	200	0.5	0.9	1.5

^aComputed from data of R. M. Diamond, K. Street, Jr., and G. T. Seaborg, *J. Am. Chem. Soc.* **76**, 1461-69 (1954).

^bParentheses indicate estimated values.

In a series of column experiments it was established that tracer strontium could be adsorbed effectively from 1 M NaCl solutions with the adsorbent initially in the ammonium form. Excellent adsorption of tracer strontium (Sr⁸⁵) was achieved even from 1 M Mg(NO₃)₂ solutions. In one experiment, for example, terminated after 150 column volumes, better than 99.5% adsorption of Sr⁸⁵ was achieved at a flow rate of 1 cm/min with a 1-cm column. Unfortunately, we have not been able so far to develop techniques for the rapid elution of the adsorbed strontium.

In a search for new anion exchange active oxides, lanthanum oxide was investigated in some detail. The material was prepared from lanthanum nitrate solutions by precipitation with ammonia, dried at 25°C, and sieved. Exchange rates with this material were relatively slow at room temperature. However, at 97°C the rates were satisfactory. Under these conditions Cr(VI) uptake as high as 3 moles per liter of bed was achieved.

Investigation of the chromatographic application of heavy-metal sulfides continued. In a recent communication³⁹ we have summarized some work on a reaction of cadmium sulfide with Ag(I),

Hg(II), and Cu(II). Cadmium sulfide undergoes essentially a metathetical reaction with these ions. The reaction goes substantially to completion. Reaction rates were sufficiently fast to permit column operation at high flow rates.

Additional work was carried out on a number of other sulfides (ZnS, PbS, and As₂S₃), and some typical reactions, all evaluated by column techniques, are summarized in Table 6.12. Inspection of Table 6.12 shows that the extent of the reactions and their rates are not related in any simple manner to the free energies of the metathetical reactions. Thus, the reaction with the highest free energy change, ZnS with Hg(II), occurs to only a small extent even at slow flow rates. In this case presumably only a surface reaction occurs. In most other cases, where at 50% breakthrough the reaction is 40% or more complete, surface conversion cannot be limiting and bulk conversion presumably occurs. This implies rapid diffusion rates of the metal ions in the pertinent solids.

³⁹H. O. Phillips and K. A. Kraus, *J. Am. Chem. Soc.* **85**, 486 (1963).

Table 6.12. Uptake of a Number of Metals by Various Sulfides

Sulfide	Metal Ion	Flow Rate (cm/min)	Uptake at 50% Breakthrough			
			Moles per Kilogram	Moles per Liter of Bed	Moles per Mole of $M_x S_y$	Percent of Theoretical
ZnS	Ag(I)	7	13.5	18.9	1.3	66
	Cu(II)	4	6.2	8.7	0.6	61
	Hg(II)	0.3	0.5	0.7	0.05	5
CdS	Ag(I)	3	13.5	12.1	1.95	97.5
	Cu(II)	5	4.8	4.3	0.7	69
	Hg(II)	2	4.4	4.0	0.6	64
	Au(III)	3	3.6	3.2	0.5	78
PbS	Ag(I)	5	7.1	11.4	1.7	85
	Cu(II)	5	1.8	2.9	0.4	43
	Hg(II)	5	4.2	6.7	1.0	98
As ₂ S ₃	Ag(I)	7	11.1	5.5	2.7	46
	Cu(II)	3	0.9	0.5	0.2	7
	Hg(II)	4	2.1	1.1	0.5	17

PHYSICAL CHEMISTRY OF ION EXCHANGERS

Osmotic and Activity Coefficients of Some Quaternary Ammonium Halides in Aqueous Solution at 25°C

S. Lindenbaum G. E. Boyd

Aqueous solutions of the symmetrical quaternary ammonium halides (tetramethyl-, tetraethyl-, tetra-*n*-propyl-, tetra-*n*-butyl-, ...) present an attractive opportunity for a study of the effect of cation size on osmotic behavior. It has therefore been the objective of this work to search for the existence of a systematic behavior in this thermodynamic property as a function of the size of the cation, R_4N^+ , with dilute and concentrated aqueous solutions of these salts. Freezing-point depression measurements on dilute solutions of many of these compounds were reported by Ebert and Lange⁴⁰ in

⁴⁰L. Ebert and J. Lange, *Z. Physik. Chem. (Leipzig)* **A139**, 584 (1928).

1928 and by Lange⁴¹ in 1934. Their values for the osmotic coefficients for the chlorides in dilute solutions showed a behavior characteristic of strong 1-1 electrolytes. The values for the iodides, however, were below the limiting-law prediction, suggesting ion association even in dilute solution. Recently activity coefficients at 25°C of tetramethyl-, tetraethyl-, tetrapropyl-, and tetrabutylammonium iodides were reported by Devanathan and Fernando,⁴² who performed measurements with cells having liquid junctions. Extremely high coefficients (e.g., $f_{R_4NI} = 13.5$ for 1 *N* Et₄NI) were quoted. In a recent communication by Stokes⁴³ it was suggested that these results are unreasonable and in disagreement with those of

⁴¹J. Lange, *Z. Physik. Chem. (Leipzig)* **A168**, 147 (1934).

⁴²M. A. V. Devanathan and M. J. Fernando, *Trans. Faraday Soc.* **58**, 784 (1962).

⁴³R. H. Stokes, *Trans. Faraday Soc.* **59**, 761 (1963).

Ebert and Lange even if the difference in temperature for the two sets of measurements is considered. Robinson⁴⁴ has determined the osmotic and activity coefficients of tetraethylammonium iodide by use of the gravimetric isopiestic method, and his results are in good agreement with the values reported by Ebert and Lange, confirming the view that there is a serious error in the work of Devanathan and Fernando. Our measurements are also in good agreement with those of Robinson for tetraethylammonium iodide. Measurements of the osmotic and activity coefficients of tetramethyl-, tetraethyl-, tetrapropyl-, and tetrabutylammonium chlorides and bromides and of tetramethyl- and tetrapropylammonium iodides also were made and are presented below.

Osmotic Coefficient Measurement. — Osmotic coefficients were determined by the gravimetric isopiestic vapor-pressure method of Robinson and Sinclair,⁴⁵ using a special apparatus constructed from a "low" form Pyrex vacuum desiccator provided with a mechanism for the remote-control closure of the sample dishes.

Duplicate samples of the dry salts were weighed into the tared dishes, and sufficient water was added to dissolve the salt. In addition, two dishes that contained either sodium chloride or, at the lower water activities where NaCl solutions were saturated, sulfuric acid were used as a standard. In a depression in the center of the copper block was a large gold-plated silver dish which contained either a saturated solution of known vapor pressure⁴⁶ or, at the higher water activities, a solution of sodium chloride.

The desiccator was immersed in a large constant-temperature water bath held at $25.000 \pm 0.005^\circ\text{C}$, evacuated with an aspirator, and subjected to a gentle rocking motion during evacuation and equilibration. The dishes were always covered (by remote control) before admitting air into the desiccator and removing the unit from the bath. Changes in solution composition were thus avoided during the time required for removing the unit from the constant-temperature bath and weighing the sample dishes. The dishes were weighed at intervals varying from three days to two weeks;

equilibrium was assumed if all duplicate dishes arrived at the same molality and if the molality of standard solutions agreed with the water activity of the saturated solution in the large center dish. Equilibrium was approached alternately from higher and lower water activities.

Results and Discussion. — Osmotic coefficients were evaluated from the equation valid for 1:1 electrolytes:

$$\nu m\phi = \nu m_r \phi_r, \quad (1)$$

where

ν = the number of ions = 2,

m = molality of quaternary ammonium salt,

ϕ = osmotic coefficient (molal scale) of quaternary ammonium salt,

m_r = molality of reference electrolyte (NaCl),

ϕ_r = osmotic coefficient of reference electrolyte.

Values for ϕ_r were interpolated from tables of Robinson and Stokes.⁴⁷ For water activities lower than that of saturated NaCl, the following equation was used:

$$\nu m\phi = -55.51 \ln a_w. \quad (2)$$

Tables of a_w (water activity at 25°C) for various saturated aqueous solutions are available.⁴⁶ Osmotic coefficients for the quaternary ammonium chlorides and bromides are plotted in Figs. 6.13 and 6.14, respectively, as a function of molality. In Fig. 6.15 our osmotic coefficients for the iodides are compared with those of Ebert and Lange⁴⁰ and Robinson.⁴⁴ Mean molal activity coefficients, γ , were calculated with the Gibbs-Duhem equation,

$$-\ln \gamma = 1 - \phi + 2 \int_0^{\sqrt{m}} [(1 - \phi)/\sqrt{m}] d\sqrt{m}, \quad (3)$$

and tables of osmotic and activity coefficients for a range of concentrations have been prepared.

The osmotic coefficients for dilute solutions (below 1 m) of the chlorides increase with increasing cation size: $\text{Bu}_4\text{N}^+ > \text{Pr}_4\text{N}^+ > \text{EtN}^+ > \text{Me}_4\text{N}^+$. This sequence is consistent with the idea that organic cations act to enforce the water structure, and the more carbon atoms surrounding the charge, the greater this effect will be. The bromides and iodides, however, show exactly the

⁴⁴R. A. Robinson, private communication, April 1963.

⁴⁵R. A. Robinson and D. A. Sinclair, *J. Am. Chem. Soc.* **56**, 1830 (1934).

⁴⁶R. H. Stokes and R. A. Robinson, *Ind. Eng. Chem.* **41**, 2013 (1949).

⁴⁷R. A. Robinson and R. H. Stokes, *Electrolyte Solutions*, 2d ed., Academic Press, New York, 1959.

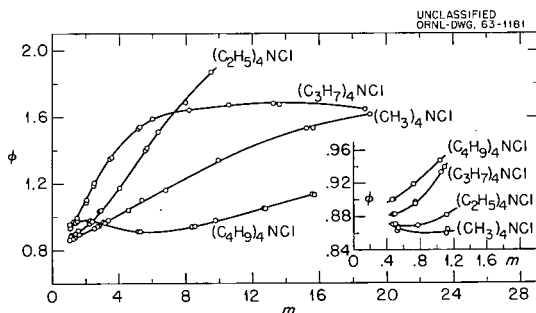


Fig. 6.13. Molal Osmotic Coefficients of Tetraalkyl Ammonium Chlorides.

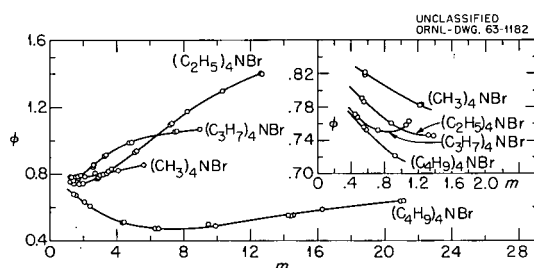


Fig. 6.14. Molal Osmotic Coefficients of Tetraalkyl Ammonium Bromides.

reverse order. It is suggested that for these larger, more-polarizable anions the effect of ion association is predominant, and the larger cation will associate more strongly.

At concentrations above 1 *m* the osmotic coefficients for the larger-cation salts decrease sharply and some of the orders given above are reversed. This behavior suggests that aggregation or micelle formation occurs. Preliminary investigations using the "spectral change" method of Corrin and

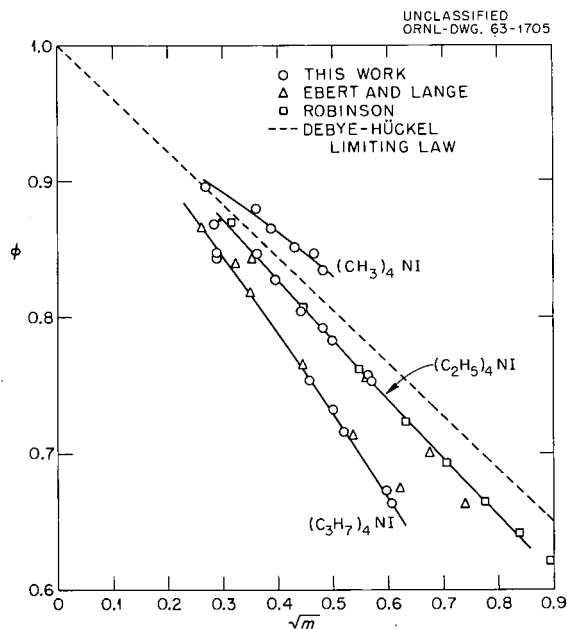


Fig. 6.15. Molal Osmotic Coefficients of Tetraalkyl Ammonium Iodides.

Harkins⁴⁸ have indicated that the critical micelle concentration of tetrabutylammonium chloride is approximately 0.5 *m*.

Maxima in the osmotic coefficient curves for the sodium salts of the fatty acids have been observed by Smith and Robinson.⁴⁹ In this case, too, micelle formation is very probably the explanation, for Debye⁵⁰ has shown "that micelle formation does occur with the potassium salts of the fatty acids."

⁴⁸M. L. Corrin and W. D. Harkins, *J. Am. Chem. Soc.* **69**, 679 (1947).

⁴⁹E. R. B. Smith and R. A. Robinson, *Trans. Faraday Soc.* **38**, 70 (1942).

⁵⁰P. Debye, *J. Phys. Colloid Chem.* **53**, 1 (1949).

7. Electrochemical Kinetics and Its Application to Corrosion

The Electrochemistry of the Dissolution of Zirconium in Aqueous Solutions of Hydrofluoric Acid

R. E. Meyer

The study of the dissolution of zirconium in aqueous solutions containing HF was continued with measurements of the capacity, additional polarization experiments, and rotating disk studies. In these investigations, the concentration of HF was varied from 0.001 to 0.02 *N*, and attention was centered upon solutions which also contained either 1 or 1.8 *N* H₂SO₄. All experiments were conducted at 25°C in cells in which only Teflon, platinum, and the electrodes were allowed to make contact with the solution.

Capacity Measurements. – The capacities of the electrodes were determined by measuring the initial slope of the voltage-time curves resulting from the application of constant-current pulses. The values of the capacity were calculated from Eq. (1):

$$C = \frac{i}{dV/dt}, \quad (1)$$

where *C* is the capacity per unit area, *i* is the current density, and *dV/dt* is the initial slope of the voltage-time curve. Because it was desired to use currents large compared to the dissolution rate, current densities up to 100 μa/cm² were used. The measured capacities ranged from 2 to 15 μf/cm², and therefore slopes as great as 5 × 10⁴ v/sec had to be recorded. An oscilloscope was used to record the initial voltage-time trace.

Capacities were measured as a function of potential and HF concentration. Values of the capacity increased with increasing HF concentration, ranging from 2.2 to 5 μf/cm² as HF concentration increased from 0.001 to 0.01 *N*. As the

potential was made more anodic with the potentiostat, capacity decreased at constant HF concentration. For 0.0067 *N* HF, for example, the capacity decreased by about 50% as the potential was changed from –700 to –500 mv vs the S.C.E.

Values of capacity in experiments in which both HF and H₂SO₄ were present ranged from 2 to 15 μf/cm². Normal values for film-free electrodes are 20 to 40 μf/cm². Low values of capacity are generally assumed to be evidence for the existence of a film on the electrode surface. A capacity of 5 μf/cm² can be explained if it is assumed that a film is present with a thickness of 25 Å and a dielectric constant of 15.

Polarization Measurements. – Further evidence that a film is present is provided by the fact that the slopes of the voltage-time traces obtained upon polarizing the electrode anodically have the same values as those obtained in anodizing experiments in solutions containing no HF. These slopes have values of about 2 v/sec at a current density of 1 ma/cm²; they should not be confused with the much larger slopes obtained when the capacity of the electrode is charged. The relatively slow and linear rise of voltage with time observed on these electrodes is characteristic of anodizing and is evidence for the existence of a film of ZrO₂ on the electrode.

It has been reported¹ that the dissolution of these electrodes is under mass transfer control. In order to confirm this, steady-state polarization experiments were conducted in which the electrodes were held at various anodic potentials and the current recorded as a function of time. These experiments showed the expected constant-current plateau characteristic of mass transfer control. The height of the constant-current plateau was

¹T. Smith and G. R. Hill, *J. Electrochem. Soc.* 105, 117 (1958).

proportional to the HF concentration. In some of the experiments, the electrodes were held at least 200 mv more anodic than the open-circuit potential for extended periods of time, and the weight losses of the electrodes were determined. These weight losses agreed well with the weight losses calculated by determining the total charge passed and applying Faraday's law. In this calculation, it was assumed that zirconium dissolves with a normal valence of 4. A method was described for calculating the dissolution rate from transient polarization data in a previous report.² However, it was found that a valence of 3 had to be assumed in order to calculate the correct dissolution rate from the transient data. Since the potentiostatic methods described here are the more accurate and reliable, it appears that zirconium probably always dissolves with a valence of 4 and that the transient data contain a small but reproducible systematic error.

Rotating Disk Studies. — The dissolution of the zirconium electrodes is controlled by the rate of mass transfer of undissociated HF to the electrode surface. With the methods described above, only the net rate of the dissolution process can be measured. In the steady state, however, the net rate of dissolution must be equal to the rate of mass transfer of HF to the surface and also to the rate of the surface dissolution reaction. These equalities are expressed by Eq. (2):

$$R_{\text{diss}} = nFD(C_{\text{HF}}^0 - C_{\text{HF}}^s)/\delta = \bar{k}_s(C_{\text{HF}}^s)^p, \quad (2)$$

where R_{diss} is the rate of dissolution, D is the diffusion coefficient of HF, C_{HF}^0 is the HF concentration in the bulk of the solution, C_{HF}^s is the HF concentration at the electrode surface, δ is the effective thickness of the diffusion layer, and p is the kinetic order. It may be seen from Eq. (2) that measurement of the net rate of dissolution gives only the product $\bar{k}_s(C_{\text{HF}}^s)^p$ and does not give the value of \bar{k}_s . The concentration of HF at the surface is not known and is not simply related to the concentration in the bulk of the solution.

Two general methods are available for obtaining information on the kinetics of electrochemical charge-transfer processes in the presence of appreciable mass transfer control: (a) use of a rotating disk electrode and (b) application of various types of high-frequency electrical signals

such as dc pulses. In the case of corroding systems, the electrical methods give some information but not the desired rate constant, \bar{k}_s . The rotating disk method therefore had to be used for the present system. It has been shown³ that if an electrode is used in the form of a disk spinning about its axis, the mass transfer equations may be solved exactly. If a number of stringent experimental conditions can be met, the steady-state anodic current at constant potential will be given by Eq. (3):

$$i = \frac{nF\bar{k}_s C_{\text{HF}}^0}{1 + \bar{k}_s/A(\omega)^{1/2}}, \quad (3)$$

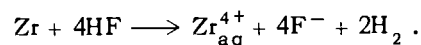
where ω is the rotational velocity and A is a constant. Equation (3) may be rearranged to the following useful form:

$$\frac{1}{i} = \frac{1}{nF\bar{k}_s C_{\text{HF}}^0} + \frac{1}{A(\omega)^{1/2} nF C_{\text{HF}}^0}. \quad (4)$$

If $1/i$ is plotted vs $1/(\omega)^{1/2}$, a straight line should be obtained whose intercept is $1/nF\bar{k}_s C_{\text{HF}}^0$. The rate constant can then be determined if n and C_{HF}^0 are known.

A rotating disk experimental cell was designed and put into operation. Preliminary experiments showed that linear plots of $1/i$ vs $1/(\omega)^{1/2}$ were obtained, and experimentation at various HF concentrations is being carried out. Plots of $1/i$ vs $1/(\omega)^{1/2}$ for one set of experiments are shown in Fig. 7.1. The plots are linear as expected and give intercepts from which the rate constants may be calculated. The experiments performed so far indicate that these rate constants are almost independent of potential and of the bulk concentration of HF, but further experiments are being carried out to confirm these results.

Summary and Conclusions. — The dissolution of zirconium may be represented by the following simple equation:



The investigation of the kinetics of this reaction has shown that it is actually quite complicated. Separate consideration must be given to the formation of a film of ZrO_2 on the electrode surface, the reduction of H^+ on the surface of this film, the

²R. E. Meyer, *Chem. Div. Ann. Progr. Rept. June 20, 1962*, ORNL-3320, p 89.

³V. G. Levich, *Physicochemical Hydrodynamics*, Prentice-Hall, Englewood Cliffs, N. J., 1962.

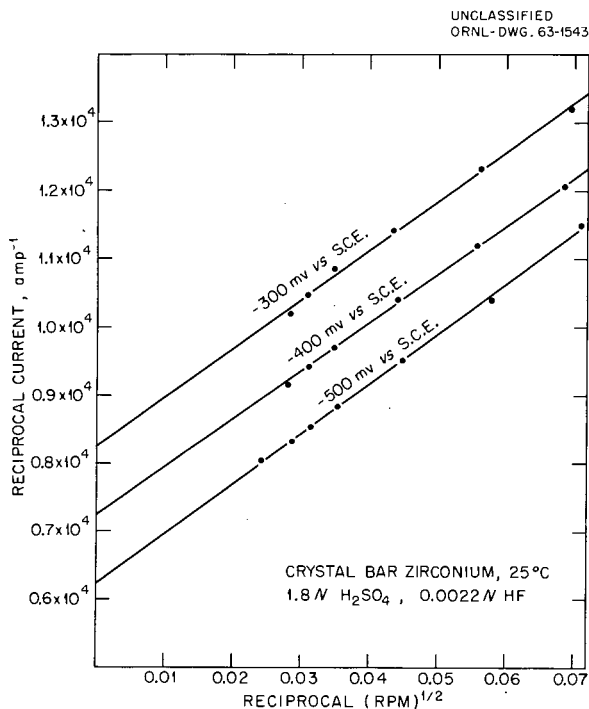


Fig. 7.1. Rotating Disk Determination of Rate Constants.

dissolution of the film, and the mass transfer of HF molecules to the surface of the film.

The formation of the film of ZrO_2 is governed by the same rate laws as those obeyed by the formation of ZrO_2 in solutions containing no HF. The dissolution of the film is first-order with respect to HF at the surface and is an extremely rapid reaction. Because of the great rate of the surface reaction the rate of dissolution is actually governed by the rate of mass transfer of HF to the surface.

Ion Exchange Properties of the Passive Film on Iron and Steel

G. H. Cartledge

Experiments were described previously⁴ which showed that the passive film on iron or steel retains chromate ions tenaciously and that these ions may be slowly exchanged by other anions. The first phase of the study of the kinetics of

⁴G. H. Cartledge and D. H. Spahrber, *Chem. Div. Ann. Progr. Rept. June 20, 1962*, ORNL-3320, p 83.

this process has been completed and published.⁵

It was found that the results may be interpreted only by a complex mechanism based upon the assumption of an activation energy which increases linearly with the extent of the exchange reaction.

In later experiments, it was found that the same type of kinetics is observed whether the exchanging electrolyte is alkaline sulfate, phosphate, molybdate, or chromate (pH ~ 9), the constants being so similar as to make it likely that the exchange is effected by OH^- ions in all these cases. With exchange by sulfate at pH 2.4, the exponential kinetics is still observed. When $Cr^{5+}(VI)$ is exchanged by $Cr^{6+}(VI)$ at pH 2.4, the rate curves apparently indicate a fast initial process involving exponential kinetics, parallel with a slow process which is first-order with respect to residual Cr^{5+} . Measurements at temperatures from 24 to 77.5° indicate that the slow process has an activation energy of ~ 10 kcal/mole. Observations on the effect of pretreatments of the specimen upon the fraction of total Cr^{5+} that is exchangeable are tentatively interpreted by the assumption that, even after thorough passivation in an aerated acidic sulfate solution, the film still contains some constituent that rapidly reduces a small amount of $Cr(VI)$.

Electrochemical Behavior of the Active Iron Electrode

E. J. Kelly

A comparative study has been made of the electrochemical behavior of the active iron electrode in typical noninhibiting and inhibiting media. Zone-refined electrolytic iron electrodes were studied by means of galvanostatic and potentiostatic polarization techniques.

In noninhibiting media, such as deoxygenated acidic sulfate, perchlorate, and chloride solutions, the corrosion of iron consists in the anodic oxidation of iron to ferrous ions and the simultaneous cathodic reduction of protons to molecular hydrogen. Previous attempts to determine the mechanisms of the iron dissolution and hydrogen evolution reactions have produced a variety of

⁵G. H. Cartledge and D. H. Spahrber, *J. Electrochem. Soc.* 110, 644 (1963).

conflicting results.⁶⁻⁹ The present investigation, carried out in 0.5 M (H₂SO₄ + Na₂SO₄), shows that the steady-state anodic dissolution of iron is characterized by a Tafel slope of 40 mv/decade, that is, $\frac{2}{3}(2.303RT/F)$, and a first-order dependency on the hydroxyl ion activity. The hydrogen evolution reaction is first-order in proton activity, and the Tafel line corresponding to this reaction has a slope of -120 mv/decade, that is, $-2(2.303RT/F)$. These observations, together with the pH dependencies of the corrosion potential E_{corr} and the corrosion rate i_{corr} , are summarized by Eqs. (1) through (4):

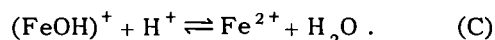
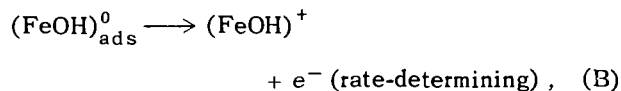
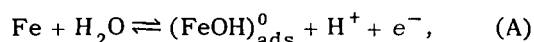
$$i_a = k_a \cdot a_{(\text{OH}^-)} \cdot \exp(3FE/2RT), \quad (1)$$

$$i_c = k_c \cdot a_{(\text{H}^+)} \cdot \exp(-FE/2RT), \quad (2)$$

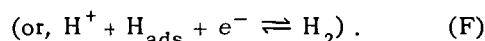
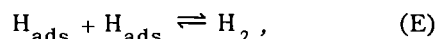
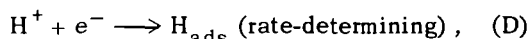
$$E_{\text{corr}} = -0.232 - (2.303RT/F)\text{pH}, \quad (3)$$

$$\log i_{\text{corr}} = -3.38 - (\frac{1}{2})\text{pH}, \quad (4)$$

in which E is the potential of the electrode with respect to the standard hydrogen electrode, and the other symbols have their customary significance. These results are consistent with the following mechanism for the iron dissolution reaction:



The mechanism of the hydrogen evolution reaction is:



Specific adsorption of an inhibitor complicates the picture presented above. Excluding from

⁶K. E. Heusler, *Z. Elektrochem.* **62**, 582 (1958).

⁷T. Hurlen, *Acta Chem. Scand.* **14**, 1533, 1555, 1564 (1960).

⁸A. C. Makrides, *J. Electrochem. Soc.* **107**, 869 (1960).

⁹J. O'M Bockris and D. Drazic, *Electrochim. Acta* **7**, 293 (1962).

consideration those cases where the inhibitor itself is oxidized or reduced, the inhibitor may function by altering the rates of the normal anodic and/or cathodic reactions, that is, those reactions which occur in the noninhibiting media [reactions (A) through (F)], or by giving rise to entirely new reaction paths. These effects may be illustrated by the polarization behavior of iron in deoxygenated 0.1 M (C₆H₅COOH + C₆H₅COONa), pH = 5.0. In this environment, a steady-state cathodic Tafel line is observed only when the cathodic polarization exceeds approximately 250 mv (cf. Fig. 7.2). This Tafel line has a slope of -120 mv/decade, that is, $-2(2.303RT/F)$, and is virtually coincident with that predicted for the hydrogen evolution reaction in noninhibiting sulfate solution at the same pH [cf. Eqs. (2) through (4)]. For smaller cathodic polarizations, the steady-state curve lies above the extension of this Tafel line to lower current densities. The steady-state current, $i_{c,ss}^*$, is related to the current along the Tafel

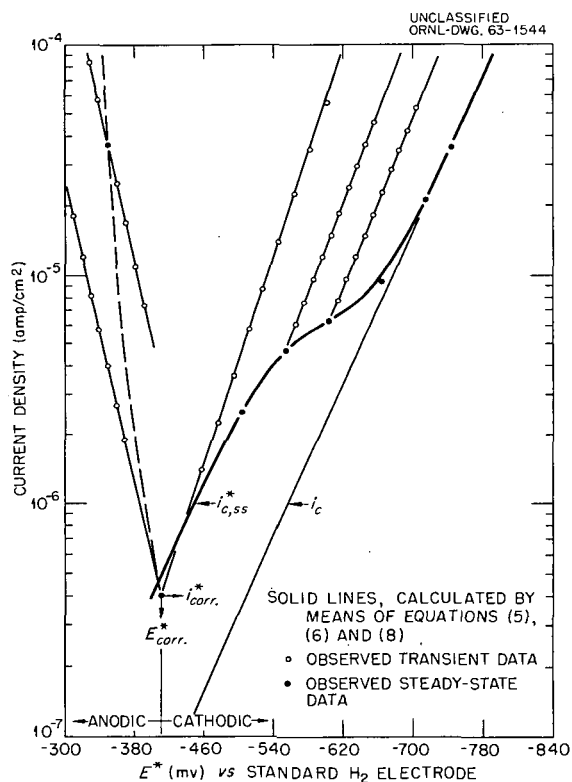


Fig. 7.2. Comparison of Calculated and Observed Current-Potential Data for Iron in 0.1 M (C₆H₅COOH + C₆H₅COONa).

line, i_c , by Eq. (5):

$$(i_{c,ss}^* - i_c)/i_c = A\{1 + \exp[-(B + CE^*)]\}^{-1}, \quad (5)$$

where E^* is the electrode potential relative to the standard hydrogen electrode, A is the limiting value of $(i_{c,ss}^* - i_c)/i_c$, which is approached as E^* approaches the steady-state corrosion potential ($E_{c,corr}^*$), and B and C are positive constants. As E^* becomes increasingly negative, $i_{c,ss}^*$ approaches and ultimately becomes equal to i_c .

Corresponding to each cathodic steady state, there exists a transient cathodic Tafel line, the slope of which is given by Eq. (6):

$$S = -104 + 16 \tanh [(B + CE^*)/2], \quad (6)$$

where S , the slope, is expressed in mv/decade, and the other terms remain as defined in Eq. (5). As E^* approaches $E_{c,corr}^*$, S approaches -88 mv/decade, corresponding to a value of unity for the hyperbolic tangent term in Eq. (6). If the electrode is in a steady state at a cathodic potential E^* , a potentiostatic shift in the cathodic potential gives rise to an initial current lying on the transient Tafel line passing through E^* . Depending upon whether the new cathodic potential is more or less negative than E^* , the current either decreases or increases, respectively, to the new steady-state current given by Eq. (5). Such potentiostatic current transients are described by Eq. (7):

$$\begin{aligned} \log (i_{c,ss}^* - i_{c,t}^*) / (i_{c,ss}^* - i_{c,0}^*) \\ = Gt - H(i_{c,t}^* - i_{c,0}^*), \quad (7) \end{aligned}$$

where $i_{c,0}^*$, $i_{c,t}^*$, and $i_{c,ss}^*$ are the current densities at times $t = 0$, $t = t$, and $t = \infty$, respectively, and G and H are constants. The application of Eq. (7) has been described in an earlier report.¹⁰ Equations (5), (6), and (7) constitute the first quantitative representation of the well-known

¹⁰E. J. Kelly, *Chem. Div. Ann. Progr. Rept. June 20, 1962*, ORNL-3320, p 88.

phenomenon of "polarization hysteresis."¹¹ As $i_{c,ss}^*$ approaches i_c [cf. Eq. (5)], S approaches a limiting value of -120 mv/decade, corresponding to $\tanh [(B - CE^*)/2] = -1$ in Eq. (6). In the potential region where $i_{c,ss}^* = i_c$, the transient polarization phenomena cease. All of the preceding observations may be interpreted on the basis of a model in which the specific adsorption of the benzoate ion is accompanied by an increase in the rate of reaction (D), that is, by a decrease in the hydrogen overvoltage.

In contrast to its effect on the hydrogen evolution reaction, specific adsorption of the benzoate ion greatly reduces the rate of the iron dissolution reaction. As the electrode potential becomes increasingly more positive, desorption of the inhibitor occurs. The anodic desorption of the inhibitor gives rise to potentiostatic current transients in which the current increases with time. Transient anodic Tafel lines, unlike the transient cathodic Tafel lines, are parallel, and have a slope of 60 mv/decade, that is, $2.303RT/F$. Under more favorable environmental conditions, as in ($0.5 M Na_2SO_4 + 0.01 M C_6H_5COOH$), complete anodic desorption of the inhibitor may be achieved, and a steady-state Tafel line is observed which is coincident with that calculated by use of Eqs. (1), (3), and (4). In $0.1 M (C_6H_5COOH + C_6H_5COONa)$, anodic passivation occurs at current densities lower than those corresponding to the steady-state Tafel region, and precludes the observation of the latter. These facts may be explained by assuming that the reduced rate of the iron dissolution results from a simple coverage effect operating on reaction (A). The transient Tafel lines correspond to a new reaction path, the anodic desorption of the inhibitor. In accordance with the 60 -mv/decade slope, the current density for the desorption reaction (i_d) may be tentatively represented by Eq. (8):

$$i_d = k_d \theta (1 - \theta) \exp (FE^*/RT), \quad (8)$$

where θ is the fraction of the electrode surface covered by adsorbed benzoate ions.

¹¹M. Stern, *J. Electrochem. Soc.* **102**, 609 (1955).

8. Nonaqueous Systems at High Temperature

The Electrical Conductivity of Solutions of Metals in Their Molten Halides

A. S. Dworkin H. R. Bronstein
M. A. Bredig

The systematic variations in the electrical conductivities of solutions of lanthanum, cerium, praseodymium, and neodymium metals in their respective trichlorides¹⁻³ and triiodides,⁴ which reflected the regular trend in stability of the dipositive rare-earth ion M^{2+} in going from lanthanum to neodymium, should also be expected in the corresponding tribromide systems. The bromide systems were of additional interest for the following reason: In the alkali⁵ and alkaline earth⁶ metal-halide systems, a trend of increasing electronic conduction with increasing atomic number of the halide ion was established by comparison of the bromide systems with the chloride and fluoride systems. This trend was found partially or fully reversed in the iodide systems. This is illustrated by Fig. 8.1, which shows, as a function of the crystal radius of the halide ion, the equivalent conductance of the metal solute in dilute, if not infinitely dilute, solution:

$$\Lambda_M^\infty = [\Lambda_{\text{soln}} - (1 - N_M)\Lambda_{\text{salt}}]/N_M; \quad N_M = 0.01.$$

It seems possible to connect the behavior of the iodide systems with two mutually opposed in-

¹H. R. Bronstein, A. S. Dworkin, and M. A. Bredig, *J. Phys. Chem.* **66**, 44 (1962).

²A. S. Dworkin, H. R. Bronstein, and M. A. Bredig, *Disc. Faraday Soc.* **32**, 188 (1961).

³A. S. Dworkin, H. R. Bronstein, and M. A. Bredig, *J. Phys. Chem.* **66**, 1201 (1962).

⁴A. S. Dworkin et al., *J. Phys. Chem.* **67**, 1145 (1963).

⁵H. R. Bronstein and M. A. Bredig, *J. Am. Chem. Soc.* **80**, 2077 (1958); *J. Phys. Chem.* **65**, 1220 (1961).

⁶A. S. Dworkin, H. R. Bronstein, and M. A. Bredig, to be published.

fluences of the size of the anion upon the motion of electrons in the molten salt medium; one, the mere cross section of the anion as a negatively charged *barrier*, and second, opposed to it, the increase in polarizability of the anion with size *facilitating* the passing of an electron. The present work on rare-earth bromide systems was to determine whether a similar, perhaps even still more pronounced, trend toward such an "iodide anomaly" existed in rare-earth systems.

The heavier-rare-earth systems were of interest because, by virtue of the smaller size of the cation, they were thought perhaps to exhibit higher electronic conductance than the lighter rare earths in the same way as dilute sodium solutions had showed such higher conductance in comparison with dilute potassium solutions.⁵

Finally, it was hoped that more examples of a conductance behavior could be found that in

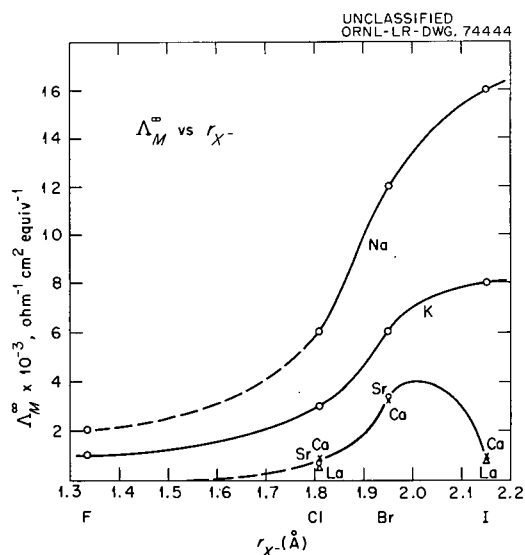


Fig. 8.1. Equivalent Conductance of the Metal Solute at Infinite Dilution vs Size of Halide Ion.

$\text{NdCl}_3\text{-NdCl}_2$ and $\text{NdI}_3\text{-NdI}_2$ was attributed earlier to an electron exchange between two ions in adjacent oxidation states.

Table 8.1 contains the results of the specific conductivity measurements of the pure trihalides. Taken together with previous results,^{1,4} these values form a regular series of specific conductivity κ vs t curves, where κ decreases with decreasing size of the cation and increasing size of the anion.

The results of the specific conductivity measurements for the metal-in-salt solutions are given in Table 8.2. The highest concentration listed represents the solubility of the metal in the salt at the temperature indicated. As expected, the solutions of lanthanum, praseodymium, and neodymium in their bromides behaved similarly to the corresponding chloride and iodide systems. The lanthanum solutions showed a rapid increase in conductivity with metal concentration, indicating

considerable electronic contribution to the total conductivity. The neodymium solutions showed little if any electronic conductance, and the praseodymium solutions are again intermediate. This has been interpreted^{1,4} to be a result of a gradual increase in the stability of the dipositive cation ($\text{La}^{2+} < \text{Pr}^{2+} < \text{Nd}^{2+}$). The increase in conductivity on addition of metal to the bromide is intermediate between those found for the chlorides and iodides. This is unlike the situation noted upon addition of the alkali and alkaline earth metals to their halides, where the iodide systems appeared to have a lower conductivity than expected (or conversely, the bromide systems showed a higher conductivity). The different behavior of the rare-earth iodide systems may have some relation to the formation of metal-like solid diiodides.⁴

The temperature dependence of conductivity in the Pr-PrBr₃ system was measured at a number of

Table 8.1. Specific Conductivity, κ , of Rare-Earth-Metal Halides

t (°C)	κ (ohm ⁻¹ cm ⁻¹)	t (°C)	κ (ohm ⁻¹ cm ⁻¹)	t (°C)	κ (ohm ⁻¹ cm ⁻¹)
	LaBr₃		NdBr₃		DyCl₃
809	0.678	713	0.466	679	0.372
812	0.683	731	0.498	704	0.424
821	0.710	743	0.519	730	0.466
831	0.720	759	0.541		
837	0.732	772	0.563		HoCl₃
851	0.755	797	0.603	747	0.431
869	0.794			776	0.488
894	0.840		GdBr₃	800	0.526
		800	0.444	819	0.562
	PrBr₃	823	0.476		
727	0.52	842	0.500		ErCl₃
750	0.56			801	0.468
770	0.60		GdCl₃	818	0.496
		629	0.382	839	0.531
		649	0.408		
		675	0.465		
		698	0.506		

Table 8.2. Specific Conductivity, κ , of MX_3 -M Systems

Mole % Metal	κ ($\text{ohm}^{-1} \text{cm}^{-1}$)	Mole % Metal	κ ($\text{ohm}^{-1} \text{cm}^{-1}$)
LaBr₃ + La at 820°C		GdCl₃ + Gd at 650°C	
0	0.70	0	0.41
1.1	0.94	0.47	0.427
3.2	1.55	0.98	0.454
6.5	3.15	1.64	0.487
10.4	7.35		
13.8	15.8	DyCl₃ + Dy at 700°C	
16.0	25.9 ± 1	0	0.415
		1.4	0.46
PrBr₃ + Pr at 740°C		4.4	0.54
0	0.54	7.8	0.65
1.46	0.66	12.3	0.76
3.06	0.80	18.4	0.90
6.35	1.10	25.0	0.98
10.3	1.47		
14.2	1.90	HoCl₃ + Ho at 800°C	
18.2	2.38	0	0.526
20.5	2.67	1.1	0.555
		5.2	0.69
NdBr₃ + Nd at 730°C		9.9	0.84
0	0.495	16.4	1.05
1.16	0.528		
4.06	0.614	ErCl₃ + Er at 820°C	
9.8	0.79	0	0.50
17.7	0.94	1.46	0.55
25.5	1.01	4.78	0.67
30.2	0.96	6	0.69
32.7	0.92		
33.3	0.92		
GdBr₃ + Gd at 820°C			
0	0.47		
1.05	0.58		
3.2	0.865		
5.6	1.27		
6.6	1.46		

concentrations and found to be 0.3%/°C, that is, similar to that in the pure salt (at 802°C, $\kappa = 2.24$ and 2.83 $\text{ohm}^{-1} \text{cm}^{-1}$; at 740°C, $\kappa = 1.90$ and 2.38 $\text{ohm}^{-1} \text{cm}^{-1}$, for 14.2 and 18.2 mole % praseodymium respectively). This has been the case for all previous systems measured except Pr-PrI₃.⁴

The conductivity vs concentration curve for the Gd-GdBr₃ system exhibits upward curvature inter-

mediate between the corresponding lanthanum and praseodymium systems. The solubility of gadolinium in GdCl₃ is too low to distinguish any curvature, but again the initial rise in conductivity is between those of lanthanum and praseodymium.

The solutions of gadolinium, dysprosium, holmium, and erbium metals in their trichlorides gave

irregular results quite different from those expected on the basis of the measurements with the lighter-rare-earth series. The solubility of the metals in the molten trichlorides at the temperatures at which the conductivities were measured rose from 1.6 mole % in GdCl_3 to 28 mole % in DyCl_3 , only to drop again to 18.5 mole % in HoCl_3 and 6% in ErCl_3 . This is in disagreement with the expectation that the stability of the M^{2+} ion, and thus the solubility, would increase in this series. The conductivity showed similar irregularities. The conductivity in the Dy-DyCl₃ system increases with metal concentration at a decreasing rate, as in the neodymium systems. In the holmium and erbium systems, the conductivity increases linearly, that is, it is intermediate between those in the praseodymium and neodymium systems.

A positive deviation from additivity in the conductance of mixtures of NdCl_3 with NdCl_2 and of NdI_3 with NdI_2 had been tentatively interpreted as reflecting an electronic contribution from an electron exchange between Nd^{2+} and Nd^{3+} ions.² The Nd-NdBr₃ system with a maximum in the curve of conductance vs composition (similar to Nd-NdI₃) and the Dy-DyCl₃ system without the maximum (similar to Nd-NdCl₃) are two more examples of this positive deviation indicating electron exchange.

An interesting observation was made in connection with the reaction between these "electron-exchange" melts and single-crystal synthetic sapphire. It had been noted earlier⁷ that the rare-earth metal-halide solutions attacked sapphire so rapidly that a conductivity measurement with the capillary cell was impossible. However, it was found that a solution of 33.3 mole % Nd in NdBr₃ (pure NdBr₂) did not attack the sapphire cell, as demonstrated by the conductivity remaining constant at the same value as that obtained with the molybdenum parallel electrodes and by the preservation of the weight of the sapphire cell. Further experiments showed that sapphire was rapidly attacked by solutions containing 20% Nd in NdBr₃, 10 and 30% Nd in NdI₃, and 30% Dy in DyCl₃. A solution containing 2% Nd in NdI₃ did not attack the cell, and in pure NdI₂ the sapphire cell showed only minimal attack.

⁷H. R. Bronstein, A. S. Dworkin, and M. A. Bredig, *J. Phys. Chem.* **64**, 1344 (1960).

An attempt was made to measure the conductivity of the Yb-YbCl₃ system. However, it was found that the pure molten YbCl₃ attacked the molybdenum crucible. This was probably due to the greater stability of YbCl₂ (similar to EuCl₂). No further measurements on this system were attempted at this time.

The Heats of Fusion of Some Rare-Earth-Metal Halides

A. S. Dworkin M. A. Bredig

We have previously measured and reported the heats of fusion of a number of lighter-rare-earth chlorides and iodides.⁸ The present report extends these measurements to other rare-earth halides with a variety of crystal structures. These data are of interest in connection with our continuing program of the interpretation of phase equilibria and electrical conductance measurements in metal-metal-halide systems.

The copper-block drop calorimeter used for the measurements and the experimental procedure were previously described in detail.⁹

Table 8.3 lists the heat and entropy of fusion, the heat content of the solid salts at their melting points, and the heat capacities of the solid and liquid in the vicinity of the melting temperature. The heat contents were measured with a precision of 0.1 to 0.2% and an estimated overall accuracy of 0.5%. The heats of fusion are believed to be accurate to at least ± 1 to 2% and the heat capacities to about $\pm 5\%$.

The compounds LaBr₃, PrBr₃, GdCl₃ (which have the UCl₃ type structure¹⁰), and NdBr₃ with the PuBr₃ type structure¹⁰ have similar entropies of fusion to those found⁸ for the chlorides of La, Pr, and Nd (UCl₃ type) and the iodides of Ce and Pr (PuBr₃ type). On the other hand, HoCl₃ and ErCl₃ (YCl₃ = AlCl₃ type¹¹) and GdBr₃, whose structure is not reported, have unusually low entropies of fusion. AlCl₃ has a much higher entropy of fusion (18.2 eu) because melting involves transformation to a liquid that unlike the crystal

⁸A. S. Dworkin and M. A. Bredig, *J. Phys. Chem.* **67**, 697 (1963).

⁹A. S. Dworkin and M. A. Bredig, *J. Phys. Chem.* **64**, 269 (1960).

¹⁰W. H. Zachariasen, *Acta Cryst.* **1**, 265 (1948).

¹¹D. H. Templeton and G. F. Carter, *J. Phys. Chem.* **58**, 940 (1954).

Table 8.3. Heat Capacity and Heat and Entropy of Fusion of Some Rare-Earth-Metal Halides

Salt	T_m (°K)	C_p , Solid (cal mole ⁻¹ deg ⁻¹)	C_p , Liquid (cal mole ⁻¹ deg ⁻¹)	$H_{T_m}(\text{solid}) - H_{298}$ (kcal/mole)	ΔH_m (kcal/mole)	ΔS_m (eu/mole)
LaBr ₃	1061	33.0	34.5	20.3	13.0	12.3
PrBr ₃	966	31.5	37.0	18.0	11.3	11.7
NdBr ₃	955	31.0	35.5	17.6	10.8	11.3
GdBr ₃	1058	32.1	32.3	19.6	8.7	8.2
GdCl ₃	875	29.1	33.7	14.8	9.6	11.0
HoCl ₃	993	29.0	35.3	17.4	7.0	7.1
ErCl ₃	1049	32.0	33.7	19.2	7.8	7.4

is not ionic but molecular in structure. The low entropy of fusion of HoCl₃, ErCl₃, and GdBr₃, in which the ionic radius $r_{M^{3+}}$ is greater than $r_{Al^{3+}}$, is in agreement with the fact that their melts are ionic like the crystals and like the melts of the lower-rare-earth trichlorides, LaCl₃, etc. The especially low value of ΔS_{fusion} may, however, suggest looking, for example, by x-ray diffraction, for a slightly different ionic structure of the melts, possibly including increased ion association to $(MCl)^{2+}$ or the like.

The Heat Content and Entropy of Strontium Chloride from 298 to 1200°K

A. S. Dworkin M. A. Bredig

The heat content and entropy of SrCl₂ from 298 to 1200°K have been measured by means of a copper-block drop calorimeter.¹² Strontium chloride, which has the CaF₂ type of structure, was recently found to have an unusually low entropy of fusion of 3.4 eu. This suggested the existence of a transition in SrCl₂ similar to that known for CaF₂, which also has an unusually low entropy of fusion.¹³ The heat content measurements shown in Fig. 8.2 do indeed show such a

second-order transition occurring in SrCl₂ about 140° below its melting point.

The measured heat contents of SrCl₂ as well as the smoothed heat content and entropy values are reported elsewhere.¹⁴ The following equations were obtained by the method of least

¹⁴A. S. Dworkin and M. A. Bredig, *J. Chem. Eng. Data* (in press).

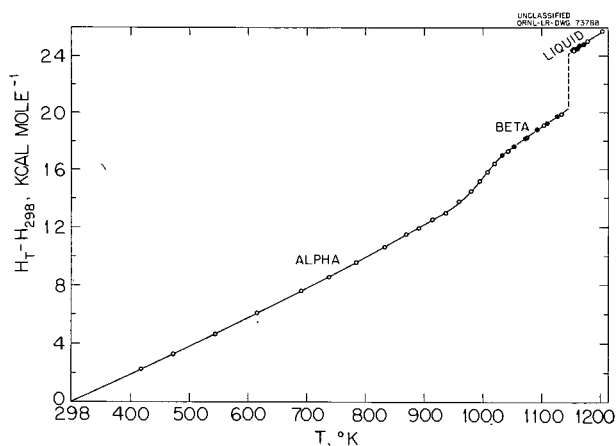


Fig. 8.2. Heat Content of SrCl₂ as a Function of Temperature.

¹²A. S. Dworkin and M. A. Bredig, *J. Phys. Chem.* 64, 269 (1960).

¹³B. F. Naylor, *J. Am. Chem. Soc.* 67, 150 (1945).

squares for $H_T - H_{298.15}$ (cal/mole):

$$H_T - H_{298.15} = -4875 + 15.28T \\ + 4.045 \times 10^{-3}T^2 \quad (298-940^\circ\text{K})$$

$$H_T - H_{298.15} = -12,430 + 28.53T \quad (1040-1146^\circ\text{K})$$

$$\Delta H_{\text{fusion}} = 3850 \quad (1146^\circ\text{K})$$

$$H_T - H_{298.15} = -7070 + 27.22T \quad (1146-1205^\circ\text{K})$$

The fit of the above equations is $\pm 0.2\%$, while the estimated overall accuracy is $\pm 0.5\%$. Figure 8.2 shows that the transition occurs gradually between the temperatures of about 940 and 1040° with no discontinuity in the heat content curve. No equation was calculated for this temperature range.

9. Chemical Physics

MICROWAVE AND RADIO-FREQUENCY SPECTROSCOPY

Paramagnetic Resonance Study of NO_3 in Irradiated KNO_3

Ralph Livingston Henry Zeldes

In the last annual report¹ a paramagnetic species in gamma-irradiated KNO_3 was tentatively identified as NO_3 . Final measurements have now been completed, and detailed results will soon be submitted for publication elsewhere. The spectrum arising from NO_3 consists of three equally intense, very sharp lines; the width between points of maximum slope is about 0.4 gauss. The lines are very strong immediately after a short, intense irradiation at 77°K with gamma rays, but after irradiation they rapidly become weaker at this temperature and disappear in about 2 hr.

Measurements were made with single crystals with the magnetic field parallel to three selected crystal planes. For all orientations the three lines remained of equal intensity, and because of the sharpness of the lines precise data were easily obtained. The three-line structure undoubtedly arises from hyperfine coupling with a single N^{14} . The spectrum is axially symmetric about the pseudohexagonal axis of KNO_3 . This direction is the perpendicular to the plane of every NO_3^- in unirradiated KNO_3 . The principal g values and hyperfine values measured at 77°K are:

$$g_{\parallel} = 2.0031 \pm 0.0004$$

$$g_{\perp} = 2.0232 \pm 0.0004$$

$$A_{\parallel} = 12.08 \pm 0.15 \text{ Mc}$$

$$A_{\perp} = 9.80 \pm 0.15 \text{ Mc}$$

¹Henry Zeldes and Ralph Livingston, *Chem. Div. Ann. Progr. Rept. June 20, 1962, ORNL-3320, p 105.*

The A_{\parallel} and A_{\perp} values correspond to line separations of 4.31 gauss and 3.46 gauss respectively. The smallness of the nitrogen hyperfine coupling is a main feature for identifying the spectrum with NO_3 .

In contemporaneous work Golding and Henschman² observed an axially symmetric spectrum for NO_3 in irradiated lead nitrate. The hyperfine parameters, which were only approximately evaluated, were somewhat smaller than those reported above, while the g values were similar to those above. Cunningham and co-workers³ observed a spectrum of three lines in irradiated KNO_3 at 4°K which had similar g values to those reported above, but the hyperfine coupling was stated to be isotropic. The spectrum was not interpreted nor was it seen at 77°K. The spectrum was probably that of NO_3 . Chantry and co-workers⁴ observed a spectrum for NO_3 in irradiated urea nitrate. There was no clearly resolved hyperfine structure, but the line widths were much greater than those reported here. The g tensor was not axially symmetric.

Paramagnetic Resonance Study of Irradiated Dimethylglyoxime

Henry Zeldes Ralph Livingston

Electron spin resonance is being used to study single crystals of dimethylglyoxime after gamma irradiation at 77°K. Dimethylglyoxime was chosen for study because of the simplicity of its structure and because of the presence of nitrogen atoms as well as hydrogen atoms which might show hyperfine structure. The unit cell is triclinic with a center

²R. M. Golding and M. Henschman, *Sixth International Symposium on Free Radicals*, Cambridge, England, 1963, p AN.

³J. Cunningham *et al.*, *J. Phys. Chem. Solids* **23**, 167 (1962).

⁴G. W. Chantry *et al.*; personally communicated by D. H. Whiffen.

of symmetry and with one molecule in the cell. Dimethylglyoxime was studied previously by Miyagawa and Gordy⁵ after gamma irradiation at room temperature. They reported parameters for a three-line spectrum due to strong hyperfine coupling to a single nitrogen atom, which they concluded was probably from ionized dimethylglyoxime with the electron spin density concentrated on one of the two nitrogen atoms.

After irradiation at 77°K, it was evident that complex spectra from several species were present. Much of the absorption disappeared on warming the crystal to room temperature, and after about one week at room temperature only the spectrum previously studied was seen. This spectrum was remeasured with greater accuracy.

Most of our work has been with a strong but complex spectrum which disappears in about three days at room temperature. This spectrum is of especial interest, since it was found to arise from a stable ground-state triplet. This was evident from the allowed ($\Delta M_S = 1$) spectrum, and it was also verified by observation of the forbidden ($\Delta M_S = 2$) spectrum. Measurements of both the allowed and forbidden spectra are well under way. The spectra are characterized by hyperfine coupling from two nitrogen atoms for which the couplings are either equivalent or very nearly so.

Many measurements of the three-line spectrum which is stable at room temperature were made at

room temperature in three crystal planes. The data were used to obtain parameters of a spin Hamiltonian of the form

$$\mathcal{H} = \beta S \cdot g \cdot H + S \cdot A \cdot I.$$

The parameters, which were obtained with the help of an electronic computer by a least-squaring procedure, are given in Table 9.1. The standard errors in the principal g values were less than 7×10^{-5} , but there is also a systematic error of about 2×10^{-4} . The standard errors in the principal hyperfine values do not exceed 0.4 Mc. The standard errors indicate that the eigenvectors for g are known within about 3°, and those for A are known within about 7°. These values agree with the previously reported⁵ values within the reported errors. A significant difference, however, is that the hyperfine coupling is not axially symmetric. An attempt will be made to relate the directions of the principal axes to structural features of crystalline dimethylglyoxime.

Paramagnetic Resonance Study of Photolyzed Hydrogen Peroxide

R. W. Holmberg Ralph Livingston

A study of species formed in single crystals of essentially 100% H_2O_2 has continued. Resumption of this work was described in the last annual report,⁶ and mention was made of three prominent

⁵I. Miyagawa and W. Gordy, *J. Chem. Phys.* 30, 1590 (1959).

⁶R. Livingston and R. W. Holmberg, *Chem. Div. Ann. Progr. Rept. June 20, 1962*, ORNL-3320, p 105.

Table 9.1. Principal Values and Directions of g and A for a Species in Dimethylglyoxime Which Is Stable at Room Temperature

Parameter	Principal Value (A 's in Mc)	Angles Between Principal Direction and Each Crystal Axis ^a (deg)		
g_1	2.0098	52.0	33.8	130.9
g_2	2.0025	125.4	56.2	89.6
g_3	2.0065	57.7	89.8	40.9
A_1	128.5	47.8	114.6	96.2
A_2	66.6	121.5	155.4	50.6
A_3	73.6	121.6	89.6	140.0

^aAxes are respectively a , b , c as defined by L. L. Merritt, Jr., and E. Lanterman, *Acta Cryst.* 5, 811 (1952).

spectra that may be observed after photolysis with uv. Additional, less intense, spectra have now been seen, and in order to simplify discussion each will be given a number. A résumé of distinct spectra that have been observed follows:

Spectrum I is formed in high yield by photolysis at low temperature. It is stable at 64°K and decays with a half-life (first-order kinetics) of a little over 1 hr at 77°K. It consists of many anisotropic lines that are moderately well resolved for some crystal orientations.

Spectrum II is found at 77°K in photolyzed samples after standing long enough for spectrum I to disappear. It consists of a large number of anisotropic lines which generally are not well resolved. Preliminary observations indicate this spectrum to be less intense than spectrum I.

Spectrum III is seen in photolyzed samples that have stood at dry-ice temperature. It consists of a bundle of poorly resolved anisotropic lines which disappear very slowly upon warming the crystal to near its melting point (−0.5°C).

Spectrum IV consists of weak lines which are distinct from spectrum II, but appear under the same conditions that give rise to spectrum II. It consists of a family of broad anisotropic lines. Each symmetry-related site for this species gives rise to one line. No hyperfine effects have been observed.

Spectrum V is formed under the same conditions that give spectra II and IV. Like spectrum IV it is of low intensity. This spectrum results from a triplet-state species.

In addition to the above five spectra there are indications that other weak spectra are present. Some measurements have been made on spectra I, IV, and V.

Considerable work has been done on spectrum I with the crystal at $\approx 64^\circ\text{K}$ during uv photolysis and during the measurements. A spectrometer was used operating at about 24,000 Mc and with the applied magnetic field parallel to planes of the form (110) and also (001) of tetragonal H_2O_2 . Study has also been made at 9000 Mc for the direction [110], and the appearance of the spectrum correlates well with that found at a higher frequency. Some of the elements of the g tensor for this species have been evaluated. Difficulty has been encountered in interpreting large splittings first thought to result from an unusually large hyperfine interaction. The possibility that these large splittings result from a D term in the Hamiltonian (triplet-

state species) is now being investigated. Smaller splittings are also present which almost certainly arise from dipolar interactions with protons, but their analysis will have to wait until the gross features of the spectrum are interpreted. Additional measurements will be needed.

Preliminary work has been done on the broad lines of spectrum IV. These lines are extremely anisotropic, and most measurements have been made on lines appearing at very high field strength in a spectrometer operating at 9000 Mc. With limited study at very high fields a g tensor was deduced, and it became clear that other lines appearing at very low fields were a part of the same spectrum. The value of the g tensor is only approximate since it represents measurement over only a small region of the entire spectrum. The g values range from 0.5 to 4 with the large value lying within 5° of the direction [110]. With additional measurement it will be possible to determine this tensor precisely. No hyperfine effects are resolved. The lines are quite intense when observed at orientations with low g values and become very weak at the higher g values.

Measurements have been made of spectrum V at 9000 Mc and at 77°K with the applied field parallel to planes of the form (110) and also (001). The spectrum arises from a triplet-state species with a characteristic zero-field splitting of lines (D term of the Hamiltonian). The splitting in an applied field reaches a maximum of about 1200 gauss for one of the two families of symmetry-related lines when the field is along the a axis. The other family of lines is at a subsidiary maximum (600 gauss) for this orientation. There is also a subsidiary maximum with the field along the c axis. From this it is concluded that the D term is about 1700 Mc (600 gauss) and the E term of the Hamiltonian is small. Apparent g values range from 2.01 to 2.04. The $\Delta M_s = 2$ transitions at half field strength have also been observed. Additional study will be needed to refine the elements of the spin Hamiltonian. The lines of the spectrum show partially resolved structure with spacings about right for concurrent spin flips of protons in the environment. Additional measurements will be needed to see if their origin is due to environmental protons or due to protons of the species itself. It is unlikely that spectrum V originates from O_2 , which is known to have a D term of $\approx 60,000$ Mc. Similarly, the species is probably not O, which is also expected to have a large D term.

Neutron-Diffraction Studies of Two Xenon
Fluoride Compounds, XeF_2 and XeF_4

P. A. Agron

H. A. Levy

Structural determinations which include anisotropic thermal motion analysis and accurate molecular parameters for the new fluoride compounds of xenon⁷ are of interest in clarifying the nature of their chemical binding. Three-dimensional neutron-diffraction analysis was first completed on a single crystal of XeF_2 . Subsequently, in collaboration with J. H. Burns,⁸ precise molecular parameters for XeF_4 were obtained from measurements on the Oak Ridge automatic neutron spectrometer.⁹

Both xenon compounds were prepared by reaction of the elements in equipment described by D. F. Smith,¹⁰ Technical Division, Oak Ridge Gaseous Diffusion Plant.

Xenon Difluoride. — A preliminary description of this work has been given earlier,¹¹ as well as a discussion in relation to other measurements.¹² The crystal is body-centered tetragonal, space group $I4/mmm$, with two linear molecules per unit cell aligned along the tetrad axes. The thermal parameters suggest that the molecules undergo a libration of about 5° about the tetrad axes. The Xe—F bond distance, after correction for this thermal motion, is 2.00 ± 0.01 A.

The structure was refined by iterative least squares, using a full matrix program for the IBM 7090.¹³ The reliability index

$$\frac{\sum(F_{\text{obs}}^2 - F_{\text{calc}}^2)}{\sum F_{\text{obs}}^2}$$

reached 0.090. A detailed comparison of F_{obs}^2 vs F_{calc}^2 is presented in Table 9.2, along with the

⁷N. Bartlett, *Proc. Chem. Soc.* **1962**, 218; H. H. Claassen, H. Selig, and J. G. Malm, *J. Am. Chem. Soc.* **84**, 3593 (1962); C. L. Chernick *et al.*, *Science* **138**, 136 (1962).

⁸Reactor Chemistry Division.

⁹W. R. Busing and H. A. Levy, *Experience with the Oak Ridge Automatic Three-Dimensional Neutron Diffractometer*, American Crystallographic Association Boulder Meeting, July 1961.

¹⁰D. F. Smith, *J. Chem. Phys.* **38**, 270 (1963).

¹¹H. A. Levy and P. A. Agron, *J. Am. Chem. Soc.* **85**, 241 (1963).

¹²P. A. Agron *et al.*, *Science* **139**, 842 (1963).

standard deviation of each observation. The resulting parameter values, with their least-squares standard errors, are given in Table 9.3.

Figure 9.1 shows the structure of the xenon difluoride crystal. The root-mean-square components of the thermal displacement are given in Table 9.4.

Xenon Tetrafluoride. — All of the 630 independent reflections out to $\sin \theta/\lambda = 0.76$ were measured. In addition, about 100 space-group absences were examined to confirm the x-ray space group, $P2_1/n$.¹⁴ The unit-cell dimensions determined from x-ray diffraction studies were adopted in this study, namely: $a = 5.050$ A, $b = 5.922$ A, $c = 5.771$ A, and $\beta = 99.6^\circ$. The atomic parameters given by Templeton *et al.*¹⁴ were taken as starting values for a least-squares refinement of the neutron diffraction data. The agreement factor, based on F^2 , reached 0.067. The final parameters and their standard deviations are given in Table 9.5.

¹³W. R. Busing, K. O. Martin, and H. A. Levy, *OR FLS, a Fortran Crystallographic Least Squares Program*, ORNL TM-305 (1962).

¹⁴J. A. Ibers and W. C. Hamilton, *Science* **139**, 106 (1963); D. H. Templeton *et al.*, *J. Am. Chem. Soc.* **85**, 242 (1963).

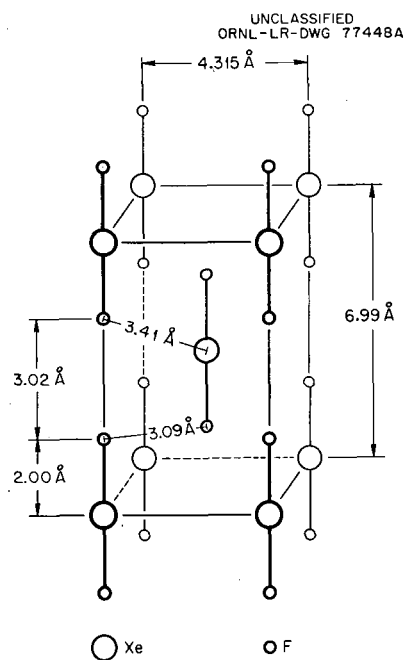


Fig. 9.1. Crystal Structure and Interatomic Distances of XeF_2 .

Table 9.2. XeF_2 , Calculated and Observed Values of the Squared Structure Factors on an Absolute Scale

h	k	l	$F^2 \times 10^3$		SD ^a	Sign ^b	h	k	l	$F^2 \times 10^3$		SD ^a	Sign ^b
			Calc	Obs						Calc	Obs		
0	0	2	1028	1197	59	-	3	3	0	1479	1567	104	+
		4	4397	4373	149	+			2	14	0	74	-
		6	55	230	68	+			4	729	642	62	+
		8	160	96	56	+			6	54	90	57	+
		10	801	692	64	+			8	63	185	60	+
1	0	1	232	190	34	+	4	0	0	1816	1908	76	+
		3	3950	3968	96	+			2	28	0	52	-
		5	491	426	47	-			4	884	827	55	+
		7	3812	3812	105	+			6	57	139	51	+
		9	242	221	45	-			8	71	0	46	+
1	1	0	7984	7258	220	+	4	1	1	139	117	53	+
		2	712	714	54	-			3	819	858	55	+
		4	3577	3533	130	+			5	8	16	40	-
		6	60	130	68	+			7	705	757	45	+
		8	146	58	59	+	4	2	0	1207	1174	58	+
		10	657	496	56	+			2	6	75	46	-
2	0	0	6431	6221	187	+			4	602	570	45	+
		2	486	521	40	-			6	50	0	40	+
		4	2915	3003	85	+	4	3	1	95	65	41	+
		6	62	31	50	+			3	389	424	46	+
		8	132	198	46	+			5	0	6	40	+
		10	539	668	52	+	4	4	0	369	344	51	+
2	1	1	213	170	38	+			2	3	56	57	+
		3	2638	2739	78	+			4	198	90	56	+
		5	222	257	54	-	5	0	1	95	91	41	+
		7	2476	2443	69	+			3	389	413	46	+
		9	113	102	42	-			5	0	69	41	+
2	2	0	4192	4173	148	+	5	1	0	662	652	49	+
		2	215	181	61	-			2	0	86	42	+
		4	1945	2003	105	+			4	343	361	39	+
		6	64	100	62	+			6	40	4	38	+
		8	109	161	57	+	5	2	1	77	151	43	+
3	0	1	190	195	43	+			3	270	212	38	+
		3	1774	1698	70	+			5	2	0	38	+
		5	92	250	52	-	5	3	0	305	257	52	+
		7	1619	1681	62	+			2	4	0	41	+
		9	49	36	42	-			4	166	8	51	+
3	1	0	3393	3467	95	+	5	4	1	40	162	50	+
		2	138	148	49	-	6	0	0	252	157	42	+
		4	1593	1712	69	+			2	5	117	37	+
		6	63	119	38	+			4	139	316	50	+
		8	98	37	38	+	6	1	1	50	183	36	+
3	2	1	164	399	56	+			3	133	0	66	+
		3	1201	1245	63	+	6	2	0	174	60	38	+
		5	32	53	45	-			2	7	145	49	+
		7	1065	1115	45	+							

^aStandard deviation.^bSign of the structure amplitude.

Table 9.3. Parameters of the Structure of XeF₂

Parameter	Xenon	Fluorine
<i>z</i>	(0.0) ^a	0.2838 ± 0.0004
β ₁₁	0.0341 ± 0.0020	0.0635 ± 0.0022
β ₃₃	0.0083 ± 0.0006	0.0087 ± 0.0004
<i>f</i> (fermi units)	(0.476) ^b	(0.550) ^c

^aValues in parentheses were not varied. The quoted errors are least-squares standard errors.

^bJ. H. Burns, P. A. Agron, and H. A. Levy, *Science* 139, 1208 (1963); J. H. Burns, P. A. Agron, and H. A. Levy in *Noble Gas Compounds* (ed. by H. H. Hyman), University of Chicago Press, Chicago, 1963.

^cG. E. Bacon, *Neutron Diffraction*, p 31, Clarendon Press, Fairlawn, N. J., 1962.

Table 9.4. XeF₂, Root-Mean-Square Components of Thermal Displacements, Å

Atom	Perpendicular to <i>c</i>	Parallel to <i>c</i>
Xenon	0.179	0.143
Fluorine	0.245	0.147

The components of thermal displacement along each of the principal axes of thermal motion were calculated for each atom as well as the orientation of these axes relative to a Cartesian system passing through the three independent atoms of the molecule. Figure 9.2 provides a pictorial representation of this thermal motion.

The large motion of the fluorine atoms normal to the bonds suggests that the molecule is librating as a rigid body. If the translational motion of the molecule is taken to be that of the xenon atom and is subtracted from the fluorine-atom displacements, the remainder can be ascribed to libratory motions of approximately 5° about each of the molecular axes. Correction for this riding model places the xenon-fluorine bonded distance at 1.95 (σ = 0.01) Å. This distance is significantly shorter than that found in XeF₂.

The XeF₄ molecule is planar by crystal symmetry, and the F(1)-Xe-F(2) angle was found to be 90.0° (σ = 0.1). The rms components of thermal displacement along the indicated Cartesian coordinates are listed in Table 9.6. These displacements are of the same order as those given for the XeF₂ molecule.

Each fluorine atom makes contact with seven other like atoms at distances of 2.99 to 3.26 Å.

Table 9.5. XeF₄, Final Parameters and Their Standard Deviations

Parameter	Xe		F(1)		F(2)	
	Parameter	σ	Parameter	σ	Parameter	σ
<i>f</i> ^a	0.476	0.003	(0.55) ^b		(0.55)	
<i>x</i>	(0.0)		0.2643	0.0002	0.2356	0.0002
<i>y</i>	(0.0)		0.1481	0.0002	0.0297	0.0002
<i>z</i>	(0.0)		-0.1536	0.0002	0.3002	0.0002
β ₁₁ ^c	0.0266	0.0004	0.0437	0.0004	0.0437	0.0004
β ₂₂	0.0129	0.0003	0.0284	0.0003	0.0248	0.0003
β ₃₃	0.0161	0.0003	0.0329	0.0003	0.0216	0.0003
β ₁₂	0.0014	0.0003	-0.0059	0.0003	-0.0008	0.0003
β ₁₃	0.0050	0.0003	0.0167	0.0003	-0.0030	0.0002
β ₂₃	-0.0002	0.0002	0.0026	0.0003	-0.0013	0.0002

^a*f* = neutron scattering factor. The value of 0.55 for fluorine is from G. E. Bacon, *Neutron Diffraction*, p 31, Clarendon Press, Fairlawn, N. J., 1962.

^bThe numbers in parentheses were not varied in the least-squares refinement.

^cThe β's are the coefficients in the asymmetric temperature factor expression: $\exp - [\beta_{11}h^2 + \beta_{22}k^2 + \beta_{33}l^2 + 2\beta_{12}hk + 2\beta_{13}hl + 2\beta_{23}kl]$.

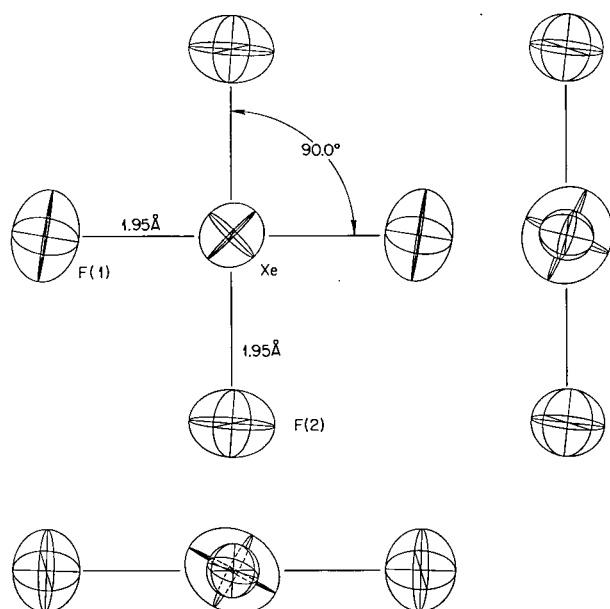
UNCLASSIFIED
ORNL-LR-DWG 77450R2

Fig. 9.2. Molecular Geometry and Thermal Motion in XeF_4 .

Table 9.6. XeF_4 , Root-Mean-Square Components of Thermal Displacement Along Molecular Axes (Å)^a

Axis	Xe	F(1)	F(2)
Xe-F(1)	0.170	0.178	0.242
Xe-F(2)	0.174	0.256	0.178
Plane normal	0.151	0.240	0.219

^a $\sigma = 0.002$ for all values in table.

Each fluorine atom has one xenon contact at 3.22 to 3.25 Å. The F to F distances are normal for fluorine in molecular crystals; however, the non-bonded xenon to fluorine distances appear considerably shorter than would be expected from consideration of van der Waals radii, 2.17 Å for xenon,¹⁵ and 1.35 Å for fluorine.

Sucrose: Precise Determination of Crystal and Molecular Structure by Neutron Diffraction

G. M. Brown H. A. Levy

The structure of the molecule of sucrose ($\text{C}_{12}\text{H}_{22}\text{O}_{11}$) has not previously been determined with the precision that modern diffraction techniques afford. An x-ray determination by Beevers and Cochran¹⁶ in 1947 of the structure of sucrose sodium bromide dihydrate (SSBD) sufficed to confirm the chemically assigned relative configurations¹⁷ of the asymmetric carbon atoms of the molecule. A subsequent x-ray determination of the structure of sucrose itself by Beevers *et al.*¹⁸ was somewhat less satisfactory, refinement having been terminated at an early stage because the data were felt to be of poor quality; the agreement between calculated and observed structure factors was just close enough to suggest that the phase problem had been essentially solved, without, however, furnishing conclusive proof of the structure proposed.¹⁹

Sucrose is a compound of very considerable biochemical importance. Also, the furanose and pyranose ring types which are represented in the sucrose molecule appear in many other important biochemical molecules. For example, furanose rings appear in the chains of deoxyribonucleic and ribonucleic acid. Not much information on the structural parameters of sugar ring systems is available; much that is available is of rather low precision. Accordingly, we have undertaken a precise neutron-diffraction analysis of the structure of crystalline sucrose, in which our starting point was the rough structure of Beevers *et al.*¹⁸ The neutron technique was chosen because it, unlike the x-ray technique, allows determination of coordinates of hydrogen atoms with nearly the same precision as can be attained for the coordinates of the heavier atoms.²⁰

¹⁶C. A. Beevers and W. Cochran, *Proc. Roy. Soc. (London)* **A190**, 257 (1947).

¹⁷See, for example, W. Pigman (ed.), *The Carbohydrates*, Academic Press, New York, 1957.

¹⁸C. A. Beevers *et al.*, *Acta Cryst.* **5**, 689 (1952).

¹⁹A. J. C. Wilson (ed.), *Structure Reports for 1952*, p 484, vol 16, Oosthoek, Utrecht, Netherlands, 1959.

²⁰We understand that x-ray analysis of the sucrose crystal structure has been resumed in Great Britain by C. A. Beevers and by J. H. Robertson, independently.

¹⁵D. R. Sears and H. P. Klug, *J. Chem. Phys.* **37**, 3002 (1962).

Determination of this structure is by far the largest problem ever undertaken in neutron-diffraction analysis, both with respect to the number of structural parameters determined and with respect to the number of data required. The precision of the determination is as high as that reached for any x-ray determination known to us in which the crystal structure even approximates the complexity of sucrose. The results provide a striking example of the power of the neutron-diffraction method in structural studies of complex crystals.

Three different crystal specimens, weighing approximately 80, 10, and 5 mg, were employed in order to detect and minimize extinction errors. About 5800 individual intensity measurements were made to provide averaged data for some 2800 independent reflections accessible to measurement on the Oak Ridge automatic neutron diffractometer.²¹ Before averaging, the intensity data were corrected for absorption effects and the Lorentz effect, then placed on an absolute scale by comparison with data from a standard crystal of NaCl.

From the coordinates of the 12 carbon and 11 oxygen atoms of the structure of Beevers *et al.*, we calculated reasonable coordinates for the 14 hydrogen atoms attached to carbon atoms.²² Refinement by the method of least squares²³ was started at once, though eight hydrogen atoms had not been placed. From three-dimensional Fourier maps, one of which was computed²⁴ after each cycle of least-squares refinement, all of the eight remaining hydrogen atoms were eventually found; and rather gross misplacements of atoms C₆' and O₆' were corrected. All other shifts were effected by the least-squares calculations. The last two

of 12 cycles of least-squares refinement of the structural parameters included adjustment of individual anisotropic thermal parameters. The value of the reliability index *R*, defined by the equation

$$R = \frac{\sum |F_{\text{obs}}^2 - F_{\text{calc}}^2|}{\sum F_{\text{obs}}^2},$$

where *F* is the structure factor, is now 0.046.

Standard errors in the coordinates²⁵ are about 0.001₀ to 0.001₅ Å for the carbon atoms and the ether oxygen atoms, 0.001₄ to 0.002₁ Å for the hydroxyl oxygen atoms, 0.002₄ to 0.004₁ Å for hydrogen atoms attached to carbon, and 0.002₃ to 0.005₄ Å for hydrogen atoms of hydroxyl groups. Coordinates of the carbon and oxygen atoms, especially the *y* coordinates, are considerably different from those of the starting structure, corresponding to an average radial shift of position for the oxygen and carbon atoms of 0.28 Å, with a minimum of 0.06 Å and a maximum of 0.91 Å.²⁶

Packing of the sucrose molecules is largely determined by hydrogen bonds O—H...O, of which there are seven per asymmetric unit, including two intramolecular bonds (see Fig. 9.3). Although the O₄ hydroxyl group does not participate in hydrogen bonding, its hydrogen atom is loosely fixed in position through two fairly close contacts with oxygen atoms in other molecules (see single dashed lines of Fig. 9.3). The observed cleavage parallel to (100) is neatly explained by the pattern of hydrogen bonds, since only one of the seven bonds extends across the plane $\frac{1}{2}, y, z$ (see also ref 18).

General features of the structure of the sucrose molecule can be seen from the two views of Figs. 9.3 and 9.4. The conformation of the molecule about the bonds of the glycosidic linkage, C₁—O₁—C₂', is surprisingly similar to that in SSBD,¹⁶ even though the hydrogen bonding is completely different — in the latter structure there

²¹W. R. Busing and H. A. Levy, *Experience with the Oak Ridge Automatic Three-Dimensional Neutron Diffractometer*, American Crystallographic Association Boulder Meeting, July 1961.

²²Our calculations use crystallographic data from neutron diffraction as follows (very similar to those of Beevers *et al.*¹⁸): space group *P*2₁, *a* = 10.86, *b* = 8.70, *c* = 7.75 Å, β = 103.0°. The estimated standard errors are about 1 part in 1000.

²³Least-squares refinement was carried out using an IBM 7090 computer program, developed by successive modifications (by J. Ibers and W. Hamilton and by C. Johnson) of a program by W. R. Busing, K. O. Martin, and H. A. Levy [*OR FLS, A Fortran Crystallographic Least-Squares Program*, ORNL TM-305 (1962)].

²⁴Fourier syntheses were computed on the IBM 7090 computer using the FORDAP program of A. Zalkin, Lawrence Radiation Laboratory, Berkeley, Calif.

²⁵A table of coordinates will appear in the complete account of this work to be published later. It will be furnished earlier to anyone interested.

²⁶In least-squares refinement for space group *P*2₁, the *y* coordinate of one atom must be held constant to fix the origin of the coordinate system. We have fixed the *y* coordinate of atom C₁ at the value reported by Beevers *et al.*¹⁸ The coordinate shifts given must be considered with this constraint in mind.

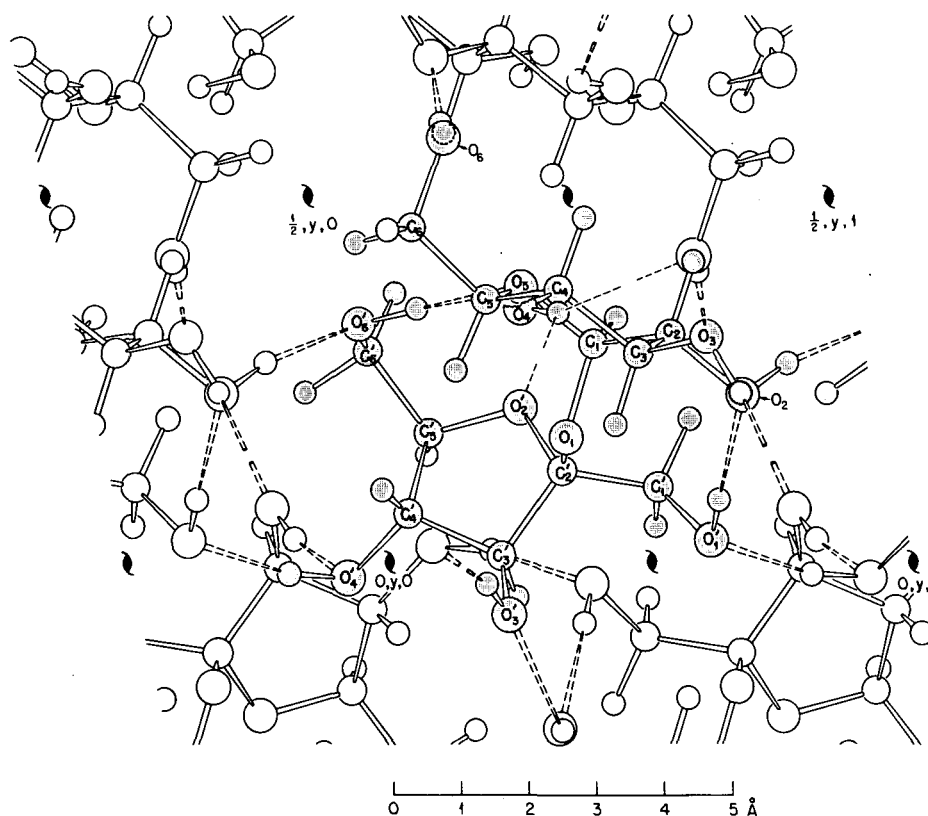


Fig. 9.3. The Sucrose Crystal Structure Viewed in Projection Along the b Axis, Showing Hydrogen Bonding. The smallest circles represent hydrogen atoms. The molecule is shown in correct absolute configuration. (Not determined in this research; see ref 17.)

are no intramolecular hydrogen bonds. The only significant difference, about 10° , is in the conformation about the C_1-O_1 bond. Conformations about the bonds C_5-C_6 and $C'_5-C'_6$ are also very nearly the same in sucrose and in SSBD. However, the conformation about the bond $C'_2-C'_1$ differs by 135° between the two structures.

We believe there is a significant difference in the conformation of the furanose ring between sucrose and SSBD, although comparison of the two structures is made difficult by the larger uncertainties of the coordinates of the latter crystal. In the SSBD crystal atoms C'_2 , C'_3 , C'_5 , and O'_2 are very nearly coplanar, and atom C'_4 is about 0.5 Å from their average plane. The furanose ring (see Fig. 9.4) in the sucrose crystal cannot be described so simply. We prefer to describe it by specifying an angle of twist about each ring bond. Consider four successive atoms around the ring, as C'_5 , C'_4 ,

C'_3 , C'_2 . We define the conformation angle of the directed bond $C'_4 \rightarrow C'_3$ as the angle, measured counterclockwise, that the projection of bond $C'_4 \rightarrow C'_5$ makes relative to the projection of bond $C'_3 \rightarrow C'_2$ when one looks in the direction of the bond $C'_4 \rightarrow C'_3$. In the furanose ring of sucrose the conformation angles for the various bonds are: $C'_4 \rightarrow C'_3$, 35.0° ; $C'_5 \rightarrow C'_4$, -27.3° ; $O'_2 \rightarrow C'_5$, 8.2° ; $C'_2 \rightarrow O'_2$, 14.6° ; $C'_3 \rightarrow C'_2$, -31.1° . Corresponding values for SSBD are: 36.5° , -34.5° , 22.9° , -1.5° , and -21.1° .

The pyranose ring is in the chair form, with $-CH_2OH$ and $-OH$ groups in equatorial positions and O_1 and five hydrogen atoms in axial positions. The six conformation angles of the ring, alternating in sign, fall within the range of magnitude 54.8° to 56.0° . The range is wider, 51.3° to 64.0° , in SSBD, probably reflecting the larger coordinate errors.

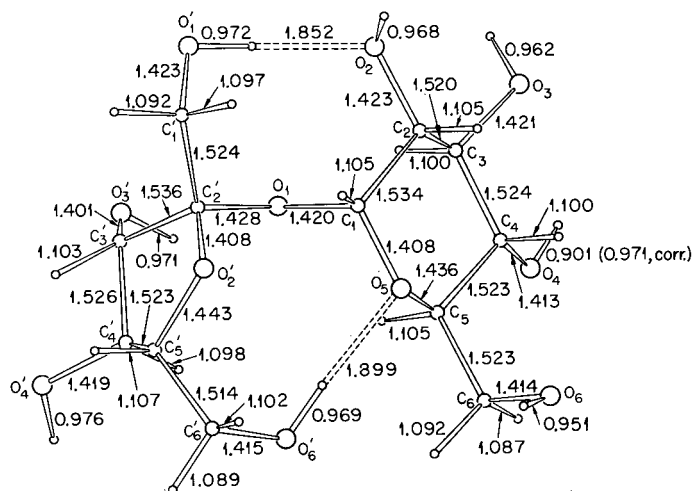
UNCLASSIFIED
ORNL-DWG. 63-1273

Fig. 9.4. The Sucrose Molecule. Numbers attached are bond lengths (Å).

Lengths²⁷ of C—C bonds (see Fig. 9.4) show remarkably small deviations from the mean of 1.525 Å, regardless of environment. The short C—C bonds, averaging 1.44 Å, reported by Beevers and Cochran in the furanose ring of SSBD can hardly be correct. Variations of length among the C—O bonds are slightly greater. In each ring the C—O bond adjacent to the glycosidic linkage appears significantly shorter than the other C—O bond of the ring. The C—H bond lengths range from 1.087 to 1.107 Å; the average, 1.099 Å, is the normal value expected for saturated molecules.

The O—H bond lengths, excluding that of the O₄ hydroxyl group, vary from 0.951 to 0.976 Å, a rather narrow range considering the possibility of perturbing effects of hydrogen bonding and of thermal motion. For the O₄ hydroxyl group, thermal motion has an especially large effect, since this group is not clamped in orientation by hydrogen bonding, and torsional motion about the C₄—O₄ bond is relatively free. The apparent bond length of 0.90 Å was approximately corrected²⁸ for the thermal motion to 0.97 Å, on the assumption that the hydrogen atom "rides" the oxygen atom. We have not yet analyzed the thermal motion in enough detail to make corrections for other bonds.

²⁷ Bond lengths may be revised slightly when more precise values of the unit-cell parameters become available.

The ether oxygen valence angles are as follows:

$C_1-O_1-C'_2$ (glycosidic linkage),	114.4°;
$C_1-O_5-C_5$,	116.0°;
$C'_2-O'_2-C'_5$,	111.5°.

Carbon valence angles in the pyranose ring range from 108.1° to 111.0°; in the furanose ring, from 102.3° to 105.7°. Other carbon valence angles range from 105.1° to 115.9°. Hydroxyl oxygen valence angles range from 104.9° to 112.3°.

Miscellaneous Computer Programs for Crystallography

G. M. Brown

As specific needs have arisen in the course of neutron-diffraction studies on the crystal structures of chloral hydrate and sucrose, a number of programs have been written for the IBM 7090 computer, in the FORTRAN language. These programs are not yet in final form, but all have proved useful.

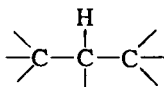
1. Averaging Program. The program accepts a previously sorted deck of data cards each of which bears the reflection indices, an integer identifying the crystal specimen, and the intensity (corrected

²⁸W. R. Busing and H. A. Levy, *Acta Cryst.* (in preparation).

for absorption) for a given observation. Averaging, with proper weighting and with simple rejection criteria, may be carried out for each independent set of indices, either over the observations for a given specimen or over those for all specimens. The function averaged may be either the intensity or the square of the structure factor. At the user's option, data cards for the Oak Ridge Fortran Least Squares Program (OR FLS)²⁹ may be produced by the program, or a set of average intensity cards may be produced. The latter cards, when sorted on intensity, are useful in appraising extinction effects by comparison of data from different crystal specimens.

2. Extinction Finding Program. Systematic comparison of observed and calculated structure factors in the final stages of refinement of a crystal is useful in detecting residual extinction errors in the observations. A short program provides data for a plot of $\langle F_{\text{obs}}^2 \rangle_{\text{avg}} / \langle F_{\text{calc}}^2 \rangle_{\text{avg}}$ as a function of the average intensity, where the averages are taken over small ranges of intensity. Input data are in a card deck produced by a slightly modified version of the OR FLS program and then sorted on the intensity values.

3. Hydrogen Coordinate Calculator. When x-ray analysis has provided coordinates of heavier atoms, it is often useful for further refinement, either by x-ray or neutron analysis, to calculate approximate coordinates for hydrogen atoms. A short program allows the calculation to be made, assuming reasonable valence angles, for such cases as the hydrogen in the grouping



or the hydrogens on plane aromatic rings. Modifications are planned to take care of other cases.

4. Composite Fourier Program. A conventional mode of display of results in determinations of structures of complex crystals is the composite Fourier map, in which parallel sections of the three-dimensional Fourier density through the centers of all atoms in the asymmetric unit are shown projected onto a single plane. A program has been prepared, utilizing a number of subroutines from the Oak Ridge Function and Error Program

²⁹W. R. Busing, K. O. Martin, and H. A. Levy, *OR FLS, a Fortran Crystallographic Least-Squares Program*, ORNL TM-305 (August 1962).

(OR XFE),³⁰ with which the synthesis may be carried out for any desired direction of projection. At present the user must write his own symmetry subroutine.

Edit Program for Crystallographic Data

K. O. Martin³¹ G. M. Brown

In reporting determinations of crystal structures, authors often present a complete table of calculated and observed values of F , the structure factor. The table, which may involve several thousand numbers, is usually prepared from typescript sheets or from computer output sheets by cutting, pasting, and photographing for reproduction on reduced scale. A program has been written to produce multicolumnar output sheets, with appropriate headings, subheadings, and spacings, from which the table of F values (or F^2) may be assembled with minimum effort. Input is from a card deck produced by a slightly modified version of the OR FLS program.³²

The Crystal Structure of the Molecular Addition Compound Xenon Difluoride-Xenon Tetrafluoride

J. H. Burns³³ R. D. Ellison
H. A. Levy

The crystalline phase previously reported³⁴ as a "high-density form of XeF_4 " is shown, by crystal structure analysis, to be a distinct compound with the composition $\text{XeF}_2 \cdot \text{XeF}_4$. The crystal is monoclinic,³⁴ with space group $P2_1/c$ and cell parameters $a = 6.64 \text{ \AA}$, $b = 7.33 \text{ \AA}$, $c = 6.40 \text{ \AA}$, $\beta = 92^\circ 40'$, and $Z = 4$. The true x-ray density is 4.02 g/cm^3 .

³⁰W. R. Busing and H. A. Levy, *A Crystallographic Function and Error Program for the IBM-704*, ORNL CF-59-12-3 (December 1959).

³¹Mathematics Division.

³²W. R. Busing, K. O. Martin, and H. A. Levy, *OR FLS, a Fortran Crystallographic Least-Squares Program*, ORNL TM-305 (August 1962).

³³Reactor Chemistry Division.

³⁴J. H. Burns, *J. Phys. Chem.* **67**, 536 (1963).

Diffraction intensities were measured using a single crystal mounted on a goniostat, MoK_α x rays, and a scintillation-counter detector. Because the crystal grew in size during the course of measurements, a normalization factor obtained from repeated measurements of a reference reflection was applied. Absorption corrections, based on a determination of the approximate crystal shape, were calculated³⁵ for each reflection.

Xenon atoms, previously shown to be in a face-centered arrangement,³⁴ dominate the scattering and determine the signs of all structure factors for which h , k , and l are unmixed (all odd or all even). The signs of the structure factors for five of the strongest mixed-index reflections were determined by Sayre's squaring method.³⁶ Fourier-synthesis electron-density maps calculated by using the structure factors with signs thus determined were interpretable and yielded a trial structure as well as the composition of the compound.

A pair of centrosymmetrically equivalent fluorine atoms was found to be bonded to each xenon atom in position 2(a): 0, 0, 0; 0, $\frac{1}{2}$, $\frac{1}{2}$; two pairs of fluorine atoms were found to be bonded to each xenon atom in positions 2(d): $\frac{1}{2}$, 0, $\frac{1}{2}$; $\frac{1}{2}$, $\frac{1}{2}$, 0. Attempts to interpret a Fourier map with xenon atoms in positions 4(e) with $x = z = \frac{1}{4}$, $y = 0$, which also gives a face-centered arrangement, did not prove fruitful.

Structure-factor calculations indicated the correctness of the model. It was refined by iterative least-squares procedures using a full-matrix program for the IBM 7090.³⁷ As the refinement proceeded, it became apparent that the 35 strongest reflections were affected by extinction; consequently they were omitted from the refinement. The agreement factor,

$$R = \frac{\sum |F_{\text{obs}}^2 - F_{\text{calc}}^2|}{\sum F_{\text{obs}}^2}$$

³⁵D. J. Wehe, W. R. Busing, and H. A. Levy, *ORABS, a Fortran Program for Calculating Single Crystal Absorption Corrections*, ORNL TM-229 (1962).

³⁶D. Sayre, *Acta Cryst.* **5**, 60 (1952).

³⁷W. R. Busing, K. O. Martin, and H. A. Levy, *OR FLS, a Fortran Crystallographic Least-Squares Program*, ORNL TM-305 (August 1962).

reached 0.050. The xenon positions are given above, and the fluorine atoms are in three sets of equivalent positions, 4(e): $\pm(x, y, z; x, \frac{1}{2} - y, \frac{1}{2} + z)$, with the following parameters:

Atom	x	y	z
F(1)	0.168	-0.187	0.153
F(2)	0.505	0.079	0.212
F(3)	0.240	0.109	0.516

Least-squares standard errors of the above parameters are all 0.001. Anisotropic temperature factors were determined and will be given in a more detailed discussion elsewhere.

The xenon-fluorine bond lengths, corrected³⁸ for thermal motion on the assumption that the fluorine atoms "ride" on xenon, are 2.01 Å ($\sigma = 0.01$) for the XeF_2 molecule, and two values, 1.94 and 1.96₅ Å (each with $\sigma = 0.01$), for the XeF_4 molecule with an F(2)-Xe-F(3) angle of 89.0° ($\sigma = 0.4$). The errors quoted are least-squares measures of precision; the corresponding measures of accuracy are estimated to be about twice as large. The hypothesis that the XeF_4 molecule is square planar is easily consistent with this study, and the individual molecular geometries are retained from pure crystalline XeF_2 and XeF_4 as determined by x-ray and neutron diffraction studies.³⁹⁻⁴¹

There are no close contacts between molecules in $\text{XeF}_2 \cdot \text{XeF}_4$ such as to indicate molecular association; instead, all intermolecular distances are comparable with those in crystals of the two components. Thus it seems appropriate to describe this as a molecular addition compound.

³⁸W. R. Busing and H. A. Levy, "The Effect of Thermal Motion on the Estimation of Bond Length from Its Diffraction Measurements," submitted to *Acta Crystallographica*; W. R. Busing and H. A. Levy, *A Crystallographic Function and Error Program for the IBM-704*, ORNL CF-59-12-3 (December 1959); see also D. W. J. Cruickshank, *Acta Cryst.* **9**, 757 (1956).

³⁹H. A. Levy and P. A. Agron, *J. Am. Chem. Soc.* **85**, 241 (1963); J. H. Burns, P. A. Agron, and H. A. Levy, *Science* **139**, 1208 (1963).

⁴⁰S. Siegel and E. Gebert, *J. Am. Chem. Soc.* **85**, 240 (1963).

⁴¹J. A. Ibers and W. C. Hamilton, *Science* **139**, 106 (1963); D. H. Templeton *et al.*, *J. Am. Chem. Soc.* **85**, 242 (1963).

X-Ray Diffraction Studies of Molten Salts, Powders, and Aqueous Solutions

M. D. Danford H. A. Levy
M. A. Bredig

Molten Alkali Halides. — Analysis of x-ray scattering from molten alkali halides is continuing. The hypothesis of a large degree of charge order in the melt is consistent with observations from analysis of the radial distribution functions and calculation of theoretical intensity functions. The probability functions for atoms as far distant as 25 Å for molten LiCl and approximately 20 Å for molten CsCl are discrete enough to warrant inclusion as distinct parameters, distances beyond being randomly distributed. These distances are to be compared with a distance of about 10 Å in the case of water.

Synthesis of the observed intensity and radial distribution functions has been attempted for molten LiCl, KCl, RbCl, and CsCl. Models considered as starting points have been the NaCl structure, the cubic ZnS structure, and the hexagonal ZnO arrangement. Attempts thus far have centered on the LiCl and CsCl data. None of the models were consistent with the observed data as long as the crystal-like regularity was maintained. The NaCl arrangement, allowing

distortions of the sort illustrated in Fig. 9.5, has shown considerable promise for all of the molten alkali chlorides.

In preliminary parameter refinements for molten CsCl using this model, P_1 and P_3 (Fig. 9.5) were varied independently, with P_2 automatically calculated from the density and P_1 . The remaining distance P_3 was somewhat shorter than $(P_2 - P_3)$, suggesting that each ion has one neighbor of opposite charge at a distance different from that for the remaining neighbors. The theoretical radial distribution function for this model is shown in Fig. 9.6, and compared with the observed RDF. The quality of fit, while not completely satisfactory at this time, suggests that the model has promise and further work is in progress.

Calcium Carbide. — Work on the structure of CaC_2 at 477°C is nearing completion. Analysis of the Bragg reflections failed to distinguish between the four models considered.⁴² Analysis of the data has continued through use of the total intensity and the radial distribution function.

⁴²M. D. Danford, M. A. Bredig, and H. A. Levy, *Chem. Div. Ann. Progr. Rept. June 20, 1961*, ORNL-3176, p 85.

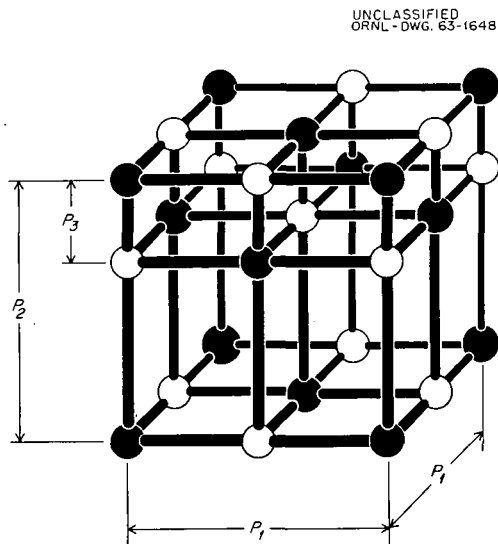


Fig. 9.5. NaCl-Like Model Used in Calculation of Theoretical Intensity Functions for Alkali Halides.

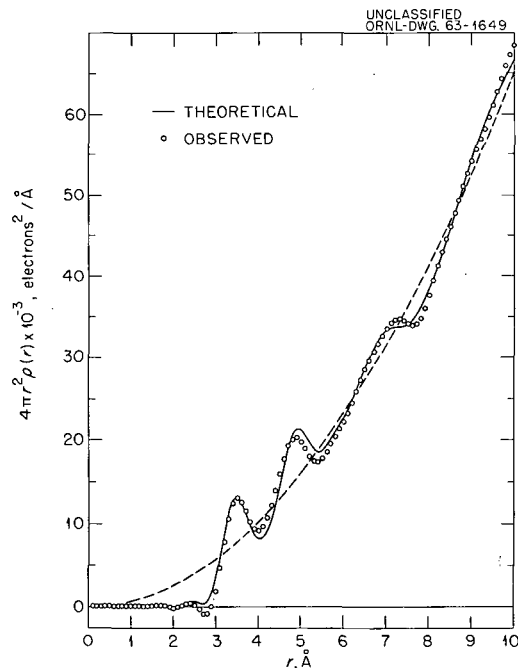


Fig. 9.6. Comparison of Observed and Calculated Radial Distribution Functions for Molten CsCl.

To this end, the experimental RDF was reinverted with cutoff at 10.0 Å, giving a broadened reduced intensity function resulting from discrete distances to 10.0 Å. This procedure makes possible the use of a model with a finite number of distances from which to synthesize the intensity function and RDF. These functions were examined in terms of the four models, namely, a model with a freely rotating C_2^{2-} ion, a disordered pyrite structure in which the C_2^{2-} ion assumes four possible orientations along the cube diagonals ($3m$ symmetry), a model in which the C_2^{2-} ion assumes three possible orientations parallel to the cube edge ($4mm$ symmetry), and a model in which the C_2^{2-} ion assumes six possible orientations parallel to the cube face diagonals (mm symmetry). In each case, the center of the randomly oriented C_2^{2-} ion occupies one set of NaCl-like positions of space group $Fm3m$.

Parameters for each model were refined by the method of least squares, first with no correction for CaO contamination and with random distribution of C–C distances. Of these models, those with free rotation and $4mm$ symmetry for the C_2^{2-} ion configuration could be eliminated immediately, while the distinction for models with mm and $3m$ symmetry was less clear. Both of these models were further examined by correcting for CaO contamination and inclusion of the longer C–C distances.

The resulting refinements gave C–C distances of 1.10 ± 0.02 Å and 1.19 ± 0.02 Å for the mm and $3m$ models respectively. Observed and calculated broadened reduced intensity functions are shown in Fig. 9.7 for the $3m$ model, with a similar comparison for the RDF's in Fig. 9.8. The Ca–Ca distance (5.885 ± 0.005 Å) compares favorably with the size of the unit cell obtained from the Bragg reflections (5.883 ± 0.005 Å). The C–C distance (1.19 ± 0.02 Å) for the $3m$ model compares very well with the normal C–C distance obtained from other results⁴³ (1.20 Å), while the distance of 1.10 Å from the mm model appears unreasonably short.

Aqueous Solutions. – Work on the structure of a 1.18 M NH_4F solution is in progress. The observed radial distribution function is compared with that for H_2O in Fig. 9.9. Clearly, there is not much difference, the differences at larger values of r being mainly due to a small density difference. These observations are in agreement with the notion that the NH_4^+ ion fits into the water structure without much disturbance,⁴⁴ the heat of solution being a relatively small negative quantity with small entropy change. Parameters for the

⁴³M. Atoji and R. C. Medrud, *J. Chem. Phys.* **31**, 332 (1959).

⁴⁴K. Fajans and O. Johnson, *J. Am. Chem. Soc.* **64**, 668 (1942).

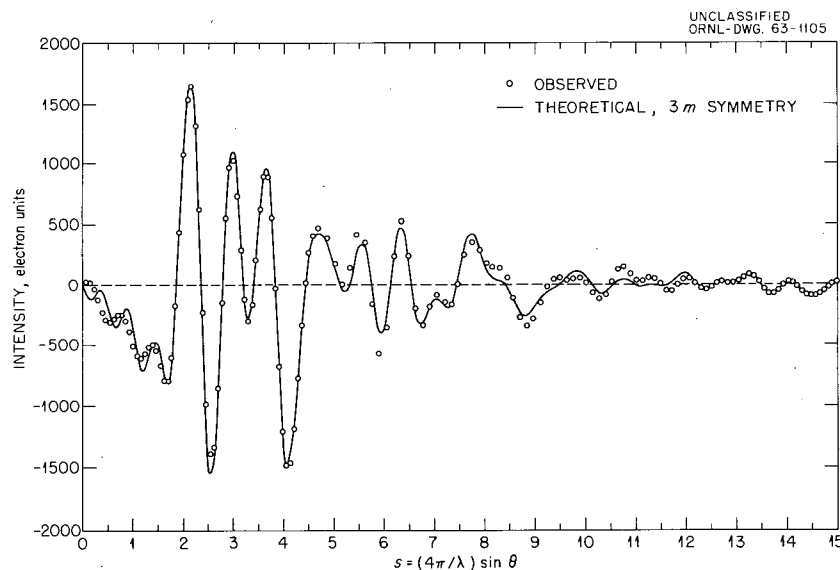


Fig. 9.7. Observed and Calculated Reduced Intensity Functions for the Disordered Pyrite Arrangement.

1.18 M NH_4F solution are being refined using the same model as that for water.⁴⁵ In this case, the N, O, and F atoms are of about the same atomic

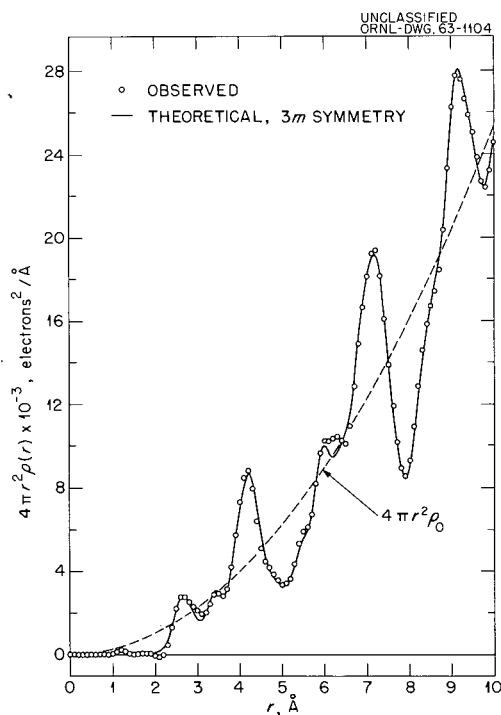


Fig. 9.8. Observed and Calculated Radial Distribution Functions for the Disordered Pyrite Arrangement.

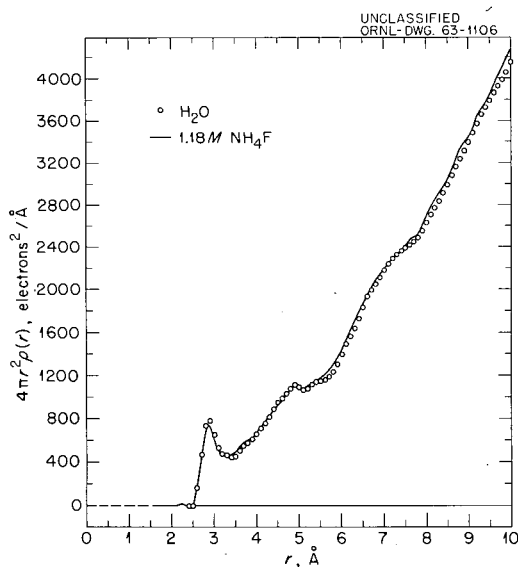


Fig. 9.9. Comparison of Observed Radial Distribution Functions for H_2O and 1.18 M NH_4F Solution.

number and have approximately the same scattering power for x rays; as a result, the observation is directly the overall effect on the water structure due to the dissolved NH_4F . A refinement of parameters for the 1.18 M NH_4F solution, using the high-angle data only, has indicated the following preliminary parameters:

1. Each network atom has three neighbors at 2.91 Å and one at 2.77 Å.
2. Each interstitial atom has three network neighbors at 2.84 Å.
3. The ratio of framework atoms to interstitial atoms is 4.11, corresponding to filling 48.7% of the cavities.

The longer network distance is thus slightly shorter than that for water, where each network atom has three neighbors at 2.94 Å. The distance of 2.77 Å is the same as that for water. The fraction of "cavities" filled is about the same in both cases, while the interstitial-atom-network-atom distance seems to be somewhat smaller than that for water (2.94 Å). Refinement of these parameters is continuing.

A solution approximately 11 M in NH_4F is currently under investigation, the data collection being incomplete at this time. Plans are also under way to study solutions of CsF. The heats of solution for salts containing the cesium ion are quite large, with the apparent partial molar volume of the Cs^+ ion at infinite dilution also large. From these observations, it would appear that the Cs^+ ion has a considerable structure-disrupting effect. Also under consideration are studies of the H_2O structure at various temperatures as well as studies of aqueous HF.

Modified Polaroid Film Holder for X-Ray and Neutron Diffraction

H. G. Smith

D. L. Holcomb

An improved adapter for the Polaroid film holder type No. 500 has been constructed and used to record x-ray and neutron diffraction patterns. The

⁴⁵M. D. Danford and H. A. Levy, *J. Am. Chem. Soc.* 84, 3965 (1962).

adapter previously used⁴⁶ was of a temporary nature, assembled to investigate the feasibility of the method. It then became desirable to construct a more permanent device, although still using the Polaroid No. 500 film holder, since it is quite suited for the purpose, requiring only minor modifications. It is also relatively inexpensive.

Although it is expected that Polaroid film will find many useful applications in x-ray diffraction, our primary use has been in taking Laue photographs and precession alignment photographs, and it was with these methods in mind that the film holder was adapted to fit the Buerger precession camera; however, it can easily be attached to other types of x-ray and neutron apparatus. The pictures may be developed in the holder without removing it from the camera.

The magnesium dovetail track attached to the back of the film holder is of such dimensions as to ensure that the plane of the phosphor can be placed exactly 60.0 mm from the crystal rotation axis of the precession camera. The phosphor is cemented in a recess which has been milled out of the interior of the film holder. The dimensions of the recess are $92 \times 107 \times 1.0$ mm.

To ensure best resolution it is advisable to have the film pressed against the phosphor during exposure, and this is accomplished by a rectangular metal frame set in a molded rubber bellows. The frame must be released before a film packet can

be inserted or removed from the holder, and a lever is provided for this movement. A drawing of the holder and adapter is shown in Fig. 9.10.

The total weight of the Polaroid holder and adapter is 1051 g as compared with 477 g for the standard commercial precession film holder. The weight of the device can be reduced to 857 g by removing the steel rollers and processing lever; however, it would be necessary to develop the film in a separate holder.

Two types of x-ray phosphors have been used — Du Pont Patterson screen "Lightning Special" and Du Pont CB-2 screen. The former is a ZnS screen and is a moderately fast phosphor with good resolution, while the latter is a ZnCdS screen, which is very fast, but the resolution is not as good. For example, exposure time for diffraction photographs with Polaroid film and the "Lightning Special" phosphor are about one-third the exposure times with Ilford Industrial G x-ray film; whereas, if the CB-2 phosphor is used the exposure times are about one-tenth the time with the Ilford film.

The neutron phosphor most commonly employed is an $\text{Li}^6\text{F}:\text{ZnS}$ mixture,⁴⁶⁻⁴⁸ but a new phosphor⁴⁹ with Li^6F dispersed in a scintillating plastic shows promise.

⁴⁷S. P. Wang, C. G. Shull, and W. C. Phillips, *Rev. Sci. Instr.* **33**, 126 (1962).

⁴⁸R. Stedman, *Rev. Sci. Instr.* **31**, 1156 (1960).

⁴⁹D. H. Vincent, J. M. Carpenter, and J. D. Sutton, *Bull. Am. Phys. Soc.* **8**, 379 (1963).

⁴⁶H. G. Smith, *Rev. Sci. Instr.* **33**, 128 (1962).

UNCLASSIFIED
ORNL-DWG 63-939

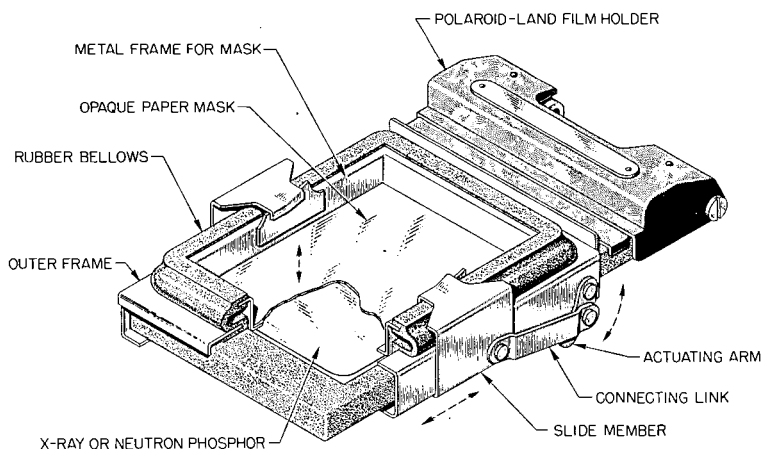


Fig. 9.10. Cutaway Drawing of Modified Polaroid Film Holder.

Neutron Study of K_2ReCl_6 at 4.2°K, 77°K, and Room Temperature

H. G. Smith⁵⁰

Potassium hexachlororhenate is of interest both for its structural properties and its magnetic properties. In its crystal structure,⁵¹ it is isomorphous with K_2PtCl_6 , and it has been shown by Morfee *et al.*⁵² that a number of compounds of this structure type exhibit peculiar anomalies in their heat capacity curves. A heat capacity study of K_2ReCl_6 by Busey, Dearman, and Bevan⁵³ shows similar anomalies at 111, 103, and 76°K and a typical λ -type anomaly at 11.9°K. Busey and Sonder⁵⁴ have shown from a magnetic susceptibility study that the heat capacity anomaly at 11.9°K is associated with antiferromagnetic ordering below this temperature. The magnetic properties of the transition metals in the platinum group are due to the 5d electrons, and an understanding of these properties should contribute greatly to the theory of chemical bonding in these compounds. For example, from a paramagnetic resonance study on $(NH_4)_2IrCl_6$, Stevens⁵⁵ has postulated that the magnetic electron of iridium spends about 30% of its time on the Cl^- ions due to the overlap of the metal $d\epsilon$ orbitals with the ligand orbitals. It is highly probable that similar effects occur in K_2ReCl_6 , and they are discussed in some detail in a comprehensive article by Eisenstein.⁵⁶

Since K_2ReCl_6 exhibits the maximum number of unpaired spins (three) of the strong-field complexes, it is particularly suited for a magnetic study of the 5d electrons by neutron diffraction. Also, since its unit cell is relatively large ($a = 9.86$ Å), the magnetic reflections occur at small scattering angles, which enables the magnetic

form factor to be extrapolated to zero scattering angle more reliably. This report describes the results of a preliminary investigation of the crystal and magnetic structure of K_2ReCl_6 by neutron diffraction.

Neutron diffraction patterns of single crystals and polycrystalline samples were recorded at 4.2°K, 77°K, and room temperature, while a limited amount of data was taken at intermediate temperatures. (The polycrystalline material was obtained from R. H. Busey of the ORNL Chemistry Division and the single crystals were grown from aqueous solution by slow evaporation.) The room-temperature data confirm the space group $Fm\bar{3}m$, reported by Aminoff,⁵¹ which requires octahedral symmetry of the hexachlororhenate ion if the crystal structure is ordered. However, Eisenstein⁵⁶ has concluded from a study of its optical absorption spectrum that the octahedron must be distorted, and hence disordered, at room temperature.

It was apparent early in this investigation that the room-temperature neutron diffraction data could not be explained satisfactorily on the basis of an ordered, rigid octahedron (i.e., chlorine atoms in the special set $x, 0, 0$), with an overall temperature factor, but the agreement between calculated and observed structure factors was substantially improved by assuming a large individual temperature factor for the chlorine atoms. However, this model is not readily distinguishable from a small disordered displacement of the chlorine atoms from their octahedral positions. In fact, as discussed below, the low-temperature data require a small ordered displacement from $(x, 0, 0)$ to $(x, \epsilon_y, \epsilon_z)$, and a least-squares analysis of the room-temperature data based on a disordered arrangement of this model gives a reliability factor, $R(F^2)$, equal to 3.7%; whereas, a model based on a rigid octahedron with isotropic thermal motion of the chlorine atoms gives an $R(F^2)$ equal to 7.1%. (Both refinements suggest a slight increase in the neutron scattering length of rhenium.)

Below 77°K additional nuclear reflections are observed which require a space group of lower symmetry, although still cubic. The most probable space group, based on the limited data available, is $Pn\bar{3}$; however, a disordered arrangement in $Pn\bar{3}m$ is not completely excluded.

Additional evidence that the crystal remains cubic below the 76°K transition has been obtained

⁵⁰Most of the experimental data were collected and some of the calculations were made while the author was on assignment at AERE, Harwell, England, from August 1961 to August 1962.

⁵¹B. Aminoff, *Z. Krist.* **94**, 246 (1936).

⁵²R. G. S. Morfee *et al.*, *J. Phys. Chem. Solids* **13**, 132 (1960).

⁵³R. H. Busey, H. H. Dearman, and R. B. Bevan, Jr., *J. Phys. Chem.* **66**, 82 (1962).

⁵⁴R. H. Busey and E. Sonder, *J. Chem. Phys.* **36**, 93 (1962).

⁵⁵K. W. H. Stevens, *Proc. Roy. Soc. (London)* **A219**, 532 (1953).

⁵⁶J. C. Eisenstein, *J. Chem. Phys.* **34**, 1628 (1961).

by Gaunt.⁵⁷ His x-ray analysis of the polycrystalline material at several temperatures between 45°K and room temperature showed anomalies of the thermal expansion coefficient in the region of the heat capacity anomalies. There was no indication of a departure from the cubic lattice, although below 90°K the α_1 , α_2 doublets at high Bragg angles were no longer resolved, suggesting some type of lattice strain or small domain size.

The point symmetry about the rhenium ion is correspondingly reduced from $4/m\bar{3}2/m$ to $\bar{3}$ (or possibly $\bar{3}m$). By a trial and error procedure it is found that $\epsilon_z \approx -\epsilon_y \approx 0.012$, but, if $\epsilon_z \equiv -\epsilon_y$, the intermediate environment of the rhenium ion (e.g., the six bonding chlorine ions) is octahedral, even though the site symmetry is lower.

It has been pointed out by Morfee *et al.*,⁵² in the isomorphous compound K_2SnCl_6 , that the structure of lowest electrostatic energy does not necessarily require the chlorine atoms to be in the set $(x, 0, 0)$, and that a small rotational displacement of the octahedra can, indeed, lead to two or more minima in the potential energy curves. This may be the explanation for the low space-group symmetry observed below 76°K in K_2ReCl_6 .

Of primary interest to the theory of chemical binding is the delocalization of the magnetic electron density onto the surrounding chlorine ligands. Unfortunately, only four magnetic reflections could be measured, and they are insufficient to determine directly the spin density associated with the metal and ligand atoms. A model describing the antiferromagnetic ordering has been formed which is consistent with the experimental data. In the terminology of P. W. Anderson, the magnetic ordering is of the first kind, that is, the spins lie in the (100) planes in a ferromagnetic arrangement and are coupled to the adjacent parallel planes antiferromagnetically. A very approximate form factor based on this model was determined from the four magnetic reflections. The resulting magnetic moment of about 2.7 Bohr magnetons is somewhat less than the expected 3.87 Bohr magnetons if three magnetic electrons are localized on the metal atoms, but it is premature to conclude that this is evidence for electron delocalization, and further studies will be necessary.

⁵⁷Paul Gaunt, University of Sheffield, private communication.

CALORIMETRY

Low-Temperature Heat Capacity of Rhenium Trichloride

R. B. Bevan, Jr. R. A. Gilbert
R. H. Busey

The increased interest in recent years in the magnetic properties of compounds of the third transition series elements, both experimentally and theoretically,⁵⁸ may be attributed to the application of ligand field theory to these problems. One of the many interesting compounds exhibiting unusual magnetic properties is $ReCl_3$. The magnetic susceptibility⁵⁹ does not follow the Curie-Weiss law, but the measurements show a low paramagnetic susceptibility only slightly dependent on temperature. A very low effective magnetic moment decreasing with temperature is calculated from the magnetic data. Presumably the salt is a binuclear complex at least in solution, since the molecular weight of the salt in glacial acetic acid is that of Re_2Cl_6 .⁶⁰ Tetrahedral coordination of the Re^{3+} is also demonstrated by the similarity of the visible spectrum of the salt in acetone and hydrochloric acid.⁶¹ In the latter solvent, the rhenium species is undoubtedly $ReCl_4^-$, since several salts $MReCl_4$ have been isolated.

No x-ray structure determination of $ReCl_3$ has been made. If the structure of the Re_2Cl_6 were two chlorine tetrahedra with one edge in common, the electronic configuration for the four $5d$ electrons would be d^4 with no unpaired electrons. The salt would then be expected to be diamagnetic, similar to $CsReCl_4$,⁶² except for the Van Vleck temperature-independent paramagnetism. If the structure in the solid were octahedral or square planar, however, paramagnetism could arise due to two unpaired spins per rhenium atom.

The magnetic entropy of a binuclear complex composed of two atoms with unpaired spins may be

⁵⁸See, for example, C. J. Ballhausen, *Introduction to Ligand Field Theory*, McGraw-Hill, New York, 1962.

⁵⁹Kerro Knox and C. E. Coffey, *J. Am. Chem. Soc.* 81, 5 (1959).

⁶⁰F. W. Wrigge and W. Biltz, *Z. Anorg. Allgem. Chem.* 228, 372 (1936).

⁶¹R. H. Busey and Q. V. Larson, *Chem. Div. Ann. Progr. Rept. June 20, 1958*, ORNL-2584, p 5.

⁶²R. J. Gillespie and R. S. Nyholm, *Quart. Rev. (London)* 11, 339 (1957).

lost as the temperature is lowered in one of two ways. The interaction energy between different magnetic ions may be the common antiferromagnetic variety⁶³ exhibited by most paramagnetic salts. For such an antiferromagnetic salt, the magnetic entropy is slowly removed as the temperature is lowered until the Néel or Curie region is reached. Below this temperature the rate of loss of magnetic entropy is more rapid. Such behavior is accompanied by a lambda transition in the heat capacity in the Curie region.⁶⁴ Alternatively, a spin-spin interaction between the two magnetic atoms of the complex may give rise to a set of energy levels consisting of a singlet ground state with degenerate excited states. The number and degeneracy of the upper electronic states depend upon the spin quantum numbers of the atoms in the binuclear complex. For both atoms with $S = 1$, the energy levels are a singlet ground state, a triplet at energy ϵ , and a quintet at energy 3ϵ above the ground state.⁶⁵ The magnetic susceptibility and behavior of the heat capacity depend upon the separation ϵ . For a weak spin-spin interaction giving rise to an $\epsilon \approx 10 \text{ cm}^{-1}$, the magnetic susceptibility would follow the Curie-Weiss law from liquid-nitrogen temperatures up, and the heat capacity would show a Schottky anomaly at the lowest temperatures (depopulation of the excited states at low temperatures). For increasingly larger separations of the energy levels (increasing spin-spin interaction), deviation of the magnetic susceptibility from the Curie-Weiss law becomes pronounced, and the Schottky anomaly becomes increasingly difficult to detect. The latter is due to the fact that depopulation of the excited states takes place over a large temperature interval and the excess heat capacity is likewise spread out.

The heat capacity of ReCl_3 from 7 to 310°K was measured in order to determine what type of heat capacity anomaly, if any, exists in the compound, and also to obtain the thermodynamic properties. The purchased ReCl_3 was carefully purified by repeated sublimations in a vacuum system. Chloride analyses gave 36.36, 36.39, and 36.33% vs 36.35% theoretical.

No lambda transition was observed, but an anomaly with a maximum near 15°K was found

which resembles a Schottky heat capacity anomaly. No heat capacity measurements on a diamagnetic compound which might represent the lattice heat capacity of ReCl_3 are available. A crude estimate of the lattice heat capacity C_l was made by fitting the C_p of ReCl_3 from 50 to 200°K with a Debye and three Einstein functions, $C_l = D(138/T) + 2E(286/T) + E(530/T)$, and making the assumption that the equation gives the lattice heat capacity below 50°K. The equation reproduced the observed C_p from 50 to 200° to within 0.5% on the average. The results of $C_p(\text{obs}) - C_l(\text{calc})$ from 7 to 50°K are given in Fig. 9.11. The curve does not represent a lambda transition, but does resemble a Schottky anomaly.⁶⁶ The crude estimate of C_l does not permit an accurate analysis of the curve to determine the number and degeneracy of the energy levels involved. The calculation does rule out the possibility of a singlet, triplet, and quintet set of energy levels, expected for a binuclear complex mentioned above with $S = 1$ for each atom. Such a set of energy levels would give a Schottky anomaly with a maximum electronic heat capacity of $1.09 \text{ cal deg}^{-1} (\text{mole ReCl}_3)^{-1}$. The observed $C_p [= C_l + C(\text{electronic})]$ is only $1.22 \text{ cal deg}^{-1} (\text{mole ReCl}_3)^{-1}$ at 15°, and C_l is most probably greater than $0.13 \text{ cal deg}^{-1} (\text{mole ReCl}_3)^{-1}$.

The heat capacity measurements show that the low effective magnetic moments calculated from the susceptibility measurements [$\mu_{\text{eff}} = 2.84(\chi T)^{1/2}$] cannot be attributed to a large antiferromagnetic

⁶⁶See, for example, R. Fowler and E. A. Guggenheim, *Statistical Thermodynamics*, p 103, Cambridge University Press, Cambridge, England, 1952.

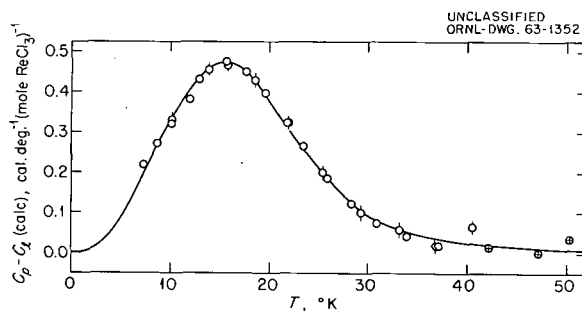


Fig. 9.11. Heat Capacity of ReCl_3 Less the Estimated Lattice Heat Capacity.

⁶³J. H. Van Vleck, *J. Chem. Phys.* **9**, 85 (1941).

⁶⁴J. W. Stout, *Pure and Appl. Chem.* **7**, 287 (1961).

⁶⁵A. Earnshaw and J. Lewis, *J. Chem. Soc.* **1961**, 396.

interaction, since no lambda transition was observed above 7°K. Further, from the anomaly at 15°K, implying a weak spin-spin interaction, one would infer that the magnetic susceptibility should follow the Curie-Weiss law from 80 to 300°K, contrary to the observed magnetic properties. Interpretation of the magnetic properties and the heat capacity anomaly at 15°K will have to await confirmation and extension of the magnetic susceptibility measurements to helium temperatures and determination of the crystal structure.

The entropy of ReCl_3 calculated from the heat capacity data by application of the third law of thermodynamics is $29.59 \text{ cal deg}^{-1} (\text{mole ReCl}_3)^{-1}$ at 298.15°K.

MOLECULAR BEAM STUDIES

Reactions of Alkali Metals

R. E. Minturn E. H. Taylor

An improved differential surface ionization gage mentioned previously⁶⁷ was applied to the reaction $\text{K} + \text{HBr} = \text{KBr} + \text{H}$. The angular distribution found was essentially identical with that reported originally,⁶⁸ but below about 20° in angle (measured from the potassium beam) the results were erratic, as in previous work.

One of the advantages of the molecular beam technique is the possibility of energy selection. The toothed-wheel velocity selector, built last year essentially to the design of Hostettler and Bernstein,⁶⁹ was installed in the potassium beam and thoroughly tested. After minor adjustments it operated satisfactorily up to 400 rps, adequate for application to all except the lightest elements. The loss in intensity, while not excessive, left too little scattered signal to perform reactive scattering experiments with the present, rather well collimated crossbeam of HBr.

These two sources of difficulty, irreproducibility at low angles and lack of enough sensitivity for more subtle experiments, led to a modification that had been considered for some years but deferred

until required. This modification is the introduction of a filter for magnetic atoms between the scattering center and the surface ionization gage, so that only the virtually nonmagnetic KBr can reach the filament. This allows direct measurement of the quantity of interest and eliminates the chief disadvantages of the two-filament gage. An inhomogeneous magnet for such a filter was copied from a standard design⁷⁰ and incorporated with a tungsten filament and a secondary-electron multiplier into a rotating gage suitable for chemical experiments. A report⁷¹ reaching ORNL after our magnet was completed showed a similar magnet developed for similar purposes independently and somewhat earlier at UCRL.

The new detector has been tested on a potassium beam alone and on scattered $\text{K} + \text{KBr}$. It appears to perform about as designed, except that it is difficult in the space available adequately to shield the electron multiplier from the magnetic field. The gain of the multiplier appears to be appreciably affected by fields not quite high enough to deflect all of the potassium. This should be curable by using a special type of multiplier not sensitive to moderate fields, or by narrowing the slits on the filter.

Interactions of Gases and Surfaces

G. E. Moore E. H. Taylor

Some details of the pseudo-specular reflection of helium, deuterium, and argon from platinum⁷² suggested an exchange of energy without adsorption, that is, during an almost elastic collision. Because such collisions preserve the phase coherence of the chopped beam it is possible to measure any resulting changes in velocity through the phase shift of the reflected beam relative to the incident. Significant phase shifts ($>20 \mu\text{sec}$) were observed, but quantitative measurement has not yet been achieved. Steps taken to improve the experiment include narrowing of the incident

⁶⁷R. E. Minturn, S. Datz, and E. H. Taylor, *Chem. Div. Ann. Progr. Rept. June 20, 1962*, ORNL-3320, p 124.

⁶⁸E. H. Taylor and S. Datz, *J. Chem. Phys.* **23**, 1711 (1955).

⁶⁹H. U. Hostettler and R. B. Bernstein, *Rev. Sci. Instr.* **31**, 872 (1960).

⁷⁰N. F. Ramsey, *Molecular Beams*, p 399 ff, Oxford University Press, Fair Lawn, N. J., 1956.

⁷¹R. R. Herm and D. R. Herschbach, *Magnetic Analysis of Atomic and Molecular Beams. I. Construction and Calibration of Inhomogeneous Deflecting Magnets*, UCRL-10526 (October 1962).

⁷²S. Datz, G. E. Moore, and E. H. Taylor, *Chem. Div. Ann. Progr. Rept. June 20, 1962*, ORNL-3320, p 124.

beam, relocation of the chopper nearer the scattering surface to preserve phase coherence, and use of a commercial lock-in amplifier. A more flexible sample holder has been built which should eliminate difficulties stemming from lack of flatness of the foil and inability to examine out-of-plane scattering.

In attempts to study surface-catalyzed (platinum) exchange reactions ($H_2 + D_2$ and $D + H_2$) and recombination reactions ($D + D$), no appreciable amounts of reflected product (HD or D_2) coherent in phase with the incident beam were observed. It is not yet clear whether this is another example of difficulties caused by high background or whether it represents an intrinsic property of the surface-catalyzed reactions, namely, a requirement for surface residence too long to preserve coherence.

MASS SPECTROMETRY

Two-Stage Mass Spectrometer

Russell Baldock L. E. Idom

Early in the fiscal year the mass spectrometry research equipment was moved to permanent quarters at the X-10 site. The two-stage machine was quickly put back in operation and has been in continuous use in support of the neutron cross-section measurement program of the Chemistry Division. All mass spectrographic analyses relative to determining the half-life of Bi^{208} have been completed.⁷³ The bismuth sample had a history of a one-year irradiation in the MTR. The Bi^{208} is formed in the reactor through the reaction $Bi^{209}(n,2n)Bi^{208}$. It was found that the material was contaminated with lead, which was most likely present in the starting material. An extensive series of measurements was necessary to establish that satisfactory chemical purification was effected prior to the ultimate determination of the Bi^{208}/Bi^{209} ratio, which was found to be in excellent agreement with measurements made by employing counting techniques.

Numerous mass spectrometric measurements relative to determining the neutron capture cross section of Rh^{105} have been made.⁷⁴ Most analyses to date have been concerned with checking various chemical procedures for yield and possible con-

tamination; extensive use has been made of the isotope dilution technique employing enriched Pd^{102} to measure the contamination by natural palladium.

Charge Spectrometry⁷⁵

T. A. Carlson C. H. Johnson
M. O. Krause Frances Pleasonton

Special use has been made of mass spectrometry to obtain data on ions that result as the direct consequence of nuclear decay. The ions were measured for their kinetic energy, their charge, and their mass. From these data information has been elicited on (1) the angular correlation in beta decay between the β^- particle and the neutrino, (2) the extent of electron shakeoff as the result of a sudden change in nuclear charge, and (3) the nature of molecular fragmentation following nuclear decay. Most recently work has been initiated on the measurement of the relative intensities of ions that result from x-ray ionization of rare gases. The following papers were prepared for publication during the last year but are not yet in print:

1. T. A. Carlson, "Electron Shake Off Following the β^- Decay of Ar^{41} ."
2. T. A. Carlson and R. M. White, "Formation of Fragment Ions from CH_3Te^{125} and $C_2H_5Te^{125}$ Following the Nuclear Decays of CH_3I^{125} and $C_2H_5I^{125}$."
3. T. A. Carlson and R. M. White, "Fragmentation of the Excited Parent Ions $[CH_3Kr^{82}]^+$ and $[CH_3O^{18}]^-$, Following the β^- Decay of CH_3Br^{82} and the β^+ Decay of CH_3F^{18} ."
4. C. H. Johnson, F. Pleasonton, and T. A. Carlson, "A Precision Measurement of the Recoil Energy Spectrum from the Decay of He^6 ."
5. M. O. Krause and T. A. Carlson, "Readjustment of the Neon Atom Following Ionization in the K-Shell by X-Rays."
6. T. A. Carlson, "Recoil Energy Spectrum of the Sodium Ions Following the β^- Decay of Ne^{23} ."

⁷⁵In collaboration with the Physics Division. C. H. Johnson and Frances Pleasonton are full-time members of that Division. T. A. Carlson is a part-time member of the Physics Division, and M. O. Krause a part-time member of the Thermonuclear and of the Physics Division.

⁷³See "Half-Life of Bi^{208} ," chap. 1, this report.

⁷⁴See "Neutron Capture Cross Section of Rh^{105} ," chap. 1, this report.

10. Water Research Program

W. H. Baldwin
M. H. Lietzke
R. J. Raridon
C. E. Higgins

D. C. Michelson
R. W. Stoughton
J. S. Johnson
T. Morozumi

K. A. Kraus
H. O. Phillips
R. D. Lanier
F. A. Posey

A little over a year ago a general water research program was initiated at Oak Ridge National Laboratory under sponsorship of the Office of Saline Water (OSW) and based on an agreement signed between the Department of the Interior and the Atomic Energy Commission. This agreement specifies that ORNL carry out fundamental research in a variety of fields, including thermodynamic and transport properties of solutions and membranes, study of phase boundaries, and corrosion. A substantial portion of this program is being carried out in the Chemistry Division, and certain aspects of this work are summarized below. Since many of the individuals working on this program are doing so on a part-time basis and since in a few other cases the work represents a cooperative program between personnel engaged in OSW and AEC activities, some parts of the work carry dual sponsorship by OSW and the AEC. The corresponding topics are appropriately identified.

Measurement of Activities of Salts by EMF Methods

Special electrodes are being evaluated for measurement of the free energies of salts in aqueous and mixed water-organic solvents. Work, so far, was concentrated on sodium chloride using, in a cell without liquid junction, special glass electrodes together with Ag-AgCl reference electrodes.

Two types of Beckman glass electrodes have been tested. Of these the Sodium Electrode (39278) was found to be excessively sensitive to acidity; the Beckman Cationic Electrode (39137), which according to the manufacturer is better for

potassium than for sodium, seems suitable for measurements with sodium chloride in water at concentrations above 0.001 *M* and in some organic-water mixtures at concentrations above 0.1 *m*. Measurements of two such cationic electrodes, each against three silver-silver chloride electrodes, gave differences in potential between 0.1 *m* aqueous NaCl solutions and 1 and 3 *m* NaCl reproducible to about 0.1 mv. The potentials for the various combinations of electrodes in a given solution were within 3 mv of one another. Comparison with values expected from literature activity coefficients of NaCl was also good: 109.1-mv difference found between 0.100 and 0.984 *m* NaCl, to be compared with 108.9 computed, and 170.0 for the difference between 3.000 *m* ($\gamma_{\pm} = 0.714$) and 0.1000 *m* ($\gamma_{\pm} = 0.778$), to be compared with 170.0 calculated.

One cannot be certain, of course, that the good performance of the electrode system in aqueous media assures that reliable results will be attained with organic-water mixtures, and literature data with which to check the point are scarce. Urea, at least, does not seem to cause serious misbehavior of the electrodes: the difference in potential of 3 *m* NaCl in water and in 10 *m* urea solution measured by these electrodes was 1.4 mv, in comparison with 1.3 mv predicted from the isopiestic measurements of Bower and Robinson.¹ Potentials in organic-water media are reproducible to about ± 0.3 mv at NaCl molalities above 0.1.

Results to date are summarized in Fig. 10.1, a graph of $\log (\gamma_{\pm\text{org}}/\gamma_{\pm\text{water}})$ obtained from the difference in potential measured in NaCl solutions

¹V. E. Bower and R. A. Robinson, in press.

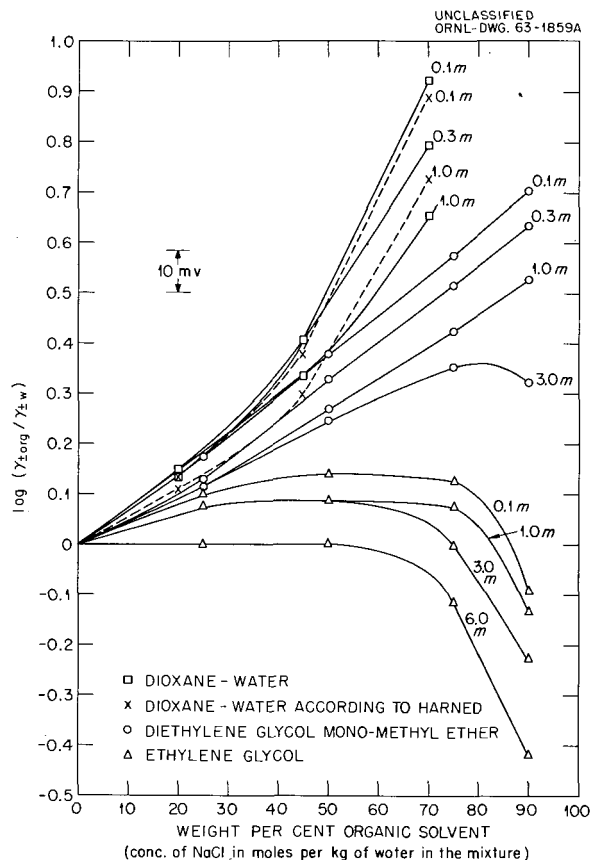


Fig. 10.1. Plot of $\log (\gamma_{\pm\text{organic-water}} / \gamma_{\pm\text{water}})$ vs Weight Percent Organic Solvent.

of a given molality in water and in mixed water-organic media. It should be noted that the concentration of salt here is expressed as moles per kg of water, rather than moles per kg of mixed solvent, as it is sometimes given. The organic diluents employed here, and their dielectric constants, are dioxane (2), ethylene glycol (38), and diethylene glycol methyl ether (no value available, but presumably intermediate between dioxane and ethylene glycol). Harned² has suggested a rule for activity coefficients of salts in organic-water mixtures that can be stated for present purposes,

$$(\gamma_{\pm\text{NaCl}})_{\text{org}} = (\gamma_{\pm\text{NaCl}})_{\text{water}} \frac{(\gamma_{\pm\text{HCl}})_{\text{org}}}{(\gamma_{\pm\text{HCl}})_{\text{water}}}$$

²H. S. Harned, *J. Phys. Chem.* **66**, 589 (1962).

where the activity coefficients are at the same molality, based on kilograms of mixed solvent. For dioxane solutions, data are available to test the rule against our measurements, and a comparison is shown in the figure. At low organic fractions and 0.1 m NaCl, agreement is very good, within a fraction of a millivolt. Divergence is greater at higher organic content and NaCl concentration, though the maximum deviation is about 8 mv in 1 m NaCl.

Activity Coefficients of HBr and KBr in HBr-KBr Mixtures

The activity coefficients of HBr in HBr-KBr mixtures have been measured up to 150°C using the cell $\text{Pt} - \text{H}_2(p) | \text{HBr}(m_2), \text{KBr}(m_3) | \text{AgBr} - \text{Ag}$. At constant temperature and ionic strength $\log \gamma_{\pm\text{HBr}}$ was found to vary linearly with m_{KBr} . Using the parameters describing this variation and a Gibbs-Duhem transformation, the activity coefficients of KBr in the mixtures were calculated. It was found that in these mixtures $\gamma_{\pm\text{KBr}}$ varies less with temperature and fraction of KBr than $\gamma_{\pm\text{HBr}}$.

Further details regarding this work, cosponsored by the AEC, are described in another section of this report.³

Activity Coefficients of HCl and NaCl in HCl-NaCl Mixtures

The activity coefficients of HCl and NaCl in HCl-NaCl mixtures have been computed from literature data. The calculations are based on the observation that at constant ionic strength and temperature $\log \gamma_{\pm\text{HCl}}$ in HCl-NaCl mixtures varies linearly with NaCl concentrations.

Further details regarding this work, cosponsored by the AEC, are described in another section of this report.⁴

Dissociation Constant of HSO_4^- and DSO_4^-

From measurements of the solubility of Ag_2SO_4 in D_2SO_4 solutions the acid constant of DSO_4^-

³See chap. 6, this report; this work has been submitted for publication in the *Journal of Physical Chemistry*.

⁴See chap. 6, this report.

was computed for the temperature range 25 to 225°C and a comparison with the corresponding values for the H₂SO₄ system given.

Further details regarding this work, cosponsored by the AEC, are described in other sections of of this report.⁵

Solubility and Activity Coefficients of Salts in Water-Organic Mixtures

A broad survey of the solubility of salts in a large number of water-organic mixtures has been initiated. The main objective of these measurements is determination of activity coefficients of these salts in the mixtures as a function of water content. So far, the measurements involved principally NaCl; a few measurements with KCl, Ba(NO₃)₂, and BaCl₂·2H₂O, as well as a few other salts, have been carried out.

Representative data are summarized in Table 10.1, which gives the activity coefficient ratios $\Gamma = \gamma_{\pm\text{org}}/\gamma_{\pm\text{aq}}$ of salts in a variety of saturated organic-water mixtures. While the measurements were carried out over a broad range of water-organic compositions, the table gives only the values where the mixed solvents contain 5% by weight of water. Activity coefficients are computed for both phases by expressing the concentration of salts in terms of moles per kilogram of water.

As part of this general survey the viscosities and densities of the organic-water mixtures are being determined at 25°C. The viscosity measurements are being carried out by use of Cannon-Ubbelohde semimicroviscometers. Densities are being determined with a micropycnometer.

Activity coefficients of NaCl and CsCl have been determined in several organic phosphates and amides by two-phase equilibration techniques, using in most cases about 0.05 M solutions of the salts. Analyses were performed radiometrically. Water content of the phases was established by Karl Fischer titrations. For all the systems studied, the activity coefficients of the salts in the organic phase were larger than unity and in a few cases very much larger. Thus, tri-*n*-butyl phosphate-water mixtures with 7.5% water had $\Gamma_{\text{NaCl}} > 50$. Of the amides studied, *t*-octyl form-

Table 10.1. Activity Coefficient Ratios $\Gamma = \gamma_{\pm\text{org}}/\gamma_{\pm\text{aq}}$ of Salts in Some 5% Water-95% Organic Mixed Solvents at Saturation (25°C).

Compound	Activity Coefficient Ratio Γ		
	NaCl	KCl	Ba(NO ₃) ₂
Acetic acid	5.3		
Acetone	140		
Acetonitrile	45		
1,3-Butanediol	3.6		
2-Butoxyethanol	7.5	25	
Dimethyl formamide	8.2		
Dimethyl sulfoxide	1.8	5.6	
Dipropylene glycol	1.5		
2-Ethoxyethanol	4.1	11	
Ethyl alcohol	10.5	23	
Ethylene glycol	0.23	0.30	0.068
Formamide	0.19	0.33	
Glycerol	0.21	0.24	0.072
Diacetone alcohol	12		
Isopropyl alcohol	60		
2-Methoxyethanol	1.2	2.8	
Methyl alcohol	1.0	2.6	6.5
<i>N</i> -Methyl-2-pyrrolidone	19	53	
Polyethylene glycol 400	0.96		
Polypropylene glycol 425	9		
1,2-Propanediol	0.52		
Propionic acid	17		
<i>n</i> -Propyl alcohol	24		

amide (5% water) had the highest activity coefficients, with $\Gamma_{\text{NaCl}} \approx 100$ and Γ_{CsCl} substantially larger than this value.

Ion Exchange

Ion exchange studies have been carried out with organic ion exchange resins of the conventional type and with inorganic ion exchange materials.

An excellent cation exchange method for the separation of calcium from magnesium, which should be applicable to moderately concentrated salt solutions, has been developed. The method takes advantage of the exceedingly high adsorbability of Ca²⁺ in concentrated HClO₄ and HClO₄-HCl solutions. Magnesium under these conditions is only slightly adsorbed; Na⁺ has negligible

⁵See chap. 6, this report; M. H. Lietzke and R. W. Stoughton, *J. Phys. Chem.* **67**, 652 (1963).

adsorption. A paper summarizing this work, cosponsored by the AEC, has been accepted for publication.⁶

The adsorptive properties of a number of sulfides have been examined. These might have application in certain special purification problems. Further details regarding this work, cosponsored by the AEC, are described in another section of this report.⁷

Hyperfiltration Studies of Membranes

A considerable amount of work is being done on the transport of various solutes and solvents through membranes. During the past year, principal emphasis was placed on "hyperfiltration" in which water is removed from salt by "filtering" water through a suitable membrane under pressure. This pressure, of course, needs to be high enough to overcome the osmotic pressure of the salt solution. Equipment has been developed for investigating the transport properties of solutes and solvents through membranes under a pressure gradient. The experiments which have been carried out are aimed toward elucidation of the mechanisms of salt rejection by the membranes and testing various films and membranes whose properties may be illuminating in this context or practically useful. Attempts are also under way to prepare hydrous oxide ion exchange barriers in a physical form suitable for hyperfiltration studies; from these we would also hope to confirm if these hydrous oxides have the rejection properties which one would predict on theoretical grounds.

A simple gas-pressurized device has been constructed, and more versatile mechanically pressurized equipment, which allows better control of experimental conditions, has been assembled; we have not as yet attained long-term, trouble-free operation of the mechanically pressurized equipment.

A number of studies have been carried out on samples of the highly promising cellulose acetate membrane developed by S. Loeb of UCLA. Some

of these are summarized in Fig. 10.2, which gives the rejection⁸ as a function of total chloride for NaCl-MgCl₂ and NaCl-CaCl₂ solutions. The mole ratio of sodium to divalent ions was about 8; this value does not appear to be critical, for calcium at least, which was rejected about the same alone as in mixtures of the same total chloride concentration. It can be seen that the divalent ions are rejected a little better than sodium, but that the percent of solute in the feed rejected varies remarkably little over a wide range of concentration. There may be some drop in rejection at very low concentrations, but it is possible that adsorption on parts of the apparatus is responsible for the apparent decrease.

The properties of this membrane are in sharp contrast to those expected for an ion exchange membrane. For the latter, rejection should be inversely related to the extent of Donnan invasion, which, in turn, increases sharply with electrolyte concentration of the surrounding medium.

Attempts to prepare ion exchange membranes suitable for hyperfiltration studies have been reasonably successful. Thus an ion exchange membrane was prepared which yielded flow rates of 1 to 2 cm/hr at 1500 psi with 0.5 M NaCl solutions. This flow rate, though appreciably smaller than for the Loeb cellulose acetate membranes (3 to 6 cm/hr), is remarkably high compared with those reported in the literature for other ion-exchange-type membranes. Further, it is approximately the same as that observed with the untreated base material (about 2 cm/hr at 1500 psi). While the base material showed no salt-rejection properties, the ion exchange material prepared from it gave 35% rejection in 0.5 M NaCl and substantially higher rejection at lower salt concentrations as shown in Fig. 10.2. In 0.01 M NaCl, rejection by this ion exchange membrane was approximately equal to that of the Loeb membranes. These measurements were carried out at 2500 psi and a moderately rapid rate of flow past the membrane. Some experiments carried out at lower flow rates and at lower pressure showed substantially less rejection.

Despite considerable work, attempts to prepare a membrane whose rejection properties result

⁶F. Nelson, J. H. Holloway, and K. A. Kraus, "Cation Exchange Separation of Calcium and Magnesium at High Ionic Strength," to be published in the *Journal of Chromatography*.

⁷See chap. 6, this report; H. O. Phillips and K. A. Kraus, *J. Am. Chem. Soc.* **85**, 486 (1963).

⁸"Rejection" is the fraction, on a mole basis, of the salt of the feed solutions which is rejected by the membrane, that is, which is not found in the solution that has passed through the membrane.

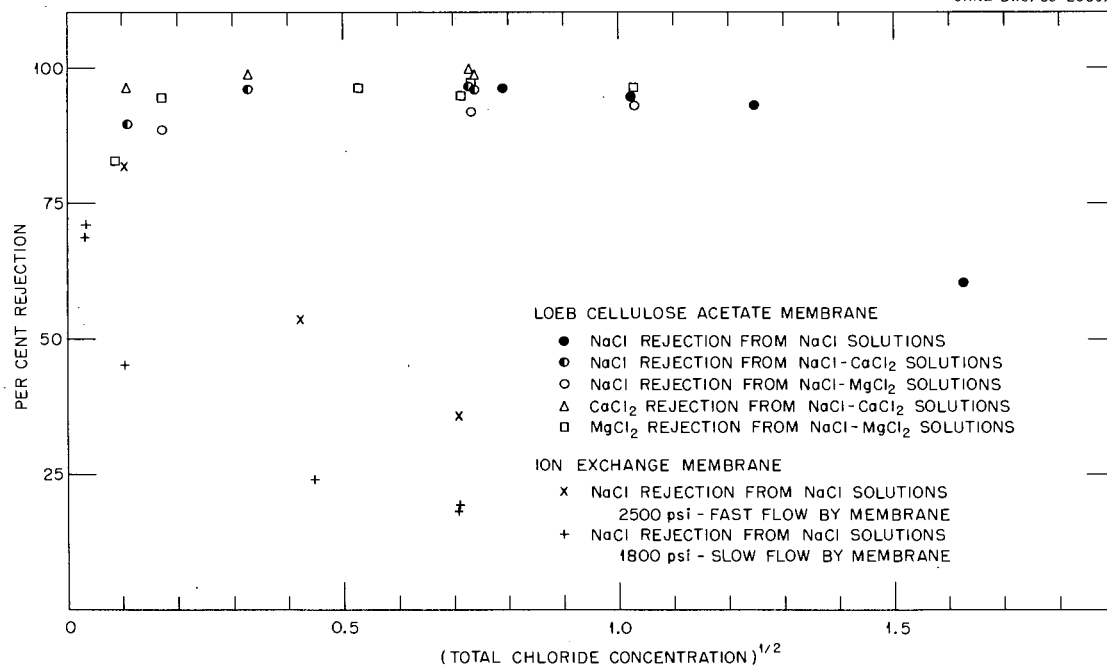


Fig. 10.2. Hyperfiltration by Cellulose Acetate (Loeb) and by Ion Exchange Membranes.

from the action of hydrous oxide ion exchangers have been so far unsuccessful. The importance of testing theoretical predictions with such materials, however, plus the wide range of practical possibilities that would be opened by success, impel us to continue our efforts in this direction.

Electrode Kinetics of Porous Conducting Electrodes

Reaction kinetics of the ferrous-ferric oxidation-reduction couple in chloride, sulfate, and nitrate solutions was studied on porous carbon electrodes under constant-potential and constant-current conditions. In addition, the effect of solution flow through the porous medium on the overall rate of the reaction in the electrode was determined as a function of electrode potential. These experiments and others were performed in order to increase understanding of the factors affecting the operation of porous electrodes.

Considerable effort was devoted to the development of a comprehensive theory of Faradaic reaction in porous electrodes. A system of equations was developed and solved for certain special cases corresponding to experimental conditions

which can be achieved or approached closely in practice. For highly conducting solutions, the interfacial potential difference is constant throughout the porous electrode and the general system of equations is explicitly soluble for overall reaction rates in both transient and steady states. For constant reactant concentrations and pure activation rate control, the distribution of current and potential was calculated exactly for three particular values of transfer coefficients of the electrochemical processes. In addition, an approximate method was developed which allows calculation of polarization behavior under very general conditions, including partial rate control by mass transfer of reactants. Results of these calculations agree well with experimental observations, and publications on both experimental and theoretical aspects are in preparation.

Electrochemical Studies of Corrosion of Iron

The rate of corrosion of polycrystalline, zone-refined iron was measured in aqueous chloride solutions as a function of temperature, acidity, and chloride ion concentration in the absence of

atmospheric oxygen. The logarithm of the corrosion rate in 0.5 M NaCl decreases linearly with increasing pH from pH = 3 to pH = 8 at all temperatures from 25 to 70°C. Corrosion rate at 50°C is given by $R = 1.21 \times 10^3 C_{H^+}^{0.38}$, while at 70°C, $R = 3.58 \times 10^3 C_{H^+}^{0.42}$, with R in $\mu\text{a}/\text{cm}^2$ and C_{H^+} in moles/liter ($1 \mu\text{a}/\text{cm}^2 \cong 2.5 \text{ mg dm}^{-2} \text{ day}^{-1}$). Comparison of data in 0.5 and 3 M NaCl shows that corrosion rate is insensitive to salt concentration at all temperatures and acidities. These measurements are being extended over a wider range of salt concentrations, from 0.5 M NaCl to saturated solutions, and polarization measurements are being made to provide data on the mechanisms of the charge-transfer processes important in the overall corrosion reaction.

rate is obtained without the necessity for weight loss or polarization measurements. A paper on the electrochemical pH-stat and its application to corrosion studies has been submitted for publication.⁹

The electrochemical pH-stat was also used to measure the extent of hydrolysis of ferrous ions produced by the corrosion of iron in 0.5 M NaCl at temperatures from 25 to 70°C. The results, corrected for activity coefficients and for the variation of the ion product of water with temperature, show that $\log K = -4.9$, essentially independent of temperature [$K = a_{\text{Fe}^{2+}} (a_{\text{OH}^-} / a_{\text{FeOH}^+})$]. Hence ΔH° is essentially zero, and $\Delta S^\circ \cong -22.4 \text{ cal mole}^{-1} (\text{°K})^{-1}$ for the dissociation of FeOH^+ . This information will be useful in interpreting other data on the corrosion of iron in saline water.

Development and Use of an Electrochemical pH-Stat

The problem of measuring corrosion rates in the pH region near neutrality over extended periods of time while maintaining constant pH was solved by development of an electrochemical pH-stat. The pH-stat controls automatically the acidity of unbuffered solutions in the region from pH = 3 to pH = 11 with a precision of approximately ± 0.01 pH unit. A potentiostat (Fig. 10.3) is used to control the potential of a platinum or other inert electrode on which the hydrogen-gas-hydrogen-ion reaction occurs in a solution saturated with hydrogen gas. The inert electrode acts as a sensing element and a regulating electrode for the control of acidity. Current from the potentiostat passes through the inert electrode and an auxiliary polarizing electrode in an external compartment separated from the main cell by a salt bridge or porous plate. The current required to maintain constant pH is equal to the corrosion rate of an isolated metallic electrode undergoing hydrogen-evolution-type corrosion in the same cell, so that a continuous record of corrosion

⁹F. A. Posey, T. Morozumi, and E. J. Kelly, "An Electrochemical pH-Stat and Its Application to Corrosion Studies," to be published in the *Journal of the Electrochemical Society*.

UNCLASSIFIED
ORNL-LR-DWG. 78264

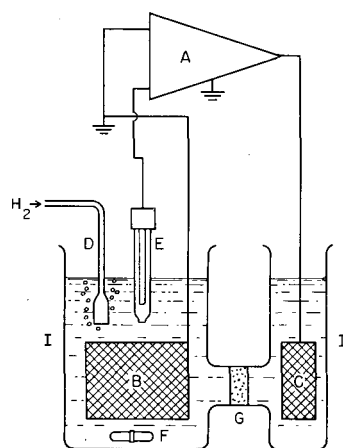


Fig. 10.3. Schematic Diagram of Potentiostat Type of Electrochemical pH-Stat. A, electronic potentiostat; B, large platinum electrode; C, auxiliary polarizing electrode; D, inlet and bubbler for hydrogen gas; E, reference electrode; F, stirrer (magnetic); G, salt bridge or porous disk; I, primary cell; II, exterior polarizing chamber.

Publications

NUCLEAR CHEMISTRY

A. R. Brosi, A. I. Galonsky, B. H. Ketelle, and H. B. Willard, "A Precision Measurement of the Longitudinal Polarization of Betas Following P^{32} Decay," *Nucl. Phys.* **33**, 353 (1962).

F. Perey, R. J. Silva, and G. R. Satchler, "Excited-Core Model of Odd-A Nuclei and the $Cu^{63}(p,p')$ Reactions," *Phys. Letters* **4**, 25 (1963).

H. W. Schmitt, J. H. Neiler, F. J. Walter, and A. Chetham-Strode, "Mass Distribution and Kinetics of U^{235} Thermal-Neutron Induced Three-Particle Fission," *Phys. Rev. Letters* **9**, 427 (1962).

H. W. Schmitt, J. H. Neiler, F. J. Walter, and A. Chetham-Strode, "Mass Distribution and Kinetics of U^{235} Thermal-Neutron Induced Three-Particle Fission" (abstract), *Bull. Am. Phys. Soc.* **8**, 69 (1963).

P. M. Lantz, "Thermal Neutron Capture Cross Section and Resonance Capture Integral of Cerium-144," *Nucl. Sci. Eng.* **13**, 289-94 (1962).

J. Halperin and J. H. Oliver, "An Upper Limit for the Effective Capture Cross Section of Po-210 for Thermal Neutrons," *Nucl. Sci. Eng.* **15**, 217 (1963).

R. W. Stoughton and J. Halperin, "Effective Cutoff Energies for Boron, Cadmium, Gadolinium, and Samarium Filters," *Nucl. Sci. Eng.* **15**, 314 (1963); *Trans. Am. Nucl. Soc.* **5**(2), 383 (1962).

J. Halperin, F. J. Johnston, R. W. Stoughton, J. H. Oliver, E. L. Blevins, R. E. Druschel, A. L. Harkness, and B. A. Swartz, "The Average Capture/Fission Ratio of U-233 for Epithermal Neutrons," *Nucl. Sci. Eng.* **16**, 245 (1963).

J. Halperin, R. E. Druschel, and C. R. Baldock, "Thermal Neutron Cross Section and Resonance Integral of Sm-150," *Trans. Am. Nucl. Soc.* **5**(2), 376 (1962).

E. Eichler, G. D. O'Kelley, R. L. Robinson, J. A. Marinsky, and N. R. Johnson, "Nuclear Levels of Ge^{74} ," *Nucl. Phys.* **35**, 625 (1962).

C. D. Goodman, G. D. O'Kelley, and D. A. Bromley, "A 20,000-Channel Pulse-Height Analyzer with Two Coordinate Address," pp 197-200 in *Proceedings of the Symposium on Nuclear Instruments, Harwell* (ed. by J. B. Birks), Academic Press, New York, 1962.

N. R. Johnson, "Decay of Re^{184} Isomers and the Level Scheme in W^{184} ," *Phys. Rev.* **129**, 1737 (1963).

G. D. O'Kelley (ed.), *Applications of Computers to Nuclear and Radiochemistry*, NAS-NS-3107, National Academy of Sciences-National Research Council, Washington, D.C., 1963.

G. D. O'Kelley, "Radioactive Sources," pp 555-80 in *Methods of Experimental Physics* (ed. by L. C. L. Yuan and C. S. Wu), vol 5B, Academic Press, New York, 1963.

R. L. Robinson, N. R. Johnson, and E. Eichler, "Decay of Cs^{132} ," *Phys. Rev.* **128**, 252 (1962).

D. E. Troutner, R. L. Ferguson, and G. D. O'Kelley, "Yields and Half-Lives in the Mass-99 Fission Product Chain," *Phys. Rev.* **130**, 1466 (1963).

R. L. Wolke, W. N. Bishop, E. Eichler, N. R. Johnson, and G. D. O'Kelley, "Ranges and Stopping Cross Sections of Low-Energy Tritons," *Phys. Rev.* **129**, 2591 (1963).

CHEMICAL SEPARATION OF ISOTOPES

A. A. Palko, G. M. Begun, and L. Landau, "Equilibrium Constant for Boron Isotope Exchange Between BF_3 and $\text{BF}_3 \cdot \text{O}(\text{CH}_3)_2$," *J. Chem. Phys.* **37**, 552-55 (1962).

G. M. Begun and A. A. Palko, "Raman and Infrared Spectra of BF_3 Complexes with Diethyl Ether and Tetrahydrofuran, and the Isotopic Exchange of These Complexes with BF_3 ," *J. Chem. Phys.* **38**, 2112-17 (1963).

A. C. Rutenberg and J. S. Drury, "The Exchange of Ammonia Between Aqueous Ammonia and $\text{Co}(\text{NH}_3)_6\text{Cl}_3$," *Inorg. Chem.* **2**, 219 (1963).

A. C. Rutenberg, "Xenon Fluorides: Fluorine-19 Nuclear Magnetic Resonance Spectra," *Science* **140**, 993 (1963).

RADIATION CHEMISTRY

G. L. Kochanny, Jr., "Radiation Chemistry Studies of Water as Related to the Initial Linear Energy Transfer of 11-23 Mev Protons," Ph.D. thesis, Michigan State University.

C. J. Hochanadel, "Photolysis of Dilute Hydrogen Peroxide Solution in the Presence of Dissolved Hydrogen and Oxygen: Evidence Relating to the Nature of the Hydroxyl Radical and the Hydrogen Atom Produced in the Radiolysis of Water," *Radiation Res.* **17**, 286-301 (1962).

H. A. Mahlman and T. E. Willmarth, "Radiation Induced Formation of Metallic Silver," *J. Appl. Phys.* **33**, 3388 (1962).

J. W. Boyle, "The Decomposition of Aqueous Sulfuric Acid Solutions by Cobalt Gamma Rays. I. Radical and Molecular Product Yields from Ce(IV) Solutions in 0.4 to 18 M Acid," *Radiation Res.* **17**, 427-49 (1962).

J. W. Boyle, "The Decomposition of Aqueous Sulfuric Acid Solutions by Cobalt Gamma Rays. II. Yields of Solvent Decomposition and Reducing Radicals from Fe(II) Solutions in 0.4 to 18 M Acid," *Radiation Res.* **17**, 450-64 (1962).

R. K. Clayton and P. S. Rudolph, "The Lethal Effects of Alpha Irradiation on Wild-Type and on a High-Catalase Mutant of *Rhodospseudomonas spheroides*," *Radiation Res.* **17**, 839 (1962).

M. D. Silverman, B. O. Heston, and P. S. Rudolph, "Radiation Damage to Freon-11, CCl_3F ," *Nucl. Sci. Eng.* **15**, 217 (1963).

H. W. Kohn, "Deuterium Exchange on Silica Gel Initiated by Cobalt-60 Irradiation," *J. Phys. Chem.* **66**, 1017 (1962).

H. W. Kohn, "Surface Carbonium Ions Produced by Irradiating Silica Gel," *J. Phys. Chem.* **66**, 1185 (1962).

H. W. Kohn and E. H. Taylor, "The Effect of Ionizing Radiations on Catalytic Activity. Hydrogenation and Isotopic Exchange on Inorganic Solids," *J. Catalysis* **2**, 32-39 (1963).

ORGANIC CHEMISTRY

C. J. Collins, M. M. Staum, and B. M. Benjamin, "Molecular Rearrangements. XX. The Deamination of *erythro*- and *threo*-1-Amino-1-phenyl-2-*p*-methoxyphenyl-2-propanol and *erythro*- and *threo*-1-Amino-1-phenyl-2-*o*-tolyl-2-propanol," *J. Org. Chem.* **27**, 3525 (1962).

C. J. Collins and B. M. Benjamin, "Stereochemistry and Radiochemistry of Deamination Reactions," reprinted from *Radioisotopes in the Physical Sciences and Industry*, International Atomic Energy Agency, Vienna, 1962.

G. A. Ropp, "Evaluation of Deuterium Isotope Effects in Photochemical Reactions of Formic-d Acid by Use of C^{14} ," reprinted from *Radioisotopes in the Physical Sciences and Industry*, International Atomic Energy Agency, Vienna, 1962.

C. E. Higgins and W. H. Baldwin, "Interactions Between Tributyl Phosphate, Phosphoric Acid and Water," *J. Inorg. Nucl. Chem.* **24**, 415 (1962).

CHEMISTRY OF AQUEOUS SYSTEMS

R. M. Rush and J. S. Johnson, "Hydrolysis of U(VI): Absorption Spectra of Chloride and Perchlorate Solutions," *J. Phys. Chem.* **67**, 821 (1963).

R. M. Rush, J. S. Johnson, and K. A. Kraus, *Hydrolysis of U(VI): Acidity Measurements in Chloride Solutions and Absorption Spectra in Chloride and Perchlorate Solutions*, ORNL-3278 (Feb. 7, 1963).

M. H. Lietzke and R. W. Stoughton, *A Mathematical Model for the Solvent Extraction of Uranyl Nitrate and Nitric Acid*, ORNL CF-62-7-10; ORNL TM-358; *Nucl. Sci. Eng.* **16**, 25-30 (1963).

M. H. Lietzke and R. W. Stoughton, "The Thermodynamics of Aqueous Electrolyte Mixtures at Elevated Temperatures," *J. Phys. Chem.* **66**, 2264 (1962).

M. H. Lietzke and R. W. Stoughton, "The Second Dissociation Constant of Deuteriosulfuric Acid from 25 to 225°," *J. Phys. Chem.* **67**, 652 (1963).

M. H. Lietzke, R. W. Stoughton, and Marjorie P. Lietzke, *A Comparison of Several Methods for Inverting Large Symmetric Positive Definite Matrices*, ORNL-3430 (May 9, 1963).

M. H. Lietzke, "Generalized Least Squares and the Inversion of Symmetric Positive Definite Matrices," pp 1-8 in *Application of Computers to Nuclear and Radiochemistry*, NAS-NS 3107, National Academy of Sciences-National Research Council, Washington, D.C., 1963.

S. Lindenbaum and G. E. Boyd, "Liquid Amine and Ion-Exchange Resin Absorption of Bromine Ion from Aqueous Salt Solutions; Variation with Aqueous Electrolyte Activities," *J. Phys. Chem.* **66**, 1383 (1962).

S. Lindenbaum and G. E. Boyd, "Spectrophotometric Investigation of the Extraction of Transition Metal Halo-Complex Ions by Amine Extractants," *J. Phys. Chem.* **67**, 1238 (1963).

H. O. Phillips and K. A. Kraus, "Adsorption on Inorganic Materials. V. Reaction of Cadmium Sulfide with Cu(II), Hg(II) and Ag(I)," *J. Am. Chem. Soc.* **85**, 486 (1963).

F. Nelson and K. A. Kraus, "Some Techniques for Isolating and Using Short-Lived Radioisotopes," *Proceedings of the IAEA Seminar on Practical Applications of Short-Lived Isotopes Produced in Small Research Reactors*, IAEA, Vienna, 1963.

ELECTROCHEMICAL KINETICS AND ITS APPLICATION TO CORROSION

G. H. Cartledge, "Recent Studies of the Action of the Inorganic Inhibitors," *Corrosion* **18**, 316t (1962).

G. H. Cartledge, "Radioisotopes in the Physical Chemistry of Corrosion Processes and Their Inhibition," p 549 in *Radioisotopes in the Physical Sciences and Industry*, International Atomic Energy Agency, Vienna, 1962.

G. H. Cartledge and D. H. Spahrber, "Ion-Exchange Properties of the Film on Passive Iron and Steel," *J. Electrochem. Soc.* **110**, 644 (1963).

R. E. Meyer, "The Reduction of Oxygen on Passive Zirconium," *J. Electrochem. Soc.* **110**, 167 (1963).

F. A. Posey and R. F. Sympson, "Effect of Adsorbed Anions on Reduction Processes on Passive Stainless Steel," *J. Electrochem. Soc.* **109**, 716 (1962).

NONAQUEOUS SYSTEMS AT HIGH TEMPERATURE

M. A. Bredig, "New Evidence for Tetrahalide Complex Ions in Cadmium Halide-Alkali Metal Halide Melts," *J. Chem. Phys.* **37**, 451 (1962).

M. A. Bredig, "Molten Salt Solutions of Electropositive Metals: Electronic Conductance and Metal Halide Stoichiometry," *J. Chem. Phys.* **37**, 914 (1962).

H. R. Bronstein, A. S. Dworkin, and M. A. Bredig, "Electrical Conductance of Solutions of Salts in Liquid Metals. II. Potassium Fluoride and Bromide in Potassium," *J. Chem. Phys.* **37**, 677 (1962).

A. S. Dworkin and M. A. Bredig, "The Heats of Fusion and Transition of Alkaline Earth and Rare Earth Metal Halides," *J. Phys. Chem.* **67**, 697 (1963).

A. S. Dworkin, R. A. Sallach, H. R. Bronstein, M. A. Bredig, and J. D. Corbett, "The Electrical Conductivity of Solutions of Metals in Their Molten Halides. VI. Lanthanum, Cerium, Praseodymium, and Neodymium in Their Molten Iodides," *J. Phys. Chem.* **67**, 1145 (1963).

CHEMICAL PHYSICS

Henry Zeldes and Ralph Livingston, "Paramagnetic Resonance Study of Production of NO_2 and NO_2^- in Irradiated KNO_3 ," *J. Chem. Phys.* **37**, 3017 (1962).

P. A. Agron, G. M. Begun, H. A. Levy, A. A. Mason, C. G. Jones, and D. F. Smith, "Xenon Difluoride and the Nature of the Xenon-Fluorine Bond," *Science* **139**, 842 (1963).

J. H. Burns, P. A. Agron, and H. A. Levy, "Xenon Tetrafluoride Molecule and Its Thermal Motion: A Neutron Diffraction Study," *Science* **139**, 1208 (1963).

W. R. Busing and H. A. Levy, "A Procedure for Inverting Large Symmetric Matrices," *Commun. Assoc. Computing Machinery* **5**, 445 (1962).

M. D. Danford and H. A. Levy, "The Structure of Water at Room Temperature," *J. Am. Chem. Soc.* **84**, 3965 (1962).

H. A. Levy and P. A. Agron, "The Crystal and Molecular Structure of Xenon Difluoride by Neutron Diffraction," *J. Am. Chem. Soc.* **85**, 241 (1963).

S. W. Peterson and H. G. Smith, "Coherent Bragg Scattering of Resonant Nuclides," *J. Phys. Soc. Japan* **17** (suppl B-II), 335 (1962).

H. G. Smith and H. A. Levy, "Neutron Diffraction Study of Ammonium Perchlorate," *Acta Cryst.* **15**, 1201 (1962).

W. R. Busing, K. O. Martin, and H. A. Levy, *OR FLS, A Fortran Crystallographic Least-Squares Program*, ORNL TM-305 (August 1962).

R. A. Gilbert, "Heat of Fusion of $3\text{LiF} \cdot \text{ThF}_4$," *J. Chem. Eng. Data* **7**, 388 (1962).

R. A. Gilbert, "Molar Enthalpies of Mixing in the Molten Lithium Fluoride-Potassium Fluoride System," *J. Phys. Chem.* **67**, 1143 (1963).

G. E. Moore, H. A. Smith, and E. H. Taylor, "Catalytic Reactions on Semiconductors: Hydrogen-Deuterium Exchange and Formic Acid Decomposition on Chemically Doped Germanium," *J. Phys. Chem.* **66**, 1241 (1962).

C. R. Baldock, "Some Unique Applications of Negative Ion Mass Spectra," *Proceedings of the ASTM Committee E-14 on Mass Spectrometry, New Orleans, La., June 3-8, 1962*.

C. E. Melton, "Ionization and Excitation Processes in Argon, Krypton, and the C₂ Hydrocarbons Produced by Various Means," *J. Chem. Phys.* **37**, 562 (1962).

T. W. Martin, R. E. Rummel, and C. E. Melton, "Higher Pressure Mass Spectrometry," *Science* **138**(3537), 77 (1962).

T. A. Carlson, Frances Pleasonton, and C. H. Johnson, "Electron Shake Off Following the β^- Decay of He⁶," *Phys. Rev.* **129**, 2220 (1963).

C. H. Johnson, Frances Pleasonton, and T. A. Carlson, "An Absolute Measurement of the He⁶ Decay Energy," *Nucl. Phys.* **41**, 167 (1963).

T. A. Carlson and R. M. White, "Mass Spectrometric Analyses of the Ions Resulting from the Nuclear Decay of CH₃I¹³⁰ and C₂H₅I¹³¹. Study of Xenon-Hydrocarbon Ions. II," *J. Chem. Phys.* **38**, 2075 (1963).

T. A. Carlson, "Electron Shake Off Following the Beta Decay of Ne²³," *Phys. Rev.* **130**, 2361 (1963).

Participation in College Instruction

C. J. Hochanadel, Visiting Professor of Physical Chemistry, 1962-63 term, Knoxville College, Knoxville, Tenn.

J. F. Riley, Lecturer "Introductory Physics," 1962-63 term, NSF Institute, Knoxville College, Knoxville, Tenn.

J. F. Riley, Lecturer, Visiting Scientist Program, 1962-63 term, Tennessee Academy of Science, Knoxville, Tenn.

Ralph Livingston, Visiting Professor of Chemistry, "Introductory Physical Chemistry," Sept. 15, 1962, to Feb. 1, 1963, Cornell University, Ithaca, N.Y.

Papers Presented at Scientific and Technical Meetings

NUCLEAR CHEMISTRY

E. Eichler, "Lecture Series on Modern Topics in Nuclear Chemistry," Israel Atomic Energy Commission Laboratories, Rehovoth, Israel, Mar. 7, 14, 21, 28, 1962.

E. Eichler, "Decay-Scheme Studies at or near Closed Shells," Gordon Research Conference on Nuclear Chemistry, New London, N.H., June 20, 1963.

J. Gilat, G. D. O'Kelley, and E. Eichler,* "Spectroscopy of Delayed Neutrons: N^{17} ," American Physical Society Meeting, Washington, D.C., Apr. 22-25, 1963 [*Bull. Am. Phys. Soc.* **8**, 320 (1963)].

G. D. O'Kelley, "Trends in Nuclear Instrumentation," invited paper presented at the Oak Ridge Radioisotope Conference, Applications to Physical Science and Engineering, Gatlinburg, Tenn., Apr. 1, 1963.

G. D. O'Kelley, "Decay Schemes of Short-Lived Nuclides," invited paper presented at the Radiochemistry Symposium, University of Missouri, Columbia, Dec. 1, 1962.

G. D. O'Kelley, "Study of the Decay of N^{17} by Scintillation Spectrometry and Time-of-Flight," invited paper presented at the Symposium on Nuclear Spectroscopy of Short-Lived Nuclides, American Physical Society, St. Louis, Mo., Mar. 28, 1963.

G. D. O'Kelley, "Special Topics in Scintillation Counting," ORINS Radioisotopes Training School, Oak Ridge, Tenn., Aug. 17, 1962, Jan. 24, Mar. 7, May 14, 1963.

G. D. O'Kelley, "Scintillation Counting," ORINS Modern Physics Institute for Physics Teachers, Oak Ridge, Tenn., July 16, 1962.

G. D. O'Kelley,* D. A. Bromley, and C. D. Goodman, "The Role of Multiparameter Pulse-Height Analyzers in Radioactivity Studies," Conference on Utilization of Multiparameter Analyzers in Nuclear Physics, Grossingers, Liberty, N.Y., Nov. 12-15, 1962.

D. E. Troutner,* R. L. Ferguson, and G. D. O'Kelley, "Nuclear Charge Division in Fission: Yields of Mass-99 Fission Products," University of Missouri, Columbia, Oct. 24, 1962.

R. W. Stoughton* and J. Halperin, "Effective Cutoff Energies for B, Cd, Gd, and Sm Filters for Spherical, Cylindrical and Slab Geometries," American Nuclear Society Meeting, Washington, D.C., Nov. 26-29, 1962.

R. W. Stoughton, "Early History of and Project Interest in Protactinium Chemistry," Protactinium Chemistry Symposium, Gatlinburg, Tenn., Apr. 25-26, 1963.

R. J. Silva, "Semiconductor Charged Particle Detectors and Some Applications in Medium-Energy Nuclear Physics," ORINS Traveling Lecture, University of Georgia, Athens, Apr. 10, 1963.

H. W. Schmitt,* J. H. Neiler, F. J. Walter, and A. Chetham-Strode, "Mass Distribution and Kinetics of U^{235} Thermal-Neutron Induced Three-Particle Fission," American Physical Society Meeting, New York, Jan. 23-26, 1963.

*Speaker

J. Halperin,* R. E. Druschel, and C. R. Baldock, "Thermal Neutron Cross Section and Resonance Integral of Sm-150," American Nuclear Society, Winter Meeting, Washington, D.C., Nov. 26-28, 1962.

P. M. Lantz,* C. R. Baldock, and L. E. Idom, "Thermal Neutron Capture Cross-Section and Resonance Capture Integral of Ce¹⁴⁰ and Effective Capture Cross Section of Ce¹⁴¹," American Nuclear Society, Annual Meeting, Salt Lake City, Utah, June 17-21, 1963.

CHEMICAL SEPARATION OF ISOTOPES

J. S. Drury,* L. Landau, and L. B. Yeatts, "Oxygen and Carbon Isotope Fractionation on Distilling Alkyl Amine Carbamates," American Chemical Society Meeting, Gatlinburg, Tenn., Nov. 1-3, 1962.

E. Von Halle and J. S. Drury,* "The Enrichment of Oxygen-17. I. Cascade Calculations," 144th National Meeting, American Chemical Society, Los Angeles, Calif., Apr. 5, 1963.

J. S. Drury,* R. M. Hill, B. B. Klima, and H. O. Weeren, "The Enrichment of Oxygen-17. II. Cascade Design and Construction," 144th National Meeting, American Chemical Society, Los Angeles, Calif., Apr. 5, 1963.

J. S. Drury, "Isotopes - Harbingers of a New Era," Chemistry Department, Brescia College, Owensboro, Ky., Mar. 19, 1963.

G. M. Begun* and W. H. Fletcher, "The Infrared and Raman Spectra of Oxalate Ion in Aqueous Solution," Symposium on Molecular Structure and Spectroscopy, Ohio State University, Columbus, June 14, 1963.

RADIATION CHEMISTRY

J. W. Boyle, "Recent Studies in Radiation Chemistry of Water," ORINS Traveling Lecture, University of Louisville, Louisville, Ky., Jan. 17, 1963.

H. A. Mahlman, "Radiation Chemistry of Concentrated Sodium Nitrate Solutions," AERE, Harwell, England, Aug. 13, 1962.

H. A. Mahlman, "The Radiation Chemistry of Aqueous Nitrate Solutions," Nuclear Research Center, Karlsruhe, West Germany, Aug. 20, 1962.

H. A. Mahlman, "The Direct Effect in the Radiation of NaNO₃ Solutions," C.E.N., Saclay, France, Aug. 28, 1962.

H. A. Mahlman, "Introduction to Radiation Chemistry," Research and Development Group - U.S. Army Reserve, Oak Ridge, Tenn., May 1, 1963.

J. F. Riley, "Radiation Chemistry," ORINS Isotope Technology Institute, July 26, 1962; ORINS Radioisotope Technique Course, Sept. 6, 1962, Mar. 8, 1962, and May 13, 1963; ORINS Health Physics Course, Sept. 28, 1962.

P. S. Rudolph, "The Radiation Chemistry of Gases," State University of New York at Buffalo, Buffalo, N.Y., Apr. 17, 1963.

P. S. Rudolph, "Elucidating Elementary Mechanisms in the Radiation Chemistry of Gases," Syracuse University, Syracuse, N.Y., Apr. 19, 1963.

P. S. Rudolph, "Radiation Effects on Glass," Technical Sessions, 8th Annual Symposium, American Scientific Glassblowers Society, Chicago, Ill., June 6, 1963.

*Speaker

H. W. Kohn, "Irradiated Catalysts," ORINS Traveling Lecture, Rice University, Houston, Tex., Nov. 19, 1962.

H. W. Kohn, "Irradiated Catalysts," Catalysis Club of Pittsburgh, Pittsburgh, Pa., Sept. 24, 1962.

ORGANIC CHEMISTRY

C. J. Collins, "Mechanism of the Deamination Reaction," University of Buffalo, Buffalo, N.Y., Sept. 26, 1962.

C. J. Collins, "The Nature of the Carbonium Ion Intermediates in Certain Deamination Reactions," California Institute of Technology, Pasadena, Calif., May 13, 1963.

C. J. Collins, "The Stereochemistry and Radiochemistry of the Deamination Reaction," Wilmington Organic Chemists Club, Wilmington, Del., May 22, 1963.

V. F. Raaen, "Some Aspects of Carbon and Hydrogen Isotope Effects," Louisiana State University in New Orleans, New Orleans, La., Mar. 22, 1963.

CHEMISTRY OF AQUEOUS SYSTEMS

R. M. Rush,* J. S. Johnson, and K. A. Kraus, "Hydrolysis of U(VI): Absorption Spectra of Chloride and Perchlorate Solutions," 14th Southeastern Regional Meeting of the American Chemical Society, Gatlinburg, Tenn., Nov. 1-3, 1962 [abstracted in the *Branched Chain* 18, 78 (1962)].

M. H. Lietzke, "The Use of a High Speed Computer in the Treatment of Thermodynamic Data Involving Complex Equilibria," and "Generalized Least Squares and the Inversion of Symmetric Positive Definite Matrices," Stetson University, De Land, Fla., Nov. 14, 1962.

M. H. Lietzke, "The Use of a High Speed Computer to Calculate Equilibrium Constants in Solvent Extraction Systems," and "The Inversion of Large Symmetric Positive Definite Matrices," University of Southwestern Louisiana, Lafayette, Nov. 30, 1962.

M. H. Lietzke, "The Use of a High Speed Computer in Analyzing Chemical Thermodynamic Systems," Loyola University, New Orleans, La., Dec. 1, 1962.

M. H. Lietzke, "The Use of a High Speed Computer to Calculate Equilibrium Constants in Solubility and Solvent Extraction Equilibria," Emory University, Ga., Jan. 11, 1963.

M. H. Lietzke, "The Use of a High Speed Computer in the Treatment of Thermodynamic Data Involving Complex Equilibria," University of Alabama, Tuscaloosa, Feb. 19, 1963.

M. H. Lietzke, "The Use of a High Speed Computer in the Treatment of Thermodynamic Data Involving Complex Equilibria," Yale University, New Haven, Conn., Apr. 11, 1963.

M. H. Lietzke, "High Temperature Aqueous Solution Chemistry," The Pennsylvania State University, State College, Apr. 12, 1963.

M. H. Lietzke, "Recent Thermodynamic Studies in Aqueous Systems at Elevated Temperatures," University of Tennessee, Knoxville, May 9, 1963.

M. H. Lietzke, "Generalized Least Squares and the Inversion of Symmetric Positive Definite Matrices," Symposium on Application of Computers to Nuclear and Radiochemistry, Gatlinburg, Tenn., Oct. 17-19, 1962.

O. L. Keller, Jr., "Identification of Niobium Double Fluoride Species in HF Solutions by Raman Spectroscopy," 14th Southeastern Regional Meeting of the American Chemical Society, Gatlinburg, Tenn., Nov. 1-3, 1962.

*Speaker

O. L. Keller, Jr., "Characterization of Protactinium Species in Crystals and Solutions by Raman and Infrared Spectroscopy," Protactinium Chemistry Symposium, Gatlinburg, Tenn., Apr. 25-26, 1963.

K. A. Kraus, Lectures on "Ion Exchange" in Summer Course on Separation Methods in Inorganic Chemistry, sponsored by the National Research Council of Italy, Rome, Italy, Sept. 17-27, 1962.

F. Nelson* and K. A. Kraus, "Some Techniques for Isolating and Using Short-Lived Radioisotopes," IAEA Seminar, Vienna, Nov. 5-9, 1962.

K. A. Kraus, "Solution Chemistry of Plutonium," Symposium on Plutonium Chemistry, University of Chicago, Feb. 18, 1963.

Fred Vaslow, "The Apparent Heats of Dilution of *p*-Ethylbenzene Sulfonate Salts and a Comparison with the Heats of Ion-Exchange Reactions," 14th Southeastern Regional Meeting of the American Chemical Society, Gatlinburg, Tenn., Nov. 1-3, 1962.

ELECTROCHEMICAL KINETICS AND ITS APPLICATION TO CORROSION

G. H. Cartledge, "Ion Exchange at the Passive Film on Iron and Steel," Second International Symposium on the Passivity of Metals, Toronto, Canada, Sept. 3-7, 1962.

G. H. Cartledge, "Factors in the Action of Inorganic Inhibitors," Seminar, The Marshall Laboratories, Philadelphia, Pa., June 11, 1963.

NONAQUEOUS SYSTEMS AT HIGH TEMPERATURE

M. A. Bredig, "Solutions of Metals in Fused Salts," Research Laboratory, General Electric Company, Schenectady, N.Y., Dec. 14, 1962.

CHEMICAL PHYSICS

Henry Zeldes, "Electron Spin Resonance Study of Irradiated Potassium Nitrate," National Physical Laboratory, Teddington, England, July 9, 1962.

Henry Zeldes, "Electron Spin Resonance Study of Irradiated Potassium Nitrate," Keele University, Keele, England, July 11, 1962.

Henry Zeldes, "Paramagnetic Species in Irradiated KNO_3 ," First International Conference on Paramagnetic Resonance, Jerusalem, Israel, July 20, 1962.

Ralph Livingston, "Paramagnetic Resonance Studies of Single Crystals Containing Free Radicals," Department of Physics, University of Alabama, Tuscaloosa, July 17, 1962.

Ralph Livingston, "Paramagnetic Resonance Studies of Irradiated Solids," Department of Physics, A & M College of Texas, College Station, Mar. 12, 1963.

Ralph Livingston, "Paramagnetic Resonance Studies of Single Crystals Containing Free Radicals," Department of Chemistry, The University of Texas, Austin, Mar. 13, 1963.

Ralph Livingston, "An Introduction to Nuclear Quadrupole Spectroscopy," Department of Chemistry, Tulane University, New Orleans, La., Mar. 15, 1963.

Ralph Livingston, "Paramagnetic Resonance Studies of Free Radicals in Solids," Department of Chemistry, University of Tennessee, Knoxville, Apr. 4, 1963.

*Speaker

H. A. Levy, "Neutron Diffraction Studies of the Structure of Some Non-Metallic Solids," Conference on Chemistry of Nonmetallic Solids, Laval University, Quebec, Canada, Sept. 5-7, 1962.

H. A. Levy, "The Impact of High Speed Computing on Experimental Crystallography," 14th Southeastern Regional Meeting of the American Chemical Society, Gatlinburg, Tenn., Nov. 1-3, 1962.

M. D. Danford* and H. A. Levy, "An X-Ray Diffraction Study of the Structure of Water at Room Temperature," 14th Southeastern Regional Meeting of the American Chemical Society, Gatlinburg, Tenn., Nov. 1-3, 1962.

H. A. Levy, "Structure of Water and the Influence of Solutes," 7th Annual Meeting of the Biophysical Society, New York, Feb. 18-20, 1963.

H. A. Levy, "Recent Neutron Diffraction Studies," Mellon Institute, Pittsburgh, Pa., Feb. 21, 1963.

M. D. Danford and H. A. Levy,* "Application of Diffraction Techniques to the Study of Structure in Non-Metallic Melts," 92nd Annual Meeting of the Metallurgical Society of AIME, Dallas, Tex., Feb. 24-28, 1963.

H. A. Levy* and P. A. Agron, "The Crystal and Molecular Structure of Xenon Difluoride by Neutron Diffraction," Annual Meeting of the American Crystallographic Association, Cambridge, Mass., Mar. 28-30, 1963.

H. A. Levy,* P. A. Agron, and W. R. Busing, "A Study of the Precision and Accuracy of Integrated Intensity Measurements with the Oak Ridge Automatic Neutron Diffractometer," Annual Meeting of the American Crystallographic Association, Cambridge, Mass., Mar. 28-30, 1963.

J. H. Burns,* P. A. Agron, and H. A. Levy, "A Neutron Diffraction Study of Xenon Tetrafluoride," Annual Meeting of the American Crystallographic Association, Cambridge, Mass., Mar. 28-30, 1963.

J. H. Burns,* P. A. Agron, and H. A. Levy, "The Crystal and Molecular Structure of Xenon Tetrafluoride by Neutron Diffraction," Conference on Noble Gas Compounds, Argonne National Laboratory, Argonne, Ill., Apr. 22-23, 1963.

H. A. Levy and P. A. Agron,* "The Crystal and Molecular Structure of Xenon Difluoride by Neutron Diffraction," Conference on Noble Gas Compounds, Argonne National Laboratory, Argonne, Ill., Apr. 22-23, 1963.

W. R. Busing* and H. A. Levy, "Experience with the Oak Ridge Automatic Three-Dimensional Neutron Diffractometer," The British X-Ray Analysis Group Conference, London, England, Nov. 16-17, 1962.

G. M. Brown, "An Example of a Precise Determination of Crystal Structure by X-Ray Analysis," Duke University, Durham, N.C., Nov. 26, 1962.

G. M. Brown, "Recent Crystal Structure Determinations by Neutron Diffraction at the Oak Ridge National Laboratory," Duke University, Durham, N.C., Nov. 26, 1962.

H. G. Smith, "Use of Polaroid Film in Neutron and X-Ray Diffraction," Symposium on Recent Experimental and Theoretical Methods in Crystal Structure Research, Munich, Germany, July 29-31, 1962.

H. G. Smith, "Neutron Diffraction at Oak Ridge," Boris Kidric Institute, Belgrade, Yugoslavia, July 19, 1962.

W. R. Busing, "Chemical Information from Neutron Diffraction Studies," University of Manchester, Manchester, England, Oct. 24, 1962; University of Glasgow, Glasgow, Scotland, Jan. 17, 1963; and Imperial College, London, England, Apr. 30, 1963.

W. R. Busing, "A Computer Program to Postulate Crystal Structures," Manchester College of Science and Technology, Manchester, England, Dec. 19, 1962.

*Speaker

W. R. Busing, "Recent Neutron Diffraction Work at Oak Ridge," Atomic Energy Research Establishment, Harwell, England, Mar. 5, 1963, and Cambridge University, Cambridge, England, May 9, 1963.

W. R. Busing* and O. S. Mills, "The Manchester On-Line X-Ray Diffractometer," University College, London, England, Mar. 1, 1963.

R. A. Gilbert, "Molar Enthalpies of Mixing in the Liquid LiF-KF System," 17th Annual Calorimetry Conference, University of California, Berkeley, Aug. 22-24, 1962.

C. R. Baldock, "Mass Spectrometric Studies of Ion-Molecule Reactions," Auburn University, Auburn, Ala., Dec. 7, 1962.

M. O. Krause* and T. A. Carlson, "The Charge Spectrum of Neon Resulting from Inner Shell Ionization by X-Rays," American Physical Society, Southeastern Section, Knoxville, Tenn., Apr. 4-6, 1963.

C. H. Johnson,* Frances Pleasonton, and T. A. Carlson, "Experimental Limit to Tensor Interaction in the β -Decay of He^6 ," American Physical Society, Washington, D.C., Apr. 22-25, 1963 [*Bull. Am. Phys. Soc.* **8**, 333 (1963)].

T. A. Carlson, "Electron Shake Off Following the β^- Decay of Ar^{41} ," American Physical Society, Washington, D.C., Apr. 22-25, 1963 [*Bull. Am. Phys. Soc.* **8**, 357 (1963)].

*Speaker

INTERNAL DISTRIBUTION

1. C. E. Larson
2. Biology Library
- 3-5. Central Research Library
6. Laboratory Shift Supervisor
7. Reactor Division Library
- 8-9. ORNL - Y-12 Technical Library
Document Reference Section
- 10-48. Laboratory Records Department
49. Laboratory Records, ORNL R.C.
50. A. M. Weinberg
51. J. A. Swartout
- 52-66. E. H. Taylor
67. E. D. Shipley
68. S. C. Lind
69. M. L. Nelson
70. W. H. Jordan
71. F. L. Culler
72. A. H. Snell
73. A. Hollaender
74. M. T. Kelley
75. W. D. Manly
76. K. Z. Morgan
77. T. A. Lincoln
78. A. S. Householder
79. M. H. Lietzke
80. F. A. Posey
81. H. E. Seagren
82. J. A. Lane
- 83-97. G. E. Boyd
- 98-105. M. A. Bredig
106. R. W. Stoughton
107. R. B. Briggs
108. G. W. Parker
109. C. J. Borkowski
110. G. H. Jenks
111. K. A. Kraus
112. H. A. Levy
113. R. S. Livingston
114. T. E. Willmarth
115. M. D. Danford
116. S. Lindenbaum
117. F. Vaslow
118. E. Eichler
119. R. A. Gilbert
120. R. B. Parker
121. G. C. Williams
122. C. H. Secoy
123. C. J. Hochanadel
124. W. H. Baldwin
125. A. R. Brosi
126. R. N. Lyon
127. S. A. Reynolds
128. P. F. Thomason
129. E. G. Bohlmann
130. C. D. Susano
131. R. Livingston
132. G. H. Cartledge
133. B. H. Ketelle
134. E. Lamb
135. R. W. Johnson
136. J. R. McNally, Jr.
137. G. D. O'Kelley
138. M. J. Skinner
139. D. S. Billington
140. H. G. MacPherson
141. J. L. Gabbard
142. R. H. Busey
143. J. J. Pinajian
144. J. Halperin
145. C. R. Baldock
146. F. F. Blankenship
147. C. J. Collins
148. J. S. Drury
149. W. R. Grimes
150. J. S. Johnson
151. W. L. Marshall
152. H. F. McDuffie
153. S. Datz
154. G. M. Watson
155. R. E. Thoma
156. D. R. Cuneo
157. P. S. Rudolph
158. G. Scatchard (consultant)
159. D. F. Hornig (consultant)
160. Isadore Perlman (consultant)
161. T. H. Davies (consultant)
162. C. A. Hutchison (consultant)

EXTERNAL DISTRIBUTION

163. H. Miller, Office of Isotope Development, AEC, Washington
164. R. W. McNamee, Union Carbide Corporation, New York
165. R. H. Schuler, Radiation Research Laboratories, Mellon Institute, 4400 Fifth Ave., Pittsburgh 13, Pa.
166. Division of Research and Development, AEC, Washington
167. Research and Development Division, AEC, ORO
168. Boeing Airplane Company
169. Union Carbide Corporation, Chemicals Division (South Charleston)
170. North American Aviation, Inc.
171. Masaharu Kondo, Professor of Chemistry, Radiation Chemistry Laboratory, Tokyo Metropolitan University, 1-950, Fukasawa-cho, Setagaya-ku, Toyko, Japan
172. M. Daniels, Department of Chemistry, University College of West Indies, Kingston 7, Jamaica
173. J. P. W. Houtman, Reactor Institute Delft, Technische Hogeschool, Delft, The Netherlands
174. Technion, Israel Institute of Technology, Department of Nuclear Science, Haifa, Israel
- 175-764. Given distribution as shown in TID-4500 (22nd ed.) under Chemistry category (75 copies - OTS)